Characterising novel, humanised and physiological mouse models of FUS-ALS



Georgia Price

DPhil in Clinical Neurosciences

Linacre College

Michaelmas 2023

Supervisors

Dr Thomas Cunningham (MRC Harwell, UCL Institute of Prion Diseases)

Professor Kevin Talbot (University of Oxford)

Word count: 46,982

Dedication

This work is dedicated to ALS patients and their families. I have been privileged to meet many people living with, and affected by, ALS during this project and their positivity and hope never failed to inspire me.

Acknowledgements

Firstly, I want to thank my primary supervisor, Tom Cunningham for his support and enthusiasm during this project. His passion and wealth of knowledge on mouse genetics is inspirational and led to countless thoughtful discussions. Thank you for your support and guidance both in and out of the lab, whilst also allowing me independence to develop my own ideas, I am a better scientist for it. Even during the closure of Harwell, Tom remained overwhelmingly positive, and I am very grateful for his constant support from afar. Throughout the project, Lizzy Fisher was a crucial figure, helping devise and guide the project from UCL. When the closure of Harwell was announced, Lizzy's support was greatly appreciated, including her eloquent arguments for the continuation of mouse research and the importance of our work. Tom and Lizzy's enthusiasm for mouse genetics and what it can help us to understand is inspiring and something I will take forward from this project.

I must also thank the members of what was the MMoN group. Remya, Samanta, Ross and Charlotte were instrumental in teaching me many of the techniques used during this project and supporting me personally. A special mention must go to Dave, without whom it would have been a very hard and lonely final two years. A fellow DPhil student in the MMoN group, Dave was a huge support both

during and after the closure, having gone through the experience together. Without Dave's help, both in the lab and out of it, the closure would have had a much greater impact on this project.

The ward staff who maintained the mice at MRC Harwell are thanked, not just for their hard work breeding and maintaining the mouse colonies, but for their cheerful support during this project, particularly after Tom had gone to UCL. There is never a dull moment in ward 5 and I thank them for that!

During my first year, Kevin Talbot kindly took me on as a student to provide stability to the project. He fully integrated me into his group, inviting me to lab meetings and social away days amongst other things, which provided a support network and a platform for rigorous scientific discussions. My project benefitted immensely from the support of his lab members.

Finally, I would like to thank my family and friends, who's love, and support made me believe I could succeed. To my parents, I am here because of your dedication and hard work, and I am eternally grateful. To my partner Dan, your unwavering confidence that I could achieve anything I put my mind to made me sure that I could. I can't thank you enough for your positive energy and encouragement.

Note on the closure of MRC Harwell

On the 18th of May 2022, during the third year of my DPhil project, MRC Harwell Mammalian Genetics Unit closed on site research. The decision to stop research was officially made during my first year, initiating two years of meetings, debates with head office, and planning for several different scenarios post-closure, which changed constantly.

In the end, mice used for this project remained at the Mary Lyon Centre at MRC Harwell and I continued using the lab space, albeit without an onsite lab group or supervisor. Dr Tom Cunningham remained as my primary supervisor, supporting the project whilst leading his new group at UCL.

The closure of the unit was a turbulent time with a lot of uncertainty about how the DPhil project would be affected. Many staff, and therefore expertise and support, left the Harwell site, and it was unclear what resources would remain available at Harwell. During this time, Prof Kevin Talbot became an additional supervisor and integrated me into his group at Oxford which provided stability.

Overall, the DPhil project progressed well and was impacted as little as was possible, but the stress and uncertainty created by the closure of MRC Harwell cannot be overlooked.

Table of Contents

Dedication 2
Acknowledgements 2
Note on the closure of MRC Harwell 4
Abbreviations 11
Abstract 13
Plain language summary 14
Impact Statement 15
1 Chapter 1: Introduction 17
1.1 Background of ALS 17
1.2 Clinical presentation of ALS 17
1.3 Pathological presentation and diagnosis of ALS 18
1.4 Genetic vs sporadic cases of ALS 19
1.4.1 Multiple hit hypothesis 21
1.5 Genetic mutations allow us to model ALS phenotypes *in vitro* and *in vivo* 22
1.6 Why do we still need additional models of ALS? 23
1.6.1 Transgenic, overexpressing models may not be representing what is happening in patients 24
1.6.2 ALS may be multiple diseases which share some pathomechanisms 27
1.7 The role of FUS in ALS 28
1.8 FUS immunoreactive inclusions are also found in FTD 30
1.9 Clinical features of FUS-ALS 31
1.10 Role of FUS and potential disease mechanisms in FUS-ALS 32
1.10.1 Transcriptional regulation 33
1.10.2 DNA damage 34
1.10.3 mRNA stability and localisation 35
1.10.4 Translation 35
1.10.5 Role of FUS in neurons and at the synapse 36
1.10.6 Liquid-liquid-phase separation 38
1.10.7 Mitochondria 39
1.10.8 Neuroinflammation 40
1.10.9 Autophagy 41
1.10.10 Role of FUS in development 41
1.10.11 The non-neuronal role of FUS 42
1.11 There is evidence for both gain and loss of FUS function in ALS 42
1.11.1 Evidence for loss of function (LOF) 43

1.11.2 Evidence for gain of function (GOF) 44
1.12 Existing mouse models of FUS-ALS 45
1.13 Summary and Aims of the Thesis 60
2 Chapter 2: Characterisation of genomically humanised *FUS* wildtype mice 62
2.1 Introduction 62
2.1.1 Humanised knock-in mouse models 62
2.1.2 *FUS* humanisation strategy 64
2.2 Aims and hypotheses 65
2.3 Contributions 66
2.4 Results 67
2.4.1 Generation of the humanised *FUS* wildtype mice 67
2.4.2 Humanisation has no effect on survival and breeding 68
2.4.3 Human *FUS* is expressed in a physiologically relevant pattern of expression in homozygous humanised *FUS* mice 69
2.4.4 Homozygous *hFUS* mice showed minimal transcriptomic changes 76
2.4.5 Homozygous humanised *FUS* mice have little to no overt phenotype up to and including 18 months old 78
2.4.6 Despite changes in FUS expression, no change in tibialis anterior muscle morphology is observed in humanised *FUS* mice 85
2.4.7 Human FUS protein is predominantly located in the nucleus, but is also present in the cytoplasm as mice age 86
2.4.8 Humanisation has no effect on spinal cord motor neuron survival 87
2.5 Discussion 89
2.5.1 Expression of human FUS can functionally replace mouse FUS 89
2.5.2 Genomically humanised mice exhibit modest reductions in *FUS* expression at the RNA and protein level 90
2.5.3 Mice expressing the *hFUS* sequence have no overt motor phenotype up to and including 18-months 93
2.5.4 Despite mild reductions in *FUS* expression, FUS localisation and function in ALS relevant tissue appears to be unaffected 93
3 Chapter 3: Characterising a novel, genomically humanised mouse model of FUS-ALS 95
3.1 Introduction 95
3.1.1 Why do we need another mouse model of a FUS-NLS mutation? 95
3.1.2 Why was the FUS^{P525L} mutation chosen? 96
3.2 Aims and hypotheses 97
3.3 Contributions 98
3.4 Results 100

3.4.1 Generation of humanised h*FUS/hFUS*^{P525L} mice 100
3.4.2 Expression of the *hFUS*^{P525L} mutation reduces survival and likely reduces fertility 101
3.4.3 *hFUS/hFUS*^{P525L} mice have a mild cognitive deficit 105
3.4.4 Heterozygous expression of *hFUS*^{P525L} is sufficient to cause a metabolism phenotype in mice of both sexes 109
3.4.5 Male *hFUS*/*hFUS*^{P525L} mice have a mild motor phenotype 112
3.4.6 Male *hFUS/hFUS*^{P525L} mice may exhibit a unilateral muscle weakness aged 21-months-old 117
3.4.7 *FUS* expression is regulated in a time, tissue and sex specific manner in *hFUS/hFUS*^{P525L} mice 122
3.4.8 RNA sequencing in *hFUS/hFUS*^{P525L} mice reveals pre-symptomatic transcriptomic changes, predominantly affecting the tibialis anterior 127
3.4.9 Total FUS is mainly localised to the nucleus despite the NLS mutation, but FUS^{P525L} is spread between the nucleus and cytoplasm 130
3.4.10 *hFUS/hFUS*^{P525L} mice show disease relevant changes in the TA muscle. 136
3.4.11 There is no evidence of neuronal degeneration in the *hFUS/hFUS*^{P525L} mice ... 140
3.5 Discussion 142
3.5.1 Expression of the *hFUS*^{P525L} mutation causes developmental defects and reduced survival 144
3.5.2 *hFUS/hFUS*^{P525L} mice display an outward behavioural and motor phenotype independent of spinal cord motor neuron loss 146
3.5.3 Total FUS becomes more cytoplasmic as *hFUS/hFUS*^{P525L} mice age 151
3.5.4 Changes at the level of the tibialis anterior muscle may be driving some of the motor phenotypes seen 154
3.5.5 There is indirect evidence both gain and loss of FUS function mechanisms are driving phenotypes seen in the *hFUS/hFUS*^{P525L} mice 157
3.5.6 The heterozygous humanised *hFUS*^{P525L} mice are likely modelling early stages of disease 158
4 Chapter 4: Using primary cell cultures from embryonic spinal cords to study cellular and molecular phenotypes 159
4.1 Introduction 159
4.2 Aims and hypotheses 160
4.3 Contributions 162
4.4 Results 163
4.4.1 Cell cultures collected from E12.5-E13.5-day old embryos were a mix of neuronal and non-neuronal cells 163
4.4.2 The amount of cytoplasmic FUS is increased in cells expressing the *hFUS*^{P525L} mutation 165

4.4.3 FUS protein is recruited to stress granules after exposure to oxidative stress in *hFUS/hFUS^{P525L}* but not wildtype cell cultures 167
4.4.4 There was no difference in cell survival after stress between genotypes 171
4.4.5 Cells expressing the *hFUS^{P525L}* mutation have altered mitochondrial function 172
4.5 Discussion 175
4.5.1 Increased FUS is localised to the cytoplasm in *hFUS/hFUS^{P525L}* cells 176
4.5.2 FUS protein is recruited to stress granules (SGs) in *hFUS/hFUS^{P525L}* cells 176
4.5.3 There is no difference in cell survival after one hour exposure to oxidative or osmotic stress between cells expressing wildtype or mutant FUS 179
4.5.4 Mitochondrial function is altered in *hFUS*/*hFUS^{P525L}* cultures 181
5 Chapter 5: Comparing the severity of two different *FUS* mutations introduced into the humanised *FUS* allele 183
5.1 Introduction 183
5.1.1 Do different *FUS* mutations have different severities? 183
5.1.2 *FUS^{P525L}* and *FUS^{Q519Ifs}* mutations 184
5.2 Hypotheses and aims 186
5.3 Contributions 187
5.4 Results 188
5.4.1 Generating *hFUS^{Q519Ifs}* mice 188
5.4.2 Generation of the phenotyping cohort to compare *FUS* mutations 188
5.4.3 Mice expressing either *FUS* mutation show no difference in survival compared to wildtype mice up to and including 14 months of age 190
5.4.4 Heterozygous expression of the *hFUS^{Q519Ifs}* mutation produces a more severe phenotype than heterozygous expression of the *hFUS^{P525L}* mutation 192
5.4.5 Different *FUS* mutations alter RNA and protein expression to different extents 201
5.4.6 Increased cytoplasmic FUS protein is observed in mice expressing the *hFUS^{Q519Ifs}* mutation 205
5.4.7 There is little difference in transcript expression between mice expressing the two *FUS* mutations 207
5.5 Discussion 212
5.5.1 Heterozygous expression of the *hFUS^{Q519Ifs}* mutation produces a more severe phenotype than heterozygous expression of the *hFUS^{P525L}* mutation 212
5.5.2 Enhanced disruption of the FUS NLS in mice expressing the *hFUS^{Q519Ifs}* mutation leads to more severe cytoplasmic FUS localisation than in *hFUS^{P525L}* mice 215
6 Chapter 6: Discussion 218
6.1 What was unknown know before this project? 218

6.1.1 Could genomically humanised mice address the historic lack of translation in ALS research? 218
6.2 What was done to address that knowledge gap? 219
6.2.1 Genomically humanised *FUS* mice were generated and characterised. 219
6.3 What was found? 220
6.3.1 Human FUS could functionally replace mouse FUS. 220
6.3.2 *hFUS/hFUS*^{P525L} male mice exhibit FUS-ALS relevant phenotypes. 220
6.3.3 Early changes in skeletal muscle may drive symptom progression in humanised *FUS* mutant mice. 221
6.3.4 Both loss and gain of function mechanisms of FUS toxicity are at play in the humanised *FUS* mutant mice. 223
6.3.5 The hFUS^{Q519Ifs} protein is more toxic than the hFUS^{P525L} protein. 225
6.3.6 Humanised models are not the answer for everything: different models are needed to answer different questions. 226
6.4 What does this work mean? 228
6.4.1 What does work characterising the humanised *FUS* mice mean for the FUS-ALS field? 228
6.4.2 What does work characterising the humanised *FUS* mice mean for FUS-ALS patients? 229
6.5 Limitations of the project 230
6.6 Future work 234
6.7 Overall summary of thesis 240
7 Chapter 7: Materials and Methods 241
7.1 Materials and equipment 241
7.1.1 Reagents and consumables 241
7.1.2 Equipment 246
7.1.3 Software 247
7.2 Mice 249
7.2.1 Ethics statement 249
7.2.2 Humane endpoints 249
7.2.3 Animal housing 250
7.2.4 Generation of mouse lines 250
7.3 Mouse experimental procedures 254
7.3.1 Genotyping 254
7.3.2 Breeding and survival data 255
7.4 Phenotyping 255
7.4.2 Tissue collection 259

7.5 Molecular biology 261
7.5.1 RNA extraction 261
7.5.2 RT-PCR and quantitative RT-PCR 261
7.5.3 RNA sequencing 263
7.5.4 SNP Sequencing Analysis 264
7.5.5 Protein extraction 264
7.5.6 Western blotting 264
7.5.7 DNA Extraction for mitochondrial copy count 265
7.5.8 Mitochondrial DNA copy count qRT-PCR assay 266
7.5.9 Simoa assay for neurofilament light (NFL) quantification 267
7.6 Histology, immunofluorescence, and immunohistochemistry 268
7.6.1 FUS immunofluorescence 268
7.6.2 Motor neuron counting 269
7.6.3 Aggregation staining in spinal cord sections 270
7.6.4 Iba1 staining in spinal cord sections 270
7.6.5 Muscle fibre typing 271
7.6.6 Muscle fibre size and central nucleation analysis 273
7.6.7 Imaging 273
7.7 Mammalian cell culture and experimental procedures 274
7.7.1 Embryo dissection 274
7.7.2 Primary cell culture disaggregation and seeding 274
7.7.3 Cell-type staining 275
7.7.4 Staining for Stress Granule Markers 277
7.7.5 Quantifying FUS localisation in primary cells 278
7.7.6 Assessing mitochondrial function (Seahorse) 278
7.7.7 Assessing mitochondrial membrane potential (TMRE Assay) 279
7.7.8 Survival assay 279
7.8 Statistical Analysis 280
8 Chapter 8: Supplementary Data 281
8.1 Chapter 2: Characterising *hFUS/hFUS* mice 281
8.2 Chapter 3: Characterising *hFUS/hFUS*^{P525L} mice 284
8.3 Chapter 4: Primary cell cultures 291
8.4 Chapter 5: Comparing *mFus/hFUS*^{P525L} and *mFus/hFUS*^{Q519lfs} mice 292
9 Chapter 9: References 298

Abbreviations

ALS	Amyotrophic lateral sclerosis
ASO	Antisense oligonucleotide
BAC	Bacterial artificial chromosome
C9orf72	Chromosome 9 open reading frame 72
CNS	Central nervous system
DAB	Diaminobenzidine (staining)
ddPCR	Droplet digital polymerase chain reaction
DNA	Deoxyribonucleic acid
EDL	Extensor digitorum longus (muscle)
EMG	Electromyography
ER	Endoplasmic reticulum
ES	Embryonic stem (cell)
FET	Family of proteins including FUS, EWSR1 and TAF15
FRT	Flippase recombinase recognition target
FTD	Frontotemporal dementia
FTLD	Frontotemporal lobar degeneration
FUS	Fused in Sarcoma
GOF	Gain of function
H&E	Haematoxylin and eosin (stain)
KD	Knock-down
KI	Knock-in
KO	Knock-out

LLPS	Liquid-liquid phase separation
LOA	Loss of allele
LOF	Loss of function
(m)RNA	(messenger) Ribonucleic acid
miRNA	Micro ribonucleic acid
MND	Motor neuron disease
NFL	Neurofilament light chain
NLS	Nuclear localisation sequence
NMD	Nonsense mediated decay
(q)PCR	(quantitative) polymerase chain reaction
RRM	RNA recognition motif
SC	Spinal cord
SG	Stress granule(s)
SNP	Single nucleotide polymorphism
SOD1	Superoxide dismutase 1
TA	Tibialis anterior (muscle)
TDP-43	Transactive response DNA binding protein of 43kDa
UTR	Untranslated region

Abstract

Amyotrophic lateral sclerosis (ALS) is a debilitating neurodegenerative condition, with mutations in the Fused in Sarcoma (*FUS)* gene accounting for particularly severe, early onset forms of the disease. Despite extensive research into ALS, there is still no cure, and almost nothing in the way of efficacious treatments. This may be in part due to a lack of physiologically relevant models. Mouse models of ALS, and other neurodegenerative diseases, have historically been transgenic and as such, the phenotypes they display may represent artefacts of overexpression, rather than disease relevant mechanisms.

In this thesis I will present data characterising genomically humanised knock-in mouse models of FUS-ALS. In these knock-in mice, the mouse *Fus* gene has been replaced with the human *FUS* sequence at the endogenous mouse *Fus* locus. The humanised knock-in FUS mice express the human *FUS* gene, from the ATG start codon through to the 3'UTR and including all introns and exons, in a physiologically relevant pattern of expression.

Initial characterisation of humanised *FUS* wildtype knock-in mice reveals minimal disruption of molecular, cellular, and overt phenotypes resulting from humanising *FUS*. Heterozygous humanised FUS-ALS mice show disease-relevant phenotypes, including progressive late-onset reduction in muscle strength from one year, hyperactivity and metabolic impairments. This is alongside cellular and molecular changes from 4 months, as shown by RNA sequencing data from the spinal cord and tibialis anterior muscle, and primary motor neuron culture studies. Two distinct *FUS*

mutations are then compared to try and understand what drives different disease severity seen in FUS-ALS patients.

The phenotypes displayed by the FUS-ALS models highlight the potential of fully humanised knock-in mice to aid in unravelling early disease mechanisms, and ultimately produce therapies targeted towards the human gene and protein, in the context of, but not limited to, ALS.

Plain language summary

Amyotrophic lateral sclerosis (ALS or MND) is a neurodegenerative condition, meaning specialised cells in the brain and spinal cord, called neurons, die. Most people with ALS develop symptoms in their 60s or 70s, however some patients with genetic variants called mutations, develop the disease much earlier.

In all cells of our body, we have thousands of genes in our DNA. These genes act as instruction manuals for making proteins, which are the building blocks of the cell. If people have a faulty gene, a faulty protein will be made which can be toxic to cells. Faulty copies of the Fused in Sarcoma (*FUS)* gene cause particularly severe forms of ALS, with symptoms developing in patients as young as 11 years old. The *FUS* gene is important for cells in our body to function normally, which could explain why variations in this gene are so severe.

It is hard to study the area affected in ALS in patients, as the brain and spinal cord are well protected and hard to access. For this reason, scientists often use mice to model human diseases, as we can study things more easily in the mouse. We have developed humanised *FUS* mice, in which we have replaced the mouse *Fus* gene

sequence with the instruction sequence to make the human FUS protein. This means when the *FUS* gene is turned on in any cell of the mouse, the human FUS protein is produced, rather than the mouse FUS protein.

We have then introduced the faulty *FUS* instruction sequence that in patients cause ALS. When the faulty instruction sequence is read, a faulty protein is produced which is toxic to neurons. The mice with the faulty human protein have many ALS-like symptoms such as leg weakness, suggesting they will be useful for future ALS research. Because the humanised mice express the human FUS gene and protein, we propose that what we learn about ALS from these humanised mice is truer of what is happening in ALS patients which will help us to design and test human targeted therapies.

Impact Statement

ALS is the third most common neurodegenerative disorder after Alzheimer's and Parkinson's disease with a lifetime risk of between 1 in 350-400 (Kiernan et al., 2011). Globally more than 200,000 people are living with ALS. The incidence of ALS is expected to increase by 69% by the year 2040 as people live longer (Arthur et al., 2016), with around six patients diagnosed every day in the UK (Brain Research UK, 2023).

Disease symptoms such as muscular paralysis means patients become dependent on carers and so the socioeconomic cost of ALS is extensive. In the US alone it is estimated that ALS costs around $1.2 billion USD a year (Berry et al., 2023). In the UK a patient in King's stage four, meaning they are experiencing nutritional or respiratory failure requiring a gastrostomy or non-invasive ventilation (NIV) respectively (Balendra et al., 2019), could cost the NHS an average of £3311 per three

months, with the largest proportion of this spend consisting of primary and secondary care costs. Healthcare costs associated with ALS are significantly higher than for other neurodegenerative diseases such as Parkinson's which costs around £529 for the same three month period (Moore et al., 2019).

The largest risk factor for ALS is aging (Alonso et al., 2009; Logroscino et al., 2010; Niccoli et al., 2017). As healthcare improves people are living longer and as a result, the number of people living with age-related conditions like ALS will increase. Scientists are also getting closer to disease slowing treatments. This will create a scenario where there are more ALS patients who are living with the disease for longer and so caring and associated costs will increase.

1 Chapter 1: Introduction

1.1 Background of ALS

Characterised in 1869 by the French neurologist Jean-Martin Charcot, amyotrophic lateral sclerosis (ALS) is a debilitating neurodegenerative condition in which upper and lower motor neurons degenerate, leading to progressive muscle weakness. Upper motor neurons originate in the motor cortex and travel down the spinal cord where they synapse onto lower motor neurons. Lower motor neurons project out of the spinal cord to innervate distal muscles.

Translated from Greek, the nomenclature neatly describes what is happening in the tissue with reduced/no (**a**) muscle (**myo**) nerve input or 'nourishment' (**trophic**) from the lateral corticospinal tract (**lateral**) leading to scarring and hardening of the area (**sclerosis**).

The lifetime risk of developing ALS is 1 in 400 for women and 1 in 350 for men, affecting around 2.16 people per 100,000 person-years in Europe (Logroscino et al., 2010) making it the third most common neurodegenerative disorder after Alzheimer's and Parkinson's disease. Global incidence is heterogeneous with populations in East, South and West Asia having much lower rates of disease (Marin et al., 2017). Despite research efforts, the average survival is still only 3-5 years from diagnosis and death usually occurs due to respiratory failure (Lyall et al., 2001).

1.2 Clinical presentation of ALS

Disease presentation varies between patients but most commonly symptoms start in distal muscles. This presentation is known as spinal onset ALS, with symptoms

including muscle weakness, slowness of movement and stiffness. Disease symptoms will often spread from the site of onset to the contralateral limb although there is debate about how this spread occurs. Muscle weakness is preceded in some patients by muscle fasciculation and mild weight loss (Masrori & Van Damme, 2020).

In 25-30% of cases, rather than spinal onset, symptoms begin in the bulbar muscles. Bulbar onset patients present with dysarthria (trouble speaking) and dysphagia (trouble swallowing), and issues with chewing and/or closing the mouth (Masrori & Van Damme, 2020). Bulbar onset is associated with a worse prognosis which cannot be completely explained by increased frequency in older patients (Chiò et al., 2009). Although bulbar onset is rarer, most ALS patients will eventually experience speech and swallowing difficulties (Masrori & Van Damme, 2020).

In addition to motor symptoms, around 35-50% of patients will experience non-motor manifestations of disease including behavioural and cognitive changes, with 15% of ALS patients co-diagnosed with frontotemporal dementia (FTD) (Masrori & Van Damme, 2020).

1.3 Pathological presentation and diagnosis of ALS

When potential ALS patients present to clinic, there is no single definitive test to diagnose the condition due to the historic lack of biomarkers. Rather, it is based on clinician assessments and multiple tests such as MRI scanning, blood tests and muscle biopsies or electromyography (EMG) nerve conduction studies. Family history will also be considered, and patients may be sent for genetic tests to look for disease-causing mutations. Post-mortem samples can be taken to confirm diagnosis and spinal cords

will show a loss of large motor neurons in the ventral horn, as well as a reduction of nerve fibres (Saberi et al., 2015).

A well-known feature of ALS pathology is the presence of inclusions in the cytoplasm of motor neurons. Bunina bodies which are positive for cystatin C, transferrin and peripherin can be seen with H&E staining. In addition to Bunina bodies, other protein inclusions are present in a variety of neurons in sporadic and familial ALS patients such as ubiquitin and TDP-43 positive inclusions (Saberi et al., 2015). TDP-43 pathology is seen in 97% of ALS patients, both sporadic and familial (Prasad et al., 2019), but the relevance of these inclusions to disease progression is unclear. TDP-43 aggregates are not specific to ALS, having also been observed in FTD, Alzheimer's, Lewy body disease and post-traumatic encephalopathy (Saberi et al., 2015).

Gliosis has been shown to correlate with disease severity and evidence of active microglia and astrocytes can also be detected in the brain and spinal cord of ALS patients (Saberi et al., 2015).

1.4 Genetic vs sporadic cases of ALS

Around 90% of ALS cases are sporadic (Chen et al., 2013), meaning there is no evidence of family history of the disease. The remaining 10% of ALS cases are familial, with mutations in several ALS-causing genes resulting in disease.

Although familial ALS cases only make up 10% of patients, they are phenotypically indistinguishable from sporadic cases when patients present at clinic (Shaw et al., 1997, Andersen and Al-Chalabi, 2011). Similar clinical presentation suggests there may be shared disease mechanisms and common pathways affected,

despite different upstream triggers. This means meaning modelling familial genetic mutations will aid our understanding of ALS more generally, including sporadic disease.

As our understanding of ALS genetics improves, to try to split ALS cases into sporadic and familial is becoming harder and less meaningful. Dominant mutations are being sequenced in apparently 'sporadic' ALS cases and their family members. For example, mutations in Fused in Sarcoma (*FUS)* account for around 1% of sporadic cases (Lai et al., 2011). There is also evidence that oligogenic inheritance of multiple risk variants can lead to disease with ALS patients carrying two genetic variants developing the disease at a significantly earlier age than those patients with only one variant (Shepheard et al., 2021).

Within familial cases of ALS, the genetic landscape is complex with mutations in over 50 genes thought to cause ALS (Mejzini et al., 2019). Despite our list of known pathogenic mutations increasing, this is not the whole story. There are suggestions that, based on population frequency, pathogenic variants of known ALS genes are not as penetrant as expected (Douglas et al., 2023). Manual examination of the gnomAD database as a proxy for the general population found that, for example, *FUS* variants were only 14% penetrant, although it is unclear if this accounts for the individual pathogenicity associated with specific *FUS* mutations. Douglas and colleagues note this could explain the identification of genetic mutations in apparently sporadic cases. Reduced penetrance suggests that whilst mutations play a role, there are clearly other factors contributing to disease phenotypes such as environmental risk factors and background genetics (Hardiman et al., 2017).

1.4.1 Multiple hit hypothesis

It has been proposed that ALS, like other neurodegenerative diseases, may be a multi-step process. ALS patients often carry ALS-causing mutations from birth but usually do not develop disease symptoms until later in life, suggesting additional 'hits' are needed. The 'multiple hit hypothesis' has been proposed to try to explain some of the complexity of ALS including the variation in disease onset in familial cases (Al-Chalabi et al., 2014).

ALS-causing mutations can also be pleiotropic. For example, repeat expansions in C9orf72, the most common genetic cause of ALS, can result in ALS, FTD, or a mix of the two. There have also been reports of heterogeneity in clinical presentations within families with C9orf72 repeat expansions, such as a broad range in age of disease onset (Hsiung et al., 2012). Pleiotropic outcomes of a mutation suggest other factors must be involved to determine the phenotype of the mutation, or the specific cell type affected.

From mathematical modelling of age of onset and incidence, it was estimated that ALS may be a six-step process, with certain factors (genetic or environmental) weighted more heavily and decreasing the number of steps (Al-Chalabi et al., 2014). Authors propose 'hits' which are specific to motor neurons make them more susceptible to degenerate, and that somatic mutations during development of the nervous system could predispose specific cell types to degeneration later in life.

The multi-step hypothesis could go some way to explaining why *in vivo* and *in vitro* models of ALS do not replicate the full phenotypic variation seen in patients. For example, mouse models maintained on a congenic background have very little genetic

variation between animals and live in tightly controlled environments where they are not exposed to environmental risk factors.

Conversely, *in vivo* disease models with a clear and replicable phenotype represent an ideal model in which to study additional factors or 'hits' to see if these hits can modify disease symptom onset and progression.

1.5 Genetic mutations allow us to model ALS phenotypes *in vitro* and *in vivo*

The discovery of ALS causing mutations opened a new avenue of research into the disease, allowing the condition to be modelled in *in vitro* and *in vivo* for the first time. This began in 1993 when the first ALS mutation, which produces a single amino acid substitution of glycine to alanine at codon 93 in the superoxide dismutase 1 enzyme (*SOD1*^{G93A}*)* was discovered (Rosen et al., 1993). Shortly after this discovery, the most widely used ALS mouse model was generated (Gurney et al., 1994). The *SOD1*^{G93A} transgenic mouse, which expresses human *SOD1*^{G93A} under the control of the *SOD1* promoter, has a robust phenotype including motor symptoms from 90 days, spinal cord motor neuron loss, and reduced survival. Much has been learnt about ALS pathomechanisms from the *SOD1*^{G93A} transgenic mouse including the relevance of oxidative stress, mitochondrial dysfunction, glutamate-linked excitotoxicity and apoptosis (Turner & Talbot, 2008).

Since 1993, mutations in over 50 genes have been found to cause ALS (Mejzini et al., 2019). Many of these mutations have been modelled *in vivo* and *in vitro* allowing hypothesis driven study in accessible and replicable systems. With the development of genetic tools, these disease models have allowed scientists to modulate the expression of mutated genes, alter when and where the dysfunctional gene and protein are

expressed, or modulate the environment. Together this work is shedding light on gain and loss of function mechanisms of disease, what role different cells and tissues play in disease progression, and how disease progression can be modulated.

One of the biggest advantages of model systems, particularly *in vivo* models, is the ability to extensively study subtle, pre-symptomatic changes which represent early disease changes. These early cellular and molecular changes are most likely to be targetable to slow or halt disease progression as they precede widespread motor neuron loss. Pre-clinical stages are almost impossible to study in sporadic ALS cases as people are unlikely to have presented to the clinic. In genetic cases when mutations are known to run in families, pre-symptomatic patients can be studied; however, this is still complicated by background genetics and variations in age of disease onset. Research is also limited to biomarker and outward phenotypic study, with access to the affected tissue limited.

1.6 Why do we still need additional models of ALS?

Despite work in the current *in vitro* and *in vivo* models, we still do not know what causes the selective degeneration of motor neurons in patients. There are many reasons for this, not least because ALS is a complex, heterogenous disorder which affects the central nervous system which is hard to access in patients.

Perhaps a more pressing issue than the lack of disease understanding is the historic lack of translatability from successful disease modifying therapies in *in vivo* models to beneficial drugs and therapies for patients. Riluzole, which was discovered nearly 30 years ago, is still the only licenced therapy in the UK for sporadic ALS; the anti-glutamatergic drug, which is thought to reduce excitotoxicity in neurons, only

extends patient life for around three months (Bensimon et al., 1994). Riluzole is far from an effective treatment and is not without its own issues; 15% of ALS patients discontinue Riluzole treatment due to gastrointestinal issues, fatigue, and liver dysfunction (Jayaprakash et al., 2020). More recently, Tofersen was approved to treat ALS caused by mutations in the *SOD1* gene. Tofersen is an ASO delivered intrathecally which aims to reduce the levels of mutant SOD1 protein (Miller et al., 2023).

Over the last 50 years, there have been over 50 failed randomised controlled clinical trials targeting ALS, meaning drugs did not have a beneficial effect on survival or disease progression (Mitsumoto et al., 2014). As discussed by Mitsumoto and colleagues, there are several likely reasons for this including the use of unsuitable disease models to generate preclinical work for the trial.

So, why is pre-clinical work in the current *in vivo* disease models not translating to success in patient trials?

1.6.1 Transgenic, overexpressing models may not be representing what is happening in patients.

The mouse is still the mammalian model of choice for *in vitro* modelling of ALS as both cellular mechanisms and the resulting overt phenotypes can be studied.

As familial ALS is caused by dominant mutations in several known genes, transgenic overexpression mouse models have been the model of choice. These models overexpress the gene, often the human sequence containing the genetic mutation of interest, under the control of a ubiquitously expressed promoter, in addition to the wildtype mouse gene. Along with overexpression, as with all transgenics, the exogenous DNA randomly integrates into the genome and may form

concatemers. An example is the most widely used model of ALS, the *SOD1*^{G93A} mouse, which has around 25 copies of the human transgene randomly inserted into the mouse genome under the control of the human *SOD1* promoter (Gurney et al., 1994).

Both overexpression and insertional mutagenesis can lead to artefactual phenotypes distinct from those caused by the mutant protein and are discussed in more detail below.

Non-physiological, over-expression

The design of transgenic mice means mutated transgenes are expressed at higher levels than would be seen in human patients. Perhaps more importantly, the mutated transgenes may have non-physiological expression patterns; expression in some cell types may be missing, or expression in other cell types may be ectopic depending on the promoter used and where the transgene becomes inserted. The local genetic environment will influence expression of the mutated transgene in a cell-type specific manner through the presence of promoters, enhancers, and repressors. When transgenes are overexpressed, there are also copy count issues due to allele instability and epigenetic silencing whereby the high copy number increases the likelihood of promoter methylation, which should be monitored (Martin et al., 1996; Garrick et al.,1998). Overexpression prevents the ability to study effects brought about by loss of function and makes it difficult to accurately study the effect of genes which are highly gene-dosage sensitive, such as *FUS* (Humphrey et al., 2020). It is known that overexpression of wildtype human *FUS* in mice is sufficient to cause loss of motor neurons in the spinal cord and or neuromuscular junction (Ling et al., 2019; Mitchell et al., 2013; Sephton et al., 2014). This motor neuron degeneration is comparable to an

ALS phenotype, possibly due to overexpression of *FUS* leading to increased cytoplasmic FUS. However, as the phenotypes seen in the mouse are not caused by physiological expression of a mutant protein, the pathways to neurodegeneration may not accurately reflect physiological changes occurring in patients.

Random insertion mutagenesis

Random insertion of the exogenous mutated transgene into the genome can cause mutagenesis. Analysis of 40 transgenic mouse strains widely used in research found around 50% had disrupted annotated genes at the insertion site (Goodwin et al., 2019). Many of the genes are known to produce phenotypes when mutated, hence the need to generate multiple independent lines to ensure the phenotypes observed are due to insertion, rather than genetic disruption. For this reason, generating valid control lines is difficult; transgenic mice expressing the wildtype protein will have different insertion sites and expression levels to the mutant lines. Ideally two independent wildtype lines should be generated, although this is often not the case.

Together, the issues associated with overexpression and random insertion bring into question the validity of transgenic overexpression models and may go some way towards explaining why existing models of ALS have struggled to translate into human therapies in the clinic. Whilst these transgenic models have proved invaluable for unpicking some of the major pathways that are disrupted in ALS, they are modelling end-stage disease within a matter of weeks. In humans, pathogenesis occurs over several decades of life. This is not to say transgenic models are not useful, but different models are needed to ask different questions.

1.6.2 ALS may be multiple diseases which share some pathomechanisms.

Until the early 2000's, rapidly progressing mutant *SOD1* transgenic mice were the only mouse models of ALS available. This meant a lot of pre-clinical work for clinical trials was based on successfully modifying the severe phenotypes seen in these models (De Giorgio et al., 2019). There are two issues with this, one being the *SOD1* transgenic mice are not without issues as discussed above, but additionally, models of SOD1-ALS may not represent what is happening in the vast majority of ALS cases. For example, TDP-43 deposits, which are found in around 97% of ALS cases (Prasad et al., 2019), are not present in SOD1-ALS patients, or FUS-ALS patients, which could suggest that upstream pathomechanisms differ in those forms of ALS.

Gene variants known to cause ALS have diverse functions; *SOD1* produces an enzyme involved in protecting the cell from reactive oxygen species, *TARDBP* and *FUS* encode nucleic acid binding proteins and C9orf72 is believed to be involved in trafficking, autophagy and the immune system. Other rare variants of genes thought to be involved in ALS have additional roles in protein trafficking and degradation, the mitochondria and cytoskeleton and axonal dynamics amongst others (Mejzini et al., 2019). Knowing the diversity of cellular pathways affected in the different genetic forms of ALS, it is unsurprising that treatments which were successful in the original rapidly progressing $SOD1^{G93A}$ or $SOD1^{G85R}$ transgenic mouse models have not been successful in clinical trials studying mixed populations of ALS patients.

Until more is understood about the missing heritability of ALS, the models used in pre-clinical work are likely to be modelling monogenic variants. So, if drugs are to be studied in large clinical trials consisting of patients with sporadic and familial ALS

caused by multiple mutations, then one would argue there is a greater probability of success if the treatment was effective across multiple models of distinct monogenic variants. Alternatively, precision medicine approaches could be used to stratify patient cohorts based on their genetics.

This further supports the need for additional models of ALS which express different known pathogenic mutations and better represent the disease pathomechanisms in a wide variety of patients.

1.7 The role of FUS in ALS

It was first discovered over a decade ago that variants in the *FUS* gene can cause ALS; it is now known around 4% of familial ALS cases are a result of *FUS* mutations (Kwiatkowski et al., 2009; Vance et al., 2009).

The *FUS* gene, located on chromosome 16, encodes a 526 amino acids long nucleic acid binding protein. Part of the FET protein family, the widely expressed RNA and DNA binding protein has roles in RNA processing of thousands of genes, along with DNA repair and translation, among others. Originally discovered as an oncogene, the FET proteins are involved in sarcoma translocations. The resulting protein contains the N terminus of the FET protein and C terminus of the ETS protein producing a potent oncogenic transcription factor (Crozat et al., 1993). Under wildtype conditions in mammalian cells, FUS, along with the other FET proteins, is mostly localised to the nucleus (Andersson et al., 2008).

The FET proteins have several conserved domains with specific functions including:

- A low complexity, SYGQ (Ser-Tyr-Gly-Gln) rich region: this region is involved in phase separation and binding of other proteins such as RNA polymerase II (Burke et al., 2015; Murthy et al., 2021).
- Multiple RGG (Arg-Gly-Gly) domains: these are known to bind nucleic acid but when methylated can bind proteins such as themselves, aiding with aggregation, and other disordered regions within proteins which is important for LLPS (Loughlin et al., 2019; Murthy et al., 2021).
- RNA recognition motif (RRM): this domain is important for RNA binding and binding other specific proteins such as PAR which is important for DNA repair (Mamontova et al., 2023).
- Zinc finger (ZnF): this domain has been shown to bind RNA, specifically via a UGGU motif, which can be a driving factor for LLPS (Loughlin et al., 2019; Maharana et al., 2018).
- Nuclear localisation sequence (NLS): this non-classical nuclear localisation sequence binds nuclear import factors directing FUS to the nucleus (Dormann et al., 2012).

Over 50 mutations in *FUS* are known to cause ALS and a large proportion of these disrupt the PY nuclear localisation sequence (NLS) (An et al., 2019; Deng et al., 2014). Mutations in the NLS lead to increased FUS in the cytoplasm where it can form inclusions. Notably, not all FUS-ALS patients have FUS inclusions, and not in all cell types (An et al., 2019; Hewitt et al., 2010; King et al., 2015; I. R. Mackenzie et al., 2010). FUS inclusions are also not specific to ALS and have been found in multiple other disorders including FTD and polyglutamine diseases including Huntington's,

some forms of spinocerebellar ataxia and dentatorubral–pallidoluysian atrophy and essential tremor (Abramzon et al., 2020; Deng et al., 2014).

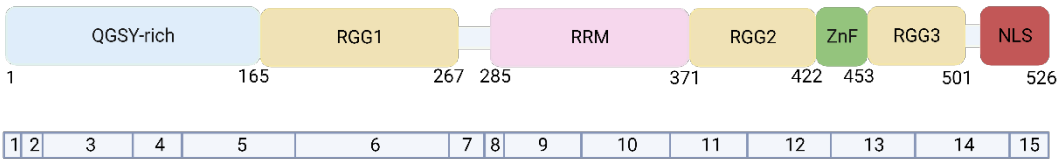


Figure 1.1 Structure of the FUS protein and the exons encoding each region. *Adapted from (Deng et al., 2014). Created with BioRender.com.*

1.8 FUS immunoreactive inclusions are also found in FTD

FTD is characterised by progressive changes in behaviour, personality, and sometimes language, with memory relatively unaffected. FTLD is a form of FTD whereby the frontal and temporal lobes are selectively affected and degenerate (Neumann et al., 2009).

In the same year that *FUS* mutations were implicated in ALS, a small proportion of FTD patients, a disease normally characterised by inclusions of TDP-43 or TAU protein, were found instead to have inclusions immunoreactive for FUS (Neumann et al., 2009). These patients, representing around 10% of all FTD patients, had a distinct pathology, and the disease was subsequently classified as FTLD-FUS (I. R. A. Mackenzie et al., 2010). Despite the presence of FUS immunoreactive inclusions, cases of *FUS* mutations leading to FTD have not been found (Tetter et al., 2023), with *FUS* mutant carriers instead presenting with ALS (I. R. Mackenzie et al., 2010).

Differences have been found between the FUS positive inclusions in FUS-ALS and FTLD-FUS which could explain why the conditions have different histochemical and

clinical presentations. In FTLD, there is evidence of increased arginine methylation of FUS RGG regions increasing the propensity of FUS to aggregate, which is not seen in FUS inclusions in ALS (Dormann et al., 2012; Hofweber et al., 2018; Loughlin et al., 2019). The proteins sequestered in FUS inclusions were also found to differ between conditions; in FTLD-FUS other FET family proteins, TAF15 and EWS, co-localise with FUS pathology, whereas in ALS other FET proteins remain nuclear suggesting different pathomechanisms involved in forming inclusions in the two diseases (Mackenzie & Neumann, 2012). More recently, it has been shown that inclusions in FTLD-FUS, although positive for FUS protein, were formed from TAF15 amyloid filaments, rather than FUS amyloid filaments, and it was thus recommended to be called FTLD-FET (Tetter et al., 2023).

Together this data suggests that FUS-positive inclusions seen in ALS and FTD occur via different molecular mechanisms in different cell types leading to distinct clinical phenotypes.

1.9 Clinical features of FUS-ALS

FUS-ALS has a distinct clinical profile to other forms of ALS and is traditionally characterised by a fast progression with early, sometimes juvenile onset. More than 60% of cases with *FUS* mutations show disease onset before 45 years of age, and *FUS* is the most commonly mutated gene in juvenile ALS defined as onset before 25 years of age (Baumer et al., 2010; Grassano et al., 2022; E. J. Huang et al., 2010; Shang & Huang, 2016).

Mutations in *FUS* are associated with a poor prognosis due to rapid disease progression, although this appears to be age dependent; FUS-ALS patients who

present with symptoms after age 45 do not differ in disease duration to patients with other mutations or sporadic disease (Grassano et al., 2022). This is supported by work from Naumann and colleagues who found the younger disease onset associated with FUS-ALS was largely driven by the prevalence of the P525L mutation and other truncation and frameshift mutations. These mutations significantly affect the NLS and have been reported in patients as young as 11 years old (Conte et al., 2012; Naumann et al., 2019). Grassano and colleagues found that in a cohort of 22 patients carrying a *FUS* mutation, those with a truncating or missense variant in the last two amino acids of the NLS had the most severe phenotype, often with juvenile onset, and were the only FUS-ALS patients with bulbar symptom onset (Grassano et al., 2022). In contrast, patients with a mutation in residues 517 or 519 had the mildest disease phenotype, which also progressed more slowly.

Wider systemic dysfunction has been noted in FUS-ALS patients, particularly in those with a NLS mutation. This includes incidences of intellectual and learning disabilities, and other cognitive dysfunction (Grassano et al., 2022; Yamashita et al., 2012) suggesting that FUS has a role in development.

Cases of FUS-ALS are characterised by FUS inclusions rather than TDP-43 inclusions (Vance et al., 2009).

1.10 Role of FUS and potential disease mechanisms in FUS-ALS

Historically considered to function solely in the nucleus, it is now becoming clearer that FUS also has many important roles in the cytoplasm (Birsa et al., 2020). Nuclear and cytoplasmic roles of FUS, and how these are known to be affected in ALS, are discussed below.

1.10.1 Transcriptional regulation

FUS was first discovered as a transcriptional activator when it was found that the FUS translocated and fused with CHOP to form an oncogenic transcription factor (Crozat et al., 1993). It has since been shown that FUS regulates several aspects of gene regulation including transcription, mRNA splicing, trafficking, and stability, all of which are known to be disrupted in FUS-ALS (Kapeli et al., 2017).

FUS is known to directly bind RNA polymerase II and other transcriptional activators such as the acetyltransferases histone CBP and p300 (Wang et al., 2008). FUS has also been found at the transcriptional start site of genes, reportedly up to 68% of expressed genes, and this enrichment is lost when *FUS* is knocked-down leading to changes in global transcription (Schwartz et al., 2012; Schwartz et al., 2014). More recently, FUS has been shown to be involved in nuclear paraspeckle formation. Found in interchromatin space, these RNA granules bind RNA and transcription factors, ultimately regulating gene expression. FUS is known to be an essential structural component of paraspeckles and mutant FUS can induce the excessive formation of dysfunctional paraspeckles, which may be toxic to motor neurons (An et al., 2019; Shelkovnikova et al., 2014).

In addition to transcriptional regulation, FUS is also a global regulator of splicing (Ishigaki et al., 2012; Lagier-Tourenne et al., 2012; Ling et al., 2013; Masuda et al., 2015; Rogelj et al., 2012). In targeted *FUS* knock-in mice, it was found that mutations in *FUS* caused a loss of function phenotype in RNA expression and splicing, mostly affecting intron retention within genes involved in the RNA metabolism pathway (Humphrey et al., 2020). Along with genes linked to RNA metabolism, FUS

and TDP-43 have both been found to preferentially regulate expression of genes with neuronal function, along with long pre-mRNAs (Lagier-Tourenne et al., 2012).

FUS is thought to directly regulate splicing by recruiting splicing factors to target genes via the C terminal domain of FUS (Yang et al., 1998). Since then, it has been shown FUS-ALS mutations which cause increased localisation of FUS to the cytoplasm can trap minor spliceosome components in cytoplasmic FUS inclusions, disrupting the splicing of many genes (Reber et al., 2016).

1.10.2 DNA damage

Since 2000, it has been known that FUS is required for chromosome stability and a functional DNA damage response from *Fus* knock-out studies in mice (Hicks et al., 2000; Kuroda, 2000). Furthermore, mouse models expressing *FUS* mutations have found defective DNA repair may contribute to disease pathogenesis (Qiu et al., 2014).

FUS is rapidly recruited to sites of DNA damage where it has been shown to be involved in DNA repair (Aleksandrov et al., 2018; Mastrocola et al., 2013). Homologous recombination (HR), one method used to repair double stranded DNA breaks, requires the formation of DNA loops, which are disrupted when FUS is knocked down (Baechtold et al., 1999; Mastrocola et al., 2013; Wang et al., 2013). More recently, studies in HeLa cells overexpressing human FUS found that under genotoxic conditions, FUS bound PARP1 at DNA damage sites leading to upregulation of PAR protein and recruitment of other DNA repair machinery (Mamontova et al., 2023). Mutations in the RGG and N terminus of FUS can affect the binding of DNA repair machinery such as PAR, meaning mutant FUS protein fails to recruit DNA repair factors to the site of damage. Furthermore, these mutant FUS proteins retain at least some

ability to bind DNA and so may act in a dominant negative fashion, preventing the binding of wildtype FUS protein to sites of DNA damage (Shang & Huang, 2016).

1.10.3 mRNA stability and localisation

Whilst in the nucleus, mRNAs have their introns removed, 5' end capped and 3' end polyadenylated to maintain mRNA stability (Nakaya et al., 2013). FUS has been shown to modulate 3' processing of specific mRNAs, such as GluA1, by regulating the polyA tail length (Udagawa et al., 2015). Authors showed when FUS was depleted, proteins which would shorten the polyA tail were no longer sequestered by FUS and so GluA1 mRNA was less stable. When Glu1A mRNA levels were depleted in the presence of mutant FUS, there were defects in synaptic plasticity, learning and memory, which could explain some of the wider behavioural changes seen in FUS-ALS.

FUS shuttles mRNA between the nucleus and cytoplasm (Zinszner et al., 1997). In FUS-ALS, cytoplasmic mutant FUS can sequester its target mRNAs to the cytoplasm (Coady & Manley, 2015; Yasuda et al., 2013). In addition to mRNA, FUS inclusions also disrupt RNA localisation by sequestering proteins required for mRNA transport, such as Kinesin-1 (Yasuda et al., 2017).

1.10.4 Translation

To initiate translation, a complex of multiple proteins is required to bind the 40S ribosomal subunit including GTP, met-tRNA, eIF2 and additional factors such as eIF4, eIF1 and eIF5 (Groppo & Richter, 2009).The exact role of RNA binding proteins in translation is not well understood but it is thought they can directly regulate translation by binding factors of the initiation complex, or by altering the availability of mRNAs at the translation start site (Birsa et al., 2020; Darnell & Klann, 2013). Both FUS

and TDP-43 co-precipitate with active translation machinery, and FUS appears to be important for local protein synthesis in axons (Birsa et al., 2020; Fujii et al., 2005).

FUS also regulates the expression of multiple genes required for translational machinery, such as the large and small ribosomal subunits, expression of which are dysregulated in a mouse model of FUS-ALS (Lopez-Erauskin et al., 2018). As well as translational machinery, FUS has also been shown to regulate expression of proteins required for the nonsense mediated decay pathway (Kamelgarn et al., 2018).

Together this highlights the multiple levels of control FUS exerts on protein biogenesis, and how this could be disrupted in ALS.

1.10.5 Role of FUS in neurons and at the synapse

Stretching from the spinal cord to distal limbs, lower motor neurons are the longest cells in the human body, with axons up to 1m long. It is thus unsurprising that, in these specialised, polarised cells, methods are employed to allow local translation of proteins in the areas they are needed, rather than carrying synthesised proteins all the way from the soma. Local protein synthesis is important for neurons to rapidly respond and grow during development, after injury and to regulate synaptic plasticity during learning (Piol et al., 2023). Both TDP-43 and FUS have been found to localise along axons and at synaptic terminals where they are important for local translation of proteins required at the nerve terminals (Fallini et al., 2012; Piol et al., 2023; Sahadevan et al., 2021; Salam et al., 2021; Schoen et al., 2015). There is growing evidence that the role of FUS at the synapse extends beyond local protein translation, as it has been found that FUS interacts with both pre- and post-synaptic proteins

leading to speculation it may be involved in synaptic vesicle processing and subsequently synaptic transmission (Salam et al., 2021).

Abundant FUS expression has been reported at NMJs, specialised junctions where motor neurons synapse onto skeletal muscles (So et al., 2018). The exact function of FUS at the NMJ is unknown but overexpression of wildtype FUS is sufficient to cause ultrastructural changes in the NMJ including loss of synaptic vesicles, fewer mitochondria, and depletion in the number of NMJs (So et al., 2018).

FUS is also implicated in axonal transport in neurons. Early studies found mutant FUS affected mitochondria trafficking in Drosophila motor neurons (Chen et al., 2016; De Vos & Hafezparast, 2017). Since then, Lopez-Erauskin and colleagues found in a mouse model of FUS-ALS, mutant FUS accumulated along axons which led to suppression of local protein synthesis and subsequent synaptic dysfunction (Lopez-Erauskin et al., 2018). FUS inclusions also sequester RNA and proteins involved in axonal transport of RNA such as SMN (Groen et al., 2013) and Kinesin-1 (Yasuda et al., 2017). Kinesin-1 modulates axonal transport of RNA by generating detyrosinated Glu-microtubules which are lost in the presence of FUS inclusions. Yasuda and colleagues note that Glu-microtubules are also lost in the presence of TDP-43 inclusions, although the mechanism by which this occurs is different stressing the importance of studying different genetic causes of ALS with distinct inclusion pathology.

Finally, FUS has been shown to play an important role in neurodevelopment by regulating neuronal morphogenesis and neuronal projections in iPSC-derived spinal and cortical organoids (Zou et al., 2022). FUS is likely controlling this dendritic morphology by regulating the expression of synaptic plasticity genes and directly

modulating axon guidance and cell adhesion pathways (Udagawa et al., 2015; Zou et al., 2022).

1.10.6 Liquid-liquid-phase separation

Liquid-liquid phase separation (LLPS) is a mechanism used by several proteins, including FUS and TDP-43, to form membrane-less organelles in the nucleus and cytoplasm. LLPS organelles perform a variety of functions and can be formed in response to several types of stress (Gao et al., 2022; Patel et al., 2015). When the stress is removed, the LLPS structure should dissipate although it has been proposed that in disease states this dispersal may not occur correctly and LLPS organelles may act as precursors to more persistent aggregates (Molliex et al., 2015; Patel et al., 2015). How transient LLPS organelles transition to become more persistent stress granules is yet to be fully elucidated.

FUS has been shown to undergo LLPS, driven by the low-complexity domains in its N terminus (Burke et al., 2015; Patel et al., 2015; Sun et al., 2011). In FUS-ALS cells, LLPS organelles have been found to remain for longer, recruiting other proteins with low complexity domains (Dormann et al., 2010). LLPS of FUS is modified by several factors including the nuclear chaperone TNPO1 (Hofweber et al., 2018). Mutations in *FUS* have been found to increase the likelihood of FUS to phase separate; TNPO1 binds FUS via the C terminus where many ALS-causing FUS mutations are located which could explain this finding. Distinct roles of LLPS and non-LLPS FUS have been proposed by analysing FUS binding partners in each state, with the former involved in DNA damage repair and the latter mRNA processing (Reber et al., 2021).

Intriguingly, it has been found that LLPS and aggregation are not themselves toxic when artificially introduced *in vitro*, making their relevance to disease pathogenesis unclear (Reber et al., 2021). This is further supported by the finding that many mouse models of FUS-ALS develop phenotypes without the detection of large aggregates (Devoy et al., 2017; Korobeynikov et al., 2022; Ling et al., 2019; Lopez-Erauskin et al., 2018; Qiu et al., 2014; Scekic-Zahirovic et al., 2016; Sephton et al., 2014; Sharma et al., 2016). It remains to be learnt whether aggregates sequester mutant protein in the cell as a form of self-defence and may be neuroprotective.

1.10.7 Mitochondria

Mitochondrial dysfunction is observed in sporadic ALS patients and is also displayed in *in vitro* and *in vivo* models of familial ALS (Muyderman & Chen, 2014). Whether this is an upstream causal factor of disease, or a downstream consequence of other triggers such as oxidative stress and inflammation is yet to be elucidated (Birsa et al., 2020).

The wildtype role of FUS in the mitochondria is not fully understood and under physiological conditions, little FUS protein localises to the mitochondria. Deng and colleagues proposed FUS localised to the mitochondria by binding HSP60 and that the presence of FUS at the mitochondria led to mitochondrial fragmentation and release of reactive oxygen species (Chen et al., 2016; Deng et al., 2015). Further work found this disruption was occurring due to FUS binding a subunit of ATP synthase which activated the mitochondrial unfolded protein response (Deng et al., 2018). Levels of FUS at the mitochondria are increased in ALS which could explain the dysfunctional mitochondrial phenotype observed in disease (Deng et al., 2018).

In addition to the direct role of FUS at the mitochondria, it has been shown in cells expressing mutant or wildtype FUS that transcripts encoding mitochondrial respiratory chain complexes are overrepresented in mRNAs sequestered by FUS protein (Tsai et al., 2020). Tsai and colleagues note that it is unclear why there is increased affinity of FUS to bind transcripts encoding mitochondrial targets, as no specific binding sequence or secondary structure have yet been found. It has been speculated this increased binding may simply be due to the increased concentration of FUS at the mitochondria when FUS is mutated. The sequestration of transcripts needed for mitochondrial proteins leads to a decrease in their translation and subsequent impairment of mitochondria, including disrupting the mitochondrial network and inhibiting aerobic respiration (Tsai et al., 2020).

1.10.8 Neuroinflammation

Neuroinflammation is an inflammatory response affecting the central nervous system and is mediated by immune cells including microglia and astrocytes.

Although seen in many models of FUS-ALS, the mechanisms by which neuroinflammation occurs is not well studied. Overexpression of wildtype FUS is sufficient to increase expression of inflammatory genes and release of pro-inflammatory factors in astrocyte cell lines, which can be neurotoxic (Ajmone-Cat et al., 2019). Astrocytes expressing mutant FUS were also found to somehow modulate AMPA receptors in co-cultured motor neurons, making the neurons more susceptible to excitotoxicity and ultimately cell death (Kia et al., 2018).

1.10.9 Autophagy

Autophagy is a process by which cells maintain homeostasis of organelles. The wildtype role of FUS in autophagy is less well studied than other RBPs such as TDP-43, however there is growing evidence that autophagy is disrupted in models of FUS-ALS. Work in neuronal cell lines expressing mutant human FUS^{P525L} found a reduction in omegasomes and LC3-positive autophagosomes, suggesting an issue in the early stages of autophagosome synthesis (Soo et al., 2015). If the autophagy pathway is impaired in FUS-ALS, then there will be defective protein degradation likely leading to the accumulation of stress granules seen in patient cells.

1.10.10 Role of FUS in development

Although not well defined, there is growing evidence that FUS has a role in development. *Fus* knock-out mice do not survive on a congenic background, with authors citing issues with the immune system and lung development (Hicks et al., 2000; Kuroda, 2000). Additionally, *fus* knock-down in Xenopus leads to defective development and gastrulation, at least in part through alterations in intron retention in genes involved in regulating developmental processes (Dichmann & Harland, 2012).

FUS appears to affect development of multiple cell and tissue types as *FUS* mutations in patients and animal models have been found to affect neurodevelopment (Ali et al., 2023; Hirayanagi et al., 2016), synapse morphology and plasticity (Fujii et al., 2005; Udagawa et al., 2015; Zou et al., 2022), and muscle development (Shefner et al., 2023; Todd & Petrucelli, 2022).

1.10.11 The non-neuronal role of FUS

Previously, much work has focussed on the role of mutant FUS in neuronal cells however work has shown that in addition to the toxic effect on motor neurons, mutant FUS can be detrimental to wider CNS cell types such as microglia and astrocytes. For example, increased expression of mutant or even wildtype FUS in astrocytes is sufficient to cause an altered inflammatory response and ultimately neuronal death (Ajmone-Cat et al., 2019; Kia et al., 2018).

FUS is also widely expressed in tissues beyond the CNS and thus *FUS* mutations have the potential to disrupt many tissues beyond those traditionally thought to be affected in ALS such as the muscle (Shefner et al., 2023). Metabolism is known to be affected in ALS and a recent paper by Ali et al. studying muscle as well as liver tissue found there was altered lipid metabolism in a mouse model expressing the $Fus^{\Delta 14}$mutation. Liver and muscle tissue showed evidence of altered fat stores and impaired lipid storage which led to a fuel preference switch and could in turn modulate the behavioural and motor phenotypes seen in the FUS-ALS model (Ali et al., 2023).

Together this shows how *FUS* mutations have the potential to cause systemic dysfunction beyond the CNS and could explain some of the wider abnormalities seen in FUS-ALS patients.

1.11 There is evidence for both gain and loss of FUS function in ALS

It has long been debated whether FUS-ALS is caused by a loss of wildtype FUS function (LOF), and/or a gain of toxic mutant FUS function (GOF). The evidence for both is discussed here.

1.11.1 Evidence for loss of function (LOF)

Mutations in *FUS* are known to be spread throughout the gene, however many mutations are clustered around the NLS causing increased localisation of FUS to the cytoplasm. Other mutations affect FUS domains responsible for binding RNA, DNA, and other proteins. Genetic variations lead to a defective FUS protein which is either in the wrong place, or cannot bind nucleic acids and proteins as effectively, both of which are necessary for FUS to carry out its wildtype function.

Some work to support the loss of function hypothesis comes from disease models comparing the phenotype of mutant *FUS* mice to *Fus* knock-out mice. Heterozygous *Fus* knock-out mice are relatively phenotypically normal and have comparable *Fus* expression; however, homozygous *Fus* knock-out mice are perinatal lethal on a congenic background emphasizing FUS function is dosage sensitive (Hicks et al., 2000; Kuroda, 2000; Scekic-Zahirovic et al., 2016). If outcrossed to a mixed genetic background, $Fus^{-/-}$ mice survive but are sub-viable, smaller, less fertile, and present with malocclusion caused by bone defects (Kino et al., 2015; Korobeynikov et al., 2022). Loss of FUS function phenotypes are modelled in FUS mutant mice, including our humanised models, suggesting loss of FUS function mechanisms are involved in the development of some disease presentations (Korobeynikov et al., 2022).

In addition to overt phenotypes, the loss of FUS function hypothesis is further supported by cellular and molecular phenotypes. For example, Humphrey and colleagues report that targeted knock-in mutant FUS NLS mice, which exhibit mild mislocalisation increased FUS protein in the cytoplasm, display loss of function effects

on expression and splicing of FUS target genes, consistent with nuclear loss of function (Humphrey et al., 2020).

Models which have physiological FUS expression, in other words do not overexpress the mutant FUS protein, are vital for unpicking loss of FUS function contributions to ALS. It could be argued that models which overexpress mutant FUS protein have artificially over inflated the contribution of gain of function mechanisms simply due to the increased concentration of toxic protein, particularly when this is additional to wildtype mouse FUS protein as seen in traditional transgenics.

1.11.2 Evidence for gain of function (GOF)

Genetic studies crossing *Fus*$^{-/-}$ mice with FUS NLS mutant mice find that a loss of FUS function cannot completely explain the phenotypes observed. NLS mutant FUS can partially rescue the FUS knock-out phenotype suggesting mutant FUS retains some functionality, whilst causing additional, distinct toxicity in a dosage dependent and mutation specific manner (Korobeynikov et al., 2022). Perhaps the strongest argument for this additional toxicity comes from the fact *Fus*$^{-/-}$ mice do not exhibit motor neuron loss whereas overexpression of wildtype or mutant FUS can cause motor neuron degeneration (Table 1.1). There is some debate about whether motor neuron loss is due to the presence of FUS in the cytoplasm; some models experience motor neuron loss without increased cytoplasmic FUS, which suggests neuronal degeneration could be caused by a nuclear gain of toxic function mechanism, rather than cytoplasmic. In many mouse models with a large proportion of nuclear mutant FUS, there are dominant negative phenotypes in FUS pathways, further supporting nuclear gain of function. For example, mutant FUS has been shown to retain some ability to bind RNA,

DNA and protein, preventing the binding of wildtype FUS, but also failing to recruit other proteins required for the correct functional response, such as during DNA damage repair or in paraspeckle assembly (An et al., 2019; Deng et al., 2014).

When mutant FUS is localised to the cytoplasm, as occurs in FUS-ALS patients if not all disease models, it can recruit FUS interacting partners including but not limited to itself, other RNA binding proteins TDP-43 and hnRNP (Korobeynikov et al., 2022), PRMT1 (Tibshirani et al., 2015) and SMN (Groen et al., 2013). This highlights how *FUS* mutations affect not only FUS function, but the function of many additional proteins. The binding of multiple proteins by mutant FUS leads to diverse cytoplasmic gain of function disease mechanisms, but also loss of nuclear function of FUS binding proteins, affecting multiple cellular pathways.

Overall, the evidence suggests that mutant FUS toxicity is a complex mix of loss and gain of function, in both the nucleus and the cytoplasm, as it does not appear that one mechanism alone can explain all phenotypes associated with FUS-ALS.

1.12 Existing mouse models of FUS-ALS

A variety of model systems have been employed to study the role of FUS, allowing researchers to investigate the disease mechanisms discussed above. Lower organisms and cell models are particularly useful for asking mechanistic questions and modifying phenotypes quickly in a high throughput system. However, the mouse is still the model of choice for studying the effects of a mutation in the wider system, providing a complex yet accessible model. The mouse CNS has many architectural similarities to the human CNS, including at the level of neuronal diversity and gene expression (Yadav et al., 2023).

Table 1.1 summarises the existing mouse models of FUS-ALS.

Table 1.1: Existing mouse models of FUS-ALS and the phenotypes they display.

FUS protein	Homozygous or heterozygous	Genetic background	Promoter and expression pattern	Expression levels	Cognitive phenotypes	Motor phenotypes	Motor symptom onset	Motor neuron loss	Survival	Other phenotypes	Limitations/to note	Reference
FUS KO	Heterozygous	C57BL/6	**Promoter:** mouse *Fus* **Expression pattern:** All cells where *Fus* is expressed	Normal	ND	ND	NA	ND	Normal	Normal	Some truncated FUS protein remains	(Hicks et al., 2000)
FUS KO	Homozygous	C57BL/6	**Promoter:** mouse *Fus* **Expression pattern:** All cells where *Fus* is expressed	Small amount of truncated FUS protein	ND	ND	NA	ND	Die within 16 hours of birth	Reduction in white blood cells Reduced cellularity of lymphoid organs Defects in pre-B cell to B-cell transition Issues with genomic stability	Some truncated FUS protein remains	(Hicks et al., 2000)
FUS KO	Homozygous	C57BL/6J x ICR	**Promoter:** mouse *Fus* **Expression pattern:** All cells where *Fus* is expressed	No FUS protein	Yes	No	NA	No	20% survive past weaning (if remove competition for resources)	No gliosis Normal muscle histology	Mixed background somehow altering phenotype	(Kino et al., 2015) Original model from (Hicks et al., 2000)
FUS KO	Heterozygous	129svev x CD1	**Promoter:** mouse *Fus* **Expression pattern:** All cells where *Fus* is expressed	Slightly reduced	ND	ND	NA	ND	Normal	ND	Low levels of truncated FUS protein	(Kuroda, 2000)

FUS protein	Homozygous or heterozygous	Genetic background	Promoter and expression pattern	Expression levels	Cognitive phenotypes	Motor phenotypes	Motor symptom onset	Motor neuron loss	Survival	Other phenotypes	Limitations/to note	Reference
FUS KO	Homozygous	129svev x CD1	**Promoter:** mouse *Fus* **Expression pattern:** All cells where *Fus* is expressed	Small amount of truncated FUS protein	ND	ND	NA	ND	Normal (129svev only don't survive to weaning)	Sterile/reduced fertility Increased sensitivity to radiation	Low levels of truncated FUS protein Mixed background somehow altering phenotype	(Kuroda, 2000)
FUS KO	Heterozygous	C57BL/6	**Promoter:** Mouse *Fus* **Expression pattern:** All cells where *Fus* is expressed	30% reduction	ND	No	NA	No	ND	No mislocalisation		(Scekic-Zahirovic et al., 2016) (Scekic-Zahirovic et al., 2017) (Scekic-Zahirovic et al., 2021)
FUS KO	Homozygous	C57BL/6	**Promoter:** Mouse *Fus* **Expression pattern:** All cells where *Fus* is expressed	Complete loss of FUS	ND	ND	NA	No	30 mins after birth (respiratory insufficiency)	No FUS		(Scekic-Zahirovic et al., 2016) (Scekic-Zahirovic et al., 2017) (Scekic-Zahirovic et al., 2021)
FUS KO	Homozygous (conditional)	C57BL/6J	**Promoter:** Mouse *Fus* **Expression pattern:** Conditional knock-down in forebrain	Decreased FUS expression in forebrain	Yes	ND	NA	ND	ND	Reduced mature dendritic spines in CA1 dendrites	Only used to assess spine formation in hippocampus	(Yokoi et al., 2017)

FUS protein	Homozygous or heterozygous	Genetic background	Promoter and expression pattern	Expression levels	Cognitive phenotypes	Motor phenotypes	Motor symptom onset	Motor neuron loss	Survival	Other phenotypes	Limitations/to note	Reference
WT (human)	Heterozygous (Additional to mouse FUS)	C57BL/6	**Promoter:** mouse PrP **Expression pattern:** Neurons, glia, testes, heart, and skeletal muscles	1.5x control	ND	None	NA	No No NMJ denervation	Normal	Largely normal	Overexpression model FUS protein is HA tagged Not normal pattern of FUS expression	(Mitchell et al., 2013) (So et al., 2018)
WT (human)	Homozygous (Additional to mouse FUS)	C57BL/6	**Promoter:** mouse PrP **Expression pattern:** Neurons, glia, testes, heart, and skeletal muscles	1.7x control	ND	Yes	28 days	60% loss spinal MNs at 8 weeks NMJ denervation at 15 days	8-12 weeks	Weak mislocalisation FUS positive inclusions Some neuronal ubiquitin inclusions Astrogliosis and microgliosis Mitochondrial dysfunction	Phenotypes much more severe than heterozygote despite only 0.2x more FUS protein FUS protein is HA tagged Not normal pattern of FUS expression	(Mitchell et al., 2013) (So et al., 2018)
WT (human)	Additional to mouse FUS	B6C3F1	**Promoter:** SBT-rAAV1 **Expression pattern:** Neurons	ND (but highest 3 weeks after birth)	ND	ND	NA	ND	ND	No mislocalisation No inclusions No gliosis TDP-43 remains nuclear	FUS is V5 tagged FUS gene is randomly integrated Only expressed in neurons so only getting cell autonomous phenotypes	(Verbeeck et al., 2012)

FUS protein	Homozygous or heterozygous	Genetic background	Promoter and expression pattern	Expression levels	Cognitive phenotypes	Motor phenotypes	Motor symptom onset	Motor neuron loss	Survival	Other phenotypes	Limitations/to note	Reference
WT (human)	Additional to mouse FUS	C57BL/6	**Promoter:** CAG **Expression pattern:** Global from germ line	Increased	ND	Yes	10 days	No spinal cord MN loss NMJ denervation	30 days	No mislocalisation No inclusions Gliosis	FUS is GFP tagged FUS gene is randomly integrated Phenotypes are very severe compared to other WT FUS models perhaps due to promoter used or random integration	(Sephton et al., 2014)
WT (human)	Additional to mouse FUS	ND	**Promoter:** mouse PrP **Expression pattern:** CNS (other expression less known)	<2-fold FUS overexpression	ND	No	NA	ND	ND	No mislocalisation	3 copies of the transgene	(Tibshirani et al., 2015)
WT (human)	Additional to mouse FUS	ND	**Promoter:** MAPT **Expression pattern:** Neuronal	Mouse FUS comparable to controls Increased human FUS	ND	No	NA	None	Normal	No mislocalisation	FUS is Myc tagged FUS is expressed in neurons but will likely be expressed elsewhere, non-physiological expression pattern	(Sharma et al., 2016)
WT (human)	Additional to mouse FUS	C57BL/6	**Promoter:** Human FUS **Expression pattern:** unknown	Comparable to control	No	No	N/A	No	ND	No mislocalisation No inclusions No gliosis	FUS gene is randomly integrated	(Lopez-Erauskin et al., 2018)

FUS protein	Homozygous or heterozygous	Genetic background	Promoter and expression pattern	Expression levels	Cognitive phenotypes	Motor phenotypes	Motor symptom onset	Motor neuron loss	Survival	Other phenotypes	Limitations/to note	Reference
WT (human)	Additional to mouse FUS	C57BL/6	**Promoter:** mouse PrP **Expression pattern:** CNS (other expression less known)	Tissue specific reduction of mouse FUS Increased human FUS	ND	Yes	12 months	No spinal cord MN loss at 12 months, sensory neuron loss 30% NMJ denervation at 12 months	ND	No mislocalisation Gliosis	FUS is HA tagged Doesn't have a normal expression pattern, leading to down regulation of mouse Fus Comparable to more severe phenotype and MN loss than R521C mutation	(Ling et al., 2019)
FUS1-359	Additional to mouse FUS	C57BL/6J	**Promoter:** Thy-1 **Expression pattern:** unknown	Tissue specific increase in total FUS Reduced mutant FUS fragment		Yes	2.5-4.5 months (dies within 2 weeks of motor symptom onset)	Spinal cord MN loss at 2.5-4.5 months NMJ denervation at 2.5-4.5 months	5 months	Inclusions (FUS and ubiquitin separately) Gliosis	FUS is GFP tagged FUS expression beyond neuronal and pattern unknown Lines had vastly different FUS expression likely due to integration environments Motor phenotype less severe when mutant fragment only expressed in neurons	(Shelkovnikova et al., 2013)

FUS protein	Homozygous or heterozygous	Genetic background	Promoter and expression pattern	Expression levels	Cognitive phenotypes	Motor phenotypes	Motor symptom onset	Motor neuron loss	Survival	Other phenotypes	Limitations/to note	Reference
R521C (human)	Additional to mouse FUS	B6C3F1	**Promoter:** SBT-rAAV1 **Expression pattern:** Neurons	ND (but highest 3 weeks after birth)	ND	ND	ND	ND	ND	Weak mislocalisation No inclusions No gliosis TDP-43 remains nuclear	FUS is V5 tagged FUS gene randomly integrated Only expressed in neurons Only aged to 3 months	(Verbeeck et al., 2012)
R521C (human)	Additional to mouse FUS	C57BL/6	**Promoter:** shPrP **Expression pattern:** unknown	Tissue specific, increased in cortex	ND	Yes	Variable	Spinal cord MN loss at 16 days NMJ denervation at 3 months	Reduced but variable	Mild mislocalisation DNA damage	FUS is FLAG tagged Not normal expression patterns Breeding strategy complicated to generate cohorts – second generation had a much more severe phenotype than first	(Qiu et al., 2014)
R521C (human)	Additional to mouse FUS	ND	**Promoter:** MAPT **Expression pattern:** Neuronal	Mouse FUS comparable to controls Increased human FUS	ND	ND	ND	Spinal cord MN loss at 60 days NMJ denervation at 40 days	Normal	Mild mislocalisation Gliosis	FUS is Myc tagged FUS is expressed in neurons but will likely be expressed elsewhere, non-physiological expression pattern Unknown if produces motor phenotype	(Sharma et al., 2016)

FUS protein	Homozygous or heterozygous	Genetic background	Promoter and expression pattern	Expression levels	Cognitive phenotypes	Motor phenotypes	Motor symptom onset	Motor neuron loss	Survival	Other phenotypes	Limitations/to note	Reference
R521C (human)	Additional to mouse FUS	C57BL/6	**Promoter:** Human FUS **Expression pattern:** unknown	Comparable to control	Yes (at 24 months)	Yes	8 months	Spinal cord MN loss at 24 months NMJ denervation at 24 months	ND	No mislocalisation No inclusions Gliosis	Random integration and not normal expression patterns	(Lopez-Erauskin et al., 2018)
R521C (human)	Additional to mouse FUS	C57BL/6	**Promoter:** mouse PrP **Expression pattern:** CNS (other expression less known)	Tissue specific reduction of mouse FUS Increased human FUS	ND	Yes	12 months	No spinal cord MN loss at 12 months, sensory neuron loss 30% NMJ denervation at 12 months	ND	No mislocalisation Gliosis	Not normal pattern of expression	(Ling et al., 2019)
R513C (mouse equivalent of R521C)	Heterozygous	C57BL/6J	**Promoter:** Mouse *Fus* **Expression pattern:** All cells where *Fus* is expressed	ND	Yes	Yes	4-7 months	Spinal cord MN loss at 2 years	ND	Gliosis		(Zhang et al., 2020)
R513C (mouse equivalent of R521C)	Homozygous	C57BL/6J	**Promoter:** Mouse *Fus* **Expression pattern:** All cells where *Fus* is expressed	Tissue specific increased FUS expression	Yes	Yes	4-7 months	Spinal cord MN loss at 2 years	ND	No mislocalisation (mislocalisation seen after Arsenite dosing) Inclusions seen after Arsenite dosing Gliosis	Large protein overexpression with almost no change in RNA Phenotype was almost identical to heterozygote	(Zhang et al., 2020)

FUS protein	Homozygous or heterozygous	Genetic background	Promoter and expression pattern	Expression levels	Cognitive phenotypes	Motor phenotypes	Motor symptom onset	Motor neuron loss	Survival	Other phenotypes	Limitations/to note	Reference
R514G (human)	Additional to mouse FUS	C57BL/6	**Promoter:** mouse PrP **Expression pattern:** CNS (other expression less known)	Tissue specific reduction of mouse FUS Increased human FUS	ND	Yes	12 months	Spinal cord MN loss at 12 months, sensory neuron loss 30% NMJ denervation at 12 months	ND	No mislocalisation Gliosis	Have chosen transgenic lines with similar expression levels so biased the results?	(Ling et al., 2019)
R521G (human)	Additional to mouse FUS	C57BL/6	**Promoter:** CAG **Expression pattern:** Global from germ line	Increased	Yes	Yes	14 days	No spinal cord MN loss Mild NMJ denervation	~60% by 30 days (some lived up to 500 days)	No mislocalisation No inclusions No gliosis	FUS is GFP tagged FUS gene randomly integrated Phenotypes less severe than WT overexpression Those that lived for over 30 days were less affected than those that died early (almost normal)	(Sephton et al., 2014)
R521H (human)	Additional to mouse FUS	C57BL/6	**Promoter:** Human FUS **Expression pattern:** unknown	Comparable to control	Yes (at 24 months)	Yes	8 months	Spinal cord MN loss at 24 months NMJ denervation at 24 months	ND	No mislocalisation No inclusions Gliosis	Random integration	(Lopez-Erauskin et al., 2018)

FUS protein	Homozygous or heterozygous	Genetic background	Promoter and expression pattern	Expression levels	Cognitive phenotypes	Motor phenotypes	Motor symptom onset	Motor neuron loss	Survival	Other phenotypes	Limitations/to note	Reference
ΔRRM and R522G	Additional to mouse FUS	C57BL/6J x CBA/J	**Promoter:** Thy-1 **Expression pattern:** unknown	Tissue specific increase in total FUS	ND	Tremor (whole body, beyond limbs) Lack of balance	2 days prior to death	No (trigeminal, facial and hypoglossal cortical nuclei studied)	20 ± 1 days	Mislocalisation FUS positive inclusions (human not mouse FUS recruited) Some overlap of FUS inclusions with ubiquitin No gliosis	Random integration 25% died suddenly, some developed a constant tremor and others didn't suggesting variable phenotype between TG littermates	(Robinson et al., 2015)
R495X	Additional to mouse FUS	ND	**Promoter:** mouse PrP **Expression pattern:** CNS (other expression less known)	3-5-fold FUS overexpression	ND	No overt motor symptoms, EMG recording defects e.g. fibrillation potentials	8-12 months	NMJ denervation and motor unit loss (unclear what tissue)	ND	Mislocalisation No FUS inclusions No ubiquitin or p62 inclusions	11-15 copies of the transgene Used WT transgenics (only 2 copies of transgene) and non-TG littermates as controls which are poor controls Large difference in symptom onset time between mice	(Tibshirani et al., 2015)
P525L (human)	Additional to mouse FUS	ND	**Promoter:** MAPT **Expression pattern:** Neuronal	Mouse FUS comparable to controls Increased human FUS	ND	Yes	1 year	Spinal cord MN loss at 30 days NMJ denervation at 20 days	Normal	Mislocalisation Gliosis	FUS gene randomly integrated Overexpression of human gene	(Sharma et al., 2016)

FUS protein	Homozygous or heterozygous	Genetic background	Promoter and expression pattern	Expression levels	Cognitive phenotypes	Motor phenotypes	Motor symptom onset	Motor neuron loss	Survival	Other phenotypes	Limitations/to note	Reference
P517L (mouse equivalent of P525L)	Heterozygous	C57Bl/6J	**Promoter:** mouse *Fus* **Expression pattern:** All cells where *Fus* is expressed	Comparable to control	ND	No	NA	Spinal cord MN loss at 18 months NMJ denervation at 12 months	90% survive to weaning 950 days	Mild mislocalisation No inclusions (but FUS in insoluble fractions) Gliosis	Expressing the mouse protein so cannot study human targeted therapies See motor neuron loss but no motor phenotype	(Korobeynikov et al., 2022)
Δ14 (human)	Additional to mouse FUS	B6C3F1	**Promoter:** SBT-rAAV1 **Expression pattern:** Neurons	ND (but highest 3 weeks after birth)	ND	ND	ND	ND	ND	Mislocalisation Inclusions No gliosis TDP-43 remains nuclear	FUS is V5 tagged FUS gene randomly integrated Only expressed in neurons Only aged to 3 months	(Verbeeck et al., 2012)
Δ14 (partially humanised)	Heterozygous	C57Bl/6J	**Promoter:** mouse *Fus* **Expression pattern:** All cells where *Fus* is expressed	Comparable to control	ND	No	NA	Spinal cord MN loss at 18 months NMJ denervation at 12 months	90% survive to weaning 950 days	Mild mislocalisation No inclusions (but FUS in insoluble fractions) Gliosis	Partially humanised	(Korobeynikov et al., 2022)
Δ14 (partially humanised)	Heterozygous	C57BL6/J	**Promoter:** Mouse *Fus* **Expression pattern:** All cells where *Fus* is expressed	Comparable to control	ND	Yes	6 months	Spinal cord MN loss at 12 months	Reduced from 19 months	Mislocalisation No inclusions Gliosis ND	Partially humanised	(Devoy et al., 2017)

FUS protein	Homozygous or heterozygous	Genetic background	Promoter and expression pattern	Expression levels	Cognitive phenotypes	Motor phenotypes	Motor symptom onset	Motor neuron loss	Survival	Other phenotypes	Limitations/to note	Reference
Δ14 (partially humanised)	Homozygous	C57BL6/J x DBA	**Promoter:** Mouse *Fus* **Expression pattern:** All cells where *Fus* is expressed	Tissue specific increased FUS expression	Yes	Yes	9 weeks	ND	Reduced from 12 weeks (seizures)	Mislocalisation No inclusions Gliosis	Unknown if due to MN loss Cross background required to survival and to avoid seizures	(Ali et al., 2023) Original model from (Devoy et al., 2017)
ΔNLS (human)	Additional to mouse FUS	C57BL/6J	**Promoter:** Mouse Thy-1.2 **Expression pattern:** unknown	Mouse FUS comparable to controls Increased human FUS	ND	Yes	8 weeks	Spinal cord neuronal loss at 1 year (ChAT+ neurons no different at 1 year)	Reduced	Mislocalisation Inclusions (FUS and ubiquitin at 2 years) Gliosis	No MN loss Not normal expression pattern	(Shiihashi et al., 2016)
Fus^{NLS} (mouse)	Heterozygous	C57BL/6	**Promoter:** Mouse *Fus* **Expression pattern:** All cells where *Fus* is expressed	Comparable to controls	Yes	Yes	10 months	15% spinal cord MN loss at birth (2016 paper) 35% spinal cord MN loss at 22 months (2017 paper)	ND	Mislocalisation in most motor neurons Occasional ubiquitin inclusions, no FUS inclusions	Differing MN loss values in different papers	(Scekic-Zahirovic et al., 2016) (Scekic-Zahirovic et al., 2017) (Scekic-Zahirovic et al., 2021)
Fus^{NLS} (mouse)	Homozygous	C57BL/6	**Promoter:** Mouse *Fus* **Expression pattern:** All cells where *Fus* is expressed	ND	ND	ND	NA	30-50% spinal cord MN loss at birth	Hours after birth (respiratory insufficiency)	Severe mislocalisation (almost no nuclear FUS)		(Scekic-Zahirovic et al., 2016) (Scekic-Zahirovic et al., 2017) (Scekic-Zahirovic et al., 2021)

ND = not determined in the current study or cannot be determined from the publication NA = not applicable

Much has been learnt from the existing mouse models of FUS-ALS, not least a clearer understanding of mechanisms which could be underpinning ALS disease progression as discussed in section 1.10. *Fus* knock-out models have allowed us to appreciate the important role of FUS in development, immunity, and fertility. Models overexpressing human wildtype FUS have shown *FUS* is a dose sensitive gene and tightly regulated expression is vital for FUS to function normally; if dysregulated it can itself lead to motor neuron degeneration and motor phenotypes. Interestingly this motor neuron loss is dependent on the cellular expression pattern of human FUS as it is not seen when FUS is expressed under the control of the CAG or MAPT promoter.

Transgenic models of FUS-ALS have the most more severe phenotypes, with motor neuron degeneration seen as early as 16 days. Targeted knock-in models usually have a much milder phenotype with symptoms not appearing until around 18 months to two years. This later onset more faithfully represents patients who live with the mutation for many years before a phenotype develops. This late-onset phenotype perhaps develops when patients are exposed to additional stochastic hits during aging or from the environment. Targeted knock-in models often do not display all aspects of disease. For example, the Fus^{P517L} model from Korobeynikov and colleagues displays motor neuron loss aged 18 months without a motor phenotype. Comparing findings from transgenic and targeted knock-in models should help us unpick which disease mechanisms are likely due to ectopic, overexpression of the mutant protein, or disruption at the site of integration, and which are due to the specific action of the mutant protein. Perhaps those disease mechanisms which are consistently found between the two types of models should be considered in more detail, such as gliosis which is regularly reported. Alternatively, existing models also indicate which cellular

and molecular phenotypes may be less important for disease progression. For example, mutant FUS can have a toxic effect on motor neurons without severe increased localisation to the cytoplasm suggesting a toxic nuclear gain of function as discussed in section 1.11.2, rather than a cytoplasmic gain of function. Moreover, five transgenic models overexpressing mutant, but also wildtype FUS, report cytoplasmic FUS inclusions compared to only one targeted knock-in model which only report inclusions after arsenite dosing. This suggests the early appearance of inclusions as seen in these mouse models are more likely when FUS is artificially overexpressed, perhaps increasing the stress the cell is under to process the toxic protein. FUS inclusions are reported in FUS-ALS patients and may also be induced by cellular stress; the relevance of FUS inclusions in patients is yet to be fully elucidated.

Existing models have shown us that the expression pattern of mutant or wildtype FUS has a strong effect on the severity of phenotype, as does the mouse genetic background. If these inconsistencies in phenotype are true, rather than being due to poor reporting and omitting negative data, then this is very interesting and relevant to human pathogenesis. The expression pattern differences support the idea that FUS has tissue and cell specific roles which are modulated by the concentration of FUS protein, and that certain cell types are more vulnerable to ectopic expression of FUS. The difference in phenotype on alternative mouse genetic backgrounds would be valuable for further study to try and uncover neuroprotective genes. For example, homozygous *Fus* knock-out and $FUS^{\Delta 14}$ mice are both perinatal lethal on congenic backgrounds but can survive on outcrossed backgrounds. It would be interesting to compare the genetic profile of each mouse strain to try and discover genes which

could be responsible for dampening the effect of mutant FUS or somehow compensating for the loss of FUS, and the mechanisms by which this is occurring.

There is emerging evidence that different *FUS* mutations leads to distinct cellular phenotypes and so additional models are needed to recapitulate the toxicity and subsequent pathomechanisms associated with individual *FUS* mutations (An et al., 2020; Salam et al., 2021).

1.13 Summary and Aims of the Thesis

In summary, the ALS field has learnt a lot from existing mouse models, however pre-clinical work done in these models has historically failed to translate into successful patient therapies. In this thesis I will present novel fully genomically humanised knock-in mouse models of FUS-ALS that aim to address some of the outstanding issues associated with existing models. The humanised *FUS* models will aid our understanding of FUS-ALS and allow the study of human targeted therapies as the mice express the human *FUS* gene and protein under the control of the endogenous mouse *Fus* promoter, in a physiologically relevant pattern of expression.

Chapter 2 – I will introduce and characterise humanised *FUS* wildtype mice in which the human *FUS* gene has replaced the mouse *Fus* gene, including all introns, exons and 3' UTR, at the endogenous mouse locus, but without mutations.

Chapter 3 – Here I will extensively characterise humanised heterozygous *hFUS*^{P525L} mice as a model of FUS-ALS. These mice are fully humanised but heterozygous for a disease-causing ALS patient mutation, representing the genetic situation observed in patients.

Chapter 4 – In this chapter I will use primary neuronal cell cultures collected from E12.5-E13.5 heterozygous *hFUS*^{P25L} mice and controls to further study molecular changes uncovered from work in the *hFUS/hFUS*^{P525L} mice.

Chapter 5 – In the final results chapter I will compare two ALS-causing patient *FUS* mutations, P525L and Q519Ifs, within the same cohort of mice. This comparison of mutations between littermates with the same genetic background will improve our understanding of what determines the severity of FUS-ALS caused by distinct *FUS* mutations.

Chapter 6 – I will draw conclusions based on findings of the previous results chapters and explore how these fit into our wider understanding of FUS-ALS.

Chapter 7 – This chapter will detail the experimental methods and protocols used throughout the project.

Chapter 8 – Contains supplementary data.

Chapter 9 – Lists references used throughout the thesis.

2 Chapter 2: Characterisation of genomically humanised *FUS* wildtype mice

Much of the phenotyping and expression data presented in this chapter were used in the publication by our group disseminating work done to generate genomically humanised mice for the major ALS-associated genes: *TARDBP, SOD1* and *FUS* (Devoy et al., 2021), on which I was co-first author.

2.1 Introduction

FUS was brought to the attention of the ALS field when mutations in the *FUS* gene were discovered to cause the disease in 2009 (Kwiatkowski et al., 2009; Vance et al., 2009). Mutations in *FUS* can cause early onset, aggressive forms of ALS, (Baumer et al., 2010; Picher-Martel et al., 2020), with mutations in *FUS* accounting for around 35% of familial ALS cases in patients younger than 40 years old (Millecamps et al., 2012).

2.1.1 Humanised knock-in mouse models

As discussed in detail in chapter 1, whilst a great deal has been learnt about ALS from traditional over-expressing transgenic mice, there are several things which should be considered but are often overlooked. These include mutagenesis at the insertion site, and the fact that dose-sensitive genes such as *FUS* may have aberrant phenotypes when more or less than two copies of the gene are expressed. In addition, loss of function effects of the mutation cannot be studied whilst the endogenous mouse genomic loci is intact, unless the transgenic mice are crossed to knock-out animals (De Giorgio et al., 2019).

Whilst targeted knock-in mice address the issues associated with ectopic overexpression and the ability to study loss of function effects, there are other considerations when drawing conclusions about the *human* disease from knock-in mouse models overexpressing the mutated *mouse* sequence. Several proteins involved in neurodegeneration have different biochemical properties between the mouse and human protein, such as APP (Xu et al., 2015) and SOD1. In the case of SOD1, the human protein has several cysteine residues which are necessary to produce certain aspects of disease such as ER stress, SOD1 protein conformational state, aggregation and ultimately protein toxicity, which are not present in the mouse protein (Crown et al., 2020; Nagano et al., 2015; Perri et al., 2020). In the case of *FUS*, the human gene sequence is 80-90% conserved and the resulting protein shares 97.67% identity with the mouse protein at the amino acid sequence. The resulting mouse FUS protein is slightly smaller, containing 518 amino acids compared to 526 in human FUS. The functional differences between mouse and human FUS are less well studied but with growing knowledge that FUS misfolds into disease relevant conformations, then we want the human protein structure to assess the human misfolded aggregates. This is even more important given the increasing evidence that proteins in many neurodegenerative diseases, including FUS, TDP-43 and Tau, have disease-specific morphological differences in aggregate amyloid filaments, and that protein seeding ability is different between these different strains, and the species from which they are derived (Arseni et al., 2022; Kumar et al., 2023; Tetter et al., 2023; Zhang et al., 2019).

The issues presented above are now able to be addressed using highly sophisticated knock-in models, such as those presented and characterised here, whereby the ALS-relevant gene sequence is replaced with the human gene sequence

at the endogenous mouse loci. These genomically humanised *FUS* wildtype mice offer the ALS field an additional tool to better understand human disease progression by conferring human protein biochemistry and expression in a physiologically relevant context.

2.1.2 *FUS* humanisation strategy

To date, few genomically humanised mouse models exist and so there is no gold standard approach for how this should be done. As detailed in our paper published in 2021, the strategy was determined based on what was known about how each gene was regulated, and how mutations may result in disease pathomechanisms (Devoy et al., 2021).

To generate fully humanised *FUS* mice, the human *FUS* sequence was introduced under the control of the endogenous mouse *Fus* promoter. The mouse *Fus* promoter was used as it was hoped that maintaining the mouse promoter sequence would enable correct binding of mouse transcriptional machinery and ensure expression of the human *FUS* sequence was physiologically relevant and as close to endogenous levels as possible. The human *FUS* sequence that was introduced started at the translational ATG start codon and included not only exons, but all introns both to allow the introduction of variations which may be relevant to human disease, and to maintain splicing complexity. It is also known intronic regions contain auto regulatory sequences which are known to influence *FUS* expression and that they can control tissue specific expression of genes (Humphrey et al., 2020). The human 3'UTR sequence was included as variations within this sequence have been reported in ALS patients suggesting the 3'UTR may play a role in disease through a miRNA regulated

protein synthesis pathway (Dini Modigliani et al., 2014; Sabatelli et al., 2013). In addition, there are reports of *FUS* frameshift mutations in patients whereby the resulting *FUS* sequence includes part of the 3'UTR. If the *FUS* 3'UTR sequence was not humanised this could result in different peptides being produced which could impact pathogenicity (An et al., 2020).

LoxP sites were introduced upstream of exon 15 and downstream of the 3'UTR to allow for future conditional studies which would remove the NLS sequence completely.

The decision was taken not to include a tag within the *FUS* sequence so as not to interfere with expression and function. If differences were observed between wildtype mice and mice expressing the human *FUS* sequence, it could be inferred this was due to humanisation and not the presence of a tag.

2.2 Aims and hypotheses

Hypothesis:

1) FUS is highly conserved in eukaryotes (Sasayama et al., 2012) and thus human *FUS* will be able to functionally replace mouse *Fus.* The humanised wildtype mouse will be grossly phenotypically normal, and a suitable control for future humanised FUS-ALS models.

Aims:

a) Characterise humanised *FUS* wildtype knock-in mice longitudinally

- Expression of the humanised gene:
    - mRNA and protein expression.

- Assess motor function:
    - Grip strength, locotronic, wheel running test.
- Is there differential gene expression due to humanisation?
    - RNA sequencing of 14-week-old spinal cord tissue.
- Histological analysis:
    - Motor neuron counts, FUS staining, muscle fibre morphology.

2.3 Contributions

A large body of work was carried out prior to my DPhil to generate the mice used in this project. Dr. Anny Devoy engineered the humanised constructs in Prof Elizabeth Fisher's lab at UCL followed by gene targeting in embryonic stem cells by the cellular and molecular group at MRC Harwell.

The staff on ward five must also be acknowledged for their hard work to support and maintain the mouse colonies used in this chapter.

David Thompson, a fellow DPhil student in the mouse models of neurodegeneration group at MRC Harwell wrote the ImageJ plugin used for fibre type quantification in section 2.4.6.

Adele Austin in the histology lab at MRC Harwell performed the serial sectioning of the spinal cords used for motor neuron counts in section 2.4.8.

2.4 Results

2.4.1 Generation of the humanised *FUS* wildtype mice

In summary, a linearized bacterial artificial chromosome (BAC) targeting construct harbouring the human *FUS* sequence, flanked by mouse homology arms was engineered via recombineering in bacteria (Devoy et al., 2021).

The human *FUS* sequence starts from the ATG start codon, and includes all introns, exons and 3'UTR, along with an FRT-flanked neomycin selection cassette inserted 1Kb downstream of the human 3'UTR.

The resulting humanised construct flanked with mouse homology arms (57.4kb at the 5' and 71.5kb at the 3' end) was electroporated into R1 embryonic stem (ES) cells, derived from 129X1/SvJ- 129S1/SV strain mice, resulting in humanising of the *Fus* gene by homologous recombination (Figure 2.1). ES cell clones were plated at clonal density and treated with Neomycin before surviving clones were screened for the desired homologous recombination event by Loss-Of-Allele (LOA) copy via qPCR and ddPCR assays.

ES cell clones where the recombination event was successful were injected into donor blastocysts and male chimeric offspring were crossed to C57BL/6J females. When germ line transmission was confirmed, heterozygous mice were crossed with C57BL/6J mice and subsequently with mice from the Gt(ROSA)26Sor$^{tm2(CAG-flpo,-EYFP)Ics}$ line (C57BL/6Ntac background) to excise the neo selection cassette.

The resulting mice were backcrossed for 10 generations before cohort mice were bred for phenotyping and molecular studies.

Targeted long range sequencing was used to confirm allele integrity in the humanised mice (Devoy et al., 2021).

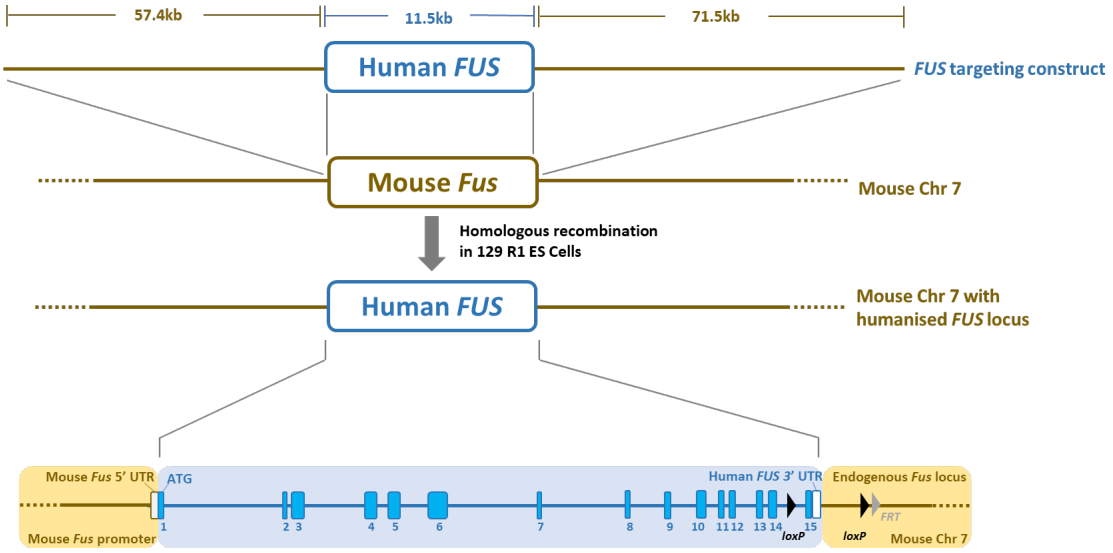


Figure 2.1: Generation of the hFUS construct. *Schematic highlighting the final humanised FUS construct and how this was generated using homologous recombination in 129 ES cells. The lowest line represents the humanised allele expressed in the humanised FUS mouse genome.*

2.4.2 Humanisation has no effect on survival and breeding

Expression of the *Fus* gene is known to be essential for viability of neonatal animals as reduced *Fus* expression leads to chromosome instability and aneuploidy (Hicks et al., 2000). Additionally, *Fus* loss-of-function is known to cause sterility in male mice who experience defects in spermatogenesis and reduced somatic growth (Kuroda, 2000)

In a cohort mice aged to 18 months, there was no difference observed in survival of mice heterozygous or homozygous for humanised *FUS*, compared to wildtype controls (Figure 2.2A).

Of the mice born, the sex split was 44.9% male pups, and 55.1% female pups born from litters used for longitudinal phenotyping (Figure 2.2B), with the gap closing

to 50.7% males and 49.3% females for all mice bred (data not shown). Offspring genotype data showed 26.3% of mice born were homozygous for mouse *Fus*, 53.9% heterozygous for mouse *Fus* and human *FUS*, and 19.8% homozygous for human *FUS* (Figure 2.2C). Hardy-Weinberg equilibrium suggests 25% of offspring should have been *hFUS/hFUS* mice suggesting homozygous *hFUS* mice may have been slightly less viable than *mFus/mFus* controls.

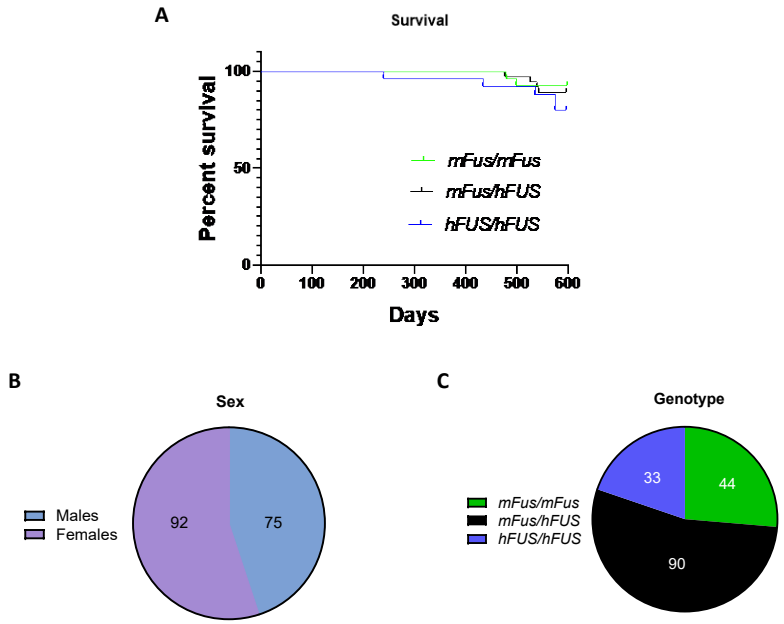


Figure 2.2: Humanisation has no effect on survival and mice breed as expected. A) *Wildtype and mice heterozygous and homozygous for humanised FUS were aged and any unexpected deaths were recorded. There was no difference in survival between genotypes up to and including 18 months.* ***B)*** *The sex split of cohort mice (167 total).* ***C)*** *The genotype split of cohort mice (167 total).*

2.4.3 Human *FUS* is expressed in a physiologically relevant pattern of expression in homozygous humanised *FUS* mice

2.4.3.1 FUS RNA expression

The introduction of the human *FUS* sequence, which includes introns and the 3'UTR, will introduce new regulatory sequences into the mouse genome and as such

has the potential to disrupt *FUS* expression. In addition, FUS is auto regulatory and binds to its own mRNA to negatively regulate expression (Humphrey et al., 2020; Zhou et al., 2013). Although the mouse and human *FUS* sequence share around 80-90% homology, the human FUS protein which is produced from the human *FUS* sequence may have an altered ability to bind to regulatory sequences in the mouse genome. To better understand the effect humanisation had on *FUS* RNA expression PCR techniques were used. Primers were designed which amplified both mouse and human *FUS,* as well as primers which were species specific.

RT-PCR on brain tissue extracted from E14.5-day old embryos confirmed that only human *FUS* was expressed in homozygous humanised mice, and both human and mouse *Fus* were expressed in heterozygous humanised animals as expected (Figure 2.3A).

Levels of *FUS* mRNA expression in spinal cord, tibialis anterior and brain were assessed using qRT-PCR to better quantify humanised *FUS* expression in ALS-disease relevant tissues. Tibialis anterior muscle was chosen as it is a hindlimb muscle predominantly made up of fast twitch muscle fibres which are more vulnerable in ALS (Frey et al., 2000). This was carried out in 3-month and 18-month-old tissue of both male and female mice to see if there was an age-dependent and sex dependent change in expression. A more extensive characterisation was carried out on tissue collected from 18-month-old mice to assess in parallel with phenotyping and histology data such as motor neuron counts.

At three months, there was no difference in total *FUS* levels between wildtype, heterozygous and homozygous humanised male mice in the spinal cord, however

there was a mild reduction in expression in the TA in *hFUS/hFUS* mice compared to *mFus/mFus* mice (Figure 2.3B).

By 18 months this expression pattern had changed. In the tissues of the central nervous system, there was a significant decrease in *FUS* expression in homozygous humanised mice, the largest of around 40-50% was seen in brain tissue ($p<0.001$), followed by 30-35% in spinal cord ($p<0.01$) compared to *mFus/mFus* mice. In the TA muscle this reduction in expression was not observed in *hFUS/hFUS* mice compared to wildtype suggesting there is tissue specific regulation of *FUS*. The pattern of *FUS* expression was consistent between sexes (Figure 2.3D).

Because of this change in expression pattern between 3 and 18 months, a qRT-PCR experiment was carried out which directly compared *FUS* expression in the spinal cord between the two time points. This longitudinal expression was interesting as it showed that over time *FUS* expression increased in both wildtype mice, and homozygous humanised mice, although to a lesser extent in homozygous humanised mice (interaction between genotype and age was significantly different, $p= 0.0040$), also shown in the 18-month time point data where levels were significantly different between *hFUS/hFUS* and control mice (Figure 2.3C).

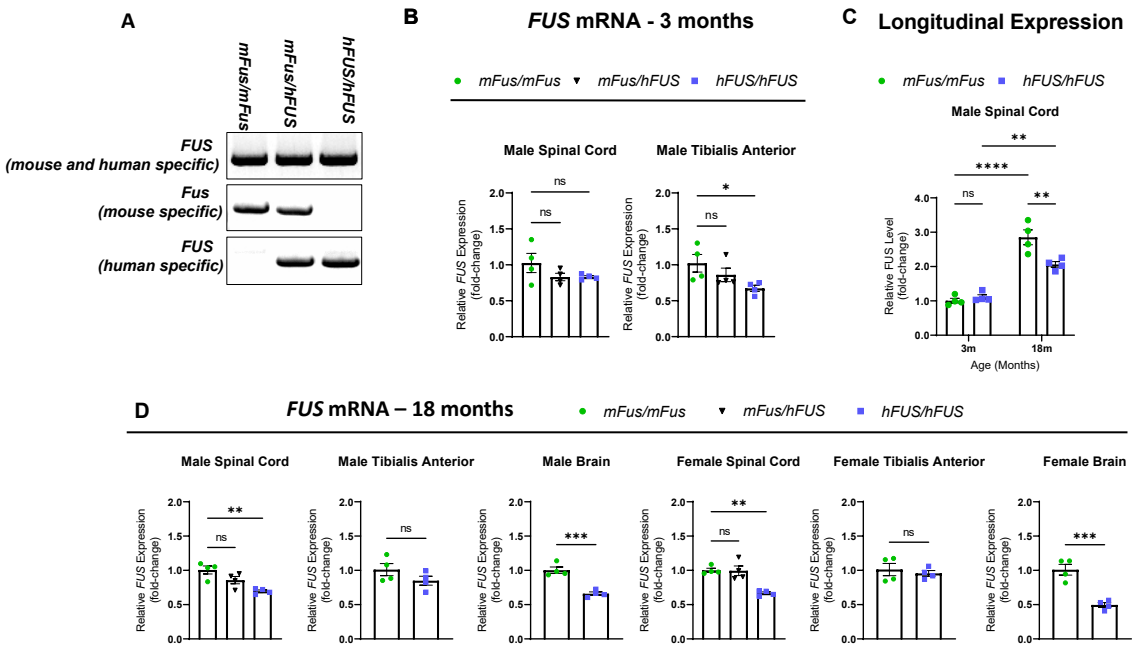


Figure 2.3: FUS expression is modestly reduced in ALS-relevant tissues in hFUS/hFUS mice. A) *Primers were designed which bound to regions specific to the mouse or human FUS sequence and RT-PCR was run on E14.5 embryonic brain tissue.* ***B)*** *FUS expression was quantified in 3-month-old tissue from male mice using qPCR techniques and primers which bound regions conserved between the mouse and human FUS sequence.* ***C)*** *FUS expression in the spinal cord was assessed longitudinally using qPCR relative to wildtype mice aged 3 months old.* ***D)*** *FUS mRNA expression was quantified more comprehensively in tissue collected from mice aged 18 months old using qPCR. The same primers were used as at 3 months. Data are shown as mean average ± SEM with significance analysed using a one-way ANOVA, two-way ANOVA, or unpaired Student's T test. ns = not significant, *=p<0.05, **=p<0.01 ***=p<0.001.*

2.4.3.2 *FUS autoregulation and intron retention*

A limitation of traditional over-expressing transgenic models for studying *FUS* mutations is that it is known *FUS* is a dosage-sensitive gene which auto-regulates (Humphrey et al., 2020; Zhou et al., 2013). Proposed mechanisms to explain this autoregulation suggest nuclear FUS protein binds to intron six and seven of *FUS* pre-mRNA causing them to be retained in mature mRNA. Introns six and seven contain several premature stop codons and so transcripts containing these introns may undergo nonsense mediated decay (NMD) (Zhou et al., 2013). *FUS* mRNA with intron six and seven retained has also been shown to be preferentially located to the nucleus

where it cannot be translated (Humphrey et al., 2020). Taken together, these mechanisms may act as tissue and developmental stage specific ways of reducing translation of *FUS* transcripts and therefore regulating overall levels of FUS protein.

Because a reduction in *FUS* mRNA and protein was observed at 18 months, a qPCR assay was designed to quantify levels of intron six and seven retaining *FUS* transcripts compared to correctly spliced *FUS,* to see if this differed between homozygous humanised mice and wildtype. RNA extracted from 18-month-old spinal cord tissue of homozygous humanised mice and control showed no difference in intron six retention in either sex (Figure 2.4A-B), however in both male and female homozygous humanised mice an increase in transcripts containing intron seven was observed compared to wildtype controls (Figure 2.4C-D).

In addition to the 18-month time-point, intron retention was also assessed in male mice aged 3 months as this tissue was available from the mice used for RNA sequencing. There was no difference in the expression of *FUS* transcripts with intron six or seven retained between *hFUS/hFUS* male mice and controls in 3-month-old spinal cord tissue however the data was more variable and was trending towards an increase in both intron six and seven retention (Figure 2.4E-F). The lack of a significant increase in intron retention correlates with data at 3 months old showing no difference in expression of *FUS* mRNA between wildtype and humanised *FUS* mice.

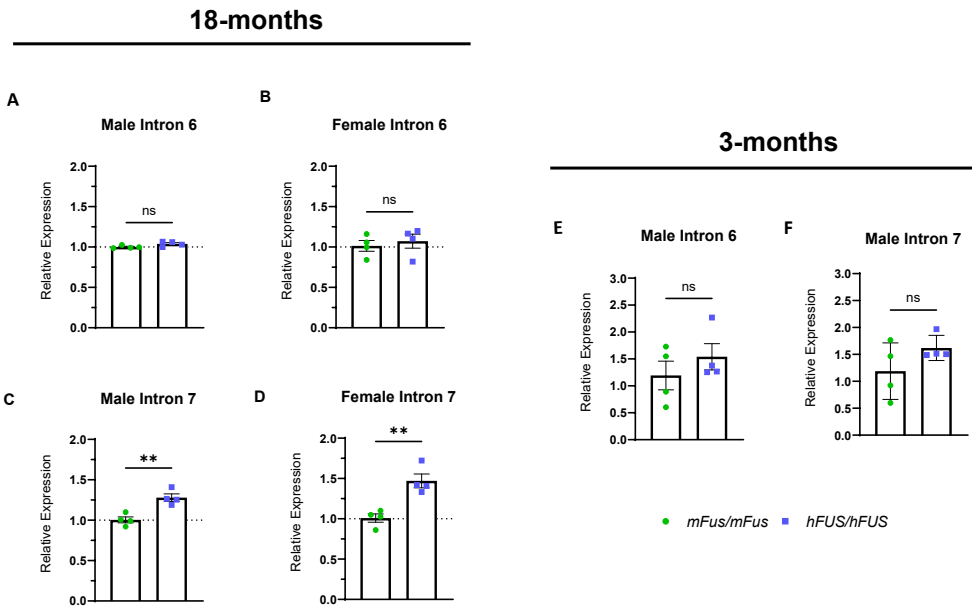


Figure 2.4: Expression of FUS transcripts with intron seven retained may explain the difference in FUS expression in the spinal cord. *qPCR was used to assess expression of FUS transcripts with intron six and seven retained in 3 month and 18-month-old spinal cord tissue.* ***A, B)*** *There is no difference in expression of FUS transcripts with intron six retained in spinal cord tissue of 18-month-old male and female hFUS/hFUS mice compared to controls.* ***C, D)*** *FUS transcripts with intron seven retained are more highly expressed in hFUS/hFUS mice compared to controls in both male and female spinal cord tissue.* ***E, F)*** *At 3 months old, when there is no significant difference in FUS expression, there is no difference in expression of intron six and intron seven retaining FUS transcripts in the spinal cord of male mice. Data are shown as mean average ± SEM with significance analysed using an unpaired Student's T test. ns = not significant, **=p<0.01.*

2.4.3.3 FUS protein expression

Having observed the modest reduction in mRNA levels, the corresponding protein levels were also assessed in tissue from the same animals so the RNA and protein expression could be directly compared. An antibody raised against the C-terminus of the FUS protein, which is conserved between mouse and human FUS, was used in immunoblots to quantify FUS protein expression.

FUS protein expression largely followed the RNA expression pattern seen in the qPCR data, except notably in the TA muscle where there seemed to be a more severe reduction in FUS protein than might be expected from the RNA levels.

At three months, there was no difference in FUS expression between wildtype, heterozygous and homozygous humanised male mice in the spinal cord or the TA (Figure 2.5A,B).

At 18 months, the spinal cord showed a trend towards a decrease of FUS protein in homozygous *hFUS* mice of both sexes compared to controls; however, these results were not significant. FUS expression in the brain was decreased, as was seen in the qRT-PCR data, with female homozygous *hFUS* mice showing a 35% decrease in FUS protein ($p<0.05$), with the same trend observed in males albeit not significant. In the TA muscle, homozygous humanised mice had a 40% decrease in FUS protein compared to controls, despite no reduction in *FUS* mRNA, however this was only significant in the males ($p<0.05$) (Figure 2.5D, Figure 8.1).

A western blot was also carried out to directly compare FUS protein expression at the early and late timepoints in the same experiment. There was no change in FUS expression in *mFus/mFus* mice between 3 and 18-months, however in the humanised *FUS* mice there was significantly lower levels of FUS protein expressed in the spinal cord at 18 months compared to the early timepoint (Figure 2.5C, Figure 8.2).

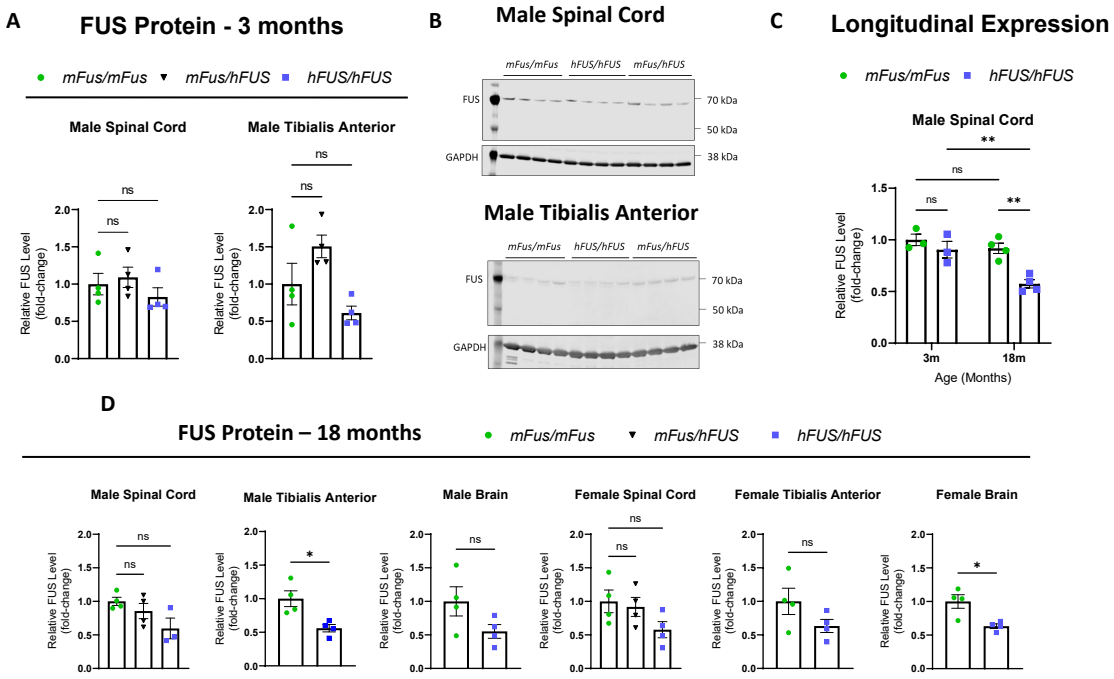


Figure 2.5: FUS protein expression is modestly reduced in ALS-relevant tissues in hFUS/hFUS mice. *FUS expression was quantified using western blotting techniques and a FUS antibody raised against the C-terminus of the FUS protein, which is conserved between the mouse and human protein.* ***A)*** *FUS expression was quantified in 3-month-old tissue from male mice.* ***B****) Images of immunoblots used for FUS expression quantification in 3-month-old mice****. C)*** *FUS expression in the spinal cord was assessed longitudinally using western blotting relative to wildtype mice aged 3 months old.* ***D)*** *FUS expression was quantified more comprehensively in tissue collected from mice aged 18 months old using western blotting techniques. Data are shown as mean average ± SEM with significance analysed using a one-way ANOVA, two-way ANOVA, or unpaired Student's T test. ns = not significant, *=p<0.05, **=p<0.01.*

2.4.4 Homozygous *hFUS* mice showed minimal transcriptomic changes

FUS is a global regulator of splicing (Ishigaki et al., 2012; Lagier-Tourenne et al., 2012; Ling et al., 2013; Masuda et al., 2015; Rogelj et al., 2012) and thus humanisation has the potential to disrupt regulation of many genes. Bulk RNA sequencing was carried out on spinal cord tissue from 14-week-old *hFUS/hFUS* knock-in mice to ensure humanisation was not causing major changes to the transcriptome.

Tissue from heterozygous *Fus* knock-out mice (*Fus*$^{+/-}$) was also included, as it is known these mice have a modest reduction in FUS protein (Humphrey et al., 2020), as seen in homozygous humanised *FUS* mice. This would inform on whether any potential

transcriptomic changes seen were caused by loss of FUS function, or by gain of function specific to humanisation of the *FUS* gene.

A lot of the RNA sequencing analysis was completed by Dr. Thomas Cunningham and published in Devoy et al 2021. An amended figure is shown here.

At 14-weeks, only 46 transcripts were differentially expressed between homozygous *hFUS* and wildtype mice, of which 21 were downregulation of mouse *Fus* and upregulation of human *FUS* (Figure 2.6, Table 8.1). Two were *Fus* pseudogenes which were believed to be mapping errors. 13 were mapped to chromosome seven, near the *Fus* locus*,* which are likely due to mouse strain differences between 129 and C57BL/6J, leaving only 10 'non-*Fus*, non-chromosome seven' transcripts changed.

To confirm that the differences in transcripts expressed from chromosome seven were strain dependent, SNP sequencing was carried out (data not shown). Primary (C57BL/6J) and secondary (129X1/SvJ) background SNPs were localised to chromosome seven as expected due to how the humanised mice were generated (see section 2.4.1). The SNP sequencing confirms it is likely that the 13 genes differentially expressed on chromosome seven are due to the presence of the 129 background. Despite showing the transcript changes are likely due differential regulation in different background strains, it may be that the small number of transcripts changed are causing some of the minor phenotypes seen in the *hFUS/hFUS* mice.

Importantly, humanising the *FUS* gene led to fewer transcript changes than were seen in the $Fus^{+/-}$ mice, which are phenotypically normal, despite the mild changes in FUS expression in the *hFUS/hFUS* mice.

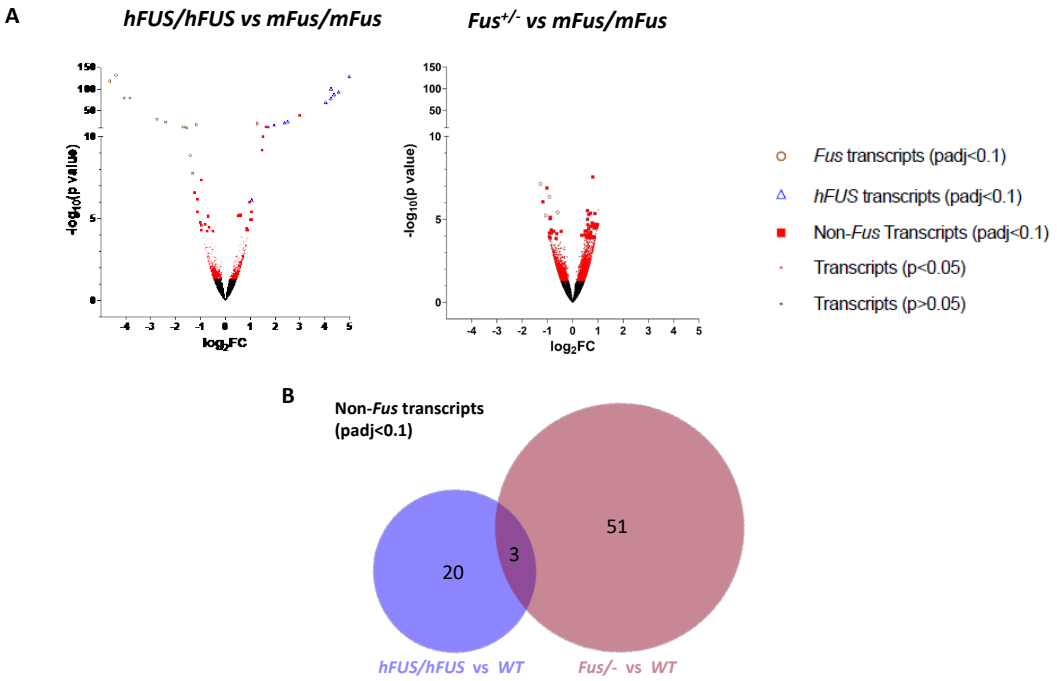


***Figure 2.6**: **hFUS/hFUS mice have minimal transcriptome disruption. A)** RNAseq volcano plots showing the distribution of differentially expressed transcripts between hFUS/hFUS and mFus/mFus (WT; left) and FUS/- and WT (right), from 3-month-old spinal cord tissue (n=4 for each genotype). Significant (padj<0.1) mouse Fus transcripts are shown by brown open circles, significant human FUS transcripts are shown by blue open triangles, significant non-Fus transcripts are shown by red squares, and other transcripts are shown by red dots (p<0.05) and black dots (p>0.05). **B)** Venn diagram comparing the number of significant non-FUS differentially expressed transcripts between hFUS/hFUS and WT (blue; left) and Fus/- and WT (red; right).*

2.4.5 Homozygous humanised *FUS* mice have little to no overt phenotype up to and including 18 months old

2.4.5.1 Humanised male mice are marginally heavier than wildtype controls, but this difference is not observed in females

The weights of homozygous and heterozygous humanised *FUS* mice were measured longitudinally starting from around six months of age.

Male heterozygous and homozygous humanised *FUS* mice were heavier than wildtype controls. This was seen at the earliest timepoint recorded and homozygous

mice were marginally but significantly heavier until the penultimate timepoint recorded. In heterozygous mice this difference was only significant until around 10 months of age (Figure 2.7A).

Interestingly, no difference in weights was recorded at any timepoint in the female humanised *FUS* mice (Figure 2.7B).

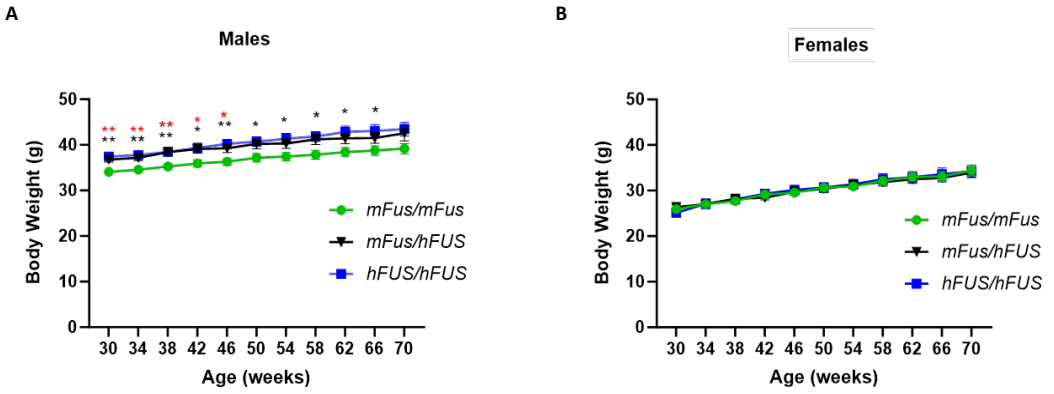


Figure 2.7: hFUS/hFUS male mice are significantly heavier than wildtype controls. *Mice were weighed every three weeks from six months old by ward staff.* ***A)*** *Weights of male hFUS/hFUS, mFus/hFUS and wildtype mice.* ***B)*** *Weights of hFUS/hFUS, mFus/hFUS and wildtype female mice. Data are shown as mean average ± SEM with significance analysed using a mixed-effects analysis with Dunnett's multiple comparisons post-hoc test. Black asterisks denote significant differences between mFus/mFus and hFUS/hFUS mice. Red asterisks denote significant differences between mFus/mFus and mFus/hFUS mice. *=p<0.05, **=p<0.01.*

2.4.5.2 Humanised FUS mice of both sexes have no overt motor phenotype

To examine the effect humanising the *FUS* gene had on motor function, homozygous humanised, heterozygous humanised and wild type control mice were put through an extensive motor phenotyping pipeline. As will be discussed in chapter

3, homozygous humanised *FUS* mice are important controls for when studying ALS mutations introduced into the human *FUS* sequence and thus, it was important to fully understand the baseline motor ability of the humanised wildtype mice.

The same mice were assessed longitudinally at 6, 12 and 18 months.

2.4.5.2.1 Grip strength

Grip strength is a test commonly used when assessing the motor ability of a mouse. It involves holding the mouse by the base of the tail and pulling it downwards along a metal ladder which can detect the force the mouse exerts as it grips onto the rungs. The mouse was held so that initially only the forelimbs could grip onto the rungs and forelimb grip strength could be assessed. Next, the mouse was held so all four limbs could grip the ladder, giving a read out of combined fore and hindlimb grip strength.

Grip strength data shows no differences in combined grip strength between wild type mice and homozygous humanised wild type mice of either sex (Figure 2.8B, D). Male mice homozygous for humanised *FUS* showed a 25% increase in forelimb grip strength compared to wildtype controls (Figure 2.8A).

Female mice recorded stronger grip strength readings in both fore and combined grip strength than male mice during this test. Although perhaps unexpected, it was noted that male mice were more lethargic and reluctant to grip onto the grid than female mice, which could explain this observation.

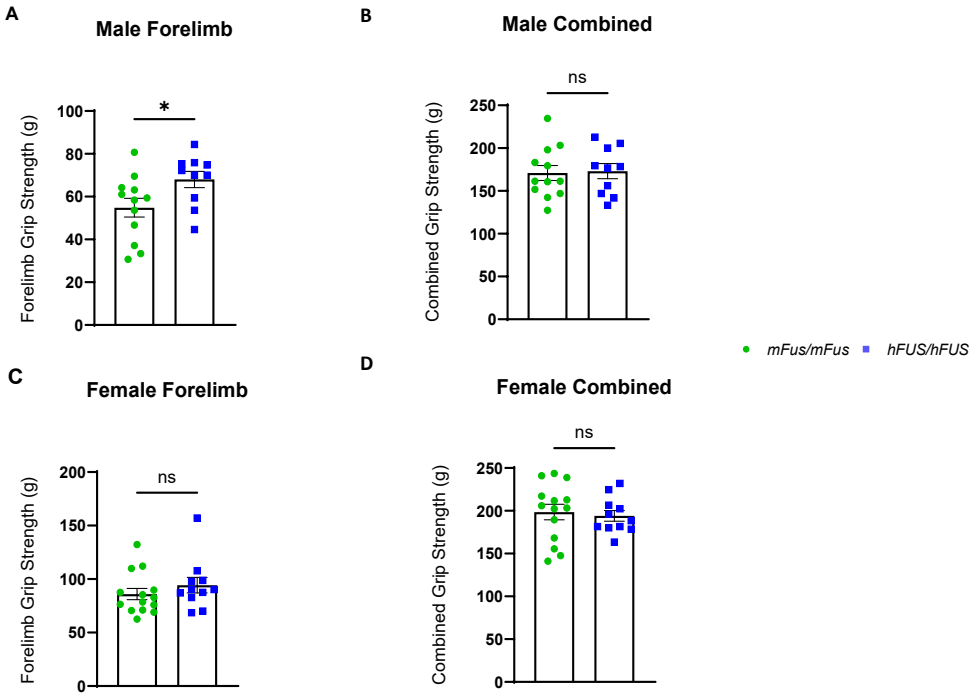


Figure 2.8: Mice homozygous for humanised FUS do not exhibit a change in combined grip strength compared to controls. *The grip strength of fore and hindlimbs was assessed at 18 months for both sexes.* ***A)*** *Male humanised FUS mice exhibited a small but significant increase in forelimb grip strength compared to controls.* ***B)*** *Males homozygous for humanised FUS showed no change in combined grip strength compared to wildtype controls.* ***C)*** *Female mice homozygous for humanised FUS showed no change in forelimb grip strength compared to control mice at 18 months.* ***D)*** *Females homozygous for humanised FUS showed no change in combined grip strength compared to wildtype controls. Data are shown as mean average ± SEM with significance analysed using an unpaired T test. ns = not significant, *=p<0.05.*

2.4.5.2.2 Locotronic

The locotronic test equipment comprises of a narrow corridor with rungs for the mouse to walk along. The walls of the corridor contain lasers which detect if a mouse's paw breaks the plane indicating the foot has fallen through the rungs. This test is used as an indication of a mouse's coordination and ability to navigate walking along an uneven surface.

The software produces a variety of readouts including front limb errors, hindlimb errors and crossing time. The software cannot always tell if a mouse is facing forwards or backwards and therefore, error readout split by front and hindlimbs could

be misleading. To counteract this, data is displayed as total leg errors. Whilst mice were completing the locotronic experiment, some mice ran straight across the rungs, and others took more breaks, sometimes turning around and moving back towards the start of the corridor or stopping to clean themselves.

There was no difference in the number of total leg errors for either sex (Figure 2.9A-B). Female mice homozygous for the humanised *FUS* mice trended towards an increase in total leg errors and trended towards an increase in crossing time but this was also not significant ($p= 0.1971$) (Figure 2.9D). Upon further analysis it was found there was a strong positive correlation between crossing time and number of leg errors ($r= 0.5603$, $p<0.0001$) (Figure 2.9E) therefore this trend towards an increase in crossing time could explain the trend towards an increase in leg errors for *hFUS/hFUS* female mice. There was no difference in crossing time in male mice.

The correlation between crossing time and number of leg errors should be considered when drawing conclusions from locotronic data. Those mice which took longer than 30 seconds to cross the ladder were excluded from leg error analysis to try and limit this effect.

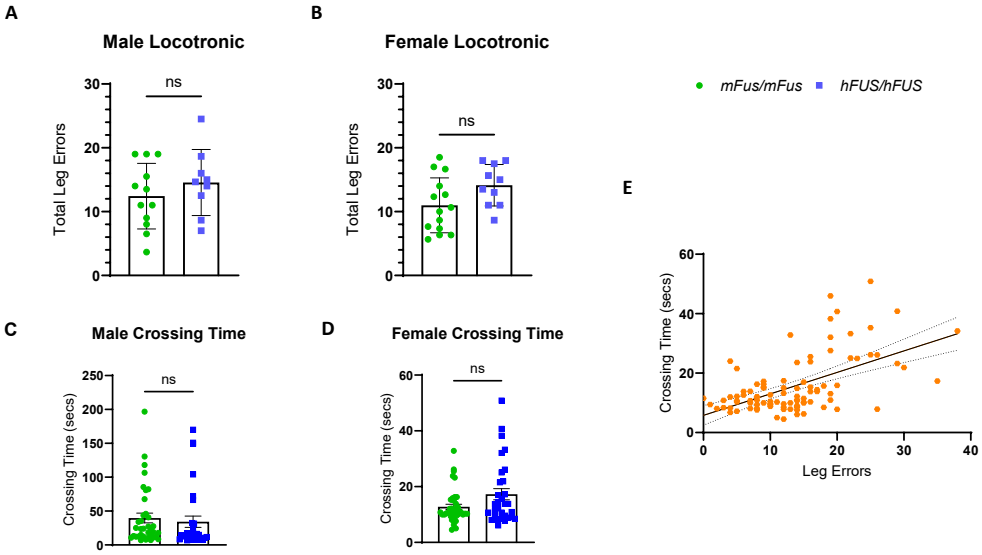


Figure 2.9: Mice homozygous for humanised FUS do not exhibit a change in the number of leg errors produced during the locotronic test. *The number of leg errors when running across the locotronic ladder were recorded at 18 months for both sexes.* ***A)*** *Neither male homozygous humanised FUS mice or* ***B)*** *female homozygous humanised FUS mice produced more leg errors in the locotronic test compared to controls.* ***C)*** *Male mice homozygous for the humanised FUS gene showed no difference in crossing time compared to wildtypes whereas* ***D)*** *Female hFUS/hFUS mice showed no significant difference in crossing time compared to mFus/mFus mice.* ***E)*** *There is a strong positive correlation between the time taken to cross the locotronic ladder and the number of leg errors produced. Data are shown as mean average ± SEM with significance analysed using an unpaired Student's T test or Mann-Whitney non-parametric test for comparing crossing time. ns = not significant, *=p<0.05. The leg error vs crossing time data was analysed using Pearson r correlation, r=0.5603, p<0.0001.*

2.4.5.2.3 Wheel running test

The wheel running motor function test is an in-depth analysis of a mouse's coordination and ability to run on a running wheel, and its motivation to do so. Briefly, mice were singly housed for three weeks in a cage which contained a running wheel which could be used ad libitum. The wheels are connected to a computer which records wheel-activity and produces a variety of read outs including maximum speed of the wheel turning, number of rotations and the time spent on the wheel. After two weeks of habituation, the wheel is exchanged for one with several rungs missing to

present a motor challenge. Phenotypically normal mice are expected to exhibit reduced maximum speeds briefly whilst they learn to navigate the complex wheel, before recovering to their previous maximum speed.

No difference was recorded in the maximum wheel running speed of genomically humanised *FUS* mice of either sex compared to wildtype controls (Figure 2.10A-C).

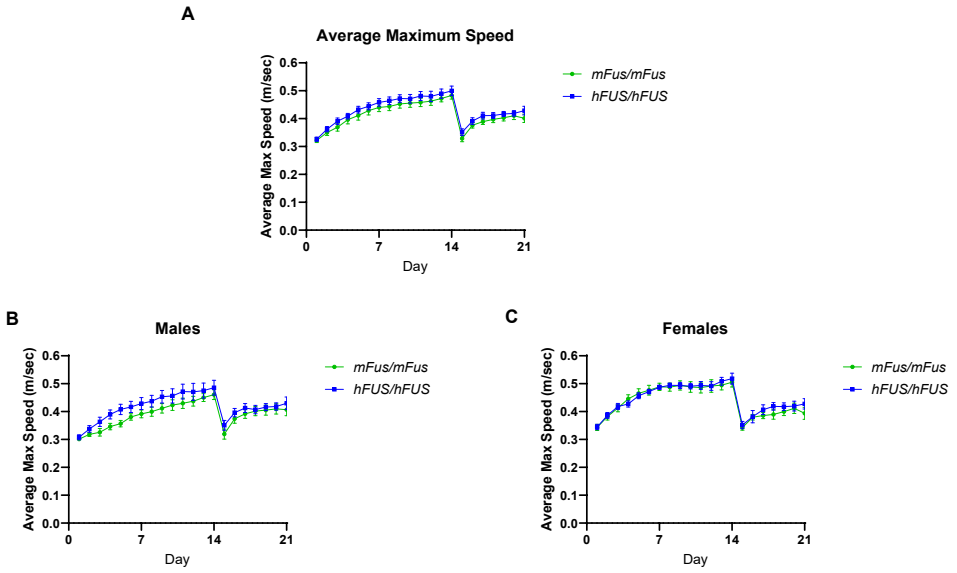


Figure 2.10: Humanised FUS mice have no motor phenotype as shown by the Wheel Running (Motor Function) Test at 18 months. *Homozygous hFUS mice and their wildtype litter and cage mates were put through the wheel running test at 18 months of age.* ***(A)*** *The average maximum speed of the running wheel during the three weeks is shown in the graph. There is no significant difference in the average maximum speed for the humanised FUS mice compared to wildtype litter and cage mates. Both genotypes were equally able to adapt when the wheel was changed at two weeks (n=18 for each genotype at the start of the experiment however some mice were culled as they lost weight in weeks two and three, finished MO with n=11 mFus/mFus and n=14 hFUS/hFUS).* ***(B, C)*** *Average maximum speed of the wheel is shown for each genotype, separated by sex (n=nine for each genotype at the start of the experiment however some mice were culled as they lost weight during weeks two and three, finished MO with n=7 mFus/mFus males and n=8 hFUS/hFUS males and n=4 mFus/mFus females n=6 hFUS/hFUS females). Data are shown as mean average ± SEM with significance analysed using a mixed effects analysis with Šídák's multiple comparisons post-hoc test.*

2.4.6 Despite changes in FUS expression, no change in tibialis anterior muscle morphology is observed in humanised *FUS* mice

Loss of function mutations in *FUS* have been shown to have deleterious effects at the site of skeletal muscle such as loss of endplates and changes in fibre size (G. Picchiarelli et al., 2019). Due to the decrease in protein expression observed in the tibialis anterior muscle of the homozygous humanised *FUS* mice, muscle fibre morphology was assessed.

Sections of tibialis anterior muscles from humanised and wildtype mice were stained using haematoxylin and eosin stain to visualise muscle fibres and nuclei. There were no obvious changes in morphology (Figure 2.11A). A fellow DPhil student, David Thompson, developed an ImageJ plugin which could measure fibre diameter and the percent of fibres with a central nucleus. Myofibres with centrally positioned nuclei are present in many muscle disorders such as ALS and are used as an index of myopathy (Folker & Baylies, 2013). Neither quantitative measure showed any difference between humanised *FUS* mice and wildtype controls however this was a small pilot study with n of only 2 or 3 animals per genotype due to tissue availability at the time of the experiment (Figure 2.11B).

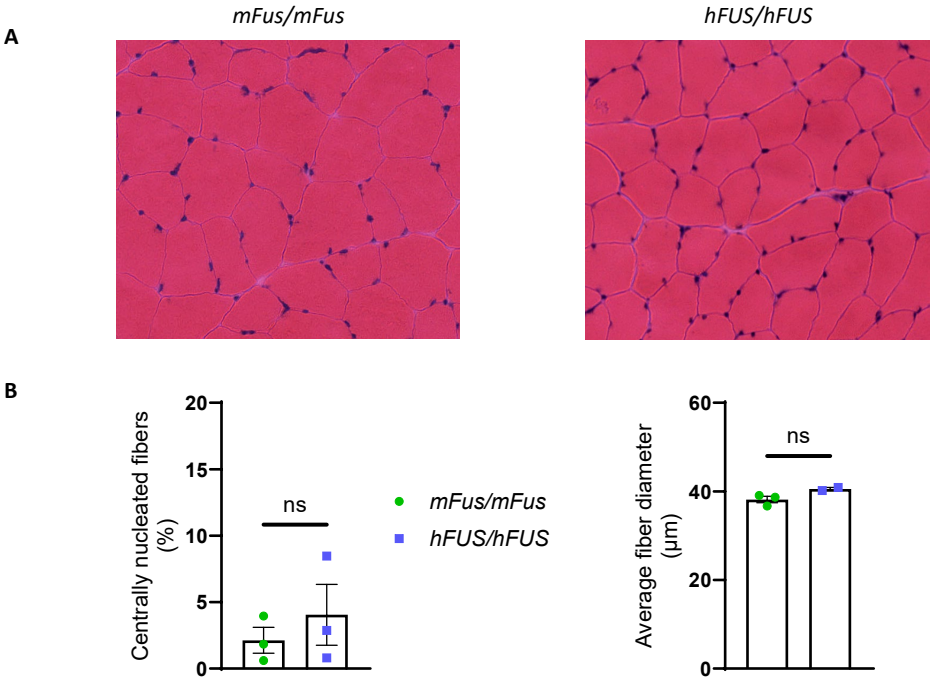


Figure 2.11: Tibialis anterior fibre morphology in hFUS/hFUS mice seems comparable to wildtype mice. ***A)*** *Haematoxylin and eosin staining of tibialis anterior muscle from 18-month-old hFUS mice. Scale bar = 100µm.* ***B)*** *Quantification of fibre size and central nucleation in tibialis anterior muscle from hFUS mice (n=2-3 per genotype). Data are presented as mean average ± SEM with significant analysed using an unpaired Student's t-test. Ns = non-significant.*

2.4.7 Human FUS protein is predominantly located in the nucleus, but is also present in the cytoplasm as mice age

The FUS protein is predominantly localised to the nucleus where it carries out its major role in RNA processing (Lagier-Tourenne et al., 2010). As discussed in chapter 1, FUS is also known to have many emerging roles in the cytoplasm such as at the mitochondria and synapses (Birsa et al., 2020).

Immunofluorescence staining was used to assess FUS localisation within cells of the motor cortex and motor neurons in the ventral horn of the spinal cord, as these areas are relevant in ALS.

Courtesy of staining performed by Dr Remya Nair, a previous post-doctoral researcher in the lab, it was shown that at eight months of age, FUS was predominantly nuclear in cells of the motor cortex in both wildtype controls and homozygous humanised *FUS* mice (Figure 2.12A). I carried out FUS staining on spinal cord sections dissected from 18-month-old mice and saw FUS was both nuclear and cytoplasmic in motor neurons of the ventral spinal cord. This staining pattern was consistent between wildtype and *hFUS/hFUS* mice (Figure 2.12B).

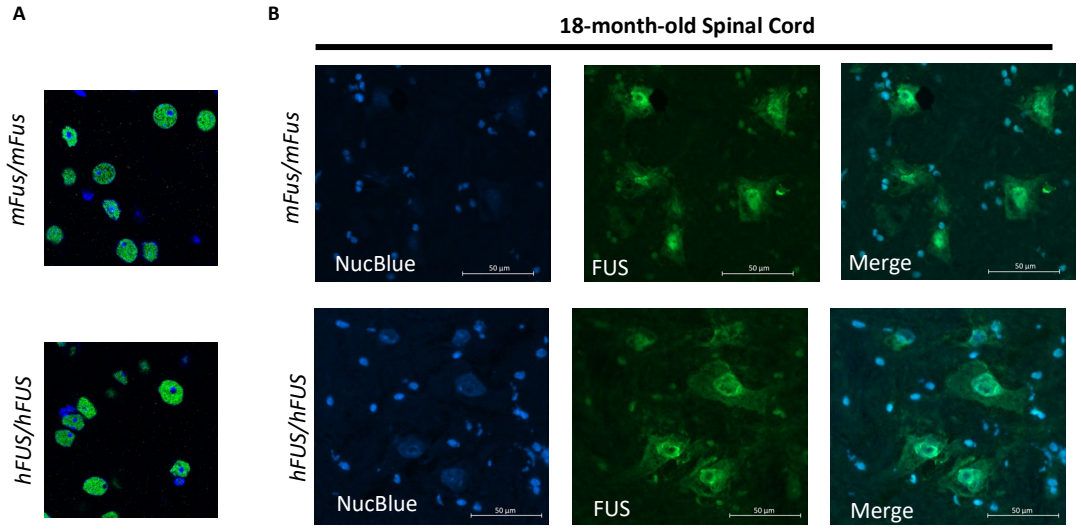


Figure 2.12: FUS cellular localisation in hFUS/hFUS mice is consistent with wildtype mice. *Total FUS staining was carried out using an antibody raised against the C-terminus of the FUS protein, which is conserved between mouse and human FUS.* ***A)*** *Immunofluorescent staining of FUS (green) in 8-month-old motor cortex showing nuclear localisation of FUS in both hFUS/hFUS mice and wildtype controls. Scale bar = 20µm.* ***B)*** *Immunofluorescent staining of FUS (green) in motor neurons of the ventral spinal cord of 18-month-old mice shows FUS is localised to the cytoplasm as well as the nucleus (blue), and the pattern of staining is consistent between homozygous FUS mice and wildtype controls. Scale bar = 50µm.*

2.4.8 Humanisation has no effect on spinal cord motor neuron survival

Motor neuron disease is characterised by the degeneration and loss of motor neurons in the spinal cord. To be a valid control for humanised FUS-ALS mice, it was essential to understand if humanising the *FUS* gene had any effect on motor neuron

survival. In addition, it is known motor neurons are vulnerable to FUS expression changes as overexpression of human wildtype FUS alone is sufficient to induce motor neuron degeneration (Ling et al., 2019; Mitchell et al., 2013).

No difference was found between the number of motor neurons in homozygous humanised *FUS* female mice compared to wildtype controls, suggesting humanising the *FUS* gene, and any potential resulting changes in *FUS* expression, are not impacting motor neuron survival to any detectable degree in the spinal cord (Figure 2.13A-C).

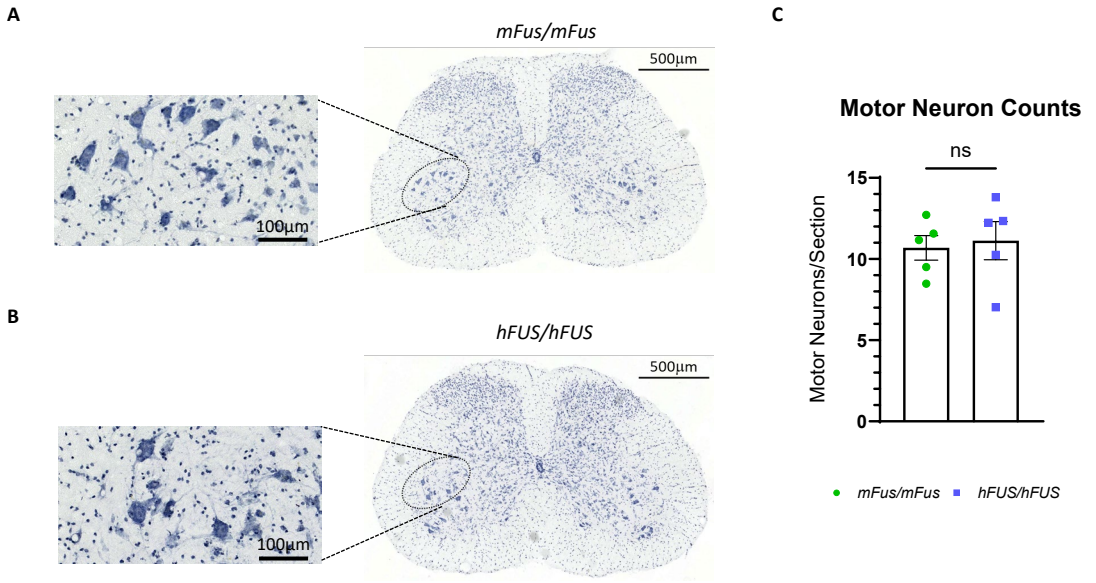


Figure 2.13: Female mice homozygous for the humanised FUS gene have no change in the number of motor neurons in the spinal cord aged 18 months. *Lumbar spinal cord sections were stained with a Nissl stain and the number of motor neurons per section were counted by eye. A motor neuron was included if it had a large cell body, a clear nucleolus, and 3+ dendrites extending from the cell body.* ***A, B)*** *Representative images of lumbar L5 spinal cord sections stained with gallocyanine from 18-month-old wildtype and homozygous humanised FUS mice. The circle indicates the location of the ventral pool of motor neurons to be counted.* ***C)*** *The number of motor neurons were quantified, and no difference was found between hFUS/hFUS and wildtype mice. Data are shown as mean average ± SEM with significance analysed using an unpaired T test. Ns = not significant.*

2.5 Discussion

Advances in the field of genetics have enabled scientists to generate more sophisticated targeted knock-in mouse models of human disease, in the hope these more faithfully replicate the genetic landscape of human disease. The work described in this chapter extensively characterises one such knock-in, whereby the mouse *Fus* gene has been replaced by the full-length human sequence at the endogenous locus, under the control of the endogenous mouse *Fus* promoter. In this study, the aim was to characterise the humanised *FUS* knock-in model to see if human *FUS* could functionally replace mouse *Fus*. This was a necessary first step to justify introducing disease-causing ALS mutations into the humanised *FUS* allele, and ultimately using the homozygous humanised wildtype mice as baseline 'wildtype' controls in future experiments.

2.5.1 Expression of human FUS can functionally replace mouse FUS

Genomically humanised *FUS* mice survive in homozygosity showing that the human *FUS* gene can functionally replace the mouse *Fus* gene at the endogenous loci both during development and throughout adult life as there was no difference in survival of fully humanised *FUS* mice. This confirms other reports whereby crossing *Fus*$^{-/-}$ mice with transgenic mice expressing human *FUS* mostly rescued the loss of function *FUS* phenotype (Ling et al., 2019). Reduction in *Fus* expression is known to cause sterility in male mice (Kuroda, 2000) so it was important to understand if humanising the *FUS* gene had an effect on breeding and fertility, particularly given the slight decreases in *FUS* expression seen at the level of mRNA and protein. There was

no evidence of sterility in the humanised *FUS* cohort which bred successfully to generate cohorts for longitudinal analysis.

2.5.2 Genomically humanised mice exhibit modest reductions in *FUS* expression at the RNA and protein level

The mild reduction in *FUS* expression at the RNA and protein level seen in some of the tissue analysed was interesting. Generally, the pattern of *FUS* (RNA and protein) expression was the same between sexes, albeit significant in one sex and not the other. Perhaps more interestingly were the changes in *FUS* expression seen between tissues, at different ages, and the fact RNA and protein expression did not always align.

Expression was analysed in the spinal cord, brain and TA muscle as these tissues are predominantly affected in ALS and it is important to understand baseline *FUS* levels.

RNA expression

At the level of RNA, the brain saw the largest decrease in *FUS* expression in *hFUS/hFUS* mice, followed by the spinal cord, whereas the TA had no significant difference at 18-months. These modest decreases in the human gene expression, which have been observed in other humanised mouse models of ALS genes (Devoy et al., 2021), suggest there may be discrepancies in transcriptional control regions between mouse and human genomes.

It is understood that *FUS* expression is tightly controlled through an auto-regulatory negative feedback loop whereby FUS binds to its own mRNA to cause intron retention and subsequently reduced translation (Humphrey et al., 2020; Zhou et al.,

2013) and this intron retention in *FUS* mRNA is an event which appears to be conserved across species and cell types (McLaughlin, 2023). The increased expression of *FUS* transcripts with intron seven retained in the spinal cord is consistent with the reduction in *FUS* mRNA expression and may suggest human FUS protein has an increased propensity to bind the human *FUS* intron seven sequence versus mouse. There is evidence that intron six- and seven-retained *FUS* is kept within the nucleus suggesting it does not undergo translation, nor nonsense mediated decay, both of which occur in the cytoplasm (McLaughlin, 2023). McLaughlin goes on to propose the shorter half-life of intron retained *FUS* at approximately three hours compared to 10-12 hours of fully/correctly spliced *FUS* (McLaughlin, 2023; Sharova et al., 2009) means it is unlikely to be retained so that splicing into fully spliced *FUS* can occur later if induced, however it cannot be ruled out. Alternatively, McLaughlin hypothesises intron retained *FUS* is slowly degraded within the nucleus suggesting that any event which leads to an increase in the intron retained *FUS* isoforms would decrease total FUS levels, as is seen in the *hFUS/hFUS* mice. Interestingly, McLaughlin also reports a difference in half-life of intron retained *FUS* in different cell types (ventral horn cells vs MEFs) which could suggest this is a mechanism by which to regulate tissue specific *FUS* expression and could go some way to explaining the differences in *hFUS* expression in different tissues in the genomically humanised *FUS* mice.

The human FUS protein which is translated in the *hFUS/hFUS* mice may also be less able to bind regulatory sequences within the mouse genome more generally, although the small number of transcripts altered as measured by RNA sequencing, suggests this is not likely to be a widespread issue. The RNA sequencing depth did not

however allow for analysis of more subtle mis-splicing or un-annotated events which may be occurring.

Protein expression

It has previously been shown that FUS protein expression decreases after post-natal developmental then remains stable in adulthood in C57BL/6 mice, and that there is a different expression pattern in different tissues (C. Huang et al., 2010). This is consistent with what is shown in Figure 2.5B whereby FUS protein expression did not change in wildtype mice from 3 to 18 months of age. Interestingly, there was a decrease in FUS in humanised mice between 3 and 18 months which suggests human FUS expression is differentially regulated as the mice age. This was different to what was seen at the RNA level where there was an increase in *FUS* expression at 18-months versus 3-months in both wildtype controls and *hFUS/hFUS* mice, although to a lesser extent in the latter. There is increasing evidence that transcript levels for many genes are not always indicative of the corresponding protein levels (Liu et al., 2016) and so this may go some way to explaining this difference.

It must also be considered that the reduction in FUS protein quantified may not be because there is less human FUS protein in the tissue, but rather that the FUS antibody is not equally able to bind mouse and human FUS. The antibody used for densitometry was raised against the C-terminus of the FUS protein, mapping to a region between residues 500 and 526, the peptide sequence of which is conserved between mouse and human FUS. This antibody was chosen to try and limit the species difference effect; however, it cannot be guaranteed that conformation of the proteins is similar enough to allow comparative binding of the antibody.

2.5.3 Mice expressing the *hFUS* sequence have no overt motor phenotype up to and including 18-months

The modest changes in expression are well tolerated as evidenced by the fact the homozygous humanised *FUS* mice are overtly phenotypically normal.

Apart from the slight increase in weight of homozygous humanised *FUS* male mice, very few changes were seen in motor-related function of *hFUS/hFUS* mice up to and including 18 months of age. Grip strength data was consistent between *hFUS/hFUS* mice and controls apart from forelimb grip strength measures in which *hFUS/hFUS* male mice had significantly increased strength. In the locotronic test, *hFUS/hFUS* performed as well as control mice. The more intensive wheel running test found no differences between *hFUS/hFUS* mice and wildtype controls of either sex suggesting there was not an issue with co-ordination, motor ability or motivation to use the running wheel.

2.5.4 Despite mild reductions in *FUS* expression, FUS localisation and function in ALS relevant tissue appears to be unaffected

FUS protein was found to be localised to both the nucleus and to a lesser extent the cytoplasm in motor neurons of aged *hFUS/hFUS* and wildtype mice, consistent with reports by others that FUS localisation naturally changes as mice age (C. Huang et al., 2010). Huang and colleagues found evidence of speckled FUS staining in the cytoplasm from sections from mice aged 200 and 600 days whereas in the humanised *FUS* mice and wildtype controls, FUS protein appeared to be more diffuse within the cytoplasm, with no evidence of speckles. In my experience, FUS staining required a lot of optimisation therefore these differences in staining could be due to

the way sections were prepared. Huang and colleagues transcardially perfused mice and post fixed tissue with 4% PFA whereas the FUS staining in Figure 2.12 was carried out on tissue which was fixed for 10 minutes in 4% PFA post sectioning. Huang and colleagues also used DAB rather than immunofluorescence antibody staining which is a more sensitive technique. The conclusion remains that increased FUS is localised to the cytoplasm as mice age, without *FUS* mutations, and this molecular behaviour was replicated in the humanised *FUS* mice.

ALS relevant tissues and cell types, such as motor neurons and TA myofibres, are known to be sensitive to FUS expression changes (Mitchell et al., 2013; G. Picchiarelli et al., 2019). Despite the trend towards a reduction in FUS expression in the spinal cord and the significant reduction in FUS protein in the TA, neither motor neuron survival nor gross muscle morphology appeared to be affected; however, it must be noted that muscle morphology data was carried out on tissue from a small number of animals (n of 2 or 3).

In summary, it has been shown from extensive characterisation of the homozygous humanised *FUS* mouse that human FUS can replace mouse FUS with minimal disruption at the transcriptomic, protein, and whole organism level. Whilst modest expression changes are seen, these do not have large, overt effects on ALS relevant molecular and cellular phenotypes such as motor neuron counts, FUS cellular localisation and motor function. As this chapter has shown, the humanised *FUS* mice are not identical to wildtype mice and so are required as the most accurate and valid control for studies looking into humanised *FUS* mice with mutations.

3 Chapter 3: Characterising a novel, genomically humanised mouse model of FUS-ALS

3.1 Introduction

In this chapter, the *FUS*^{P525L} point mutation was introduced into exon 15 of the humanised *FUS* allele, using CRISPR/Cas9 endonuclease mediated repair in zygotes. An unbiased characterisation of the phenotype of fully humanised *hFUS/hFUS*^{P525L} mice of both sexes was carried out, with a range of readouts explored.

3.1.1 Why do we need another mouse model of a FUS-NLS mutation?

There are existing models of *FUS* NLS mutations, each with their own advantages and disadvantages as shown in Table 1.1 and discussed in section 1.12. A lot has been learnt about FUS-ALS from these models, however many are traditional transgenics and so given the issues discussed in detail in section 1.6, caution must be employed when drawing conclusions about the effect of the mutation itself in these models. As *FUS* is a dose sensitive gene, this further highlights the importance of physiologically relevant expression of the mutated gene when trying to unpick relevant disease mechanisms. Some of the existing models express the human *FUS* gene and protein, but so far, no fully genomically humanised, targeted *FUS* knock-in mice exist. As increasing evidence emerges about the role of disease and species-specific strains of protein aggregates in many neurodegenerative diseases, including ALS, the need for humanised models will increase. Additionally, as will be discussed in chapter 5, it is becoming clear that different *FUS* mutations have distinct gain of toxic functions, and so more models are needed to better understand the complexity associated with individual *FUS* NLS mutations.

3.1.2 Why was the *FUS*^{P525L} mutation chosen?

Over 30 patients with the *FUS*^{P525L} mutation have been reported in the literature, making it one of the most common *FUS* mutations in ALS (Goldstein et al., 2022; Korobeynikov et al., 2022; Zhou et al., 2020). The *FUS*^{P525L} mutation is also known to cause a particularly aggressive, early onset form of ALS with poor prognosis, with the youngest patient presenting with this *FUS* mutation only 11 years of age (Baumer et al., 2010; Chiò et al., 2009; Conte et al., 2012; Kwiatkowski et al., 2009; Zhou et al., 2020). Clinical cases and their symptoms are summarised by Zhou and colleagues (Zhou et al., 2020).

The autosomal dominant missense mutation means at amino acid position 525 a leucine is added in the place of a proline disrupting the nuclear localisation sequence (NLS) (Figure 3.1). In patient tissue, the disrupted NLS means increased FUS protein is localised to the cytoplasm where it forms aggregates (Baumer et al., 2010; Kwiatkowski et al., 2009; Vance et al., 2009).

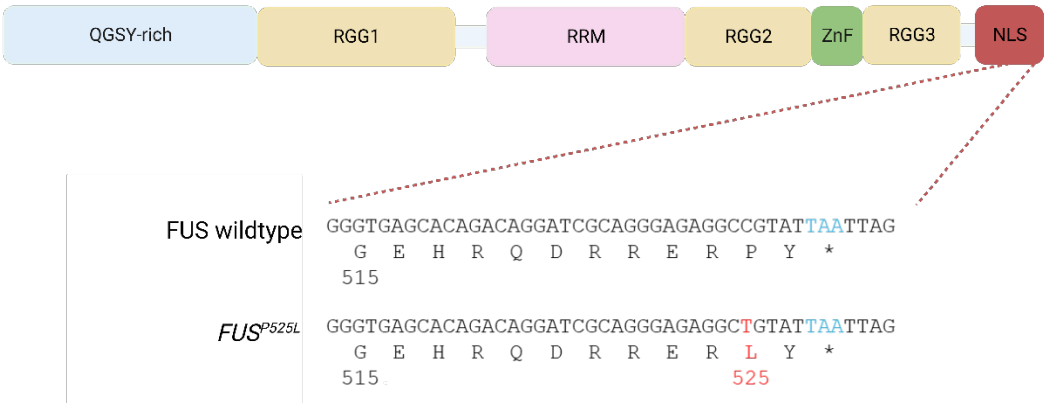


Figure 3.1: P525L mutation in the NLS of the human FUS gene sequence. *Blue letters and asterisk represent a stop codon. Red letters represent the mutated sequence and resulting amino acid. Created with BioRender.com*

The *FUS*^{P525L} mutation was chosen as it was thought that due to the aggressive nature of the disease in ALS patients, there was a higher chance of modelling a rapid disease progression with an early phenotype onset in the much shorter lifespan of the mouse.

During my characterisation of the *hFUS/hFUS*^{P525L} mice, Korobeynikov and colleagues published on a non-humanised heterozygous *mFus*/*mFus*^{P517L} knock-in mouse model (Korobeynikov et al., 2022). The *Fus*^{P517L} mutation is the mouse equivalent of the human *FUS*^{P525L} mutation, as the mouse FUS protein is only 518 amino acids long. In their model, the mutated *Fus*^{P517L} gene is expressed under the control of the endogenous mouse *Fus* promoter. There are interesting similarities and differences between the phenotype of their *Fus*^{P517L} model and our *hFUS/hFUS*^{P525L} mice which will be discussed throughout this chapter.

3.2 Aims and hypotheses

Hypotheses:

1) Based on what is observed in other targeted knock-in FUS-ALS models, a mild phenotype is expected, likely modelling the early stages of disease.
2) Increased FUS protein will be localised to the cytoplasm, leading to both gain and loss of function mechanisms of disease.
3) Cellular and molecular changes will manifest in an outward motor phenotype, like is seen in patients, which will progress as the mice age.

Aims:

a) Characterise humanised *hFUS/hFUS*^{P525L} knock-in mice longitudinally

- Expression of the humanised gene:
    - mRNA and protein expression.
- Assess cognitive function
    - Open field, social dominance tube test, Y maze, marble burying.
- Assess motor function:
    - Grip strength, locotronic, wheel running test, muscle electrophysiology.
- Is there differential gene expression due to the presence of the *hFUS*^{P525L} mutation?
    - RNA sequencing of 14-week-old spinal cord tissue and tibialis anterior tissue.
- Histological analysis:
    - Motor neuron counts, FUS staining, aggregate staining, muscle fibre morphology.

3.3 Contributions

Prior to my DPhil, the genome engineering work was carried out to generate the mice used in this project. Dr. Anny Devoy engineered the humanised constructs in Prof Elizabeth Fisher's lab at UCL. The introduction of the P525L mutation and gene targeting in embryonic stem cells was done by the cellular and molecular group at MRC Harwell.

The staff on ward five are acknowledged for their hard work to support and maintain the mouse colonies used in this chapter, including weighing the mice every three weeks.

Members of the mouse models of neurodegeneration lab helped to perform some of the phenotyping tests in this chapter including Dr Charlotte Tibbit who performed the grip strength experiments, and Dr Zeinab Ali who carried out the male 6-month echoMRI experiment.

David Thomspon stained the tibialis anterior muscles used for fibre typing in section 3.4.10.1.

The histology lab at MRC Harwell performed the serial sectioning of the spinal cords used for motor neuron counts in this chapter.

The necropsy team at MRC Harwell perfused and dissected the spinal cords used for FUS staining in section 3.4.9.

The FUS^{P525L} specific antibody used in section 3.4.9 was designed and generated by Dr Marc-David Ruepp and Dr Anny Devoy at King's College London.

Dr Mhoriam Ahmed carried out the muscle electrophysiology experiments detailed in section 3.4.6.

The phenotyping team at MRC Harwell collected the blood plasma used for neurofilament light chain quantification in section 3.4.11.2.

3.4 Results

3.4.1 Generation of humanised h*FUS/hFUS*^{P525L} mice

To generate the humanised *hFUS/hFUS*^{P525L} mice, targeted CRISPR/Cas9 gene editing was carried out in mouse zygotes from the fully humanised *FUS* mice described in chapter 2. Briefly and as detailed in Figure 3.2A, a mix of Cas9 mRNA, a small guide RNA and ssODN (the sequences of which are detailed in section 7.2.4.2) were injected into the pronucleus of one-cell-stage homozygous humanised *FUS* embryos. The injected zygotes were then implanted into pseudo pregnant female mice and the F0 progeny genotyped using Sanger sequencing. Correctly edited F0 animals were then crossed to C57BL/6J for one generation and the *hFUS*^{P525L} allele was confirmed at the F1 stage. Successfully generated *hFUS*^{P525L} mice were then backcrossed to C57BL/6J mice for at least 5-10 generations.

Two point mutations were introduced into the *FUS* sequence, the first a C to T substitution meaning a leucine amino acid is coded for in the place of a proline at position 525 producing the *FUS*^{P525L} mutation. An additional silent mutation at amino acid position 526 was introduced to aid with genotyping (Figure 3.2B).

To generate cohorts, first *mFus/hFUS*^{P525L} mice on the C57BL/6J background were crossed with *hFUS/hFUS* mice (also on the C57BL/6J background). To maintain the line and produce experimental cohorts, fully humanised *hFUS/hFUS* mice were crossed with *hFUS/hFUS*^{P525L} mice.

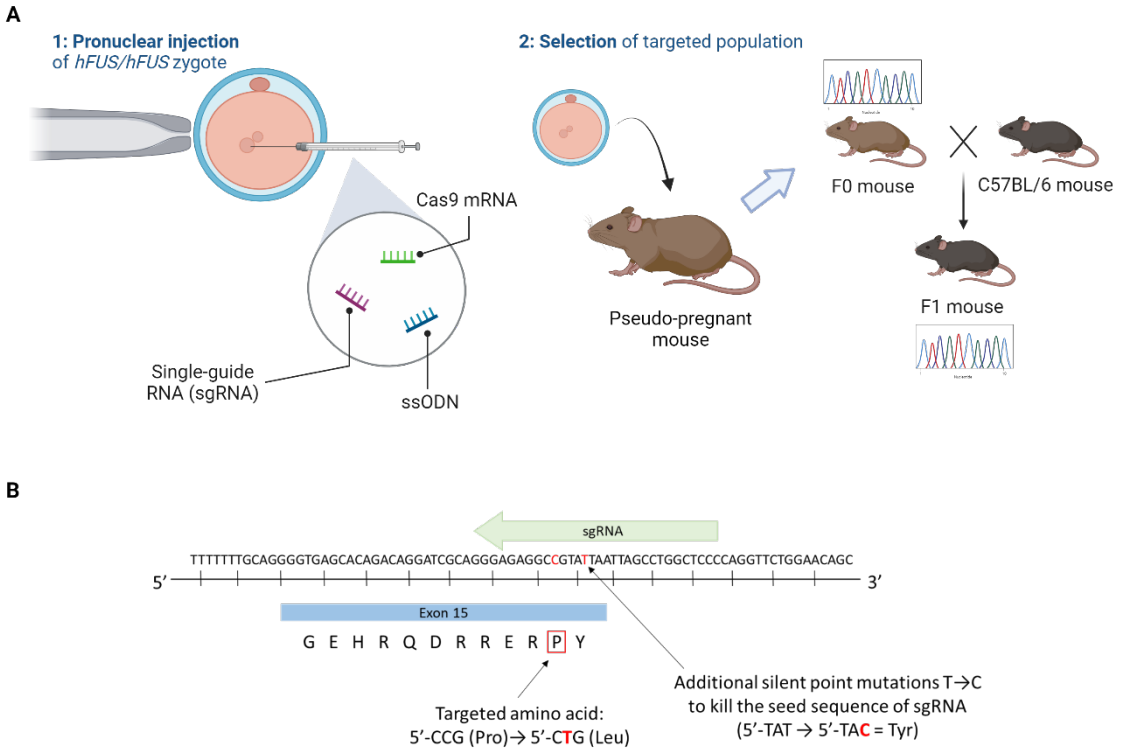


Figure 3.2: Generation of the hFUS/hFUS^{P525L} mice. A) *Depicts the steps to introduce the P525L mutation into the humanised FUS sequence using CRSIPR Cas9 techniques.* ***B)*** *Shows the FUS exon 15 sequence which is targeted and where the sgRNA binds. Created with BioRender.com.*

3.4.2 Expression of the *hFUS^{P525L}* mutation reduces survival and likely reduces fertility

3.4.2.1 Male hFUS/ hFUS^{P525L} mice have significantly reduced survival rates

Overall, the sex split of cohort mice was 53% male and 47% female (Figure 3.3A). 43.1% of mice that reached weaning age and could be genotyped were heterozygous for the *hFUS^{P525L}* mutation, lower than the 50% expected from the breeding strategy to generate the cohort, suggesting that expression of the *hFUS^{P525L}* mutation leads to marginal sub-viability in the mice (Figure 3.3B).

hFUS^{P525L}/hFUS^{P525L} mice were embryonic lethal and when dissected at day E18.5, were much smaller than *mFus/mFus* embryos (Figure 3.3C).

To assess whether expression of the humanised *hFUS*^{P525L} mutation led to a decrease in lifetime survival, a survival analysis was completed. All deaths were recorded as an event unless mice were culled for fighting related injuries or for scheduled cohort dissections.

Overall survival of mice heterozygous for the *hFUS*^{P525L} mutation was modestly but significantly reduced from around three weeks of age (Figure 3.3D, p=0.0015). When the data was split by sex, this difference was driven by a reduced survival in male mutant mice (Figure 3.3E, p=0.0017) as females showed no significant difference in survival rates (Figure 3.3F, p=0.42).

To understand what was causing male mutant mice to be die prematurely, a search through welfare records was carried out. The main cause of death was issues relating to malocclusion. This led to mice being unable to eat, losing weight and becoming generally unwell leading to welfare culls. Additionally, seven mice were found dead aged between 23 and 84 days old. Two of the mice had masses in their intestines, and several had issues with wound healing. One male and one female mouse were culled with hydrocephalus and two mice had abnormal gaits and head tilts.

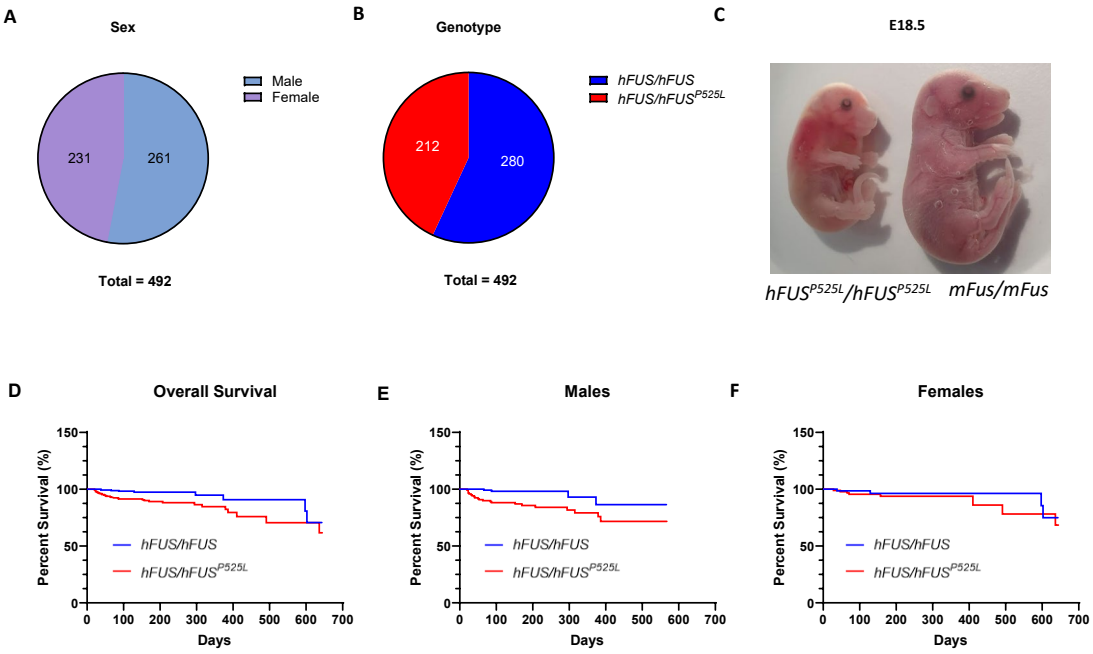


Figure 3.3: Heterozygous humanised FUS^{P525L} mice have decreased survival compared to humanised wildtype FUS mice. A) *The sex split of cohort mice.* ***B)*** *The genotype split of cohort mice.* ***C)*** *Representative image of hFUS^{P525L}/hFUS^{P525L} and mFus/mFus embryo aged E18.5.**D)** Survival of heterozygous humanised FUS^{P525L} mice (both sexes combined) is significantly decreased (p=0.0015) compared to homozygous humanised FUS wildtype mice as shown by a Kaplan-Meier survival graph. When separated by sex, this decrease in survival is seen to be due to a reduction in the survival of **E)** male mutant mice (p=0.0017) whereas there is no significant difference in survival of **F)** female mutant mice (p=0.42). Data are shown as percent survival at a specific timepoint (days after birth) and significance was calculated using the Log-rank (Mantel-Cox) test.*

3.4.2.2 There is a malocclusion phenotype in heterozygous hFUS^{P525L} mice

Malocclusion is a dental disorder caused by the improper alignment of teeth. Rodent teeth grow throughout their lifetime and when the top and bottom front teeth align, they are naturally worn down and maintain a healthy size. If the jaw is misaligned, the incisors do not contact one another and thus become overgrown. This leads to welfare issues whereby the mouse struggles to eat and loses weight, with teeth having to be regularly clipped to prevent this occurring. C57BL/6J mice naturally have a malocclusion incidence of around 0.05% (The Jackson Laboratory, 2016).

Malocclusion was observed in 3.3% of heterozygous *hFUS*^{P525L} female mice, with a 2.5 times greater incidence of 8.3% observed in males. Malocclusion was observed at a much lower rate in the humanised *hFUS/hFUS* wildtype mice with no females displaying this phenotype and only 0.7% of male mice.

3.4.2.3 There was a low incidence of seizures in the cohort, with both wildtype and hFUS^{P525L} mice affected

Of all the mice born and studied in this cohort, only three were observed having seizures. All three mice were male, two *hFUS/hFUS* mice and one *hFUS/hFUS*^{P525L} mouse. Seizure behaviour was described as excessive or repetitive grooming, jerky movements, abnormal jaw movements (chomping or gasping), and saliva coming from the mouth. All seizures lasted <10 seconds and the mouse fully recovered within one hour. Interestingly, all three mice had multiple seizures, two or three in total over several days. The seizures occurred when being handled and so it is assumed they were brought on by stress. Additional mice may have had seizures whilst in their home cages which were not observed.

3.4.3 *hFUS/hFUS^{P525L}* mice have a mild cognitive deficit

3.4.3.1 Male mice aged six months old have a hyperactivity phenotype seen during open field assessments

The open field test was used to assess both motor and anxiety-like phenotypes displayed by the cohort longitudinally as cognitive defects are seen in other *FUS* NLS mutant mouse models (Scekic-Zahirovic et al., 2021).

Male *hFUS/hFUS^{P525L}* mice showed no anxiety-like phenotypes in open field as there was no difference in the time these mice spent exploring the centre of the open field arena (Figure 3.4A). Male mice did however exhibit a hyperactivity phenotype at 6 months as evidenced by the significant increase in distance travelled (Figure 3.4B, p= 0.0427). This trend continued at the later timepoints but was not significant (p= 0.0569 and p= 0.1223 respectively).

In female mice, the phenotype was different. At 18 months old, *hFUS/hFUS^{P525L}* mice spent significantly longer in the centre of the arena than wildtype controls (Figure 3.4B, p=0.0023). *hFUS/hFUS* female mice spent significantly less time in the centre as they got older; mean average 221.2 seconds aged 6 months compared to 120.5 seconds aged 18 months (p= 0.0121) whereas the time spent in the centre did not change between the timepoints in the *hFUS/hFUS^{P525L}* mice which could suggest a deficit in long-term memory. The female mice did not exhibit the hyperactivity phenotype seen in males (Figure 3.4D).

There was no difference in vertical episode counts for either sex at any timepoint studied (Figure 3.4E-F).

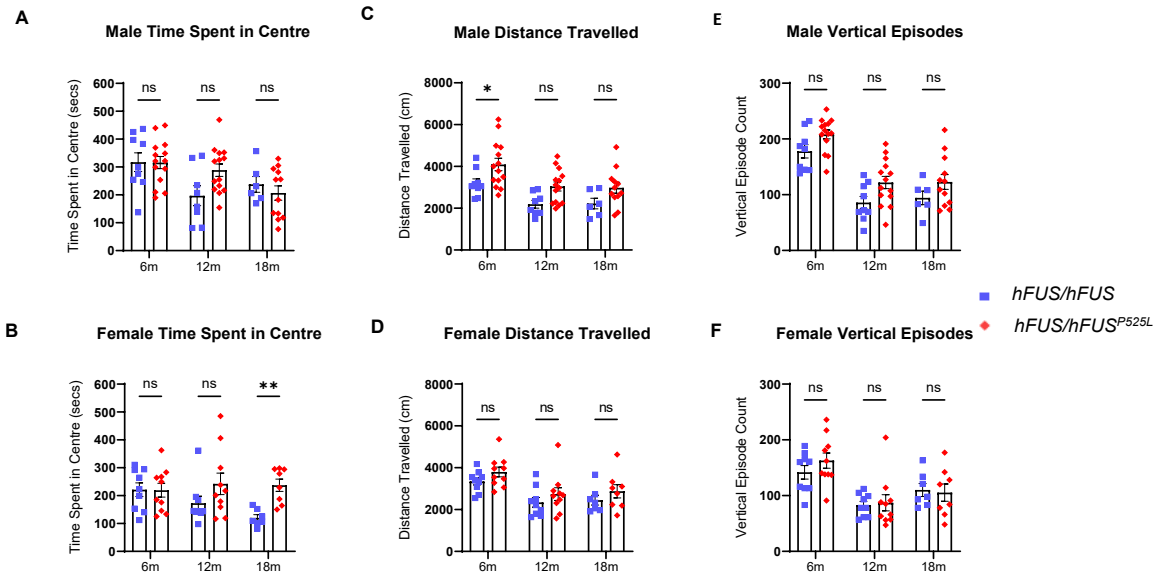


Figure 3.4: Mutant hFUS^{P525L} mice were not more anxious than hFUS/hFUS mice. *Mice were assessed longitudinally using open field to study anxiety-like phenotypes and additional motor parameters.* ***A,B)*** *Time spent in the centre of the arena is used as a read out of anxiety behaviour. No differences were seen in either sex until 18 months of age when female hFUS/hFUS^{P525L} mice spent more time in the centre than controls.* ***C,D)*** *Male hFUS/hFUS^{P525L} mice travelled further than controls aged 6 months but there were no significant differences at any other timepoints in either sex.* ***E,F)*** *There were no significant differences in vertical episode counts at any timepoint studied. Data are shown as mean average ± SEM with significance analysed using a mixed-effects analysis with Šídák's multiple comparisons post-hoc test. ns=not significant, *=p<0.05, **=p<0.01.*

3.4.3.2 Mice expressing the hFUS^{P525L} mutation may be less socially dominant than hFUS/hFUS mice

A lot of fighting between males was recorded in this cohort, with several mice lost due to fight wounds, and the ward staff noting an increased aggression when handling the mice. The tube dominance test was carried out on male mice aged 21 months to see which of the genotypes, if either, were more dominant.

Interestingly, the *hFUS/hFUS* mice appeared to be more dominant, winning 68% of interactions (data not shown).

3.4.3.3 *hFUS/hFUS^{P525L} mice aged six months do not have a spatial working memory deficit*

Y maze is a technique commonly used to assess spatial working memory in mice, which requires input from neurons within the hippocampus (Kraeuter et al., 2019).

Mice aged 6 months were trained with one arm closed off and then the time spent exploring the novel arm was calculated. No differences were observed for mice of either sex (Figure 3.5A-B).

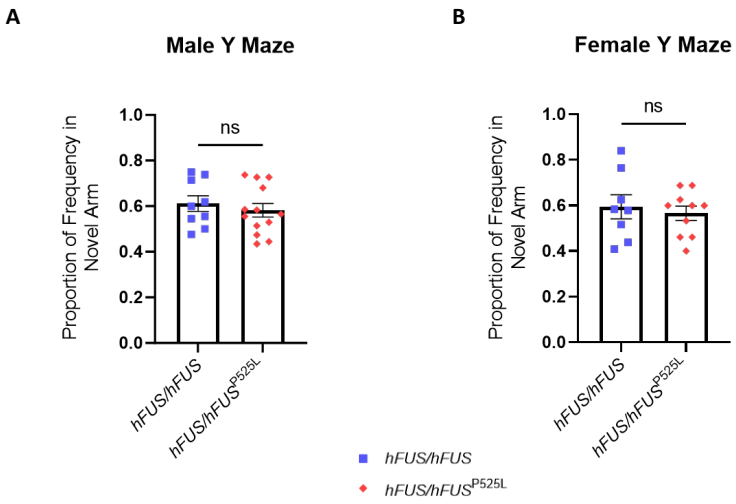


Figure 3.5: hFUS/hFUS^{P525L} mice aged 6 months do not have a spatial working memory deficit. *Mice were put through the Y maze experiment aged 6 months. Mice were trained with one arm blocked and the proportion of time spent in the novel arm recorded. There were no differences compared to controls in **A)** male or **B)** female mice. Data are shown as mean average ± SEM with significance analysed using an Unpaired T test. ns=not significant.*

3.4.3.4 *Marble burying data does not show an overall issue with wellbeing in hFUS^{P5252L} mice*

Marble burying is an innate mouse behaviour which requires motivation and can be a crude read out of wellbeing and apathy (Keszycki et al., 2023). The marble

burying test involves placing nine marbles in a repeated pattern then giving the mouse 30 minutes to interact with the marbles, after which the number of marbles buried, partially buried, moved, or ignored are quantified.

Mutant *hFUS*^{P525L} mice of neither sex showed a difference in marble burying behaviour compared to controls aged 18 months old, although there was a trend towards a decrease in marbles fully buried (Figure 3.6, p=0.1062 in males and p=0.0509 in females).

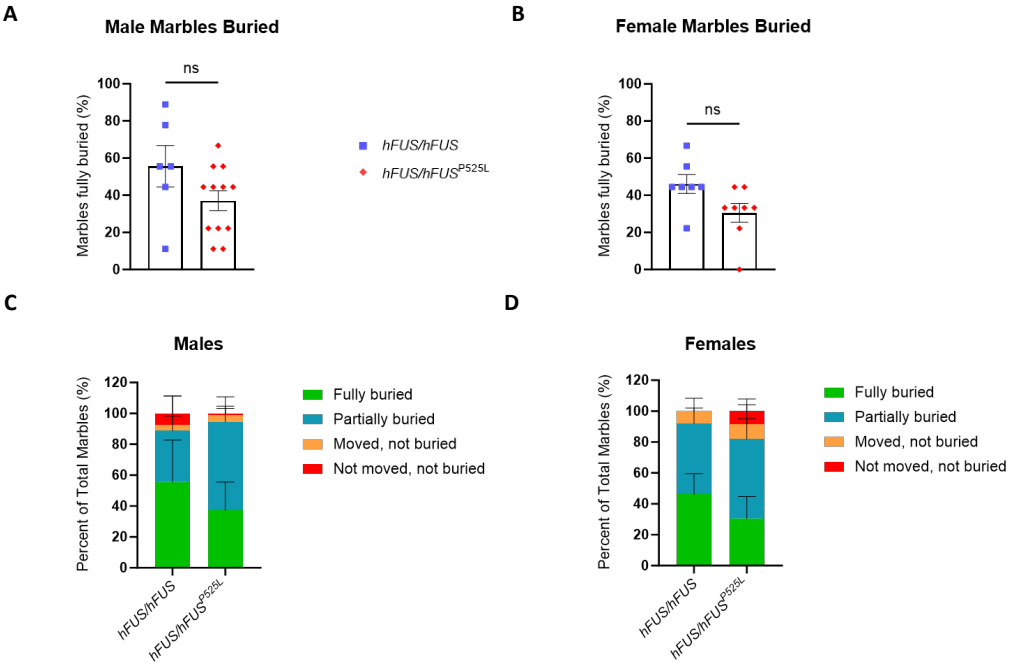


Figure 3.6: Neither male nor female mice display a marble burying deficit at 18 months. *Mice were placed into individual cages with nine marbles evenly spaced apart. After 30 minutes, the location of the nine marbles was observed. Marbles were considered fully buried if ≥2/3*^{rds} *of the marble was buried.* ***A,B)*** *The percent of marbles fully buried after 30 minutes was quantified and analysed. No differences in number of marbles fully buried were observed at any timepoint for male or female mice with expressing the hFUS*^{P525L} *mutation.* ***C,D)*** *The fate of all nine marbles is shown in graphs C and D. Data are shown as mean average ± SEM with significance analysed using an Unpaired T test. ns = not significant.*

3.4.4 Heterozygous expression of *hFUS*^{P525L} is sufficient to cause a metabolism phenotype in mice of both sexes

3.4.4.1 Mice expressing the hFUS^{P525L} *mutation are smaller than wildtype controls*

The weight of cohort mice was recorded every four weeks. Mice of both sexes gained weight; however, *hFUS/hFUS*^{P525L} mice were smaller than controls. *hFUS/hFUS*^{P525L} male mice were significantly smaller than controls at the earliest timepoint studied aged eight weeks and this difference remained significant until around 40 weeks except for one reading at 20 weeks old (Figure 3.7A). Aged 56 weeks, *hFUS/hFUS*^{P525L} male mice were significantly smaller; around 30% lighter than control mice. Weight differences between 40 and 68 weeks were all approaching significance (p=0.0501-0.0968).

Female *hFUS/hFUS*^{P525L} mice were only significantly smaller aged 12 and 88 weeks, although they trended towards this at all ages recorded (Figure 3.7B).

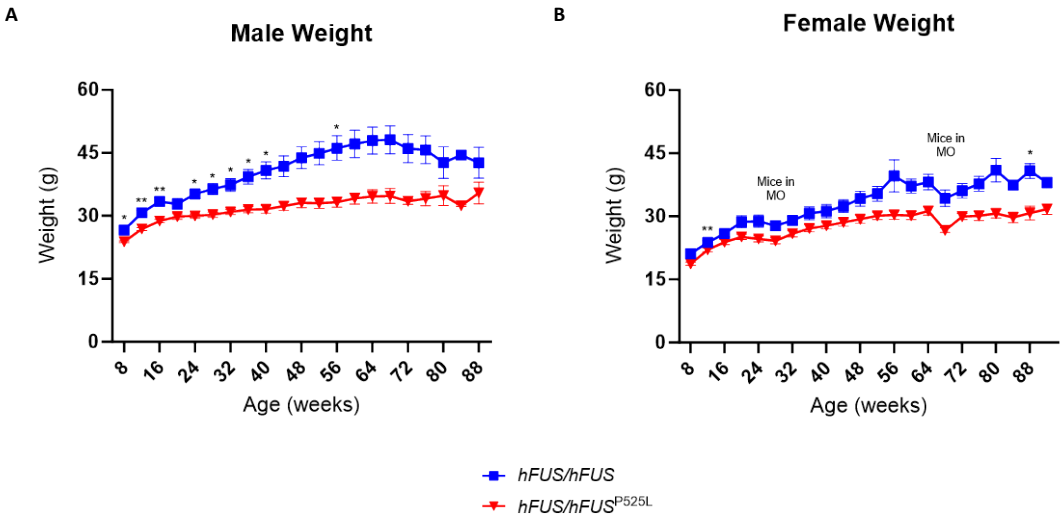


Figure 3.7: Male and female mice heterozygous for the hFUS^{P525L} mutation are smaller than wildtype controls. A) *Weight change in males was assessed.* ***B)*** *Weight change in females was assessed. Female cohort mice were put through the motor wheel-running test aged 6 and 12 months explaining the weight loss during this time. Data are shown as mean average ± SEM with significance analysed using a mixed-effects analysis with Šídák's multiple comparisons post-hoc test.*

3.4.4.2 Mice expressing the hFUS^{P525L} mutation have an altered metabolic composition as shown by EchoMRI

Body composition of *hFUS/hFUS^{P525L}* mice and controls was assessed using echoMRI which assesses body fat, lean weight, free water, and total mass of live animals using the principle of nuclear magnetic resonance (NMR).

Both male and female mice heterozygous for the *hFUS^{P525L}* mutation were significantly smaller than controls at all timepoints studied using echoMRI (Figure 3.8A-B). This is comparable to what was seen when mice were weighed longitudinally whereby *hFUS/hFUS^{P525L}* mice were smaller, albeit the difference not always statistically significant.

Male mice had an additional reading at 6 months as a colleague, Dr Zeinab Ali, carried out and included this 6-month data in her study of metabolism.

In male *hFUS/hFUS*^{P525L} mice, the reduction in weight was coming in part from a reduction in fat mass as this made up a significantly smaller proportion of their total mass compared to controls; 18.42% versus 27.8% in controls (Figure 3.8C). At 12 and 18 months, the *hFUS/hFUS*^{P525L} mice had a mild but significant increase in lean mass as a percent of total mass, around 10% more than controls (Figure 3.8E, p=0.0110 and 0.0113 respectively).

There was no difference in the composition of fat or lean mass in *hFUS/hFUS*^{P525L} female mice despite them being around 20% smaller than humanised controls (Figure 3.8B, D, F).

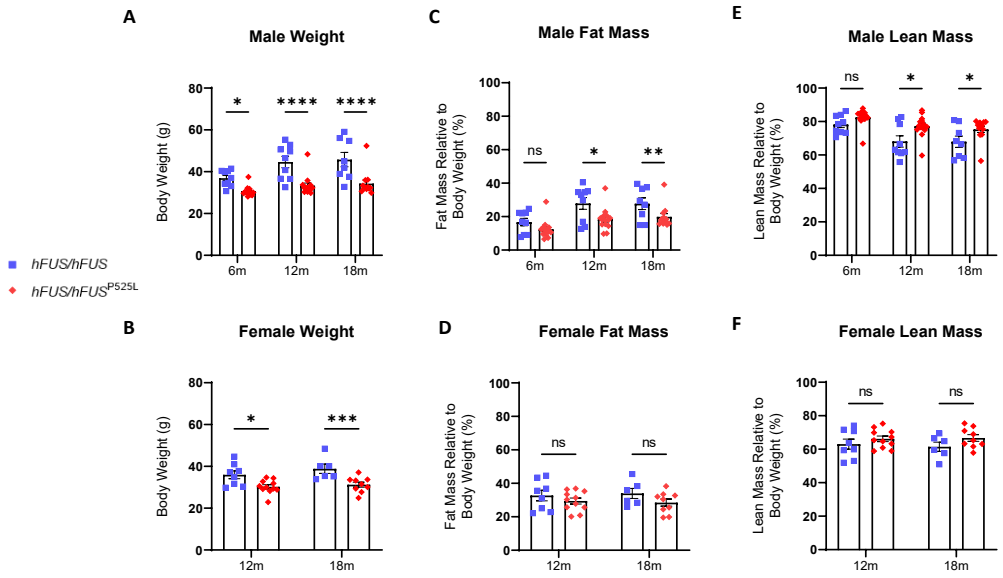


Figure 3.8: Mutant hFUS/hFUS^{P525L} mice of both sexes are smaller than wildtype controls, however only male mice heterozygous for hFUS^{P525L} show changes in fat and muscle composition. *Mice were assessed longitudinally using echoMRI, a technique which can assess fat and muscle composition of live mice.* ***A,B)*** *Both male and female mice heterozygous for the hFUS^{P525L} mutation were significantly smaller at all timepoints studied.* ***C,D)*** *Male hFUS/hFUS^{P525L} mice had a lower percent fat mass relative to body weight compared to wildtype controls, which was significant at 12 and 18 months. This reduction was not seen in mutant females.* ***E,F)*** *hFUS/hFUS^{P525L} male mice had a significantly higher lean mass than controls at 12 and 18 months old. This difference was not seen in females. Data are shown as mean average ± SEM with significance analysed using a mixed-effects analysis with Šídák's multiple comparisons post-hoc test. ns=not significant, *=p<0.05, **=p<0.01, ***=p<0.001, ****=p<0.0001.*

3.4.5 Male *hFUS/hFUS^{P525L}* mice have a mild motor phenotype

3.4.5.1 Male mice heterozygous for the hFUS^{P525L} mutation have a late-onset, degenerative grip strength phenotype

Grip strength was used to assess muscle strength in *hFUS/hFUS^{P525L}* mice longitudinally. Male mice heterozygous for the *hFUS^{P525L}* mutation developed a grip strength phenotype aged 12 months when mice had a 20% reduction in grip strength compared to controls (p= 0.0012). This muscle weakness progressed until the final time-point studied aged 18 months (Figure 3.9A).

No significant difference in grip strength was recorded in female mice at any timepoint studied (Figure 3.9B). Despite post-hoc tests at individual timepoints finding no significant differences, there was a trend towards female *hFUS/hFUS*^{P525L} mice having a reduction in grip strength compared to *hFUS/hFUS* mice. A mixed effect analysis comparing genotypes confirmed this trend and approached significance (p=0.0528).

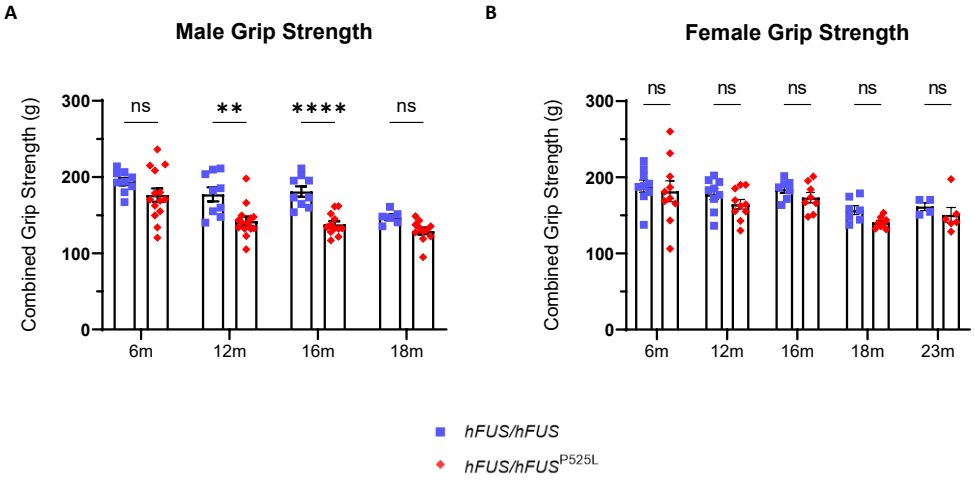


Figure 3.9: Males heterozygous for the hFUS^{P525L} mutation have a progressive, late onset reduction in muscle strength. *The combined grip strength of fore and hindlimbs was assessed longitudinally in a cohort of mice.* ***A)*** *Males heterozygous for the hFUS^{P525L} mutation demonstrated a decrease in combined grip strength by 12 months of age which progressed until the final timepoint studied at 18 months.* ***B)*** *Female hFUS/hFUS^{P525L} mice were also assessed longitudinally and no significant difference in grip strength was observed at any timepoint. Data are shown as mean average ± SEM with significance analysed using a mixed-effects analysis with Šídák's multiple comparisons post-hoc test. ns=not significant, **=p<0.01, ****=p<0.0001.*

3.4.5.2 *Male hFUS/hFUS^{P525L} mice exhibited fewer leg errors than control mice, but also crossed the ladder quicker during the locotronic test*

On the locotronic ladder, male mice heterozygous for the *hFUS^{P525L}* mutation exhibited significantly fewer leg errors than wildtype controls at all timepoints assessed (Figure 3.10A). Interestingly, at 6 and 12 months the *hFUS^{P525L}* mice also travelled across the ladder significantly faster than controls which could indicate a hyperactivity phenotype. If mice stop during the locotronic test to explore their surroundings, this can inflate the number of errors read as the paws sit between the rungs which are subsequently called as errors. There is a strong positive correlation between crossing time and leg errors (Figure 3.10E, r=0.66, p <0.0001). As the *hFUS/hFUS^{P525L}* mice cross the ladder significantly faster, this may explain why they had fewer leg errors detected.

In female mice, there was no difference in the number of leg errors or crossing time at any individual timepoints assessed but there was a trend towards a reduction in both parameters in *hFUS/hFUS^{P525L}* mice compared to *hFUS/hFUS mice*. When comparing genotypes using a two-way ANOVA there was a significant difference between genotypes (p= 0.0366 for leg errors, p= 0.0398 for crossing time) (Figure 3.10B, D).

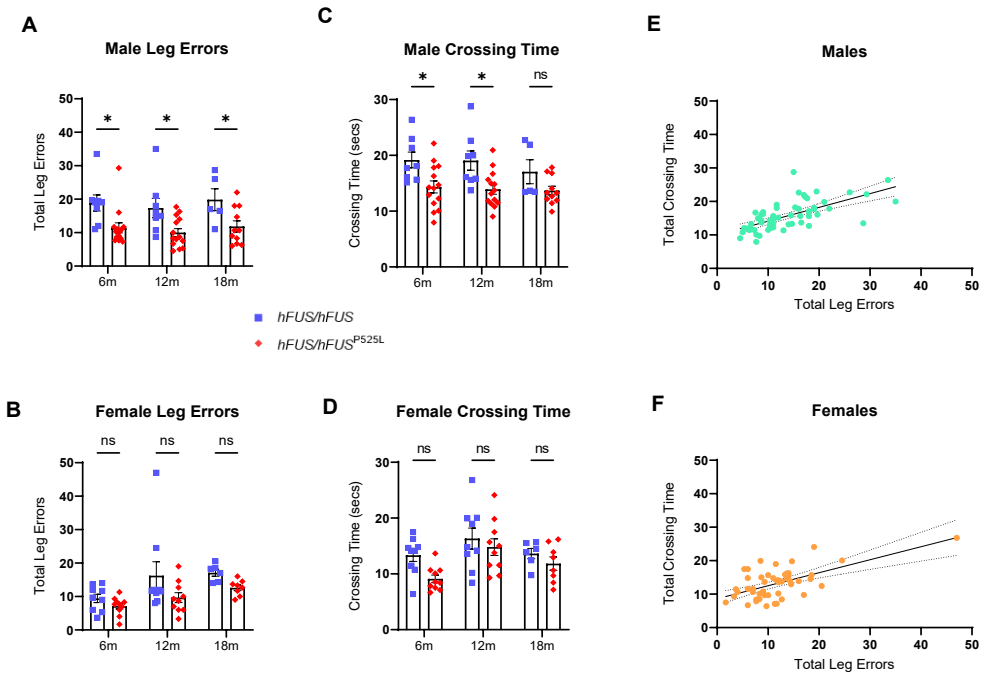


Figure 3.10: Male mice heterozygous for the hFUS^{P525L} mutation demonstrated fewer leg errors, but also ran across the ladder faster than control mice.. *The locotronic ladder uses lasers to quantify the number of times a mouse's paw falls through a ladder rung, recorded as a leg error.* ***A,B)*** *Male mice expressing the hFUS^{P525L} mutation exhibited significantly more leg errors than wildtype controls. The humanised mutant female mice showed no difference in the number of leg errors compared to wildtype mice.* ***C,D)*** *Crossing time was also analysed. Male mice expressing the hFUS^{P525L} mutation crossed the locotronic ladder significantly quicker than wildtype mice. There was no significant difference in crossing time with females expressing the FUS mutation. Data are shown as mean average ± SEM with significance analysed using a two-way ANOVA analysis with Šídák's multiple comparisons post-hoc test. ns=not significant, *=p<0.05.* ***E,F)*** *The number of leg errors vs crossing time was plotted. For male mice, the r value was 0.66 with a p vale of <0.0001. For female mice, the r value was 0.60 with a p value of <0.0001.*

3.4.5.3 Rotarod shows hFUS/hFUS^{P525L} mice are able to hold on for longer than hFUS/hFUS mice

Rotarod was used as a measure of motor co-ordination and balance. There was no difference in the time mice spent on the rotating rod in male mice at any individual timepoints, however a mixed-effects analysis comparing genotypes showed male *hFUS/hFUS^{P525L}* mice were able to remain on the rod for longer than controls (p= 0.0041) (Figure 3.11A).

In females, *hFUS/hFUS^{P525L}* mice remained on the rotarod for significantly longer than controls at all timepoints studied (Figure 3.11B).

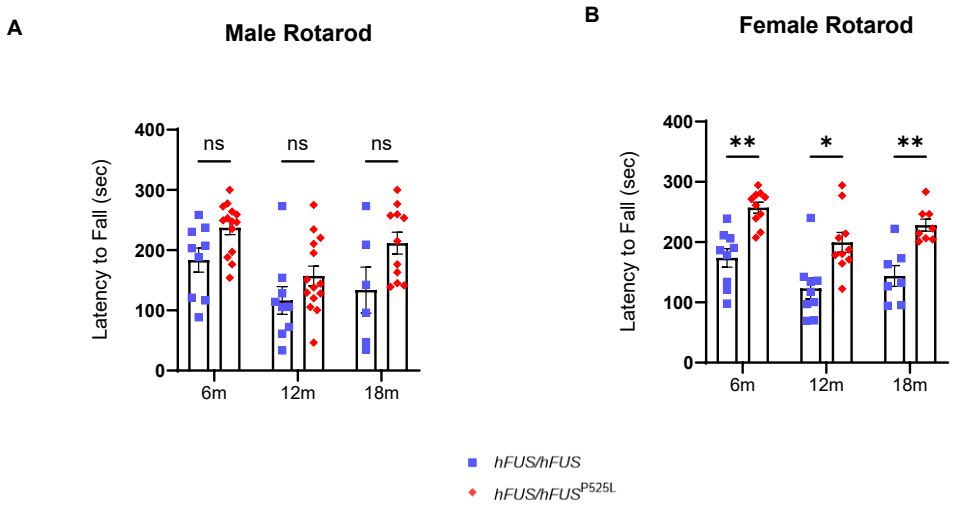


Figure 3.11: Female hFUS^{P525L} mice remained on the rotating tube for significantly longer than hFUS/hFUS controls. ***A)*** *Male mice expressing the hFUS^{P525L} mutation were no different to controls in the rotarod experiment.* ***B)*** *The hFUS/hFUS^{P525L} mutant female mice remained on the rotating tube significantly longer than control mice. Data are shown as mean average ± SEM with significance analysed using a mixed-effects analysis with Šídák's multiple comparisons post-hoc test. ns=not significant, *=p<0.05, **=p<0.01.*

3.4.5.4 The wheel running test showed no difference in motor ability or coordination in hFUS/hFUS^{P525L} female mice

Female mice were analysed using the running wheel test for two weeks at a time aged 6 and 15 months. Males could not be assessed at these timepoints as the test requires mice to be singly housed and males cannot be reintroduced to group cages after two weeks apart due to fighting and subsequent welfare issues.

There were no differences observed in the maximum speed of the running wheel female mice could achieve at any timepoint, even when a complex wheel was

introduced, compared to controls (Figure 3.12A-B). No complex wheel was introduced when mice were aged 15-months as the wheel test system was being upgraded at MRC Harwell and no complex wheels were available at that time.

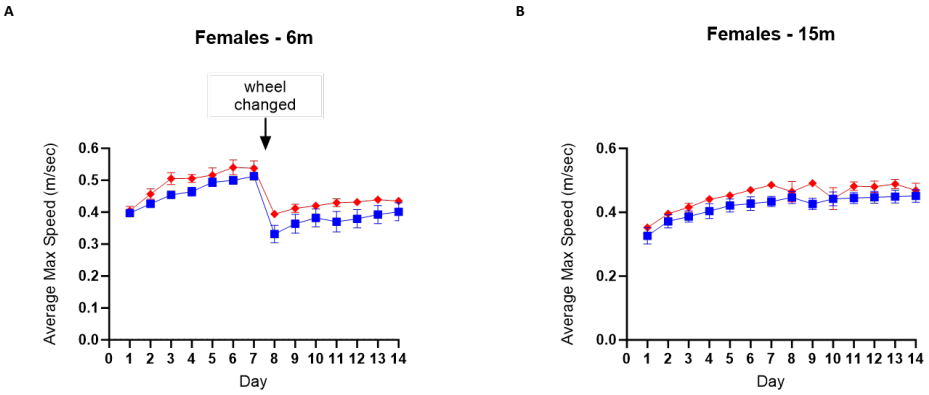


Figure 3.12: The running wheel test showed no significant difference in motor ability or coordination between hFUS/hFUS and hFUS/hFUS^{P525L} female mice. A) *Mice were studied for two weeks aged 6 months and no difference in average max speed of the running wheel was observed, even when the wheel was exchanged for a complex wheel.* ***B)*** *Aged 15 months there was still no difference observed in max speed of the running wheel in female mice. No complex wheel was used in the 15-month experiment. Data are shown as mean average ± SEM with significance analysed using a mixed-effects analysis with Šídák's multiple comparisons post-hoc test.*

3.4.6 Male *hFUS/hFUS^{P525L}* mice may exhibit a unilateral muscle weakness aged 21-months-old

21-month-old male *hFUS/hFUS^{P525L}* mice and wildtype littermate controls were sent to UCL to undergo muscle electrophysiology experiments using published techniques to assess changes in muscle function (Ahmed et al., 2016; Ahmed et al., 2023).

Mice were deeply anaesthetised, and the tibialis anterior (TA) and extensor digitorum longus (EDL) muscles exposed and attached to isometric transducers. The sciatic nerve was also revealed, and electrodes were attached to stimulate the nerve.

Several muscle electrophysiology parameters were assessed including twitch and maximum tetanic force of the TA and EDL, and number of motor units and fatigue resistance in the EDL muscle.

Twitch force is the first measurement recorded for each muscle and is the amplitude of force produced by the muscle after one impulse sent via the electrode, equivalent to one action potential. Maximum tetanic force refers to the maximum force the muscle can generate after being given a series of impulses via the electrodes. This is repeated several times, careful not to fatigue the muscle, and the maximum force recorded is taken.

3.4.6.1 Tibialis anterior muscle readings

In the TA muscle, when comparing the mean average of both legs, there was no difference between the two genotypes in either twitch or maximum tetanic force (Figure 3.13A-B). However, analysis driven by Dr Ahmed found that when the data was split by leg, it produced some interesting trends. In the *hFUS/hFUS*^{P525L} mutant mice, there appears to be a weaker leg. This is also true of humanised control mice, but to a lesser extent. The difference in readings between legs was calculated to reflect this unilateral weakness and both trended towards a larger difference in *hFUS/hFUS*^{P525L} mutant mice, which was significant for maximum tetanic force despite large variation in the data (Figure 3.13E-F).

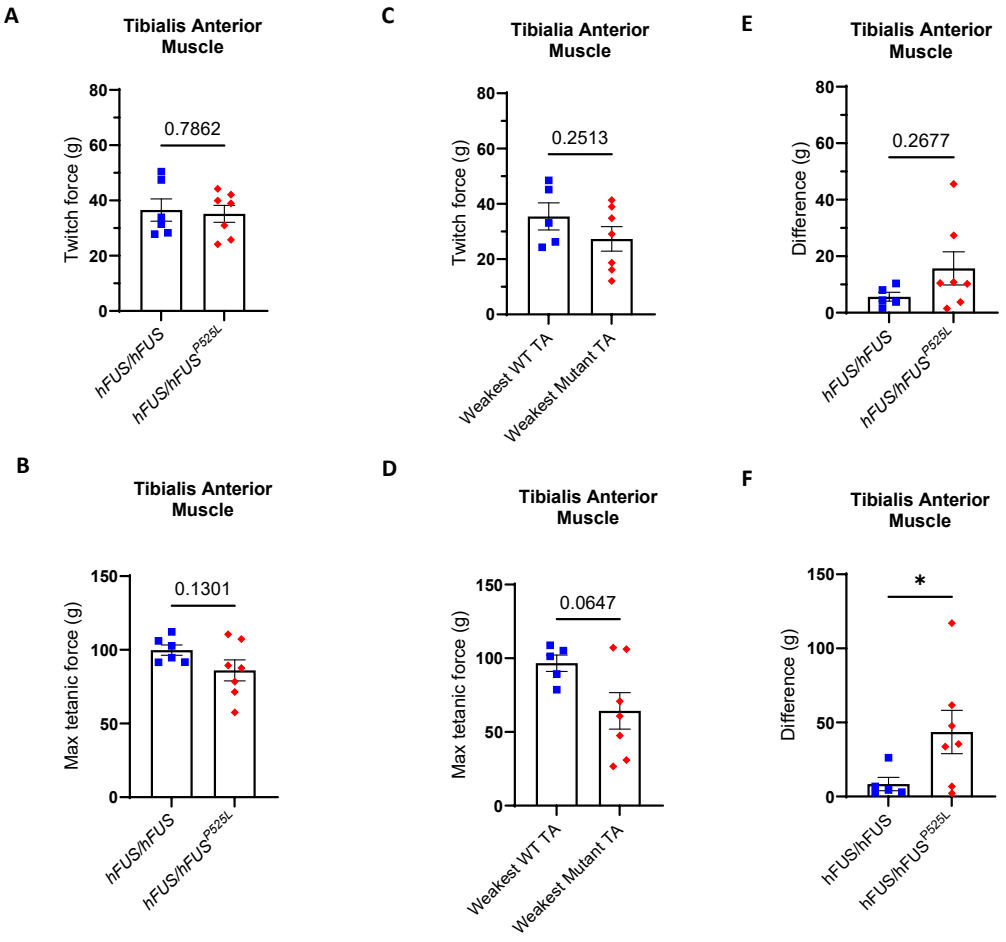


Figure 3.13: Electrophysiology readings trend towards decreased force exerted by the tibialis anterior muscle and this appears to be unilaterally driven. A) *Mean average twitch force and* ***B)*** *maximum tetanic force readings of both legs of hFUS^{P525L} mice and wildtype controls.* ***C)*** *Comparing twitch force and* ***D)*** *maximum tetanic force readings of the weakest leg from FUS mutant mice and controls.* ***E)*** *Comparing the difference in twitch force and* ***F)*** *maximum tetanic force produced by the strongest and weakest leg of mutant mice compared to controls. Data are shown as mean average ± SEM with significance analysed using an Unpaired t test or Mann-Whitney non-parametric test. Ns=not significant, *=p<0.05.*

3.4.6.2 Extensor digitorum longus readings

The same analyses were carried out on the EDL muscles. There was no significant difference recorded when averaging both legs together (Figure 3.14A-B), or when comparing the weakest leg of both genotypes (Figure 3.14C-D).

When comparing legs, both humanised wildtype mice and mutant mice appeared to have an EDL which was able to produce a stronger force than the

alternate leg with no significant difference between the forces exerted by each side likely in part due to variability of the data (Figure 3.14E-F).

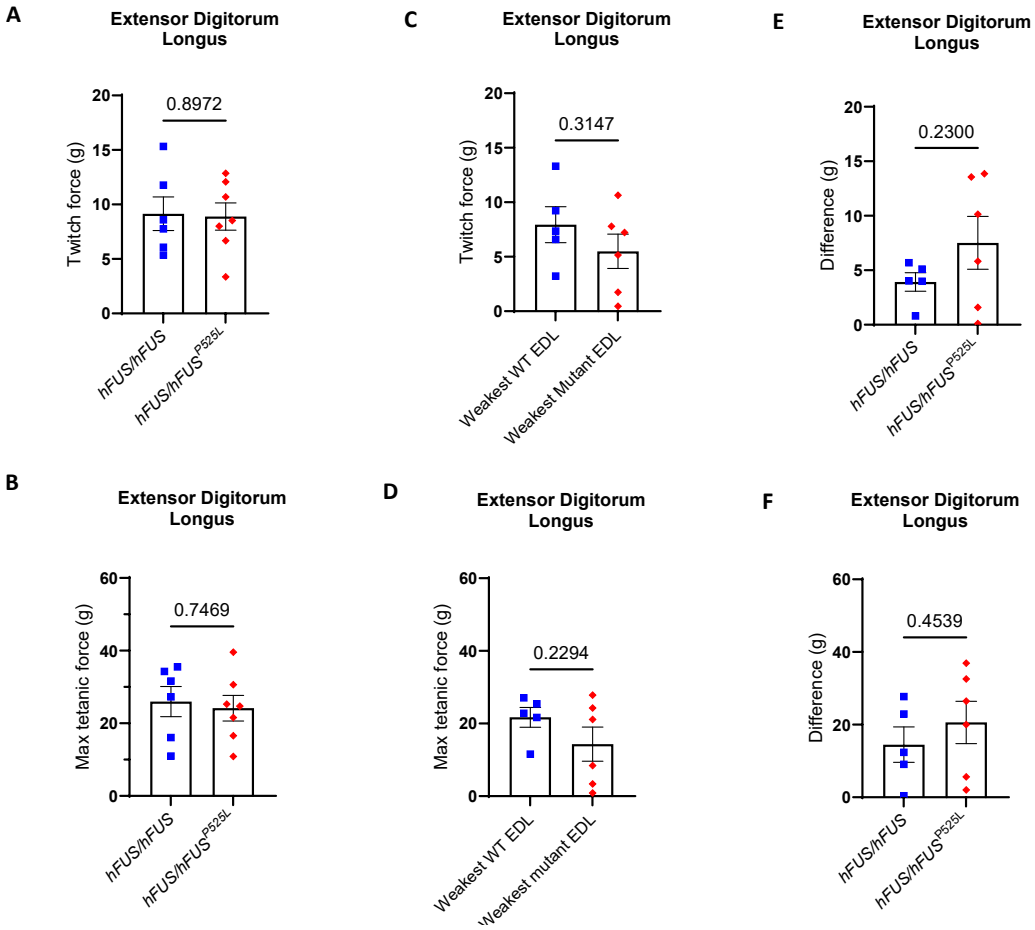


Figure 3.14: Electrophysiology readings trend towards decreased force exerted by the extensor digitorum longus, but this is less apparent than in the TA. A) *Mean average twitch force and* ***B)*** *maximum tetanic force readings of both legs of hFUS^{P525L} mice and wildtype controls.* ***C)*** *Comparing twitch force and* ***D)*** *maximum tetanic force readings of the weakest leg from FUS mutant mice and controls.* ***E)*** *Comparing the difference in twitch force and* ***F)*** *maximum tetanic force produced by the strongest and weakest leg of mutant mice compared to controls. Data are shown as mean average ± SEM with significance analysed using an Unpaired T test. Ns=not significant, *=p<0.05, **=p<0.01.*

The number of motor units can also be quantified by stimulating the EDL muscle with impulses of increasing intensity and measuring the muscle twitch tension recorded. The stepwise increase in muscle twitch tension corresponds to the recruitment of individual motor axons or units which can be quantified.

When the number of motor units was compared between genotypes when taking the average of both legs, there was no significant difference (Figure 3.15A); however, when the legs with the lowest motor unit counts were compared, there was a significant decrease in the *hFUS/hFUS^{P525L}* mice (Figure 3.15B). When the difference between motor unit counts from both legs was compared between genotypes, there was a trend towards *hFUS/hFUS^{P525L}* mice having a larger difference, but this was not significant (Figure 3.15C, p=0.1306).

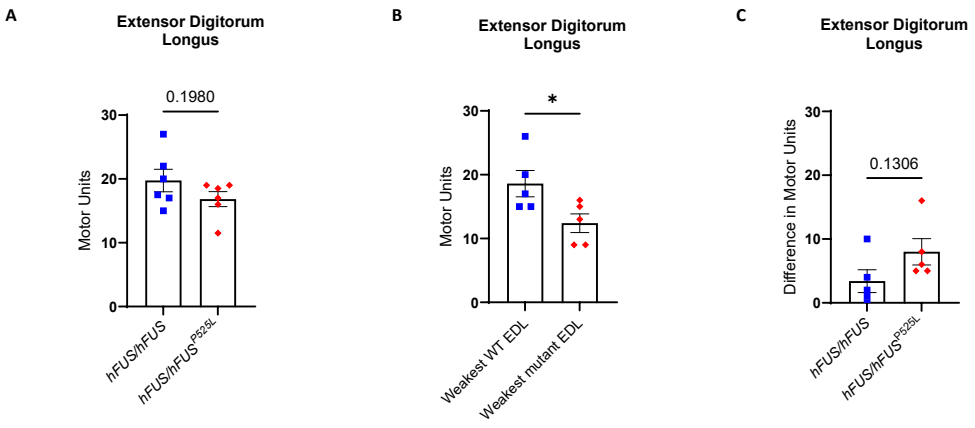


Figure 3.15: Electrophysiology readings suggest the EDL muscle of hFUS^{P525L} mice has fewer motor units than hFUS/hFUS mice, and this may be worse in one leg. A) *Mean average motor unit count of both legs of hFUS^{P525L} mice and wildtype controls.* ***B)*** *Comparing motor unit counts of the leg with the least motor units in FUS mutant mice and controls.* ***C)*** *Comparing the difference in motor unit counts between legs of mutant mice compared to controls. Data are shown as mean average ± SEM with significance analysed using an Unpaired t test. Ns=not significant, *=p<0.05.*

Finally, muscle fatigue can be quantified as this can indicate if there are large differences in the fibre type composition of muscles, some of which are more prone to

fatigue resistance. The muscle is repeatedly stimulated and the difference in force between the first (strongest) and last (weakest) peak is calculated.

No difference in fatigue properties of the EDL muscle were observed in *hFUS/hFUS^{P525L}* mutant mice (Figure 3.16).

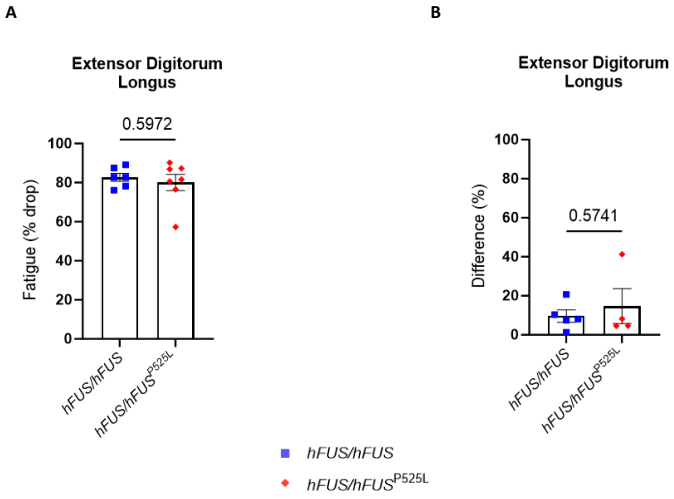


Figure 3.16: Electrophysiology readings showed no difference in EDL muscle fatigue resistance in mutant FUS mice. A) *Mean average fatigue of EDL muscles from both legs of hFUS^{P525L} mice and wildtype controls.* ***B)*** *Comparing fatigue properties found no differences between legs of hFUS^{P525L} and control mice. Data are shown as mean average ± SEM with significance analysed using an Unpaired T test. Ns=not significant.*

3.4.7 *FUS* expression is regulated in a time, tissue and sex specific manner in *hFUS/hFUS^{P525L}* mice

3.4.7.1 FUS RNA expression

FUS expression was assessed at an early and late time-point using quantitative qRT-PCR. Primer pairs were designed to amplify *FUS* mRNA both with and without the *hFUS^{P525L}* mutation.

Focus was given to ALS-relevant tissues such as the spinal cord, brain, and hindlimb muscles. The TA and EDL muscles are predominantly composed of fast-fatigable muscle fibres which are preferentially affected in ALS. The soleus is predominantly made up of slow twitch fibres which are more resistant to ALS.

FUS RNA expression was extensively characterised in tissue from 4-month-old mice of both sexes. Interestingly, expression patterns differed between the sexes. Male mice heterozygous for the *hFUS*^{P525L} mutation had a small but significant increase in *FUS* expression in the spinal cord, TA, and EDL, with the largest expression change seen in the TA, followed closely by the EDL compared to male *hFUS/hFUS* mice (Figure 3.17A,E,G).

In the female *hFUS/hFUS*^{P525L} mice, there was no significant difference in *FUS* expression in the spinal cord or the brain compared to *hFUS/hFUS* mice, although the brain was trending towards a decrease in *FUS* expression (Figure 3.17B,D). As seen in male mice, *hFUS/hFUS*^{P525L} female mice exhibited increased *FUS* expression in the TA muscle, but there were no significant differences in the EDL or soleus compared to *hFUS/hFUS* mice (Figure 3.17F,H,J).

Intron retention differences could not explain the changes in *FUS* expression (Figure 8.3).

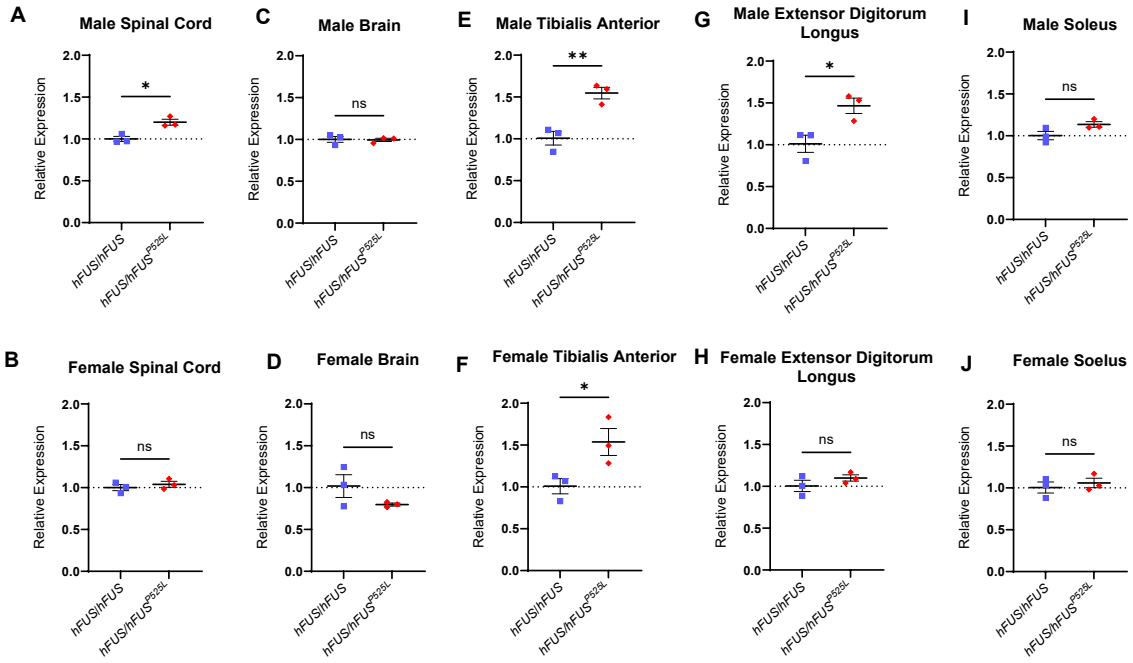


Figure 3.17: Expression of the hFUS^{P525L} mutation causes changes in FUS expression patterns in a tissue and sex specific manner in mice aged 4 months. *Tissue was collected from male and female mice aged 4 months old and total RNA was extracted and FUS expression quantified using qRT-PCR and primers bound regions in exon two and exon four, which amplified both wildtype and mutant FUS. Multiple disease relevant tissues were analysed for both sexes including **A,B)** spinal cord, **C,D)** brain, **E,F)** tibialis anterior, **G,H)** extensor digitorum longus and **I,J)** soleus. Data are shown as mean average ± SEM. Significance was calculated using an Unpaired T Test. ns = not significant, *=p<0.05, **=p<0.01.*

FUS expression was also studied in male mice post-motor symptom onset at the end of the phenotyping pipeline. Expression patterns were mostly consistent with those seen at the earlier timepoint. There was a mild increase in expression in the spinal cord of *hFUS/hUS^{P525L}* mice, but this was no longer significant (Figure 3.18A), and in the TA there was a significant increase in *FUS* expression (Figure 3.18B, p= 0.0468).

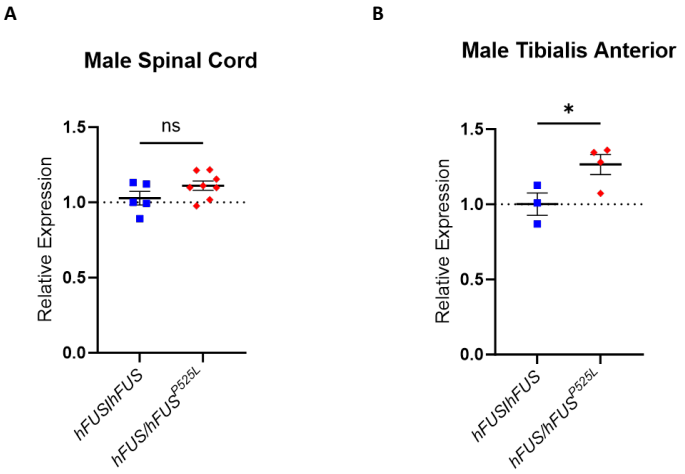


Figure 3.18: FUS RNA expression in 21-month-old male hFUS/hFUS^{P525L} mice. *Tissue was collected from male mice aged 21 months old and total RNA was extracted and FUS expression quantified using qRT-PCR and primers bound regions in exon two and exon four, which amplified both wildtype and mutant FUS. Disease relevant tissues were analysed including **A)** spinal cord, and **B)** tibialis anterior. Data are shown as mean average ± SEM. Significance was calculated using an Unpaired T Test. ns = not significant, *=p<0.05.*

3.4.7.2 FUS protein expression

In addition to *FUS* RNA expression, FUS protein expression was also analysed in male mice post-motor symptom onset**.** Total protein was extracted from the whole tissue sample. To note, there was an insoluble fraction remaining after homogenisation with RIPA buffer from both genotypes.

There was no significant difference in total FUS protein levels in the spinal cord or TA muscle from aged male *hFUS/hFUS^{P525L}* mice compared to controls, although there was a trend towards increased expression in the TA with large variation in the expression values, particularly in *hFUS/hFUS^{P525L}* tissue (Figure 3.19A-B).

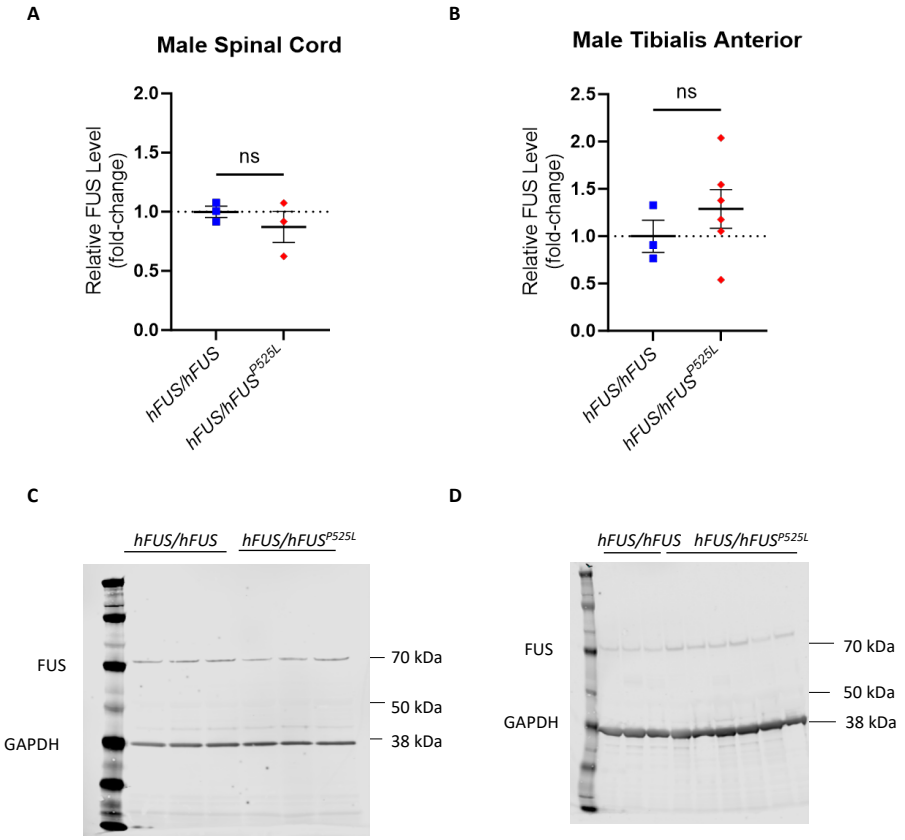


Figure 3.19: FUS protein expression in aged hFUS/hFUS^{P525L} male mice. *Tissue was collected from male mice aged 15-months-old (spinal cord) and 12-months-old (tibialis anterior muscle). Total protein was extracted and FUS expression quantified using a FUS antibody raised against the N-terminus of the FUS protein, which is unaffected by the presence of the P525L amino acid change. Disease relevant tissues were analysed including **A)** spinal cord, and **B)** tibialis anterior. **C,D)** Images of immunoblots used for FUS expression quantification in the spinal cord and tibialis anterior muscle respectively. Data are shown as mean average ± SEM. Significance was calculated using an Unpaired T Test. ns = not significant.*

3.4.8 RNA sequencing in *hFUS/hFUS^{P525L}* mice reveals pre-symptomatic transcriptomic changes, predominantly affecting the tibialis anterior

Spinal cord and tibialis anterior tissue collected from 4-month-old *hFUS/hFUS^{P525L}* mice and controls was sent for bulk RNA sequencing.

PCA plots comparing all four conditions (spinal cord and tibialis anterior tissue in both genotypes) showed that the largest variation came from the tissue type (Figure 3.20). Little variation was found between spinal cord transcriptomic data of the two genotypes. There was however variation between transcript expression from tibialis anterior muscles and genotypes grouped separately, albeit with a large spread in the *hFUS/hFUS^{P525L}* condition.

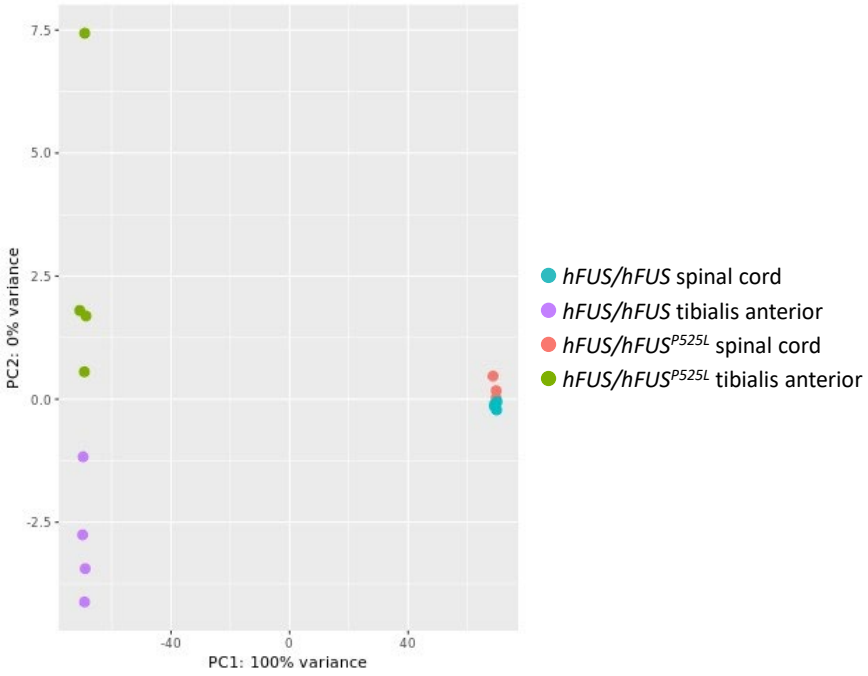


Figure 3.20: PCA plot highlighting variation in RNA sequencing data between tissue type and genotype.

Over five times more transcripts were found to be differentially expressed in the tibialis anterior muscle compared to the spinal cord of *hFUS/hFUS*^{P525L} mice (Figure 3.21C-D).

Transcripts which were up and down regulated in each tissue were assessed for GO terms to try and unpick relevant cellular and molecular pathways which may be affected by the presence of the *hFUS*^{P525L} mutation. A list of transcripts differentially expressed between *hFUS/hFUS* and *hFUS/hFUS*^{P525L} mice (adjp<0.1) is submitted as additional data alongside this thesis.

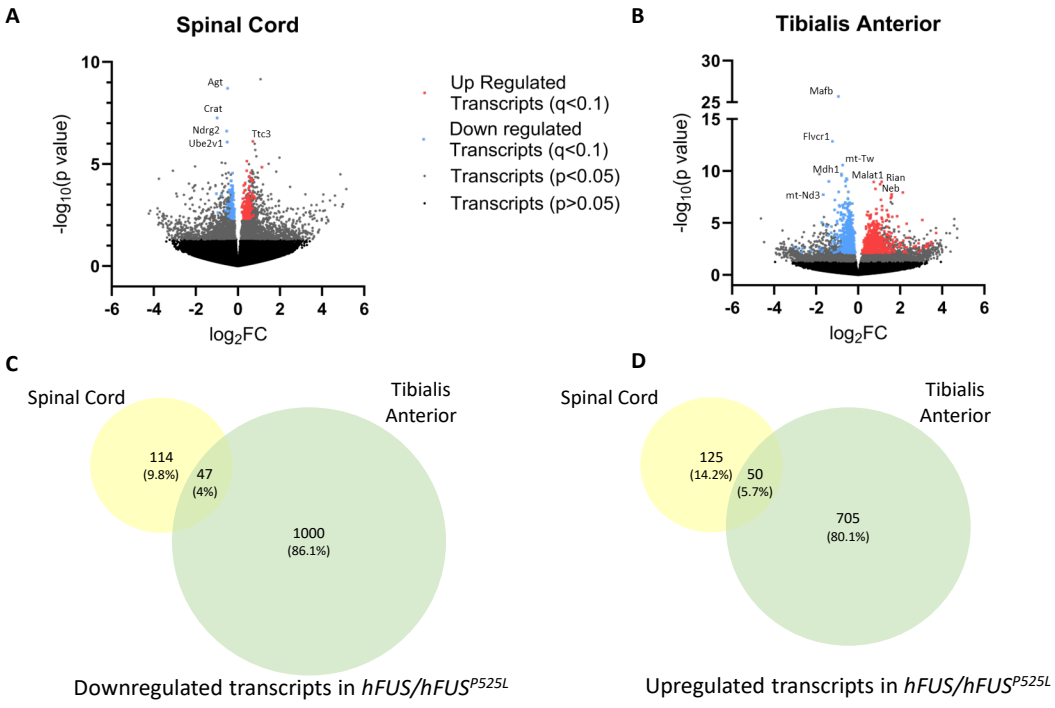


Figure 3.21: RNA sequencing data from spinal cord and tibialis anterior tissue collected from 4-month-old male mice hFUS/hFUS and hFUS/hFUS^{P525L} mice shows increased transcript changes in the tibialis anterior muscle compared to the spinal cord. A) *Volcano plot showing differentially expressed transcripts in the spinal cord of hFUS/hFUS^{P525L} mice compared to hFUS/hFUS mice.* ***B)*** *Volcano plot showing differentially expressed transcripts in the tibialis anterior muscle of hFUS/hFUS^{P525L} mice compared to hFUS/hFUS mice.* ***C)*** *The number of downregulated transcripts in the spinal cord and tibialis anterior muscle.* ***D)*** *The number of upregulated transcripts in the spinal cord and tibialis anterior muscle.*

In the spinal cord, upregulated transcripts were associated with *protein binding, cellular component organisation*, and *nervous system development* amongst others (Figure 8.4). Fewer GO terms were found for the down regulated transcripts, with the *cytoplasmic cellular component* the most significant hit, followed by *organonitrogen compound biosynthetic process*, the *synapse* and *ribosomal dysfunction* (Figure 8.5).

Many more GO terms were found for up and downregulated transcripts in the TA muscle. Upregulated transcripts were associated with *binding*, the *cytoplasm*, *muscle system processing, DNA binding* and *synaptic vesicle recycling* (Figure 8.6).

Downregulated transcripts were strongly associated with the *mitochondria* and many aspects of mitochondrial function including *aerobic respiration, organisation*, and *electron transfer activity*. *Ribosomal transcripts* were also downregulated, as in the spinal cord, including some related to the ribosomal subunit, which could suggest a global issue with translation (Figure 8.7).

As part of the RNA sequencing experiment, spinal cord tissue from $Fus^{+/-}$ mice was also included, as it is known heterozygous *Fus* knock-out mice experience a mild loss of *Fus* expression and therefore FUS function. Interestingly, when comparing the fold change of those transcripts which were significantly differentially expressed in $hFUS/hFUS^{P525L}$ mice ($q<0.1$) to the fold change of the equivalent transcripts in $Fus^{+/-}$ mice, there was a strong negative correlation (Figure 3.22, $r=-0.8890$, $p<0.0001$).

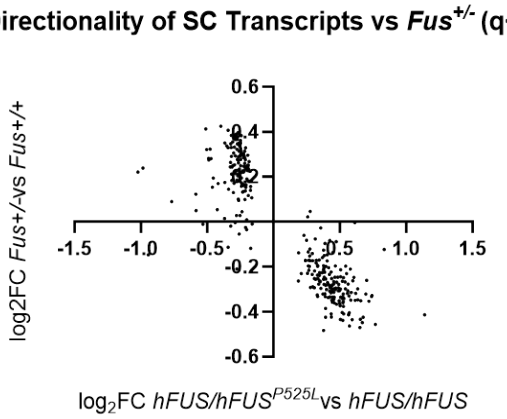


Figure 3.22: Transcripts which were significantly differentially expressed in hFUS/hFUS^{P525L} mice compared to hFUS/hFUS controls have a negative correlation in fold change compared to transcripts differentially expressed between Fus$^{+/-}$ and Fus$^{+/+}$ mice.

3.4.9 Total FUS is mainly localised to the nucleus despite the NLS mutation, but FUS^{P525L} is spread between the nucleus and cytoplasm

Mutations in the *FUS* gene, particularly those located in the NLS, are known to increase the amount of FUS in the cytoplasm, likely due to impaired binding of nuclear import factors (Dormann et al., 2012; Dormann et al., 2010). FUS staining was carried out to assess the extent of cytoplasmic FUS staining in *hFUS/hFUS^{P525L}* mice. Tissue collected from young *Fus$^{-/-}$* mice was also included as a negative control (Figure 8.8).

Mice aged 4 and 21 months were culled and then perfused with 4% PFA and the spinal cord dissected out and sectioned prior to staining. Two different FUS antibodies were used, one which recognised the N terminus and therefore should bind both wildtype and mutant FUS (total FUS) and one which was donated by the Ruepp

lab which was raised to bind human FUS^{P525L} (FUS^{P525L}) specifically. Sections were co-stained with NeuN as a neuronal marker, or ChAT as a motor neuron specific marker.

In spinal cord tissue collected from 4-month-old mice, when staining with total FUS, there was no clear increase of FUS protein to the cytoplasm in either male or female tissue of both genotypes although only a small number of sections were analysed (Figure 3.23). When *hFUS/hFUS^{P525L}* sections were stained using the FUS^{P525L} specific antibody there was increased cytoplasmic staining of FUS^{P525L}, with some nuclear staining also present (Figure 3.23). As expected, there was no FUS^{P525L} staining in neuronal cells in sections collected from *hFUS/hFUS* controls, although some structures which appear to be blood vessels were stained non-specifically.

FUS staining was specific as there was no staining in primary and secondary only controls (Figure 8.9).

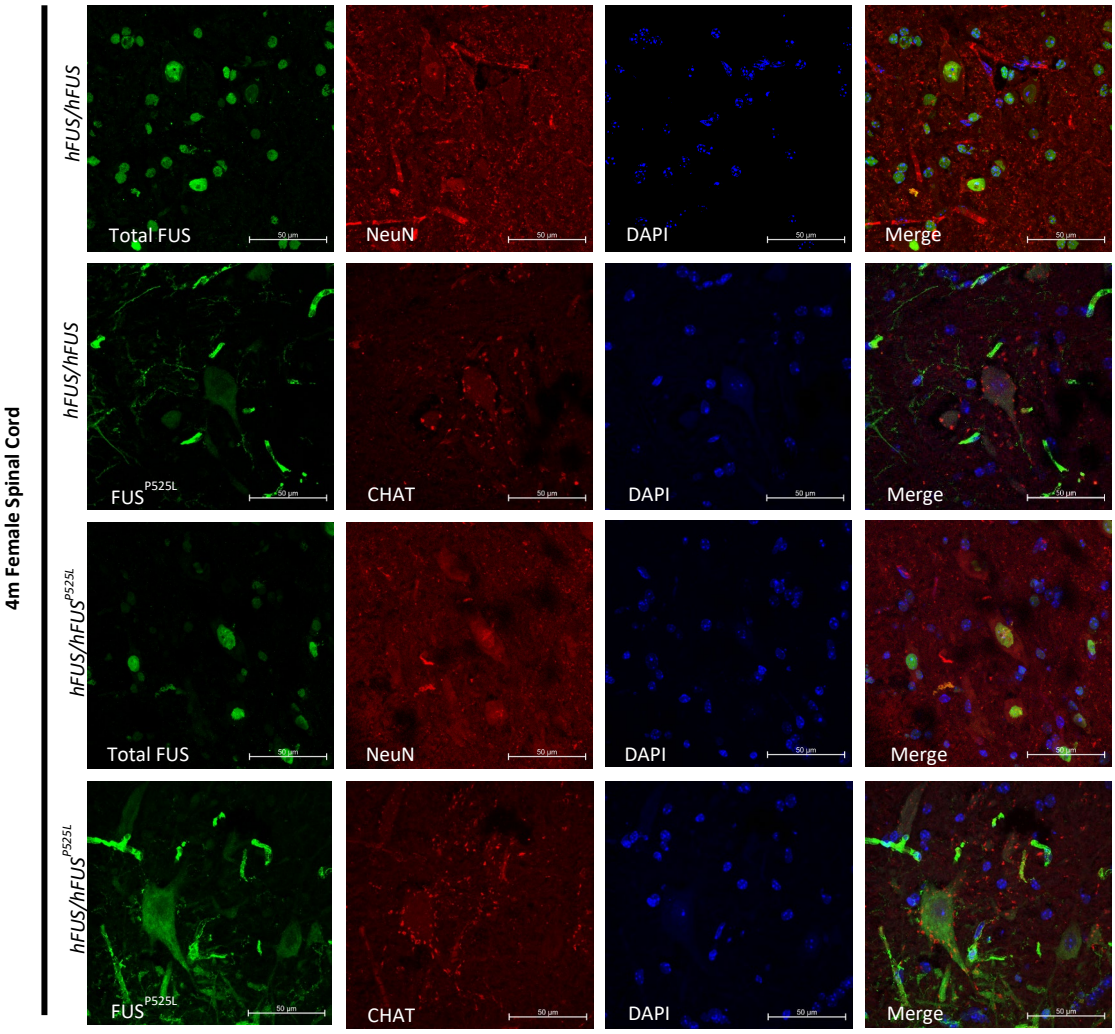


Figure 3.23: FUS staining in spinal cord neurons in hFUS/hFUS^{P525L} mice aged 4 months. *FUS staining was carried out using an antibody raised against the N-terminus of the FUS protein (Novus 565, green) and a FUS^{P525L} specific antibody (green), with ChAT or NeuN (red) used as neuronal markers. DAPI staining shows nuclei (blue). Scale bars = 50µm.*

In aged mice, there was a mild but consistent increase of total FUS located in the cytoplasm in *hFUS/hFUS^{P525L}* mice. FUS^{P525L} specific staining showed the same pattern as at 4 months with staining consistent throughout the nucleus and cytoplasm. Structures which look to be microglia also stain in *hFUS/hFUS^{P525L}* mice (Figure 3.24).

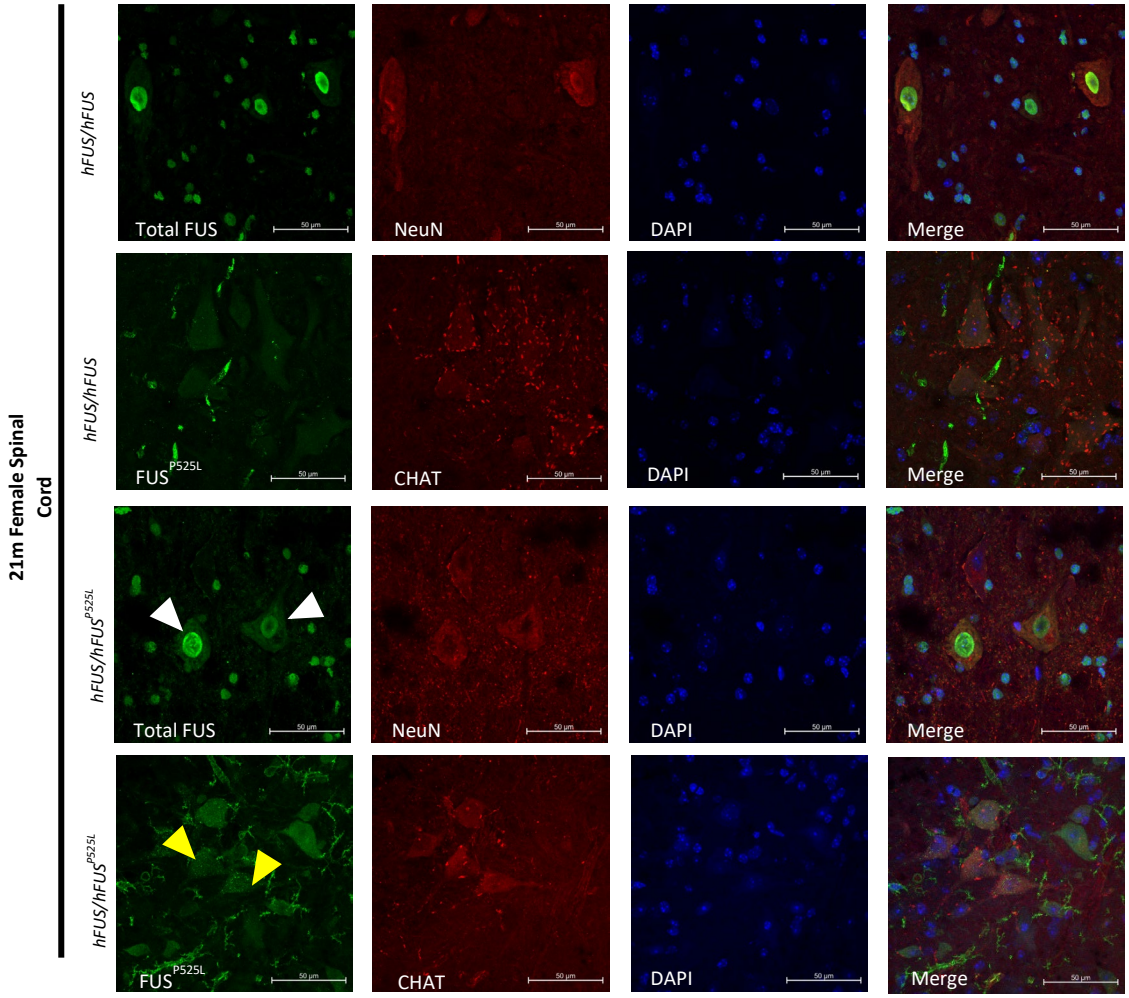


Figure 3.24: Cytoplasmic FUS is increased in spinal cord neurons in hFUS/hFUS^{P525L} mice aged 21 months. *FUS staining was carried out using an antibody raised against the N-terminus of the FUS protein (Novus 565, green) and a FUS^{P525L} specific antibody (green), with ChAT or NeuN (red) used as neuronal markers. White arrows indicate cytoplasmic total FUS. Yellow arrows indicate cytoplasmic FUS^{P525L}. DAPI staining shows nuclei (blue). Scale bars = 50µm.*

3.4.9.1 Despite an increase in cytoplasmic FUS, large aggregates were not observed

Cytoplasmic FUS staining was diffuse when stained using antibodies against FUS, with no large aggregates detected. H&E staining has been used to observe basophilic inclusions in tissue from FUS-ALS patients (Nolan et al., 2016). Spinal cord sections were collected from 21m old female *hFUS/hFUS^{P525L}* mice and controls.

Despite increased FUS in the cytoplasm in *hFUS/hFUS^{P525L}* mice, basophilic inclusions were not observed (Figure 3.25).

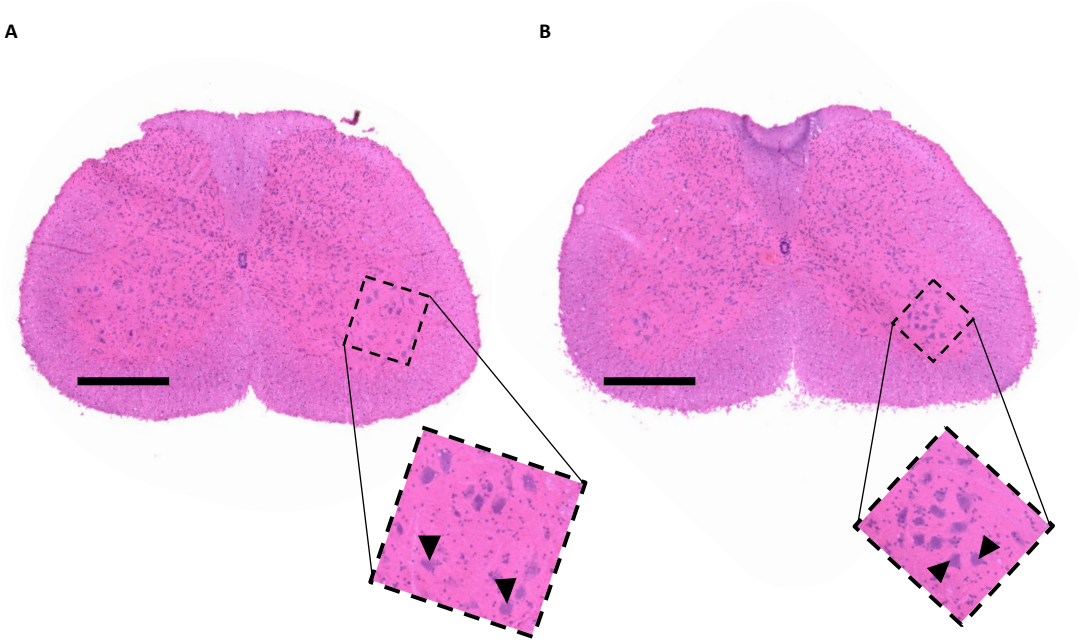


Figure 3.25: Large aggregates were not observed in ventral motor neurons. *Black arrows highlight motor neurons in the ventral spinal cord of aged female mice.* ***A)*** *Representative image of a spinal cord section dissected from a hFUS/hFUS mouse.* ***B)*** *Representative image of a spinal cord section from a hFUS/hFUS^{P525L} mouse. Scale bar represents 500μm.*

3.4.9.2 Expression of hFUS/hFUS^{P525L} does not cause microglial activation in the ventral spinal cord of aged female mice

Microglial activation in the spinal cord has been shown to play a role in ALS disease progression and other models of FUS-ALS have shown evidence of this occurring (Korobeynikov et al., 2022; Sharma et al., 2016).

Perfused tissue from 21-month-old females was collected and stained for Iba1 as a microglial marker (Figure 3.26A-B). The percent of the ventral horn which had a positive signal for Iba1 was quantified as a readout of microglial activation. There was no difference in the percent of ventral horn covered by microglia between *hFUS^{P525L}* and humanised *FUS* wildtype controls (Figure 3.26C). There was also no evidence of differences in Iba1 staining between the left and right ventral horn of heterozygous *hFUS^{P525L}* and wildtype mice (Figure 3.26D).

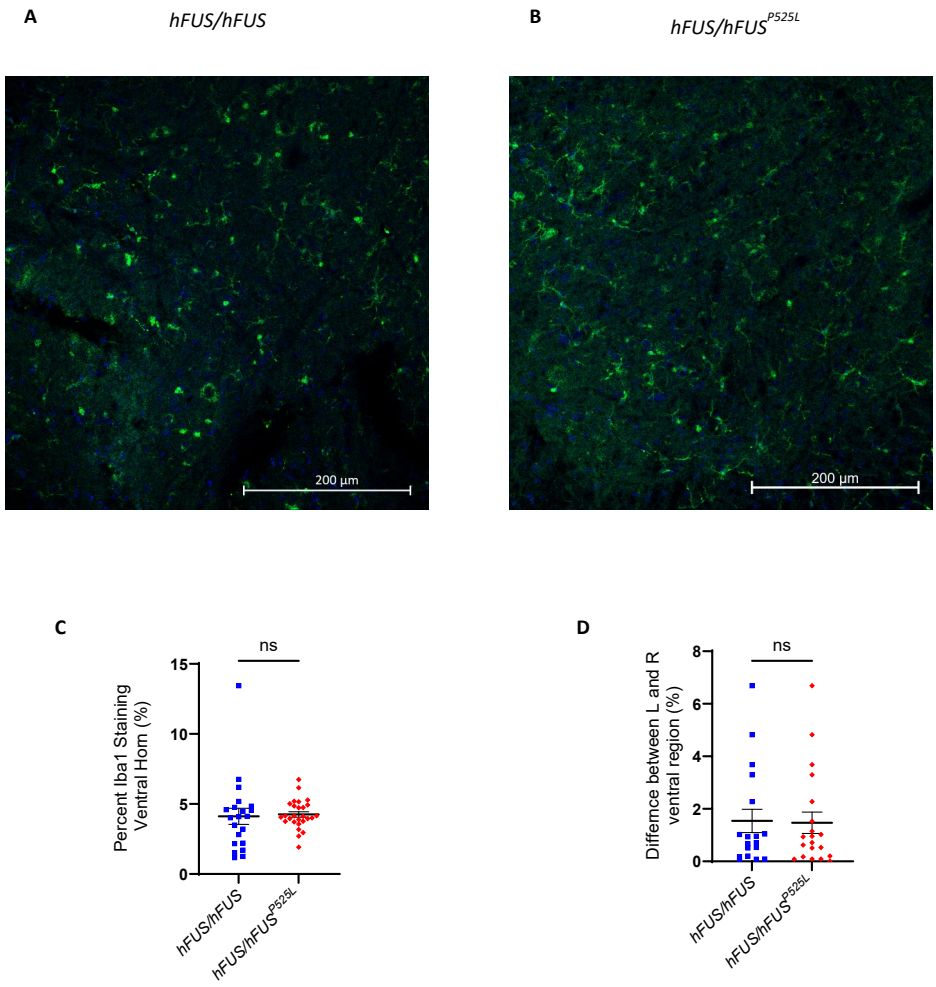


Figure 3.26: Iba1 staining in the ventral horn of 21-month-old female spinal cord shows no difference in microglial activation between hFUS/hFUS^{P525L} mice and wildtype controls. A) *Representative image of Iba1 staining (green) and DAPI (blue) in hFUS/hFUS spinal cord.* ***B)*** *Representative image of Iba1 staining (green) and DAPI (blue) in hFUS/hFUS^{P525L} spinal cord.* ***C)*** *The percent of the ventral horn of the spinal cord covered by Iba1 signal was quantified on ImageJ using image segmentation to quantify microglial activation and proliferation.* ***D)*** *The percent of Iba1 staining in the left vs right ventral horn was quantified to see if there was a topographic difference in Iba1 staining. Data are shown as mean average ± SEM with significance analysed using an unpaired T test or Mann-Whitney test for differences between left and right ventral regions. ns = not significant. n=4 hFUS/hFUS and n=5 hFUS/hFUS^{P525L} mice with multiple spinal cord sections per animal quantified. Scale bars = 200µm.*

3.4.10 *hFUS/hFUS^{P525L}* mice show disease relevant changes in the TA muscle.

3.4.10.1 Tibialis anterior muscles from hFUS/hFUS^{P525L} mice have a different fibre type composition aged 15-months

Fibre type composition was analysed in unfixed TA sections from 15-month-old *hFUS/hFUS^{P525L}* male mice using an ATPase stain which enables fibre type to be differentiated based on colour. The TA sections were stained by David Thompson, a fellow DPhil student in the lab.

Type II fast-fatigable fibres made up 73% of the TA in control mice, however this decreased to 64% in *hFUS/hFUS^{P525L}* mice (Figure 3.27C, p= 0.0167).

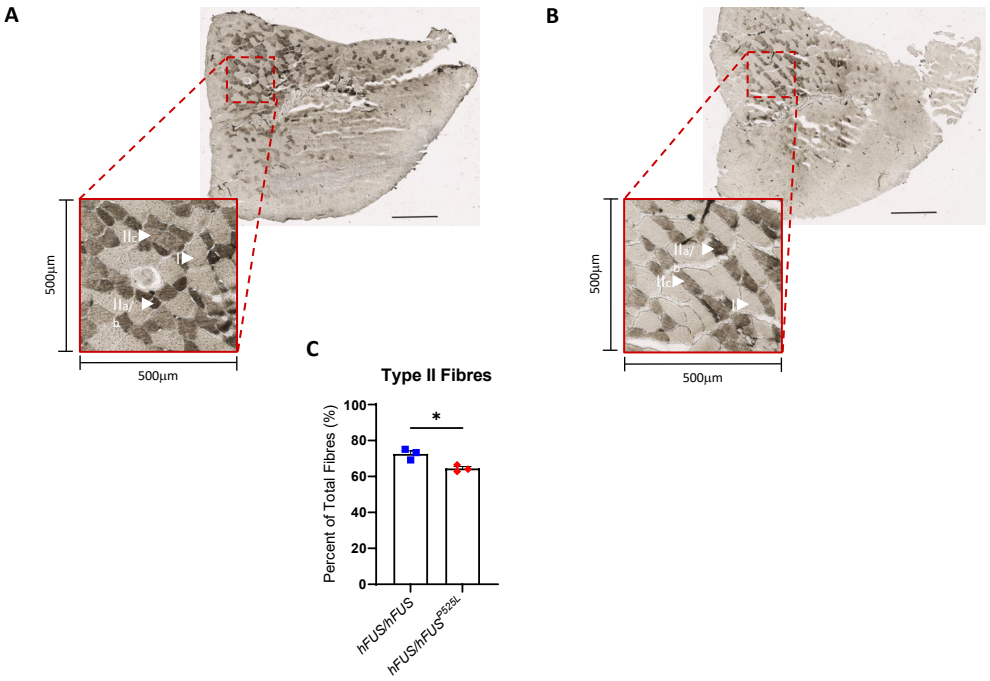


Figure 3.27: Tibialis anterior muscles were dissected from 15-month-old male mice and the fibre type composition assessed using an ATPase staining method which differentiates fibre type based on colour. A) *representative image of a TA stained from a hFUS/hFUS mouse highlighting each fibre type (white arrows) in the zoomed in box (red).* ***A)*** *representative image of a TA stained from a hFUS/hFUS^{P525L} mouse highlighting each fibre type (white arrows) in the zoomed in box (red).* ***C)*** *Quantification of the percent composition of type II fibres. Data are shown as mean average ± SEM with significance analysed using an Unpaired t test. *=p<0.05.*

In addition to fibre type composition, TA sections from the same 15-month-old *hFUS/hFUS^{P525L}* mice were used to assess fibre type morphology.

Haematoxylin and Eosin staining to visualise muscle fibres revealed there was a trend towards a decrease in fibre size in *hFUS/hFUS^{P525L}* mutant mice compared to controls (Figure 3.28D-E). TA muscles also trended towards being hypertrophic in *hFUS/hFUS^{P525L}* mutant mice (Figure 3.28A,F).

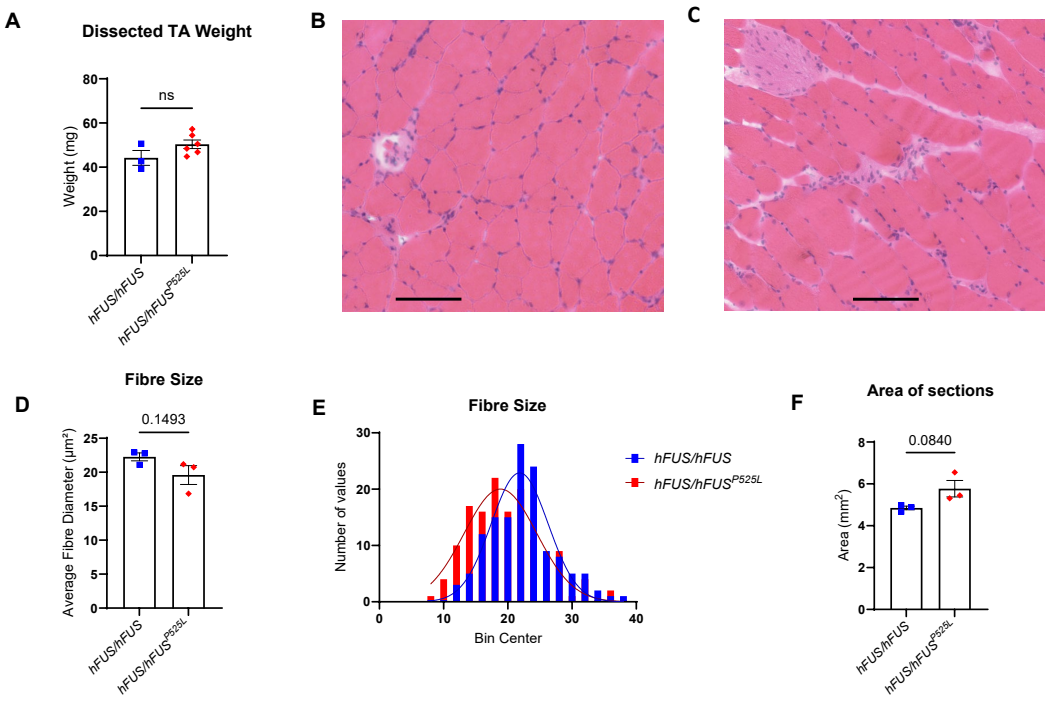


Figure 3.28: Tibialis anterior fibre morphology trends towards a decrease in fibre size in hFUS/hFUS^{P525L} mice compared to controls. A) *Weight of dissected TA muscles from the right leg of male mice aged 15 months old.* ***B)*** *Representative images of TA sections from hFUS/hFUS mice stained with H&E used for fibre sizing. Scale bar = 100µm.* ***C)*** *Representative images of TA sections from hFUS/hFUS^{P525L} mice stained with H&E used for fibre sizing. Signs of inflammatory cell infiltration were more apparent in sections from hFUS/hFUS^{P525L} mice. Scale bar = 100µm.* ***D)*** *Quantification of fibre size and* ***E)*** *histogram showing the distribution of fibre size within the TA muscles from mutant and control mice.* ***F)*** *Total area of TA sections was quantified. Data are presented as mean average ± SEM with significant analysed using an unpaired Student's T test. ns = non-significant.*

3.4.10.2 Dissected TA muscles from hFUS/hFUS^{P525L} male mice aged 21m are significantly smaller than control mice

Aged 15 months, there was no difference in TA weight between *hFUS/hFUS* and *hFUS/hFUS^{P525L}* mice however aged 21 months old, TA muscles from *hFUS/hFUS^{P525L}* mice were 10% smaller than humanised wildtype controls (Figure 3.29A, p=0.0221).

Noo significant difference between the weight of muscles from the left versus right leg was recorded but the variation in the data was very large meaning the comparison was underpowered (Figure 3.29B).

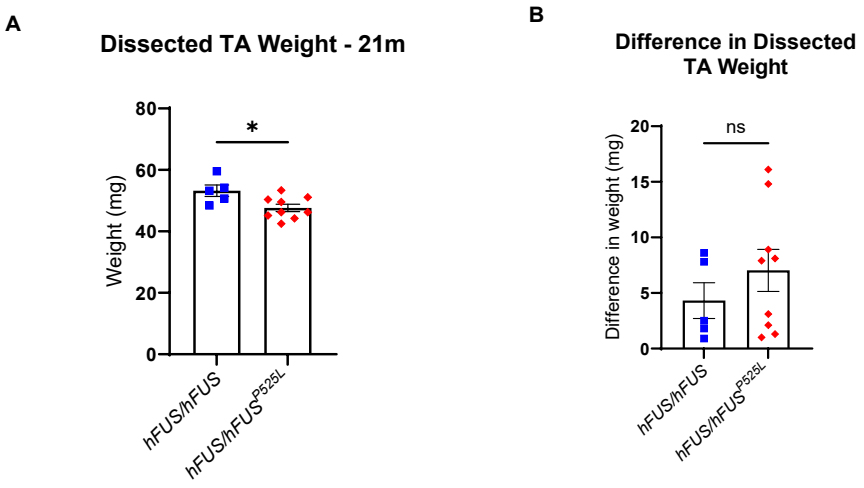


Figure 3.29: Weight of tibialis anterior (TA) muscle dissected from 21-month-old male mice. A) *Mean average weight of the TA muscles from both legs of male mice aged 21 months old.* ***B)*** *Difference in weight of dissected TA muscles from the left and right hindlimbs. Data are shown as mean average ± SEM with significance analysed using an Unpaired t test. Ns=not significant, *=p<0.05.*

3.4.10.3 hFUS/hFUS^{P525L} have a lower mitochondrial DNA copy count in their tibialis anterior muscles

Transcriptomic data from TA muscles of 4-month-old mice showed a large downregulation of mitochondrial related genes. To investigate whether this was due to the muscles having fewer mitochondria a qRT-PCR mitochondrial DNA copy count assay was carried out.

The ratio of mitochondrial DNA compared to genomic DNA is compared as a readout of the number of mitochondria present in a sample.

TA tissue collected from mice aged 4 months found there was a trend towards a decrease in mitochondrial DNA, but this was not significant (Figure 3.30A). This was repeated in tissue collected from mice aged 12 months and at this timepoint, the decrease in mitochondrial DNA was significant likely because the analysis had more power (Figure 3.30B, p=0.0406).

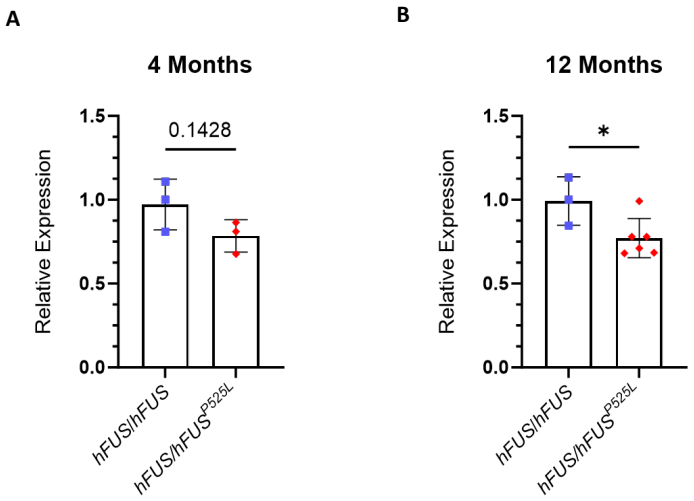


Figure 3.30: hFUS/hFUS^{P525L} male mice have a decrease in mitochondrial DNA in tibialis anterior muscles. A) *qRT-PCR was carried out on TA tissue from male mice aged 4 months old to quantify mitochondrial DNA. There was no significant difference in the quantity of mitochondrial DNA between hFUS/hFUS^{P525L} mice and controls.* ***B)*** *When this qRT-PCR experiment was repeated on TA tissue from 12-month-old mice, there was a significant decrease in mitochondrial DNA.*

3.4.11 There is no evidence of neuronal degeneration in the *hFUS/hFUS^{P525L}* mice

3.4.11.1 Motor neuron counts

Motor neuron counts were carried out in male mice aged 21-months, at the end of the longitudinal phenotyping pipeline.

There was no significant difference in the number of motor neurons in the ventral horn of the lumbar spinal cord in *hFUS/hFUS^{P525L}* mice compared to controls (Figure 3.31).

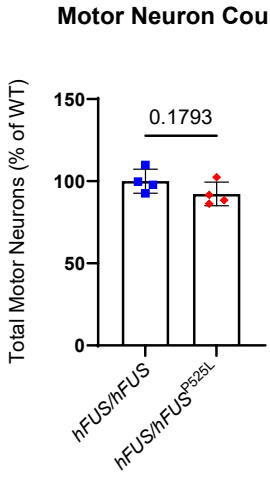


Figure 3.31: There was no loss of ventral motor neurons in the lumbar spinal cord of 21-month-old male hFUS/hFUS^{P525L} mice compared to controls. *Spinal cord sections from 21-month-old male mice were stained with gallocyanine and motor neurons in the ventral horn manually counted. Data are shown as mean average ± SEM with significance analysed using an Unpaired T test. ns = not significant.*

3.4.11.2 There is no difference in NFL levels in blood plasma of aged hFUS/hFUS^{P525L} mice of either sex

Neurofilament light chain (NFL) in blood plasma is used as a biomarker in ALS as a proxy measure of neuronal degeneration (Thompson et al., 2022).

A Simoa assay was used to quantify NFL concentration in blood plasma from tail bleeds collected from humanised *FUS* male and female mice aged 15-months with and without the *hFUS^{P525L}* mutation. There was no difference in the concentration of NFL in blood plasma of either sex (Figure 3.32).

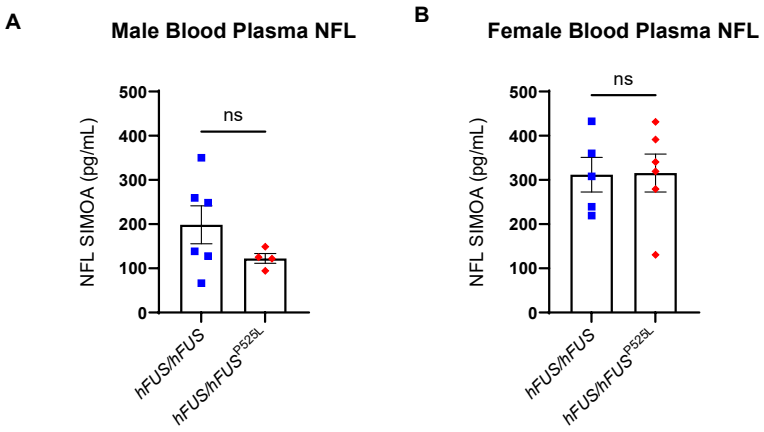
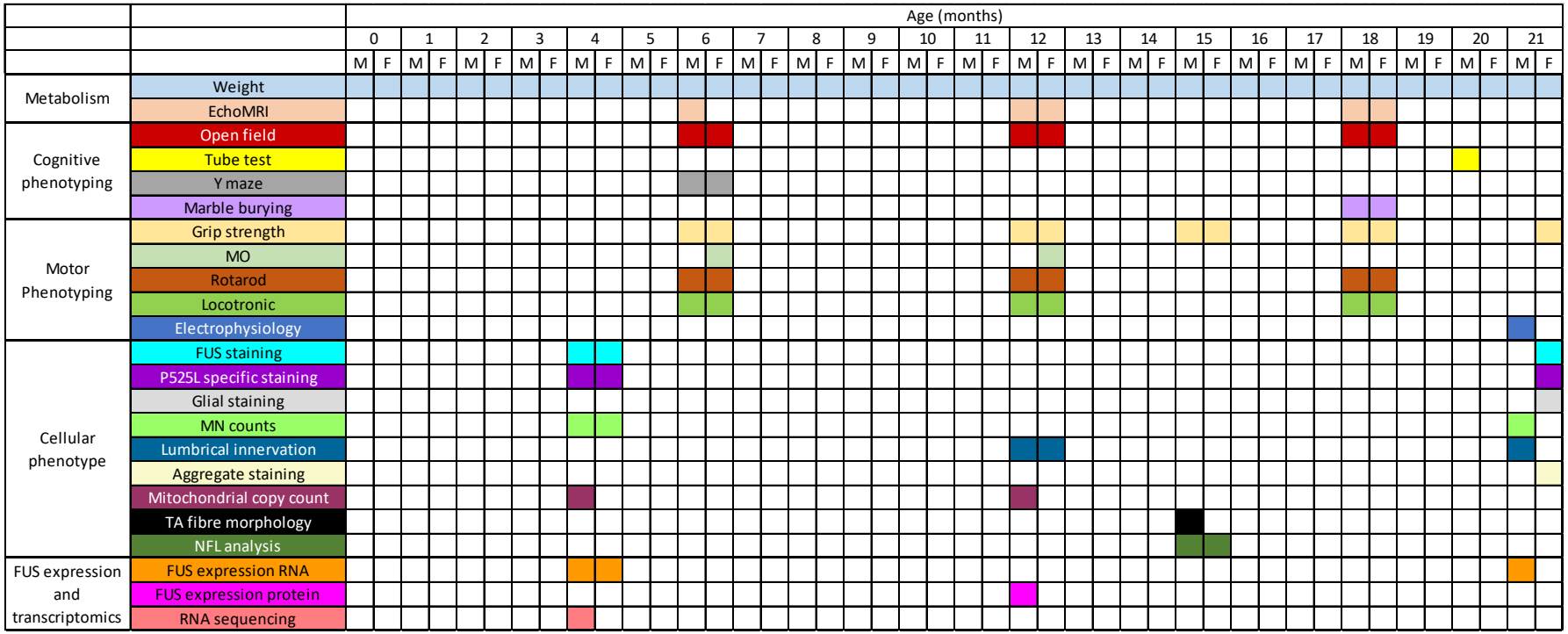


Figure 3.32: There was no difference in blood plasma levels of neurofilament light chain (NFL) in 15-month-old hFUS/hFUS^{P525L} mice of either sex. *A SIMOA machine was used to quantify levels of NFL in the blood plasma taken from tail bleeds of 15-month-old male and female mice. There was no difference in blood plasma levels of NFL in* ***A)*** *male or* ***B)*** *female mice. Data are shown as mean average ± SEM with significance analysed using a Mann Whitney test (males) or Unpaired T test (females). ns = not significant.*

3.5 Discussion

The aim of this project was to generate a targeted knock-in mouse model which expressed the mutated human *FUS^{P525L}* gene and protein at physiologically relevant levels, but perhaps more importantly in a physiologically relevant pattern of expression, under the control of the endogenous mouse *Fus* promoter. An assessment of phenotypes, both at the whole organism and cellular and molecular level, was then carried out to see what effect the human *FUS^{P525L}* mutation was having in the mouse system. Every effort was made to study all phenotypes in both sexes and at a range of timepoints; Table 3.1 provides a summary of all data collected.

Table 3.1: Summary of data collected from hFUS/hFUS^{P525L} mice.



M = male

F = female

3.5.1 Expression of the *hFUS^{P525L}* mutation causes developmental defects and reduced survival

FUS is known to play a crucial role in development as *Fus$^{-/-}$* mice are embryonic lethal (Hicks et al., 2000). Homozygous expression of the *hFUS^{P525L}* mutation is also embryonic lethal; embryos are smaller and poorly developed, which is consistent with what is seen in other homozygous P525L mouse models (Korobeynikov et al., 2022) and suggests there is insufficient wildtype FUS function remaining to enable normal development. Korobeynikov and colleagues provide evidence however that FUS^{P525L} does retain some FUS function as it is able to partially rescue a *Fus* knock-out phenotype in compound heterozygosity with a *Fus* null allele (Korobeynikov et al., 2022).

Male mice heterozygous for the *hFUS^{P525L}* mutation were sub-viable and had worse survival probability as they aged, consistent with other *FUS^{P525L}* mouse models (Korobeynikov et al., 2022). In the humanised *hFUS/hFUS^{P525L}* mice the decrease in survival was mainly driven by issues associated with malocclusion leading to mice struggling to eat and losing weight. Malocclusion is a developmental defect likely caused by issues with bone development and asymmetrical patterning, although how FUS modulates this is not well understood. Malocclusion is known to affect C57BL/6J mice naturally however an increased prevalence of this phenotype is seen in FUS-ALS mouse models with varying degrees of penetrance (Korobeynikov et al., 2022). Interestingly Korobeynikov and colleagues observed seizures in their P517L/KO mice, but not in the P517L/WT or Δ14/WT mice. Seizures were recorded in the *hFUS/hFUS^{P525L}* and *hFUS/hFUS* mice which could suggest this phenotype is related to the mild loss of FUS expression we are seeing by humanising the *FUS* gene, as discussed in chapter 2.

This data clearly supports a role of *FUS* in development and shows how mutations in *FUS* may bring about systemic changes in patients. This is becoming more widely accepted as juvenile ALS cases caused by *FUS* mutations are often accompanied by wider abnormalities such as learning and intellectual disabilities and seizures (Ali et al., 2023; Dodd et al., 2019; Goldstein et al., 2022; Picher-Martel et al., 2020; Yamashita et al., 2012; Zou et al., 2013) and mutations in *FUS* can stunt brain development more generally (Hirayanagi et al., 2016).

Metabolism was also clearly affected in the *hFUS/hFUS*^{P525L} mice which were smaller than controls from a young age; echoMRI data also indicated an altered fat/lean mass ratio in *hFUS/hFUS*^{P525L} male mice. It is proposed that metabolism deficits can affect nervous system development and are also linked to seizure phenotypes (Ali et al., 2023; Godoy-Corchuelo et al., 2022). Weight loss is observed in ALS patients, due to the degeneration of muscle mass paired with a reduction in fat mass, but prior to disease onset a lower BMI is associated with a higher risk of developing ALS, and a more rapid disease progression in patients (Ngo et al., 2014). There is evidence of hypermetabolism, defined as an increase in metabolic rate at rest, in ALS patients and *in vivo* models, in the symptomatic stage of disease (Ngo et al., 2014). A decreased fat mass may result in a weaker capacity to compensate for this hypermetabolic state as energy stores are more quickly depleted (Ngo et al., 2014). Indeed a high glucose diet was shown to prevent FUS toxicity in a C.elegans model of FUS-ALS (Tauffenberger et al., 2012). Data from the humanised *FUS*^{P525L} mice suggests there are developmental changes causing the mutant mice to be smaller than controls to begin with, with a reduction in fat mass observed in males. If these developmental changes are also occurring in FUS-ALS patients, this leanness could make them less

able to compensate for hypermetabolism leading them to develop ALS symptoms earlier in life. More work would be needed to study hypermetabolism and lipid homeostasis in the *hFUS/hFUS^{P525L}* mice to see if, when, and in what tissue, these changes could be observed.

3.5.2 *hFUS/hFUS^{P525L}* mice display an outward behavioural and motor phenotype independent of spinal cord motor neuron loss

Male *hFUS/hFUS^{P525L}* mice were found to be hyperactive aged 6 months, which was not due to increased anxiety. Whether hyperactivity is a symptom associated with ALS remains speculative (Lule et al., 2008), but other behavioural and social changes such as apathy, and social and communication skills can often precede motor symptoms (Beeldman et al., 2020; Rusina et al., 2021). Changes in social behaviour were also seen with male *hFUS/hFUS^{P525L}* mice being less socially dominant than controls. Female *hFUS/hFUS^{P525L}* mice aged 18 months also trended towards burying fewer marbles which can indicate an issue with wellbeing. It would have been interesting to follow up on cognitive changes at additional timepoints, to see if social changes occurred before the motor phenotype, or if a spatial memory deficit developed after 6 months as is seen in other heterozygous *FUS$^{NLS/+}$* mutant mouse models as they age (Scekic-Zahirovic et al., 2021).

hFUS/hFUS^{P525L} mice were analysed longitudinally to see if they developed a motor phenotype. At 6 months, there was no difference in grip strength of mice of either sex but from 12 months male *hFUS/hFUS^{P525L}* mice had a significantly weaker combined grip strength compared to wildtype mice which got progressively worse until the latest timepoint studied aged 18 months. By 18 months several wildtype mice had

been lost from the longitudinal phenotyping cohort making the 18-month timepoint less powered. This was due to the *hFUS/hFUS* mice having a higher propensity to become obese, and subsequently a higher propensity for weight loss in old age that approached the maximum 20% loss cut-off, resulting in welfare culls. To note, collaborators working with *hFUS/hFUS*^{P525L} independently found a grip strength deficit in male *hFUS/hFUS*^{P525L} mice beginning around 12 months.

Combined grip strength of female *hFUS/hFUS*^{P525L} mice was no different to controls at any individual timepoint studied although data trended towards a decreased grip strength in *hFUS/hFUS*^{P525L} mice. Interestingly, collaborators found a hindlimb-specific grip strength phenotype in female mice aged 12 months. Hindlimb specific grip strength was not assessed in the mice at MRC Harwell so this phenotype may have been missed. Alternatively, the lack of grip phenotype seen in female mice at MRC Harwell could be due to confounding variables from different mouse housing environments, and experimenter variables.

Other motor phenotyping tests studied included the locotronic ladder test, rotarod and the automated running wheel. In these tests the *hFUS/hFUS*^{P525L} mutant mice of both sexes either performed as well as controls, or even better. Male *hFUS/hFUS*^{P525L} mice produced fewer leg errors in the locotronic ladder test however they also crossed the ladder significantly faster, and the number of leg errors correlates strongly with crossing time which could explain this result; female mice trended towards this too. In the rotarod test, female *hFUS/hFUS*^{P525L} mice outperformed control mice, staying on the rotating rod for longer; male *hFUS/hFUS*^{P525L} mice also stayed on the rod significantly longer than *hFUS/hFUS*

controls although this wasn't significant at individual timepoints. Watching mice during the rotarod test, it was clear the larger *hFUS/hFUS* control mice were struggling to remain on the foam coating of the rotarod; sometimes their weight was so much that it started to pull the foam from the rod. Rotarod data was very spread, with two minutes between the best and worst performers within genotypes suggesting it was not the most accurate test to measure motor performance in these mice. In the wheel running test there was no difference in wheel running ability between *hFUS/hFUS*^{P525L} female mice and controls.

It is interesting to consider that of the four motor tests carried out, the three which required self-motivation from the animals found equal or better motor ability in the *FUS* mutant mice compared to controls. From discussions with clinicians, this is something that is seen in patients in early stages of disease, whereby patients are known to outperform controls.

Perhaps the most interesting and unexpected result was seen in the muscle electrophysiology data collected at UCL. When the electrophysiology data was first analysed by colleagues at UCL, the normal protocol was followed to average readings from both legs together. Upon further discussion within the lab at UCL, they started to split the data by left and right leg as there appeared to be differences between the two sides. It was not always the left, or always the right leg which produced the lower reading, but a 40/60 split which suggests it was not due to a transducer error. When the readings from both legs were averaged, there were no differences observed between *hFUS/hFUS*^{P525L} mice and controls. When the weakest leg of the mutant mice was compared to the weakest leg of the control mice, some trends started to emerge,

with a significant decrease in motor units seen in the EDL (p= 0.0401). The difference in readings between the legs was also compared between genotypes; this was not significant for most readings, except the difference in maximum tetanic force of the TA. Particularly in the TA muscle, the difference in muscle performance between legs was widely spread, meaning in some mice there was almost no difference between the left and right leg, and in others the difference was very large making the data underpowered. It would be interesting to try to stratify those mice with the greatest topographical differences in muscle performance to see if any additional factors could explain why one side was more affected. The trends towards unilateral weaknesses could go some way to explain why motor tests which assess gross motor function found only mild deficits. The subtle, perhaps unilateral weakness may have been missed as the leg which had comparative strength to the wildtype mice may be compensating; thus, the motor tests used may not be adequately sensitive to detect these fine motor changes.

Although the unilateral effect of the *FUS* mutation on muscle electrophysiology data was mostly trending, it would be important to follow this up in future cohorts, at different timepoints and with more power to see if this phenotype was replicable. If so, to the best of my knowledge this is the first mouse model of ALS which represents a unilateral weakness, like that seen in ALS patients. Further work would be needed to see if this unilateral phenotype could be studied at a cellular and molecular level, to see what was driving the changes. Neuromuscular junction innervation of the affected muscles could be assessed to see if this correlated with the muscle weakness seen. Additionally, RNA sequencing and proteomics could be carried out on tissues from the weaker and stronger side, such as skeletal muscle and motor neurons, to see if novel

pathways could be found. If the phenotype was replicable enough to be studied at the cellular level it would be vital to understand what was ultimately causing the side-specific changes, such as stochastic 'second' hits beyond the *hFUS*^{P525L} mutation, when these were occurring, and ultimately how they could be prevented in patients, in addition to how pathology subsequently spread to the contralateral side.

At 21-months old, there is no significant motor neuron degeneration in the spinal cord of *hFUS/hFUS*^{P525L} mice

Interestingly, the phenotypes observed in the *hFUS/hFUS*^{P525L} mice were occurring independently of detectable motor neuron degeneration and neuroinflammation as measured by Iba1 staining, which were not observed in the spinal cord of *hFUS/hFUS*^{P525L} mice in this study. Of note, Iba1 staining was carried out in tissue from female mice which did not exhibit a degenerative motor phenotype. It would have been useful to assess for neuroinflammation in other tissue types and from male mice which did display motor phenotypes. Other mouse models expressing the *FUS*^{P525L} mutation have found the opposite, with mild age-dependent motor neuron degeneration occurring without producing an overt motor phenotype (Korobeynikov et al., 2022). Differences in motor neuron loss observed in the two P525L mouse models could relate to the experimental techniques used. Korobeynikov and colleagues counted Choline Acetyltransferase (ChAT) positive motor neurons in the *Fus*^{P517L} mice whereas a Nissl stain was used in this project. There is evidence that ChAT expression is not specific to cholinergic motor neurons; ChAT-Cre labels a significant number of GABAergic and glutamatergic neurons in the adult spinal cord (Alkaslasi et al., 2021; Patel et al., 2022). Additionally, some dysfunctional motor

neurons may no longer stain with ChAT but may not have been lost completely and so would still be detected with a Nissl stain; with only an 11-22% decrease in motor neurons observed in the *Fus*^{P517L} mice aged one and a half to two years, that would equate to a difference of around two motor neurons per spinal section. In addition, in this project the Nissl stain gallocyanin was used which stained sections weakly making it hard to distinguish motor neurons from inter-neurons. Motor neuron counting was subsequently optimised and is being repeated with sections stained with cresyl-violet. Assessment of distal hindlimb lumbrical muscle innervation is also ongoing in *hFUS/hFUS*^{P525L} mice as this can precede motor neuron loss in the spinal cord (Korobeynikov et al., 2022).

If the difference in motor neuron loss is not due to experimental differences but a true phenotype, then it may be considered that the presence of the *hFUS*^{P525L} mutation is less toxic to motor neurons than the *Fus*^{P517L} mutation. This could be for two reasons, 1) the mouse P517L protein is intrinsically more toxic than the human P525L protein or 2) there may be lower levels of mutant FUS protein in the *hFUS/hFUS*^{P525L} mice compared to P517L mice as humanising the *FUS* gene is known to produce lower levels of the FUS protein (as shown in chapter 2). Korobeynikov and colleagues have proposed that the severity of gain of function toxicity of *FUS* mutations is dose-dependent (Korobeynikov et al., 2022).

3.5.3 Total FUS becomes more cytoplasmic as *hFUS/hFUS*^{P525L} mice age

Heterozygous expression of the *hFUS*^{P525L} mutation did not lead to a significant increase in cytoplasmic total FUS in spinal cord motor neurons from 4-month-old mice, but rather the majority of the FUS protein remained nuclear and diffuse from analysing

a small number of sections. When spinal cord sections were stained with a FUS^{P525L} specific antibody the mutant FUS protein was found to be distributed throughout the nucleus and the cytoplasm. This data supports the finding that FUS nuclear import is achieved in some degree through binding of NLS-independent chaperone proteins such as transportin-3, importin β, importin 7 and the importin β/7 heterodimer which would be unaffected by the P525L mutation (Baade et al., 2021; Gonzalez et al., 2021).

Interestingly, the pattern of total FUS staining appeared to change as mice aged. When spinal cord sections were analysed from *hFUS/hFUS^{P525L}* mice aged 21 months, there was a visible increase in cytoplasmic total FUS. It is hard to directly compare as the spinal cord sections were prepared in different ways (perfused versus post fixed) but in chapter 2 it was also found there was an increase in cytoplasmic FUS in aged mice, consistent with other reports (C. Huang et al., 2010). The idea that cytoplasmic FUS increases with disease duration is not novel (Suzuki et al., 2012), and there is speculation that increased FUS in the cytoplasm may actually signal phenoconversion (Caputo et al., 2020). This is not to say that the role of mutant FUS in the nucleus is not important for disease progression, as it is likely both loss and gain of toxic function are occurring in the nucleus prior to increased localisation to the cytoplasm. Various factors could induce increased cytoplasmic localisation of FUS such as stress granule formation which are themselves formed in response to many different types of stress. For example, there is evidence stress granules can be induced by altered mRNA splicing; perturbation of genes involved in the spliceosome, regulating pre-mRNA splicing and RNA processing/export led to stress granule formation in human cell models (Berchtold et al., 2018). Further work would be needed to see if mutant FUS altered the expression of these splicing genes, and

whether this could create a feedforward loop whereby dysregulated gene expression induced cytoplasmic stress granule formation, increasing cytoplasmic FUS and sequestration.

Increased cytoplasmic and decreased nuclear FUS protein means autoregulation is affected and levels of FUS protein are usually elevated in FUS mutant models (Zhou et al., 2013). At the RNA level, there were small but significant increases in *FUS* expression in ALS-relevant tissues of *hFUS/hFUS*^{P525L} mice of both sexes. In male mice, increased *FUS* expression was seen in the spinal cord and the predominantly fast-fatigable TA and EDL muscles, but interestingly not in the slow-twitch soleus muscle which is less vulnerable to degeneration in ALS. These expression changes were small however, and it is hard to say if they would be having a functional effect. Changes in intron retention could not explain the small increases in *FUS* RNA as there were no differences between the levels of FUS transcripts with intron six and seven retained between *hFUS/hFUS*^{P525L} mice and controls (Figure 8.3). The RNA changes were not mirrored at the protein level where there were no significant differences in total FUS expression in the spinal cord or TA muscle. The minimal FUS expression changes further support the argument that transgenic models which highly overexpress the mutant FUS protein are not accurately representing the pattern of expression seen in a physiologically relevant system.

FUS protein expression was only analysed in the RIPA soluble fraction of total tissue homogenate. It would have been interesting further work to see if there was increased FUS protein in the insoluble fraction and whether this was increased further in *hFUS/hFUS*^{P525L} mice.

3.5.4 Changes at the level of the tibialis anterior muscle may be driving some of the motor phenotypes seen

Pre-symptomatic transcriptomic changes suggested the presence of the *hFUS*^{P525L} mutation was having a larger effect on the predominantly fast-twitch tibialis anterior muscle compared to the spinal cord. The RNA sequencing experiment was done on bulk tissue which means subtle changes affecting specific vulnerable neuron populations and supporting cells specifically may have been diluted. However, the RNA sequencing data does provide an interesting picture of wider tissue-specific changes.

Ribosomal related transcripts were downregulated in both the spinal cord and tibialis muscle suggesting there could be a global issue with translation. Translation has shown to be dysregulated in *in vitro* and *in vivo* models of FUS-ALS (Birsa et al., 2021; Lopez-Erauskin et al., 2018; Sévigny et al., 2020).

In the spinal cord, upregulated transcripts were associated with protein binding and cellular compartmentalising, with many transcripts associated with the actin cytoskeleton such as *Bltp1* (Bridge-like lipid transfer protein family member 1) and *Dystonin*. *Nexilin* was the most upregulated transcript in *hFUS*/*hFUS*^{P525L} mice (fold change = 1.13, adjp=0.014) however this was a minor transcript (*Nexn-201*) and several other *Nexilin* transcripts were unchanged. There was further overlap between tissues as cytoskeletal transcripts were also upregulated in the tibialis anterior muscle with *Titin, Nebulin*, the actin binding protein *Xin* and *Dystrophin*, all having several transcripts significantly upregulated.

Several transcripts associated with muscle function were also upregulated in the TA including several isoforms of *Triadin* which contributes to skeletal muscle

contraction by regulating luminal Ca^{2+} release and maintenance of triads, functionally affecting muscle strength (Oddoux et al., 2009). Various myosin heavy chain transcripts were also upregulated.

Downregulated transcripts in the TA muscle were highly associated with mitochondria organisation and function; both mitochondrially and nuclear encoded. Other models of FUS-ALS have found reduced numbers of mitochondria within muscle synapses may be an early disease change (So et al., 2018). Other differentially expressed transcripts of note include *Mafb-201* which is part of a family of proteins which regulate type IIb, fast myofibre determination (Sadaki et al., 2023). *Vegfa, Vegfb* and *Myoglobin* transcripts were also downregulated. The resulting proteins all have roles in angiogenesis, endothelial cell growth and oxygen flow in skeletal muscle. VEGF has already been shown to promote neurogenesis, neuroprotection, and glial growth and so downregulation may make the muscle more vulnerable if exposed to nerve damage (Rosenstein et al., 2010; Shefner et al., 2023).

Taken together, the transcript changes in the muscle indicate a change in structure, altered fibre type composition and altered energy metabolism. This could suggest the TA muscle may be moving towards a composition containing an even higher percent of type II, fast-fatigable fibres. Type II fast fatigable fibres are glycolytic, containing fewer mitochondria and are used for short bursts of muscle power. Further work would be needed to see if these transcriptomic changes give rise to the proposed fibre type switch at the functional level in young *hFUS/hFUS*^{P525L} mice, and whether this switch is something which happens as the muscle develops, or whether environmental factors initiate this as the mice age. It is known that fast-fatigable fibres

are more vulnerable to degenerate in ALS, which could explain why by 15 months of age, when motor symptoms are also seen, there is a decrease in type II fibres in the TA muscle sections, consistent with what is seen in ALS patient muscle biopsies (Frey et al., 2000). Many differentially expressed transcripts pointed towards mitochondrial dysfunction, and this was confirmed by a mitochondrial DNA copy count assay which showed TA muscles from aged *hFUS/hFUS*^{P525L} mice had fewer mitochondria compared to controls suggesting the TA muscles may have issues with energy biogenesis.

Despite the fibre type changes in TA sections from 15-month-old *hFUS/hFUS*^{P525L} mice, there was no significant difference in TA size, rather the muscles trended towards being hypertrophic, which could suggest muscle swelling. By 21 months of age however, the TA muscles of *hFUS/hFUS*^{P525L} mice had atrophied and were smaller than control mice. Interestingly this muscle atrophy had to have occurred independently of spinal cord motor neuron loss but could have been due to other changes that were not analysed such as dysfunctional NMJs. This would not be surprising given that FUS regulates the expression of muscle genes including myogenic transcription factors and synaptic components such as AChR, and that mutations, including *FUS*^{P525L}, can impair NMJ structure and function (Gina Picchiarelli et al., 2019; Shefner et al., 2023; Zhou et al., 2022). Additional work has highlighted a role of FUS in the synapse, beyond local protein translation and gene regulation, as FUS co-localises with pre- and post-synaptic markers (Salam et al., 2021; So et al., 2018). If mutant FUS altered synaptic function this could explain some of the muscle phenotypes observed in the *hFUS/hFUS*^{P525L} mice, but this is speculative and further work would be needed to assess the role of hFUS^{P525L} at the synapse such as FUS localisation, the effect of

mutant FUS on mitochondrial function and if there was altered synaptic transmission in mutant mice.

Together, data collected during this project supports the dying-back hypothesis which proposes that ALS is a distal axonopathy which is triggered by changes in peripheral tissues and nerve terminals such as the neuromuscular junction.

3.5.5 There is indirect evidence both gain and loss of FUS function mechanisms are driving phenotypes seen in the *hFUS/hFUS^{P525L}* mice

Both gain and loss of function mechanisms have been proposed in FUS-ALS. The working hypothesis in the field is that increased FUS in the cytoplasm leads to depletion of wildtype FUS function in the nucleus, whilst mutant FUS also has toxic gain of function effects in the nucleus and cytoplasm (Birsa et al., 2020; Scekic-Zahirovic et al., 2016).

Loss of FUS function could explain some of the phenotypes seen in the *hFUS/hFUS^{P525L}* mice such as malocclusion and sub viability, as these phenotypes mimic those seen in *Fus$^{-/-}$* mice.

Loss of FUS function cannot however explain all phenotypes, as there were many more phenotypes present in the *hFUS/hFUS^{P525L}* mice than in the *Fus$^{+/-}$* mice, and *hFUS/hFUS* wildtype mice, both of which have a mild reduction in FUS expression and therefore function. This is consistent with what is seen by other groups modelling FUS NLS mutations whereby loss of FUS function alone could not explain the phenotypes observed in the motor neurons and NMJ of FUS mutant mice, such as motor neuron loss (Korobeynikov et al., 2022; Gina Picchiarelli et al., 2019). RNA sequencing data which compared transcriptomic expression between *hFUS/hFUS^{P525L}* mice and *Fus$^{+/-}$*

mice further supported this argument. There was a strong negative correlation in fold change of transcripts indicating presence of the *hFUS*^{P525L} mutation was having the opposite effect on transcript expression than loss of FUS function.

3.5.6 The heterozygous humanised *hFUS*^{P525L} mice are likely modelling early stages of disease

The right model for ALS research depends on the question being asked. The mild behavioural, motor, and cellular and molecular phenotypes the *hFUS/hFUS*^{P525L} mice exhibit are likely modelling an early, prodromal stage of ALS. This early stage is most likely to be targetable to slow, or even halt, disease progression in ALS-patients. The *hFUS/hFUS*^{P525L} mice are not experiencing widespread motor neuron loss, becoming paralysed or dying prematurely of clinical ALS symptoms. Instead, they are developing early signs relevant to the disease, but do not develop late-stage disease phenotypes within the lifespan of the mouse. Even in human patients with early onset of disease it takes many years to show clinical ALS symptoms which may reflect the time taken for pathological FUS assemblies to propagate and drive toxic pathways.

It is clear some of the phenotypes seen in the *hFUS/hFUS*^{P525L} mice are developmental rather than neurodegenerative. Rather than making the model less valid, this may be more faithfully replicating the wider systemic changes that occur in FUS-ALS patients. Part of what we are seeing in the *hFUS/hFUS*^{P525L} mice may be subtle developmental molecular changes which predispose disease vulnerability in certain cell types and tissues.

4 Chapter 4: Using primary cell cultures from embryonic spinal cords to study cellular and molecular phenotypes

4.1 Introduction

The cellular and molecular changes occurring within motor neurons in ALS are hard to study *in vivo* due to their location within the body. Rather researchers are largely restricted to studying changes post-mortem in patients or animal models. Primary cell cultures generated from tissue biopsies are a method used to counteract this issue, as are other *in vitro* models such as induced pluripotent stem cell (iPSC) and embryonic stem cell (ESC) derived neurons. All have their advantages and disadvantages. Primary cells have the same genetic landscape and closely mimic the physiological state of the tissue from which they were derived meaning they can be used for in depth cell biology phenotyping *in vitro*. But primary neuronal cells are also time consuming to collect, have a short lifespan with which to work, and likely represent immature, developing neurons.

For over 20 years, the generation of primary motor neuron cultures from murine tissue has been described (Arce et al., 1999). It is from this original report that the method used to yield primary neuronal cultures used in this chapter was adapted and published by the Schiavo lab at UCL (Fellows et al., 2020). To collect the primary cell cultures, spinal cords were dissected from embryonic (E)12.5-13.5-day old mouse embryos, and large motor neurons preferentially selected using centrifugation gradients. As described by Arce and colleagues, E12.5-day-old embryos were used as at this time motor neurons become specified and pruning occurs and E12.5 provided a

higher yield of motor neurons than if taken at a later embryonic stage (Arce et al., 1999, Yan and Johnson, 1988).

In this chapter, the role of mutant FUS^{P525L} in stress granule (SG) dynamics and at the mitochondria was assessed in primary neuronal cultures. FUS is known to be recruited to cytoplasmic SGs and altered SG dynamics have been reported to play a role in FUS-ALS (Baron et al., 2013; Dormann et al., 2010; Marrone et al., 2018; Sama et al., 2013; Szewczyk et al., 2023; Vance et al., 2013; Zhang et al., 2020). In a mouse model of FUS-ALS, authors also found increased expression of SG markers which co-localised with cytoplasmic FUS after a stress challenge (Zhang et al., 2020). More recently, SG disassembly was shown to be affected in motor neurons expressing the *FUS^{P525L}* mutation in a stress-specific manner, with SGs induced by heat shock showing increased disassembly time (Szewczyk et al., 2023). Mitochondrial abnormalities have also been found in transgenic and targeted knock-in models of FUS-ALS, along with our *hFUS/hFUS^{P525L}* model described in chapter 3 (Devoy et al., 2017; Scekic-Zahirovic et al., 2017; So et al., 2018; Zhang et al., 2020). The formation and disassembly of SGs is ATP-dependent and so mitochondrial function was assessed to see if this was altered by the presence of the *hFUS^{P525L}* mutation.

4.2 Aims and hypotheses

Hypotheses:

1) There will be mild increased cytoplasmic FUS protein in *hFUS^{P525L}* cells compared to cells expressing *hFUS* wildtype due to the presence of the NLS mutation.
2) Cells expressing the *hFUS^{P525L}* mutation will recruit mutant but not wildtype FUS to SGs when exposed to oxidative stress.

3) Cell survival will be decreased in *hFUS*/*hFUS*^{P525L} cells compared to wildtype after acute exposure to oxidative or osmotic stress.
4) Cell cultures expressing the *hFUS*^{P525L} mutation will display mitochondrial defects compared to cell cultures homozygous for *hFUS.*

Aims:

a) Characterise the cell culture populations:

- Stain cultures for markers of neuronal and non-neuronal cells.

b) Quantify FUS localisation in the cell cultures:

- Stain cultures for FUS and quantify FUS localisation is the nucleus and cytoplasm.

c) Determine the response of cell cultures to oxidative and osmotic stress

- Stress cultures using sodium arsenite as an oxidative stressor and sucrose as an osmotic stressor and fix immediately or allow to recover.
- Stain for FUS and SG markers to assess FUS localisation in response to stress in mutant and wildtype cells.
- Use a survival assay to see if cells expressing the *hFUS*^{P525L} mutation have a worse survival after stressing.

d) Assess mitochondrial function:

- Use seahorse assay to quantify mitochondrial function.
- Use TRME assay to determine the mitochondrial membrane potential as a readout of mitochondrial health and survival.

4.3 Contributions

The embryo dissection protocol used in this chapter was kindly provided and demonstrated by Dr David Villarroel Campos at UCL.

The staff in ward five at MRC Harwell were instrumental in setting up the timed mouse breeding to allow embryos to be collected at E12.5-E13.5 days.

The FUS^{P525L} specific antibody used in section 4.4.2 was designed and generated by Dr Marc-David Ruepp and Dr Anny Devoy at King's College London.

4.4 Results

4.4.1 Cell cultures collected from E12.5-E13.5-day old embryos were a mix of neuronal and non-neuronal cells

Cells were dissected from the ventral spinal cord of E12.5-E13.5-day-old embryos and grown for five days. Brightfield images were taken each day and over time cells started to form processes (Figure 4.1).

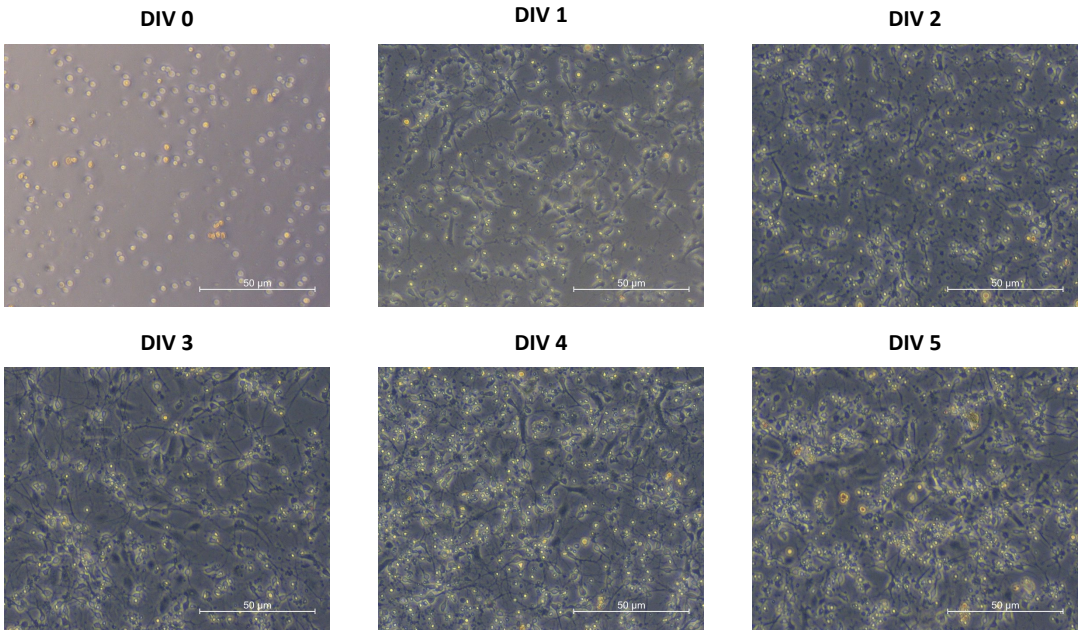


Figure 4.1: 10x brightfield images of primary cell cultures collected from E12.5-E13.5-day-old embryo spinal cords. A) *DIV 0 shows how the cells look immediately after dissociation of the embryonic spinal cord and plating.* ***B)*** *DIV 1 shows how cells look one day after plating,* ***C)*** *DIV 2 after two days,* ***D)*** *DIV 3 after three days,* ***E)*** *DIV 4 after four days,* ***E)*** *DIV 5 after five days. Scale bars represent 50µm.*

Before using the neuronal culture for downstream experiments, it was important to understand what cell types the cultures contained.

Cultures were fixed after five days and stained for neuronal and non-neuronal markers. Cultures stained strongly for markers associated with neuronal cell axons and

dendrites (MAP2, Tau and Beta Tubulin III) indicating the presence of neuronal cells in the primary culture, along with microglia and astrocytes (Figure 4.2). Islet1 and ChAT were used as markers of motor neurons specifically. Islet1 (Figure 4.2D) and ChAT (data not shown) staining suggested there were few motor neurons in the culture. As the culture did not contain a high proportion of motor neurons, the neurons present were likely sensory neurons or interneurons, but further staining would have to be carried out to confirm this.

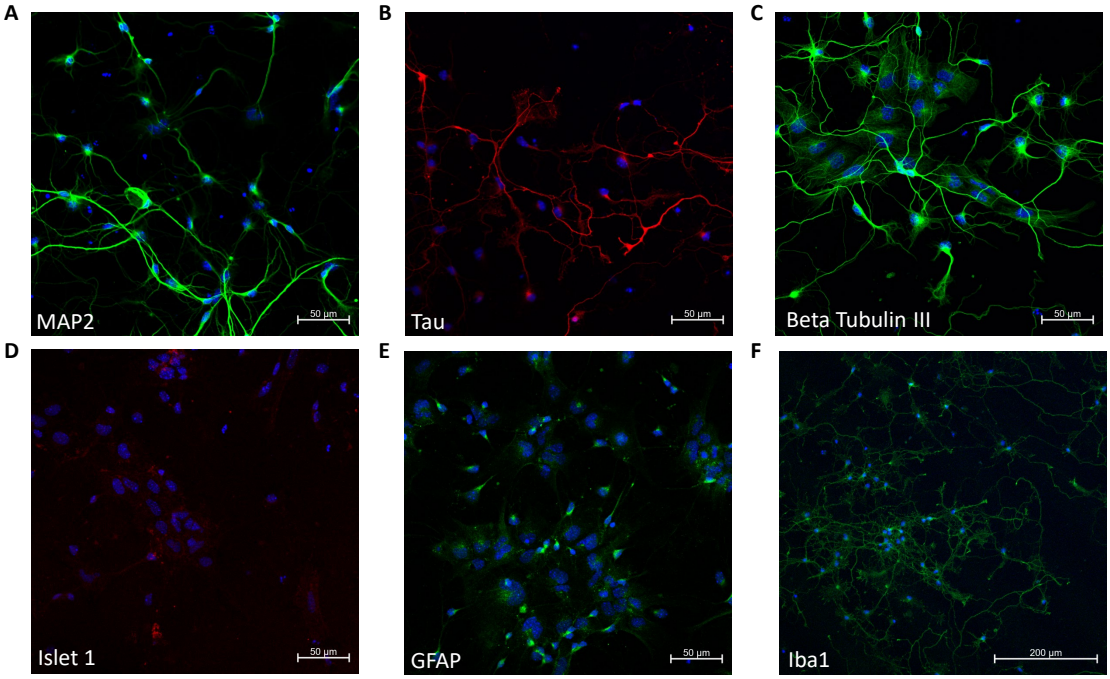


Figure 4.2: Primary cultures extracted from spinal cords of E12.5-E13.5-day-old embryos express markers indicative of neuronal and non-neuronal supporting cells. *Primary cultures were grown for five days before fixing and staining.* ***A)*** *The cultures expressed MAP2 (green) which is a neuronal specific protein expressed in neuronal dendrites.* ***B)*** *Cells within the population also expressed Tau (red) which is a marker of neuronal axons.* ***C)*** *Beta Tubulin III (green) is a marker of microtubules found in axons and was expressed strongly throughout cells in the culture.* ***D)*** *Islet 1 (red) was used as a motor-neuron specific marker. Islet 1 staining was weak and sparce suggesting there were few motor neurons in the culture.* ***E)*** *There were also cells within the population which expressed GFAP (green) which is a marker of astrocytes, glia, and ependymal cells.* ***F)*** *Iba1 (green) was also expressed within the cell culture which is a marker of microglia. Cells were co-stained with DAPI to visualise nuclei (blue). Scale bars represent 50µm (A-E) and 200µm (F).*

4.4.2 The amount of cytoplasmic FUS is increased in cells expressing the *hFUS^{P525L}* mutation

Cultures were stained with FUS antibodies, one which bound total FUS with or without the mutation, and a second which bound hFUS^{P525L} specifically.

In *hFUS/hFUS* cultures, FUS was predominantly nuclear. In contrast, FUS was clearly visible in the cytoplasm and axons of cells from *hFUS/hFUS^{P525L}* embryos, although like that seen *in vivo*, a large proportion remained nuclear (Figure 4.3B).

Staining with the P525L specific antibody showed hFUS^{P525L} was localised to the cytoplasm to varying degrees in *hFUS/hFUS^{P525L}* cells; in some cells hFUS^{P525L} was nearly all nuclear whereas in neighbouring cells there was increased hFUS^{P525L} in the cytoplasm (Figure 4.3D).

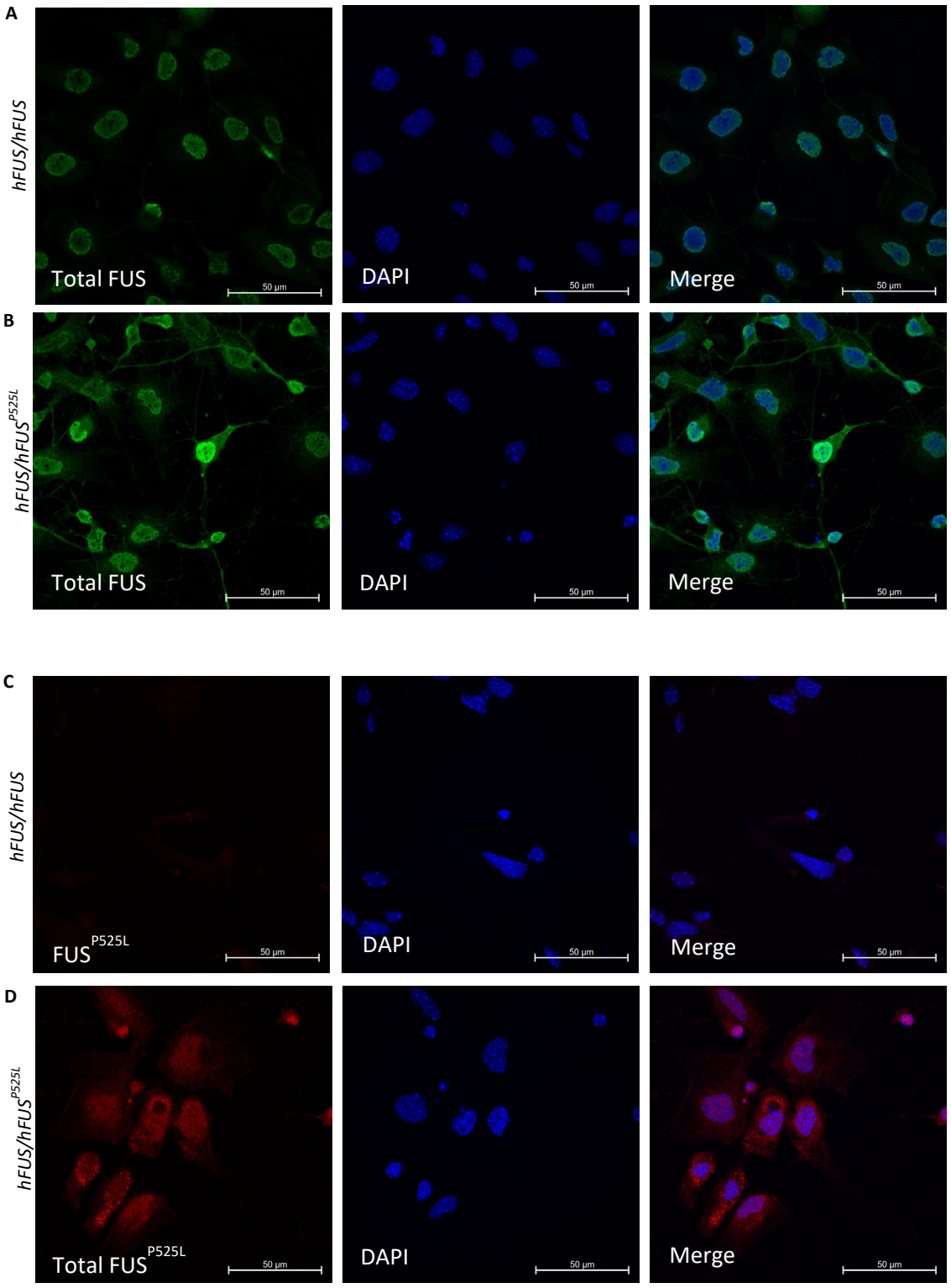


Figure 4.3: There is increased FUS in the cytoplasm in cells expressing the hFUS^{P525L} mutation. *Cells were fixed and stained with an antibody raised against the N terminus of the FUS protein (Novus 565) so binding should be unaffected by the presence of the FUS^{P525L} mutation (total FUS) or an antibody raised against FUS^{P525L}.* ***A)*** *Representative image of total FUS (green) staining in cells expressing hFUS/hFUS.* ***B)*** *Representative image of total FUS (green) staining in cells expressing hFUS/hFUS^{P525L}.* ***C)*** *Representative image of FUS^{P525L} (red) staining in cells expressing hFUS/hFUS.* ***D)*** *Representative image of FUS^{P525L} (red) staining in cells expressing hFUS/hFUS^{P525L}. Cells were co-stained with DAPI to visualise (blue). Scale bars represent 50μm.*

4.4.3 FUS protein is recruited to stress granules after exposure to oxidative stress in *hFUS/hFUS^{P525L}* but not wildtype cell cultures

Before stress was applied, there was increased FUS in the cytoplasm in *hFUS/hFUS^{P525L}* cultures compared to *hFUS/hFUS* cultures (Figure 4.3). G3BP1 co-staining allowed the cytoplasm to be visualised and FUS localisation to be quantified (Figure 4.4C). Primary and secondary only control staining suggests FUS and G3BP1 staining was specific (Figure 8.10).

In *hFUS/hFUS* cultures FUS protein was 80% nuclear on average, representing the fact FUS shuttles between the nucleus and cytoplasm to carry out its cytoplasmic roles. In *hFUS/hFUS^{P525L}* cultures, an average of 73% of FUS protein was nuclear.

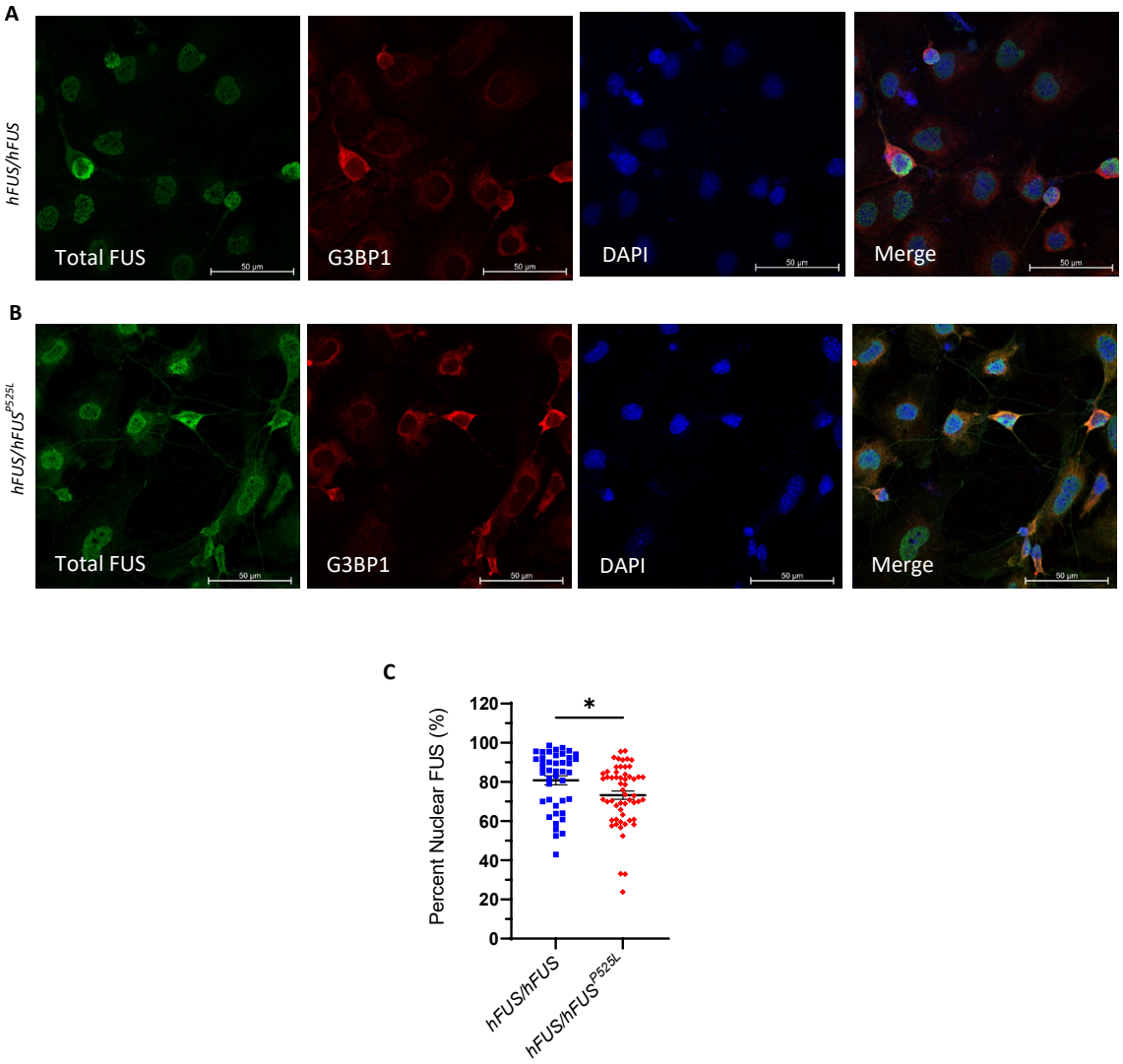


Figure 4.4: Increased FUS is localised to the cytoplasm in hFUS/hFUS^{P525L} primary cultures before oxidative stress is applied. *Primary neurons were fixed and stained with an antibody which binds residues 1 and 50 of the N terminus of the human FUS protein and so in theory will bind both wildtype and mutant hFUS^{P525L} protein. Cells were co-stained with G3BP1, a SG marker which under wildtype conditions is diffusely spread throughout the cytoplasm.* ***A)*** *In hFUS/hFUS cells, FUS (green) is predominantly nuclear.* ***B)*** *In hFUS/hFUS^{P525L} cultures, FUS (green) is seen in the nucleus and cytoplasm.* ***C)*** *Using G3BP1 (red) as a cytoplasmic marker and DAPI (blue) as a nuclear marker, the percentage of FUS protein localised to each compartment was calculated. hFUS/hFUS^{P525L} cells had a significant reduction in nuclear FUS protein compared to hFUS/hFUS cells. Scale bars represent 50μm. Data are shown as mean average ± SEM with significance analysed using an unpaired Student's T test. *=p<0.05.*

When stressed, cells produce SGs to conserve energy and protect the cell; cytoplasmic FUS liquid-liquid phase separates to bind with other SG proteins to form membrane-less SGs under stress conditions (Dormann et al., 2010; Vance et al., 2013). When the stressor is removed, SGs should dissipate. It has been proposed that in FUS-ALS SGs do not disassemble correctly and that SGs may precede more persistent FUS inclusions seen in FUS-ALS patients (Dormann et al., 2010). How SGs transition to aggregates is not well understood.

Primary cell cultures were exposed to sodium arsenite, an oxidative stressor, for one hour to evaluate SG formation in response to acute stress. G3BP1 staining was used as a marker of SG formation.

When oxidative stress was applied for one hour, primary cells produced SGs as demonstrated by G3BP1 staining forming cytoplasmic puncta. In *hFUS/hFUS* cultures, FUS staining remained predominantly nuclear (Figure 4.5A). In *hFUS/hFUS*^{P525L} cultures however, cytoplasmic FUS formed puncta which overlapped with G3BP1 staining suggesting FUS protein was recruited to SGs (Figure 4.5B). Because the FUS antibody used stained total FUS protein, it cannot be determined whether FUS protein localised to SGs in *hFUS/hFUS*^{P525L} cultures was hFUS^{P525L} or wildtype FUS protein.

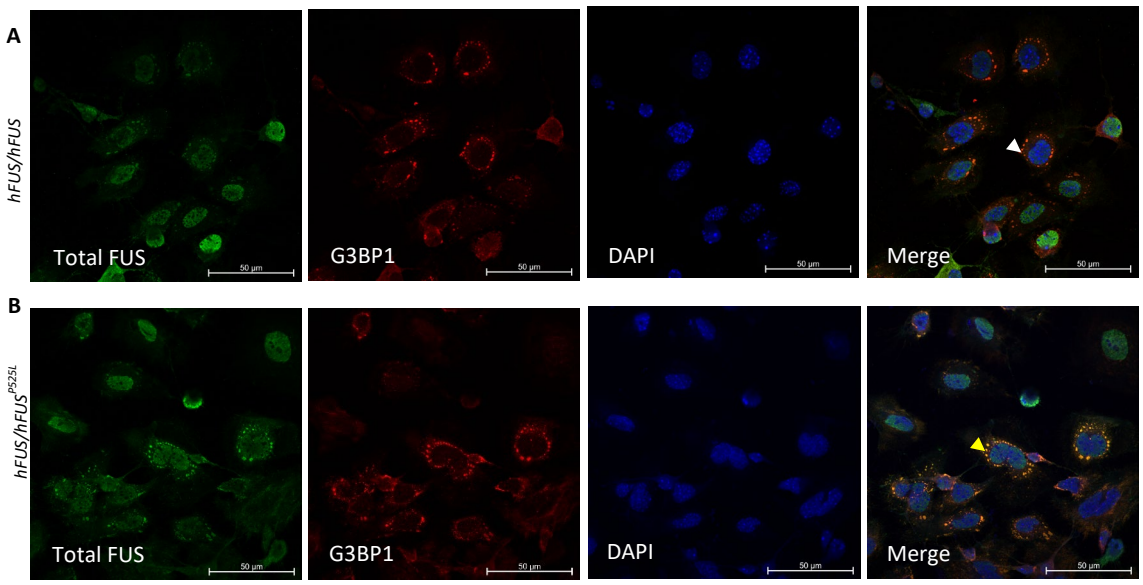


Figure 4.5: Oxidative stress induces SGs which co-localise with FUS in hFUS/hFUS^{P525L} but not wildtype primary cultures. *The primary cell cultures were stressed for one hour using 50mM sodium arsenite as an oxidative stressor. Cells were fixed immediately post stress and dual stained with an antibody raised against the N terminus of FUS (green) and G3BP1 (red) as a marker of SGs.* ***A)*** *hFUS/hFUS cultures produced SGs (white arrow) but FUS staining remained predominantly nuclear.* ***B)*** *In contrast, in hFUS/hFUS^{P525L} cells, FUS protein co-localised with cytoplasmic SGs (yellow arrow). Cells were co-stained with DAPI to visualise nuclei (blue). Scale bars represent 50μm.*

Cells were also imaged after the stressor was removed and cells were allowed to recover for 24 hours to see if SG dispersal differed between *hFUS/hFUS* and *hFUS/hFUS^{P525L}* cultures. G3BP1 staining was diffuse in cell cultures from both genotypes after 24 hours suggesting SGs had successfully dissipated.

In *hFUS/hFUS* cultures, FUS was primarily nuclear and there was no obvious overlap with G3BP1 staining (Figure 4.6A). In *hFUS/hFUS^{P525L}* cultures, although the stress granules had dissipated, the cells did not look healthy; some cell nuclei were condensed and misshapen which can indicate apoptosis (white arrows, Figure 4.6B).

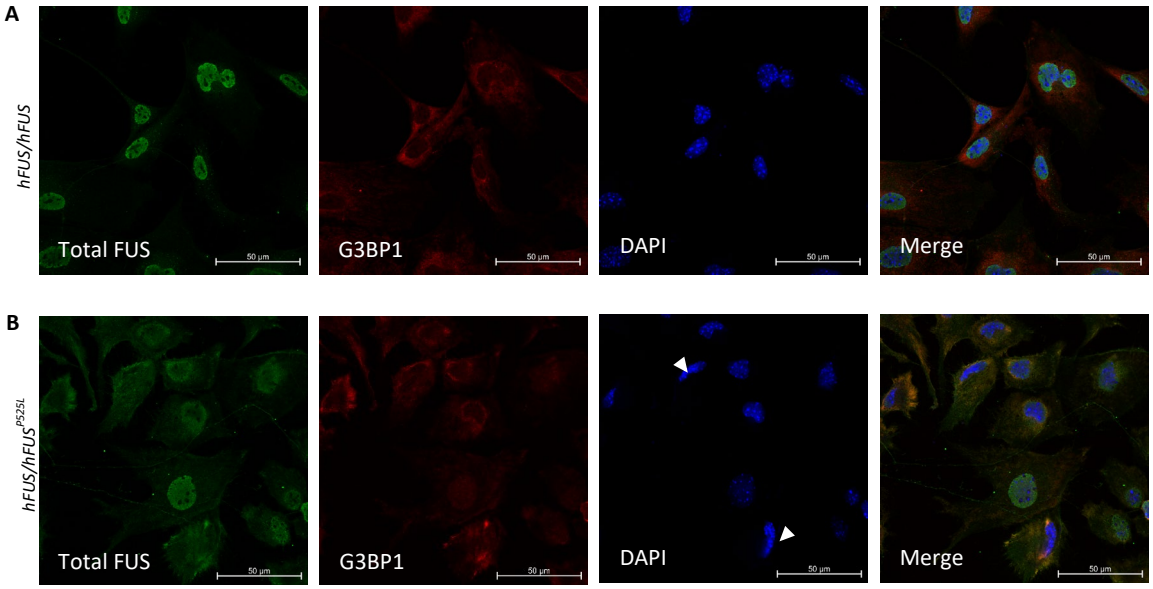


Figure 4.6: There is increased cytoplasmic FUS in hFUS/hFUS^{P525L} cultures after oxidative stress is removed. *After stressing cells for one hour with sodium arsenite, the stress was removed, cells washed and left to recover for 24 hours. Cells were then fixed and stained with an antibody raised against the N terminus of FUS (green) and G3BP1 (red).* ***A)*** *FUS protein remained nuclear and SGs were no longer visible in hFUS/hFUS cells.* ***B)*** *Cells expressing the hFUS/hFUS^{P525L} mutation no longer had visible SGs. FUS protein was spread throughout the nucleus and cytoplasm. White arrows indicate condensed nuclei. Cells were co-stained with DAPI to visualise nuclei (blue). Scale bars represent 50μm.*

4.4.4 There was no difference in cell survival after stress between genotypes

A survival assay was carried out to see if altered SG dynamics altered cell viability in primary cultures expressing the *hFUS^{P525L}* mutation. Two different stress inducers were used as it is known SG dynamics are stress dependent.

Cells were stressed with either sodium arsenite as an oxidative stressor, or sucrose as an osmotic stressor for one hour. The stressor was then removed, and cells were allowed to recover for 24 hours. After recovery, toxicity and cell viability assays were completed.

There was no difference in toxicity or viability observed in cells from either genotype (Figure 4.7).

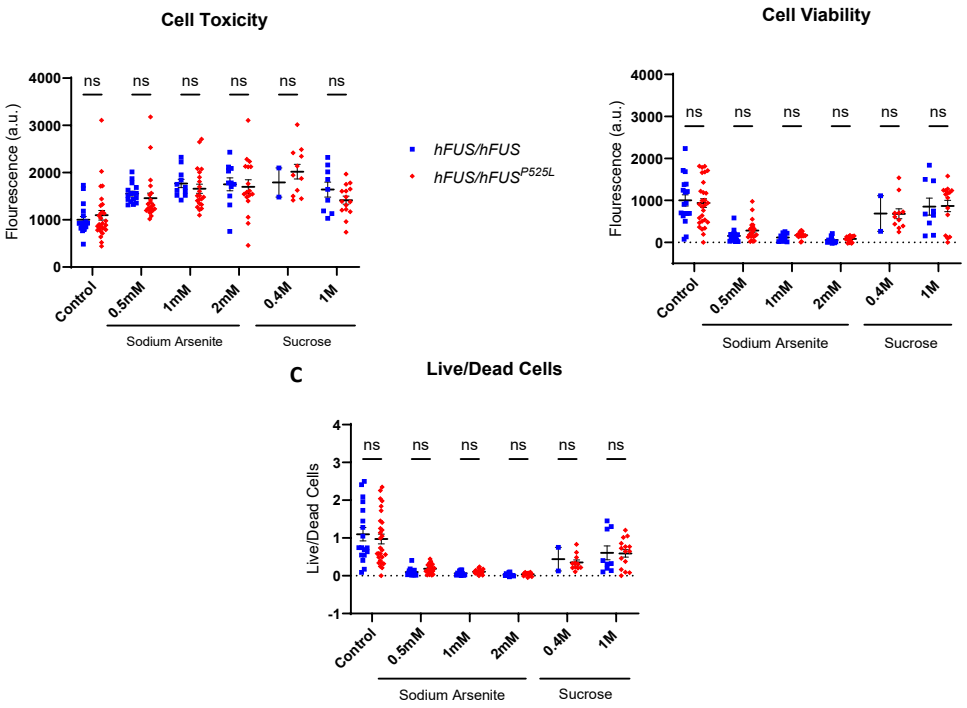


Figure 4.7: There was no difference in cell viability or toxicity between genotypes after stress. *Cells were stressed for one hour with either sodium arsenite or sucrose of varying concentrations. The stressor was then removed, and cells allowed to recover for 24 hours. After 24 hours, a cell toxicity assay was completed, followed by a cell viability assay.* ***A)*** *Cell toxicity assays showed both stressors at all concentrations caused increased cell death compared to control wells.* ***B)*** *Cell viability was reduced in both genotypes after cells were stressed with sodium arsenite. Sucrose also reduced viability, but this was less severe than was seen with sodium arsenite stress.* ***C)*** *The ratio of live vs dead cells was calculated, and this was reduced after all stress conditions compared to control wells but was not different between genotypes. Data are shown as mean average ± SEM with significance analysed using a two-way ANOVA and Šídák's multiple comparisons post-hoc test. ns = not significant.*

4.4.5 Cells expressing the *hFUS*^{P525L} mutation have altered mitochondrial function

Mitochondrial function was probed in primary cell cultures using the Agilent Seahorse Mito Stress Test kit. Three compounds were injected into the cell media allowing different aspects of mitochondrial respiration to be analysed using oxygen consumption rate (OCR) as a readout. Figure 4.8A highlights the OCR of both genotypes throughout the experiment, from which, further readouts can be calculated. Cells expressing the *hFUS*^{P525L} mutation performed significantly differently

to control cells in three areas of mitochondrial function: 1) Basal respiration, 2) ATP-linked respiration and 3) Reserve capacity (Figure 4.8B).

Basal respiration is a measure of the oxygen required to meet the ATP demands of the cell. Increased basal respiration rates seen in *hFUS/hFUS*^{P525L} cultures suggests the mutant cell cultures have an increased energetic demand under baseline conditions.

When oligomycin is injected, a potent ATP synthase inhibitor, the proportion of basal respiration driving ATP production can be calculated. *hFUS/hFUS*^{P525L} cells had a significant increase in ATP-linked respiration compared to *hFUS/hFUS* cultures.

Spare or reserve capacity is a measure of the ability of cells to respond to increased energy demand or stress. *hFUS/hFUS*^{P525L} primary cultures had a significantly lower reserve capacity than controls, likely because the basal respiration rate was already significantly higher before stress was induced.

There was no difference in mitochondrial membrane potential (MMP) as determined by TMRE staining, which is a readout of mitochondrial health and viability.

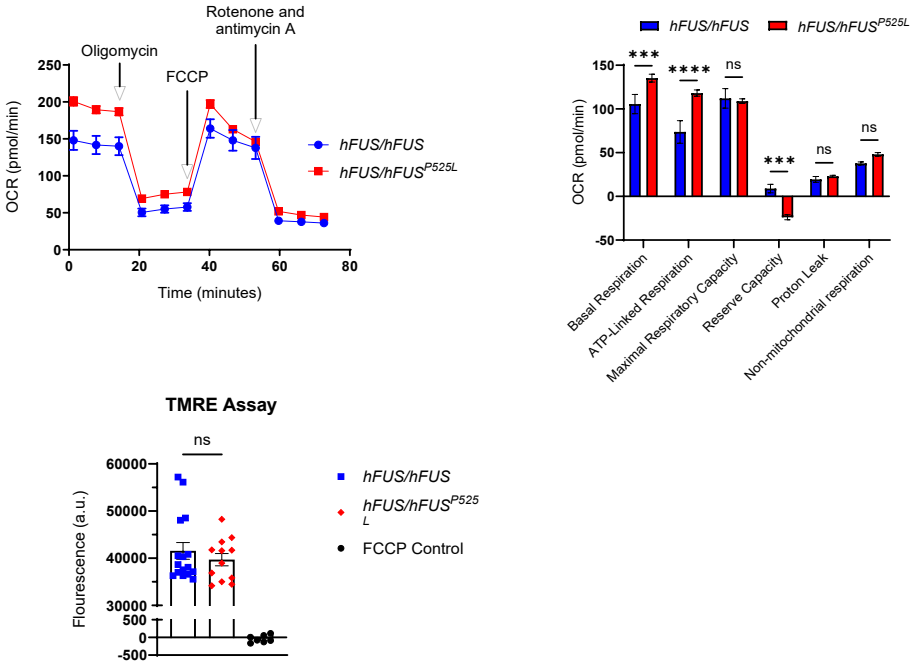


Figure 4.8: Cells expressing the hFUS^{P525L} mutation have altered mitochondrial function. *Primary cultures were grown for five days before assessing mitochondrial function using the Seahorse Mito Stress Test.* ***A)*** *Oxygen consumption rate (OCR) is measured throughout the stress test experiment to quantify mitochondrial function. After measuring basal respiration rates, oligomycin is added which inhibits ATP synthase (complex V) of the mitochondrial electron transport chain (ETC), reducing electron flow through the ETC. FCCP (Carbonyl cyanide-4 (trifluoromethoxy) phenylhydrazone) is then added which collapses the proton gradient and disrupts the mitochondrial membrane potential, increasing electron flow through the ETC and complex IV oxygen consumption reaches its maximum. Finally, rotenone and antimycin A are added which inhibit complex I and complex III respectively. Inhibition of these complexes stops mitochondrial respiration allowing the contribution of non-mitochondrial respiration to be calculated.* ***B)*** *Parameters of mitochondrial function calculated from A.* ***C)*** *TMRE Assay shows no difference in mitochondrial membrane potential between cells from hFUS/hFUS or hFUS/hFUS^{P525L} cultures. Data are shown as mean average ± SEM with significance analysed using a two-way ANOVA and Šídák's multiple comparisons post-hoc test or an unpaired T test. ns = not significant, ***=p<0.001, ****=p<0.0001.*

4.5 Discussion

In this chapter, primary neuronal cultures from *hFUS/hFUS* and *hFUS/hFUS*^{P525L} embryos were used to analyse SG dynamics and mitochondrial response to stress.

The aim of this project was to generate a primary motor neuron culture however the protocol used generated a mixed population of cells containing neurons (likely sensory neurons and interneurons), glia, and astrocytes, with a low proportion of motor neurons. More work would be needed to optimise collection to study the effect of the *hFUS*^{P525L} mutation in primary motor neurons specifically as the cells as the project had initially intended. Whilst the mixed population meant the response of a single cell type could not be assessed, the presence of multiple cell type may more faithfully replicate the spinal cord environment. Co-culturing iPSC-derived motor neurons with supporting cells such as glia has been shown to recapitulate up to 40% of up-regulated gene expression changes associated with neuronal maturation (Patel et al., 2022) highlighting the importance of additional cell types to replicate neuronal function *in vitro*.

Any *in vitro* cell system is artificial in some way and a disadvantage of the primary neuron cultures generated, beyond the fact there was a low proportion of motor neurons, is that cells which were present likely model an immature neuronal state when generated from embryonic tissue. Motor neurons are considered specified at E10.5 but reports have shown motor neurons are not functionally mature until post-natal day 21 according to gene expression profiles (Patel et al., 2022). Thus, cells collected from E12.5-E13.5-day old embryos will likely not exhibit all functionality associated with mature neurons; rather they will represent an early, immature

neuronal state. The primary cells were also only grown for five days in culture meaning they were very young; at DIV five they would not have formed functional synapses. DIV five was used for practical reasons but further work growing the cells for longer and seeing how this affected neuronal function would have been valuable future work.

If disadvantages of the model are considered when drawing conclusions, as should be the case with any model of disease, primary cell cultures represent a useful tool for studying cellular and molecular disease phenotypes in neuronal cells, likely modelling early disease changes in immature neurons.

4.5.1 Increased FUS is localised to the cytoplasm in *hFUS/hFUS^{P525L}* cells

In *hFUS/hFUS* cell cultures, FUS protein was only 80% nuclear likely because FUS protein shuttles between the nucleus and the cytoplasm to carry out its wildtype role (Zinszner et al., 1997). In *hFUS/hFUS^{P525L}* cells, cytoplasmic FUS was mildly but significantly increased compared to *hFUS/hFUS* cells, supporting what is seen in other cell and animal models, including adult *hFUS/hFUS^{P525L}* mice. Further work co-staining the primary cultures with cell type specific markers could ascertain if increased cytoplasmic FUS localisation differed between cell types, and what effect this may have on the function of different cell types in FUS-ALS.

4.5.2 FUS protein is recruited to stress granules (SGs) in *hFUS/hFUS^{P525L}* cells

SGs are defined as cytoplasmic membrane-less structures containing mRNA and other proteins (Anderson & Kedersha, 2008). SGs are formed when stressors trigger translational arrest to conserve cellular energy, disrupting mRNA biogenesis. mRNA is lost from polysomes and is subsequently recruited into SGs to be sorted. Additional SG associated proteins include eIF2α kinases which monitor the environment and

modulate translational machinery, and RNA binding proteins which alter RNA processing such as SMN and G3BP (Anderson & Kedersha, 2008). As such, the formation of SGs is vital to protect cells from external stressors and preventing their formation is not necessarily neuroprotective (Szewczyk et al., 2023). However, it has been suggested SGs act as precursors for larger cytoplasmic inclusions (Dormann et al., 2010). A two-hit model has been proposed whereby NLS mutant FUS is localised to the cytoplasm (first hit) and subsequently recruited to SGs when cells are stressed (second hit). If cells are chronically stressed, SGs may persist, leading to larger inclusions seen in FUSopathy patients (Dormann et al., 2010). Under physiological conditions, SGs disassemble once the stressor is removed, however when mutant FUS is expressed, SGs have been shown to increase in number and remain for longer (Baron et al., 2013; Dormann et al., 2010; Marrone et al., 2018; Szewczyk et al., 2023; Zhang et al., 2020).

Expression of *hFUS*^{P525L} alone was not sufficient to cause SGs in the primary cell cultures; although redistributed to the cytoplasm, FUS remained diffuse in mutant cells. This is consistent with other reports analysing mutant FUS^{P525L} in HeLa cells (Dormann et al., 2010).

FUS localisation in response to stress was assessed in the primary cells to see if this differed between genotypes. Sodium arsenite (SA) was used as an oxidative stressor, thought to induce oxidative stress through the production of reactive oxygen species (ROS). An antibody against G3BP1 was used as a marker of SGs specifically (Dormann et al., 2010).

In *hFUS/hFUS* cultures, FUS remained predominantly nuclear and there was less co-localisation with SGs. There have been conflicting reports on whether wildtype FUS

is recruited to SGs after oxidative stress (Dormann et al., 2010; Szewczyk et al., 2023) and so it may be that very low levels of FUS co-localised with SGs in *hFUS/hFUS* cultures which were not detected with the antibody used. FUS staining overlapped with G3BP1 SG staining in *hFUS/hFUS*^{P525L} cultures suggesting co-localisation, which is consistent with other reports (Dormann et al., 2010; Szewczyk et al., 2023; Zhang et al., 2020).

During this project, Szewczyk and colleagues published their work studying the effect of the FUS^{P525L} mutation on SG size, abundance, and dynamics in iPSC-derived motor neurons (Szewczyk et al., 2023). Authors found the effect of mutant FUS on SG disassembly was stress specific, likely due to the formation of distinct SG protein compositions by different stressors. Authors found that disassembly of SGs induced by heat shock was more disrupted than disassembly of SGs induced by oxidative stress. They propose that because mutant FUS was sufficient to upregulate heat shock proteins and disrupt proteostasis under baseline conditions, the chaperone system could not elevate its response sufficiently during heat stress and became overwhelmed.

Further work could be done using the primary cell cultures to assess SG dynamics in more detail such as abundance, size, and kinetics of disassembly, all of which are thought to be relevant to their function (Baron et al., 2013). Given what was seen in iPSC-derived motor neurons, it is hypothesised both size and abundance of SGs would be increased in *hFUS/hFUS*^{P525L} cultures after oxidative stress (Szewczyk et al., 2023). There are several reasons why mutant FUS may increase the abundance of SGs. The presence of the NLS mutation means there is increased FUS in the cytoplasm, and

likely an altered ability of FUS to LLPS, both of which increase the likelihood of FUS inclusions to form. Szewczyk and colleagues propose that rather than the liquid-liquid properties of FUS, it rather depends on the protein composition of SGs and how the interactions of these component proteins may be altered by the presence of mutant FUS. Further work in the primary cell cultures could focus on assessing the composition of SGs and how this differs when cells are exposed to different stressors. This could help us to understand how exposure to different stress leads to neuronal death and how this could be blocked or reduced in human patients.

4.5.3 There is no difference in cell survival after one hour exposure to oxidative or osmotic stress between cells expressing wildtype or mutant FUS

There was no difference in cell viability or toxicity after acute exposure to oxidative or osmotic stress between *hFUS/hFUS* and *hFUS/hFUS*^{P525L} cells, consistent with reports in iPSC-derived motor neurons (Szewczyk et al., 2023). As proposed by Szewczyk and colleagues, it could be that altered SG dynamics somehow protect neurons from degeneration, at least in models of immature neurons such as iPSC and primary neuronal cultures, although this may change as neurons age. What was apparent from this survival assay was that different types of stress had different effects on cell viability and toxicity, even if not between genotypes. It would be interesting further work to see what different cellular mechanisms were induced by different types of cell stress and whether certain pathways were more or less affected by the FUS mutation as has been proposed in the case of oxidative and heat shock stress (Szewczyk et al., 2023).

To note, there was a lot of variability in the viability and toxicity assays; viability in the control group with no stress applied were very spread. The concentration of plated cells and number of days in culture could have been optimised to ensure any cell death was due to the presence of the stressor and not cell conditions. The concentration of cells plated was constrained by the number of cells collected from each embryo, and the number of experimental groups in the survival assay. Cells could also not be combined as genotypes were not determined until after cells were plated. Additionally, media volumes and plate layout could have been optimised as some wells appeared to dry out, particularly around the edges of the plate, which could also cause cell death.

Although no difference in survival was found after acute stress exposure in the primary cell cultures, there is evidence of cell death after chronic stress exposure in *in vitro* and *in vivo* FUS-ALS models (Szewczyk et al., 2023; Zhang et al., 2020). Chronic stress occurs throughout human life in the form of physical, mental, and environmental stressors. It would be interesting future work to assess if exposure to chronic stress increases cytoplasmic FUS localisation in primary cultures expressing the *FUS*^{P525L} mutation, and if the formation and dissociation dynamics of SGs was altered over time. The fact that mutant FUS is more readily recruited to SGs than wildtype FUS, whether due to being in the cytoplasm when SGs are formed, or due to an altered biochemical property of the mutant protein, suggests cumulative stress would increase the probability of persistent FUS inclusions forming and exacerbate loss and gain of toxic function effects.

4.5.4 Mitochondrial function is altered in *hFUS*/*hFUS*^{P525L} cultures

In this project, primary neuronal cell cultures expressing the *hFUS*^{P525L} mutation had increased basal respiration and ATP production rates, paired with a decrease in reserve capacity. Taken together this data suggests the cells expressing mutant FUS were more stressed than cells expressing wildtype FUS under baseline conditions, requiring more energy to function under the 'resting' state. iPSC-derived motor neuron cultures expressing the *FUS*^{P525L} mutation exhibit overactive stress response pathways under basal conditions supporting this finding (Szewczyk et al., 2023). As stress pathways were not studied however, it cannot be confirmed if increased activation of stress response pathways was a factor driving increased basal respiration in the primary cultures.

From personal communication, increased basal respiration is a phenotype seen in other models of familial ALS, such as iPSC-derived motor neurons expressing mutant TDP-43. The reduced reserve capacity seen in the *hFUS/hFUS*^{P525L} cultures suggests mitochondria are already working to fulfil higher energy demands, and so cells would be less able to respond to stress given that SG formation, amongst other events, requires ATP. There was no difference in MMP staining used as a readout of mitochondrial death, suggesting that in the immature neurons, there is no loss of mitochondria. If cells expressing mutant FUS^{P525L} require more energy to function in unstressed conditions, over time this overactive energy production may become detrimental, particularly as mitochondria age and acquire additional age-associated mutations, and can no longer perform their role as efficiently (Payne & Chinnery, 2015). Neurons are highly energy demanding cells, so it is understandable that they are particularly vulnerable to mitochondria dysfunction.

Generally, in other models of familial and sporadic ALS, mitochondrial respiration has been reported to decrease, although some reports are conflicting (Smith et al., 2019). In cell models overexpressing human wildtype or mutant FUS, reductions in both MMP and ATP production have been reported (Deng et al., 2015; Smith et al., 2019; Stoica et al., 2016). It has also been shown that mutant FUS causes damage to the mitochondria; in neuronal and fly models of ALS, levels of FUS protein at the mitochondria are increased, leading to mitochondrial fragmentation and release of ROS (Deng et al., 2018). It is possible then that in overexpressing mutant FUS models, when there is increased FUS protein, this artificially induces mitochondrial dysfunction and a reduction in respiration and MMP. The differences in response to mutant FUS may also represent the different cell types used; a mixed population of neuronal primary cultures compared to HEK293 and NSC-34 cells, highlighting the need to assess phenotypes in the most relevant *in vitro* models of disease, which is not always easy to determine.

Overall, during this exploratory project, phenotypes were observed in the primary neuronal cultures which would be interesting to follow up on and explore in more detail. More work could be done to optimise neuronal collection to enrich for motor neurons, optimise plating conditions to make survival assays more reliable, and study additional stressors and SG markers to study SG dynamics further.

5 Chapter 5: Comparing the severity of two different *FUS* mutations introduced into the humanised *FUS* allele

5.1 Introduction

In this chapter, two ALS-causing *FUS* mutations were compared within a cohort of mice on the same genetic background, allowing conclusions to be drawn about how different *FUS* mutations may cause phenotypes of differing severities.

5.1.1 Do different *FUS* mutations have different severities?

Over 50 mutations in the *FUS* gene are known to cause ALS (An et al., 2019; Deng et al., 2014). Certain *FUS* mutations appear to be more severe than others, based on clinical factors such as age of onset and disease progression, and this seems to correlate with how severely the NLS is disrupted (Dormann et al., 2010; Grassano et al., 2022; Hubers et al., 2015; Naumann et al., 2019; Waibel et al., 2013). However, patients with the same mutation can have different clinical presentations suggesting that mutation alone is not enough to explain the phenotypic variability of FUS-ALS (Grassano et al., 2022; Naumann et al., 2019).

This difference in severity is likely due to mutations localised to the NLS causing a more severe increase in localisation of FUS to the cytoplasm, where it exhibits both loss and gain of function mechanisms of disease. Increased cytoplasmic FUS is observed in patients, although to differing extents and only in certain subsets of neurons and supporting cells (Hewitt et al., 2010; King et al., 2015; I. R. Mackenzie et al., 2010). Many mouse models of *FUS* mutations exist which display increased cytoplasmic localisation of FUS to different extents (Shang & Huang, 2016). However,

there are many confounding factors which could influence phenotypes in these mouse models including different promoters used leading to different expression patterns of the mutated *FUS* gene, different genetic backgrounds, and different housing environments. These and many other factors make it hard to directly compare the effect of different *FUS* mutations in mouse models.

In 2020, Haiyan et al expressed several *FUS* NLS mutations in SH-SY5Y cell lines and found there were interesting differences between the phenotypes observed. This included changes in FUS localisation and expression, the number and size of FUS aggregates, and changes in FUS protein stability, the complexity of which was not fully modelled by NLS knock-out (An et al., 2020). This suggests that different *FUS* mutations have different toxic effects, and further investigation is warranted into how these differences leads to contrasting disease presentations.

5.1.2 *FUS*^{P525L} and *FUS*^{Q519Ifs} mutations

The two *FUS* mutations studied in this chapter are both seen in patients, although *FUS*^{Q519Ifs} is much rarer, with both affecting the NLS. These mutations were chosen as they are known to cause severe forms of ALS in patients, but the way in which the NLS is affected is distinct.

The P525L missense mutation causes leucine to be made in place of proline in the PY NLS sequence due to a point mutation at c.1574 (Figure 5.1). Over 30 clinical cases of patients with the *FUS*^{P525L} mutation have been published which highlight the early onset and rapid disease progression associated with this mutation (Goldstein et al., 2022; Korobeynikov et al., 2022; Zhou et al., 2020).

In the case of the *FUS*^{Q519Ifs} mutation, at c.1554 there is a four-base deletion (c.1554_1557delACAG) leading to a frameshift truncation mutation which abolishes the NLS. At position 519 an isoleucine is made in place of a glutamine and seven further amino acids are then synthesised before a stop codon is reached in the 3'UTR sequence (Figure 5.1). This mutation was sequenced from a male patient aged 18 who presented with bilateral arm weakness quickly progressing to weakness involving neck muscles and swallowing. In addition, the patient was reported to have mild learning difficulties and congenital deformities of both feet (Baumer et al., 2010). The patient died within six months of diagnosis.

As the NLS is abolished with the *FUS*^{Q519Ifs} mutation, this may cause a more severe phenotype than is seen in mice expressing the *FUS*^{P525L} mutation.

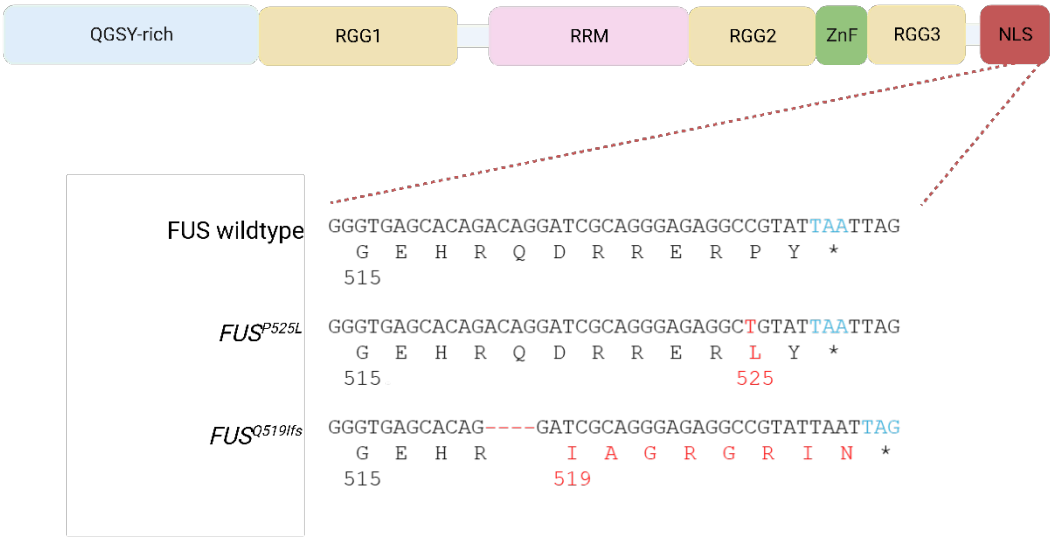


Figure 5.1: hFUS*^{P525L} *and hFUS*^{Q519Ifs} *mutations disrupt the NLS. *Blue letters and asterisk represent a stop codon. Red letters represent the mutated sequence and resulting amino acids. Created with BioRender.com.*

5.2 Hypotheses and aims

Hypotheses:

1) Mice expressing the *hFUS*^{Q519Ifs} mutation will have a more severe phenotype than mice expressing the *hFUS*^{P525L} mutation. This will be evident in outward phenotypic expression.
2) Mice expressing the *hFUS*^{Q519Ifs} mutation will display a more severe increase in localisation of the FUS protein to the cytoplasm due to the more disrupted C terminus of the protein than mice expressing the *hFUS*^{P525L} mutation.
3) Expression of the *hFUS*^{Q519Ifs} mutation will cause increased dysregulation of transcripts that FUS regulates, possibly because of increased FUS protein localised to the cytoplasm.

Aims:

a) Characterise *hFUS*^{P525L} and *hFUS*^{Q519Ifs} knock-in mice longitudinally

- Assess anxiety-like and wellbeing phenotypes
    - Open field and marble burying
- Assess motor function
    - Grip strength
- Expression of the mutated *FUS* gene and FUS protein
    - mRNA and protein expression
- Is there differential gene expression between the two mutations?
    - RNA sequencing of 4-month-old spinal cord tissue
- Histological analysis
    - FUS staining

5.3 Contributions

The generation of humanised *hFUS*^{P525L} mice has already been discussed in detail in chapter 3 and the contributions noted there. Mice expressing the *hFUS*^{Q519Ifs} gene were also generated prior to starting my DPhil by the cellular and molecular team at MRC Harwell.

The ward five team are thanked for their work to breed and maintain the mouse colonies used in this chapter, including weighing the cohort every three weeks.

Dr Charlotte Tibbit helped to carry out the grip strength experiments detailed in section 5.4.4.3.

The necropsy team at MRC Harwell perfused and dissected the spinal cords used for FUS staining in section 5.4.6.

5.4 Results

5.4.1 Generating *hFUS*^{Q519Ifs} mice

The *hFUS*^{Q519Ifs} mice were originally generated at MRC Harwell with the aim of characterising them much in the same way as the *hFUS*^{P525L} mice described in chapter 3 to act as an additional, and perhaps more severe, model of FUS-ALS. However, generating cohorts of mice expressing the *hFUS*^{Q519Ifs} mutation proved to be difficult due to a severe reduction in viability of pups and a malocclusion phenotype which caused welfare issues. Humanised *FUS*^{Q519Ifs} mutant mice were bred on a range of different genetic backgrounds to see if this reduced the penetrance of the malocclusion phenotype and improved survival to enable study. Starting in 2018, *hFUS*^{Q519Ifs} mice were bred on the C57BL/6J background and malocclusion was observed in 27% of male mice and 50% of female mice expressing the *hFUS*^{Q519Ifs} gene, of which there were only 33 in a cohort of 183 mice. The *hFUS*^{Q519Ifs} mice were also backcrossed onto the DBA and 129S1/SvImJ backgrounds however seizure and malocclusion phenotypes presented respectively. The C3H background was finally chosen as this reduced the penetrance of the malocclusion phenotype and survival was sufficient to breed cohorts. Due to the issues discussed above, there was insufficient time to generate fully humanised *hFUS/hFUS*^{Q519Ifs} mice to characterise, which were instead maintained as *mFus/hFUS*^{Q519Ifs} heterozygotes.

5.4.2 Generation of the phenotyping cohort to compare *FUS* mutations

Mice heterozygous for either the humanised *FUS*^{P525L} or the *FUS*^{Q519Ifs} mutation were crossed to generate the experimental cohort.

Humanised *hFUS*^{Q519lfs} mice were maintained as heterozygous for the *FUS* mutation and wildtype mouse *Fus* (*mFus/hFUS*^{Q519lfs}) on the C3H background for reasons discussed in section 5.4.1. *hFUS*^{P525L} mice were maintained as heterozygotes for the *FUS*^{P525L} mutation, but homozygous for humanised *FUS* on the C57BL/6J background and so a cross was first set up to generate *mFus/hFUS*^{P525L} mice (Figure 5.2).

The breeding strategy used to generate the phenotyping cohort meant the control mice were not optimal as they were wildtype mice expressing only mouse *Fus.* The aim of this chapter was to assess differences, if any, between the two *FUS* mutations. The comparison between *FUS* mutant mice is valid as the only difference between the mice is the *FUS* mutation in the human *FUS* sequence. As discussed at length in chapter 2, the differences between mouse and human *FUS* are minor, but mice are not identical and so it must be noted than any differences between 'control' mice (*mFus/mFus*) and *FUS* mutant mice in this chapter cannot be put down to mutation alone, but also the presence of human *FUS.* The *mFus/mFus* mice are included as a baseline.

To note, *mFus/hFUS*^{Q519lfs} mice were maintained on a C3H background, whereas *hFUS*^{P525L} mice were maintained on a C57BL/6J background, so when mice were crossed to generate the phenotyping cohort, F1 offspring were on a hybrid genetic background. The background is identical between offspring, with a 50% contribution of C3H and 50% C57BL/6J.

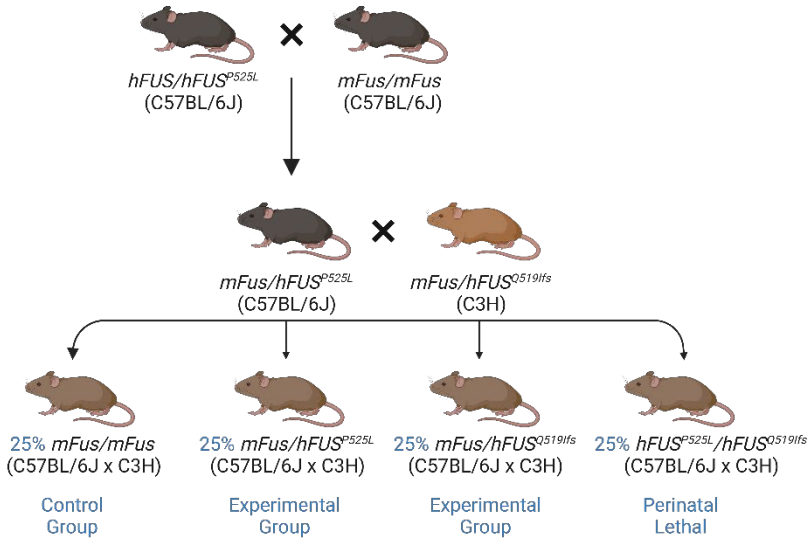


Figure 5.2: Generation of the cohort to compare hFUS^{P525L} and hFUS^{Q519Ifs} mutations. *Created with BioRender.com.*

5.4.3 Mice expressing either *FUS* mutation show no difference in survival compared to wildtype mice up to and including 14 months of age

Cohort mice were aged up until 14 months when tissues were collected. There was no difference in survival between genotypes (p=0.6105, Figure 5.3A).

5.4.3.1 Breeding data and malocclusion rates

Breeding data was also considered to see if the presence of either *FUS* mutation influenced fertility. Of the 166 mice born from this cross, 36 died before weaning. Genotypes from 12 mice were not determined and so they were not included in phenotyping or further analysis. Of the mice born, the sex split was as expected with 46.6% male pups, and 53.4% female pups born from cohort litters (Figure 5.3B). Offspring genotype data indicated that no compound heterozygous mice survived to weaning as expected as there would likely be very little functional FUS protein. The remaining genotype split was around 1/3rd each (Figure 5.3C).

One male *mFus/hFUS*^{Q519Ifs} mouse displayed malocclusion, representing 5% of male *mFus/hFUS*^{Q519Ifs} mice and 2.22% of all *mFus/hFUS*^{Q519Ifs} mice of both sexes, albeit from a small cohort to extrapolate this prevalence. Starting from one month of age, the affected mouse needed weekly teeth trimming until it was culled. The fact malocclusion was observed in this cohort is likely due to the hybrid background and re-introduction of the C57BL/6J genetic strain, on which the malocclusion phenotype had the highest penetrance in mice expressing the *hFUS*^{Q519Ifs} mutation.

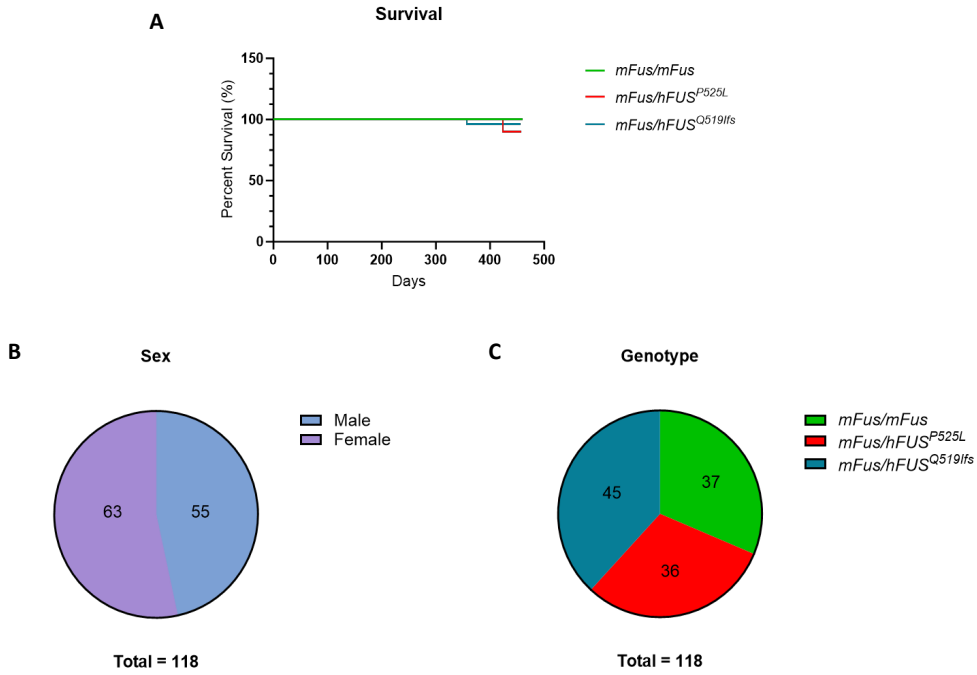


Figure 5.3: Neither FUS mutation effects survival and mice breed as expected. ***A)*** *Wildtype and mice heterozygous for humanised FUS*^{P525L} *or humanised FUS*^{Q519Ifs} *were aged up to 14-months and any unexpected deaths were recorded. There was no difference in survival between genotypes.* ***B)*** *The sex split of cohort mice.* ***C)*** *The genotype split of cohort mice.*

5.4.4 Heterozygous expression of the *hFUS*^{Q519Ifs} mutation produces a more severe phenotype than heterozygous expression of the *hFUS*^{P525L} mutation

5.4.4.1 Male mice expressing hFUS^{Q519Ifs} *are significantly smaller than those expressing hFUS*^{P525L} *or control mice*

Mice were weighed every three weeks from six weeks of age to assess weight changes over their lifetime (Figure 5.4).

Mice of all genotypes and sexes gained weight; however, both male and female mice expressing the *hFUS*^{Q519Ifs} mutation were smaller than controls. In females, this was significant until 3 months of age. Male mice expressing the *mFus/hFUS*^{Q519Ifs} were significantly smaller than controls at all timepoints studied.

Mice expressing the *hFUS*^{Q519Ifs} mutation were significantly smaller than mice expressing the *hFUS*^{P525L} mutation aged 6 weeks. This was significant until 3 months of age in both males and females. In males, this difference became significant again when the mice were aged around seven months, until around one year when the *hFUS*^{P525L} mice weights started to decline. The pattern suggests the weight of male mice expressing the *hFUS*^{Q519Ifs} mutation started to plateau earlier than mice expressing the *hFUS*^{P525L} mutation.

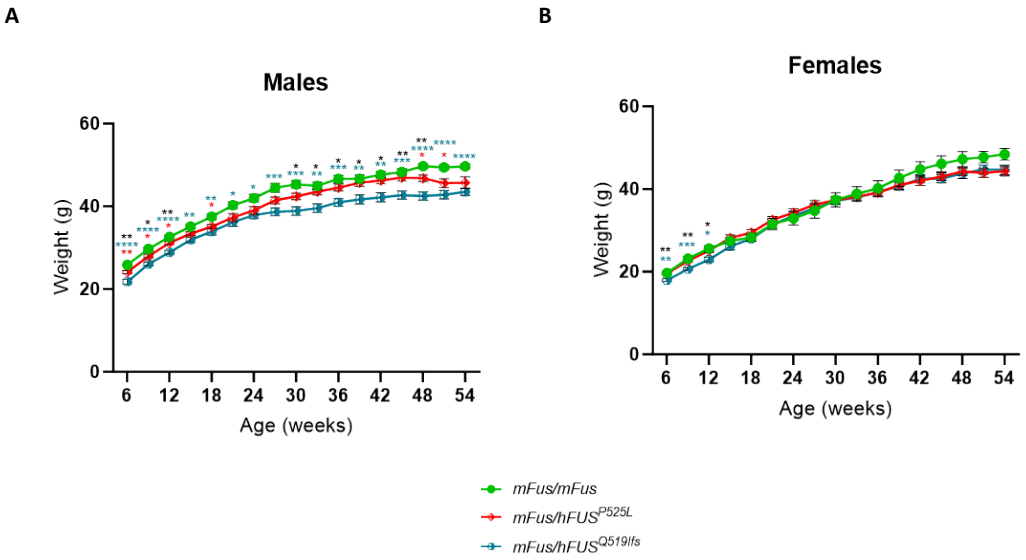


Figure 5.4: Partially humanised mFus/hFUS^{Q519Ifs} male mice are significantly smaller than wildtype controls. *Mice were weighed every three weeks from six weeks old by ward staff. Graphs show the longitudinal weights of mFus/mFus (green), mFus/hFUS^{P525L} (red) and mFus/hFUS^{Q519Ifs} (blue)* ***A)*** *male and* ***B)*** *female mice. Data are shown as mean average ± SEM with significance analysed using a mixed-effects analysis with Tukey's multiple comparisons post-hoc test. Red asterisks denote significant differences between mFus/mFus and mFus/hFUS^{P525L} mice. Blue asterisks denote significant differences between mFus/mFus and mFus/hFUS^{Q519Ifs} mice. Black asterisks denote significant differences between mFus/hFUS^{P525L} and mFus/hFUS^{Q519Ifs} mice. *=p<0.05, **=p<0.01, ***=p<0.001, ****=p<0.0001.*

5.4.4.2 Male mice heterozygous for the hFUS^{Q519Ifs} mutation have a mild open field phenotype

As in previous chapters, open field was used to assess both motor and anxiety-like phenotypes displayed by the cohort. Cohort mice were studied at 6 months, and again aged 12 months.

Female mice with either *FUS* mutation showed no difference in time spent in the centre of the arena versus controls at either timepoint (Figure 5.5B). In contrast, male mice heterozygous for the *hFUS^{Q519Ifs}* mutation spent more time in the centre compared to mice with the *hFUS^{P525L}* mutation and controls aged 12 months, suggesting a deficit in the mouse's natural prey instinct to remain in the periphery of the arena (Figure 5.5A).

Distance travelled and rearing behaviour in the open field arena was also analysed as a readout of hyperactivity and motor function. There was no significant difference in distance travelled for any genotype studied, however data was variable, (Figure 5.5C, D) suggesting expression of either mutation does not cause a hyperactivity-like phenotype like that seen in fully humanised *hFUS/hFUS*^{P525L} male mice aged 6 months. In addition, there was no observable difference in rearing (Figure 5.5E, F) suggesting that the mouse's motor skill and coordination required to rear was unaffected by presence of the *FUS* mutations.

It is worth noting that after completing the open field test, two male mice had a seizure lasting less than 10 seconds. One was heterozygous for *hFUS*^{P525L} and the other heterozygous for *hFUS*^{Q519lfs}. It is possible the seizures were stress-induced and were recorded as adverse events of the experiment. Although a strong anxiety phenotype was not observed during the open field test, anecdotally this cohort of mice were 'skittish' when handled, more so for example than the fully humanised *hFUS/hFUS*^{P525L} mice.

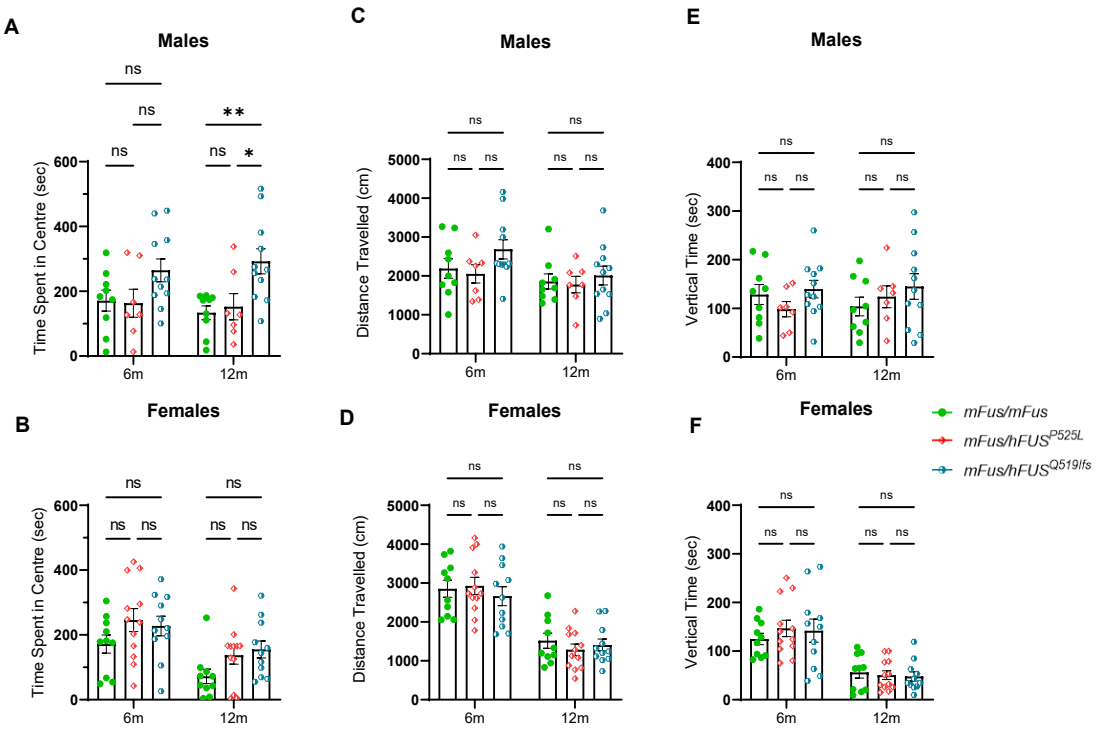


Figure 5.5: Open field data shows male mice heterozygous for the hFUS^{Q519Ifs} mutation have an increased affinity for the centre of the open field arena at 12 months. *Male and female mice were analysed for 20 minutes in an open field arena. Various parameters were measured and analysed such as* ***A, B)*** *time spent in the centre of the arena as opposed to the periphery,* ***C, D)*** *total distance travelled in the arena during the 20 minutes and* ***E, F)*** *time spent rearing. Data are shown as mean average ± SEM with significance analysed using a two-way ANOVA with Tukey's multiple comparisons post-hoc test. Ns = not significant, *=p<0.05, **=p<0.01.*

5.4.4.3 *Mice expressing the hFUS^{P525L} mutation and hFUS^{Q519Ifs} mutation have a weakened grip strength compared to control mice*

Forelimb and hindlimb grip strength was analysed to assess motor function in mice with the ALS-causing *FUS* mutations.

Male mice expressing the *hFUS^{P525L}* mutation had a significantly reduced forelimb and combined grip strength at both timepoints studied (Figure 5.6A, C).

Female mice expressing the *hFUS^{P525L}* mutation did not have significantly reduced grip strength compared to controls at any timepoint studied (Figure 5.6B, D).

In comparison, mice expressing the *hFUS^{Q519Ifs}* mutation had a significant decrease in both forelimb and combined grip strength, which was present from 6 months old in both males and females (Figure 5.6A-D).

By 12 months, male mice heterozygous for *hFUS^{Q519Ifs}* had a 26% reduction in combined grip strength ($p<0.0001$), with a mean average of 187.24g compared to 251.72g in wildtype mice (Figure 5.6C). The deficit was still significant, but smaller for mice heterozygous for *hFUS^{P525L}* with a decrease of 15% compared to wildtype controls ($p<0.01$, Figure 5.6C). For female mice the pattern was similar but not identical. Female *mFus/hFUS^{Q519Ifs}* mice had an 18% decrease in combined grip strength at 12 months ($p<0.01$), compared to a 10% decrease in *mFus/hFUS^{P525L}* which was not significant compared to controls (Figure 5.6D).

Expression of the *hFUS^{Q519Ifs}* mutation produced a significantly worse grip strength than the *hFUS^{P525L}* mutation in the forelimb grip strength of female mice at 12 months (Figure 5.6B) and combined grip strength of male mice aged 6 months ($p<0.05$, Figure 5.6C). Looking at combined grip strength of male mice, expression of *hFUS^{Q519Ifs}*

trended towards a significantly worse grip deficit aged 12 months (p=0.0627) compared to mice expressing the *hFUS*^{P525L} mutation (Figure 5.6C). In female mice, this trend was further from significance (p=0.2060, Figure 5.6D).

Owing to the two male mice having seizures after open field, they were removed from future phenotyping experiments. As a result, statistical analysis of subsequent male phenotyping data (grip strength and marble burying) was done using a mixed effect analysis rather than a two-way ANOVA, to account for missing longitudinal data points. No mice were lost from the female cohort and thus a two-way ANOVA was used to analyse data for all phenotyping tests.

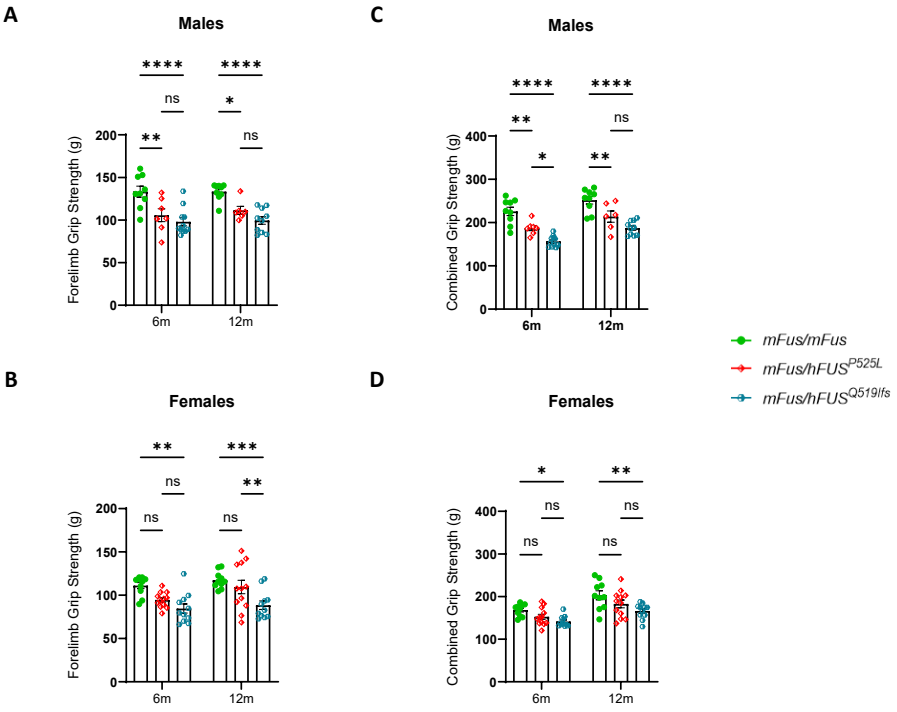


Figure 5.6: Mice heterozygous for FUS mutations have decreased grip strength compared to controls. *Forelimb and combined forelimb and hindlimb grip strength was measured at 6 and 12 months for all mice in the cohort.* ***A, B)*** *Forelimb grip strength of male and female mice.* ***C, D)*** *Combined fore and hindlimb grip strength of male and female mice. Data are shown as mean average ± SEM with significance analysed using a mixed-effects analysis with Tukey's multiple comparisons post-hoc test for males and two-way ANOVA with Tukey's multiple comparisons post-hoc test for females. Ns = not significant, *=p<0.05, **=p<0.01, ***=p<0.001, ****=p<0.0001.*

5.4.4.4 Female mice expressing the hFUS^{Q519lfs} mutation develop a marble burying phenotype

Burying novel objects is an innate behaviour in mice. Failure to do so can be a crude way to indicate an issue with wellbeing and apathy to be explored further.

For male mice expressing either *FUS* mutation, there was no difference in the way mice interacted with the marbles at both timepoints compared to wildtype controls (Figure 5.7A). In contrast, female mice expressing *hFUS*^{Q519lfs} had a marble burying phenotype at 12 months, fully burying only 44% of marbles on average compared to 68% in wildtype mice with no *FUS* mutation ($p<0.01$, Figure 5.7B). This marble burying deficit seen in mice expressing the *hFUS*^{Q519lfs} mutation was significantly different to mice expressing the *hFUS*^{P525L} mutation which fully buried 69% of marbles ($p<0.01$). At 12 months, female mice with the *hFUS*^{Q519lfs} mutation also showed an increased tendency to ignore the marbles altogether, with 10% of marbles not moved or buried, compared to just 1% in wildtype controls (Figure 5.7D).

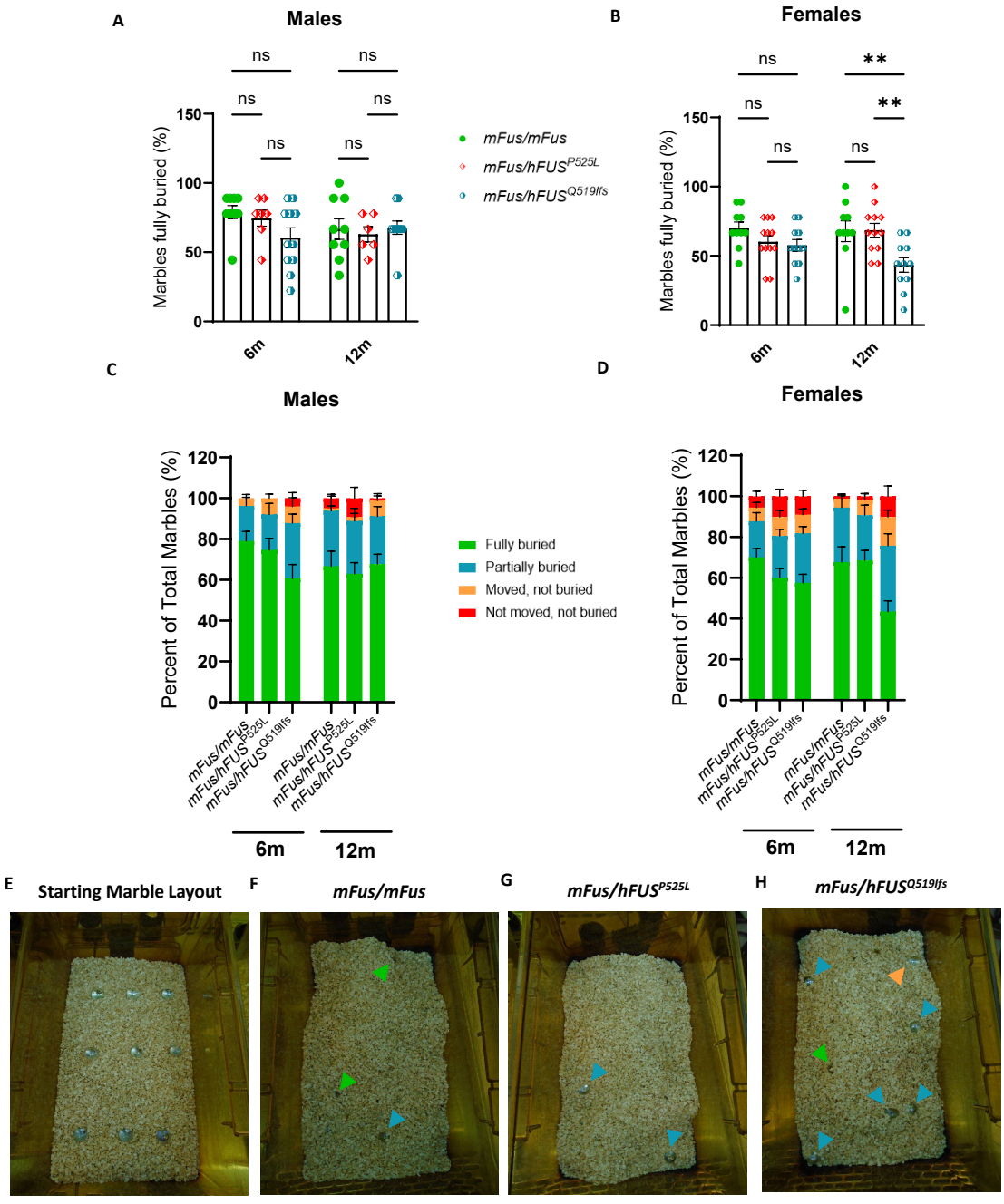


Figure 5.7: Female mice with both FUS mutations display a marble burying deficit at 12 months, whereas no differences are seen in male mice with either FUS mutation. *Mice were placed into individual cages with nine marbles evenly spaced apart. After 30 minutes, the location of the nine marbles was observed.* ***A, B)*** *The percent of marbles fully buried after 30 minutes was quantified and analysed in 6- and 12-month-old mice.* ***C, D)*** *The fate of all nine marbles is shown in graphs C and D.* ***E-H)*** *Representative images of cages from female mice at the 12-month timepoint.* ***E*** *shows how the marbles are arranged at the start of the phenotyping test.* ***F*** *shows a representative image from wildtype mice with arrows showing fully buried (green) and partially buried (blue) marbles.* ***G*** *shows a representative image from mice expressing the hFUS^{P525L} mutation with partially buried marbles indicated (blue arrows) and* ***H*** *shows a cage from a mouse expressing the hFUS^{Q519Ifs} mutation with fully (green), partially (blue) and moved but not (orange) buried marbles with arrows. Data are shown as mean average ± SEM with significance analysed using a mixed-effects analysis with Tukey's multiple comparisons post-hoc test for males and two-way ANOVA with Tukey's multiple comparisons post-hoc test for females. Ns = not significant, *=p<0.05, **=p<0.01.*

5.4.4.5 *Mice expressing FUS mutations have significantly smaller TA muscles than control mice*

When mice were dissected aged 14 months, TA muscles were collected for FUS expression experiments. Before processing, the muscles of the left and right leg were weighed.

In both male and female mice expressing *FUS* mutations, the average weight of the left and right TA muscle was significantly smaller than controls. There was no significant difference in the TA weight between *FUS* mutations (Figure 5.8).

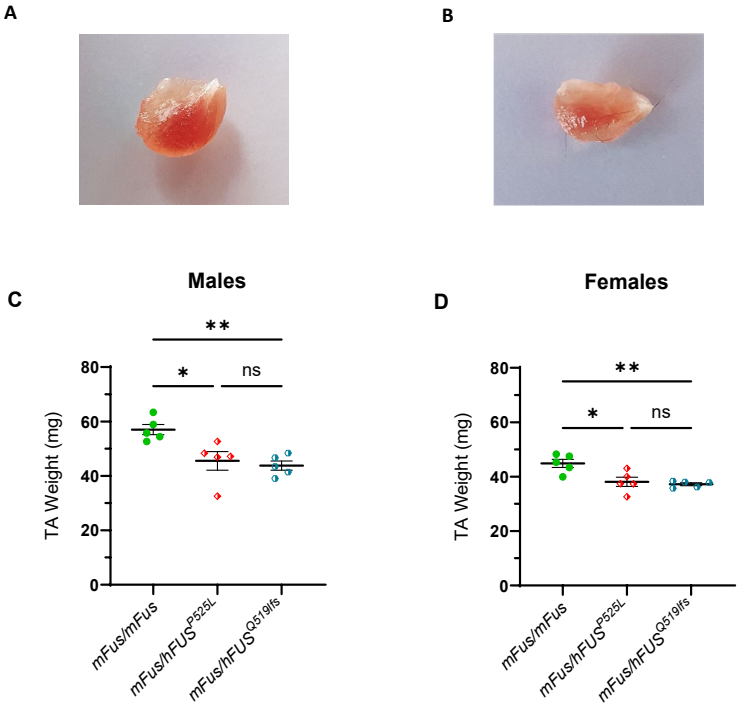


Figure 5.8: Mice expressing the FUS mutations have significantly smaller tibialis anterior muscles. *Representative images of TA muscles dissected from **A)** mFus/mFus mice and **B)** mFus/hFUS^{Q519Ifs} mice. **C-D)** Mice heterozygous for either FUS mutation have significantly smaller TA muscles compared to control mice. Data are shown as mean average ± SEM with significance analysed using a one-way ANOVA with Tukey's multiple comparisons post-hoc test. Ns = not significant, *=p<0.05, **=p<0.01.*

5.4.5 Different *FUS* mutations alter RNA and protein expression to different extents

5.4.5.1 FUS RNA expression is increased in mice expressing either the hFUS^{P525L} or the hFUS^{Q519Ifs} mutation

FUS expression in ALS-relevant tissues was quantified using qRT-PCR techniques.

FUS RNA expression was increased in mice expressing *FUS* mutations compared to controls, in mice of both sexes, in the spinal cord (SC) and to a greater extent in the tibialis anterior muscle (TA) (Figure 5.9).

Female *hFUS^{Q519Ifs}* mice had a small but significantly increased *FUS* expression relative to *hFUS^{P525L}* mice in the spinal cord.

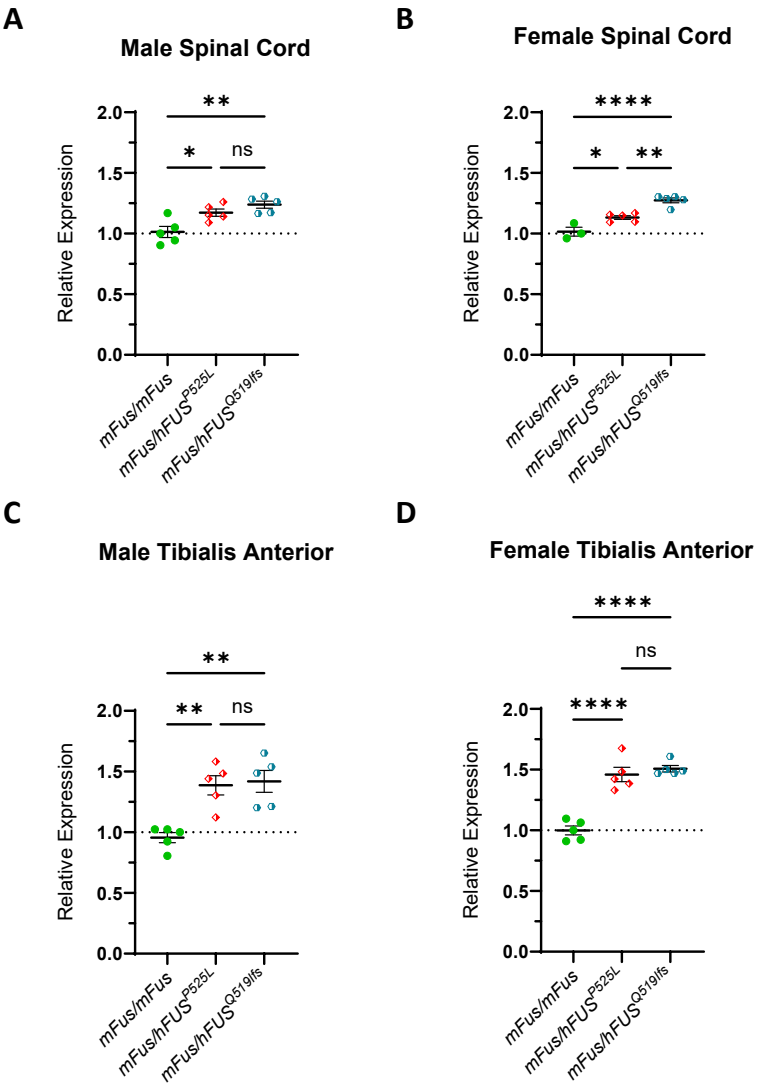


Figure 5.9: Mice which express the hFUS^{P525L} mutation or the hFUS^{Q519Ifs} mutation have increased FUS expression in ALS disease relevant tissues, but there is no difference between mutations. *Tissue was collected from male and female mice aged 14 months old and total RNA was extracted and FUS expression quantified using qPCR. Primers were designed which bound regions in exon two and exon four which are identical between mouse Fus and human FUS and are unaffected by the presence of the C terminal mutation. FUS expression was analysed in mice of both sexes in RNA extracted from **A-B)** spinal cord and **C-D)** tibialis anterior muscle. Data are shown as mean average ± SEM. Significance was calculated using a one-way ANOVA with Tukey's multiple comparisons post-hoc test. Ns = not significant, *=p<0.05, **=p<0.01, ****=p<0.0001.*

5.4.5.2 Mice expressing the $hFUS^{Q519Ifs}$ mutation have an increase in FUS protein expression

Total protein was extracted from SC and TA tissue to quantify FUS protein expression in ALS-relevant tissues.

Male and female mice both showed a similar pattern in FUS expression. In the SC, there was no significant difference in FUS expression between control and *FUS* mutant mice of either sex, although in $hFUS^{Q519Ifs}$ mice this trended towards increased FUS expression and data was variable (Figure 5.10A-B, Figure 8.11, Figure 8.12). In male mice, FUS expression was modestly but significantly increased in mice heterozygous for the $hFUS^{Q519Ifs}$ mutation compared to $hFUS^{P525L}$ mice. This significant difference was not seen in the SC of female mice although due to the spread of data, analysis was likely underpowered and there was a trend towards increased protein expression in mice heterozygous for the $hFUS^{Q519Ifs}$ mutation compared to $mFus/hFUS^{P525L}$ mice and controls.

In the TA muscle of male mice, the expression pattern was like that observed in the SC. Although not statistically significant in males, there was increased FUS expression in $hFUS^{Q519Ifs}$ mice (Figure 5.10C-D). In both sexes, expression of the $hFUS^{Q519Ifs}$ mutation was significantly increased compared to mice expressing the $hFUS^{P525L}$ mutation.

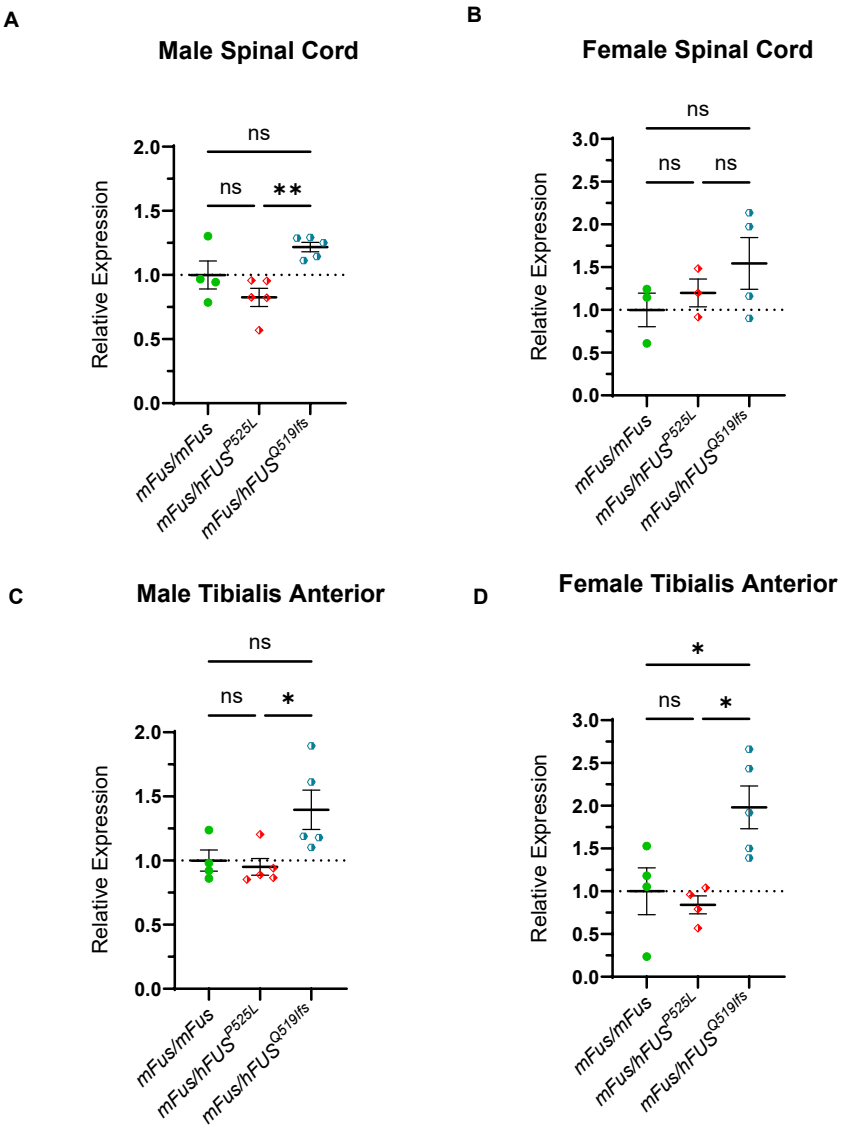


Figure 5.10: Mice which express the hFUS^{Q519Ifs} mutation have increased FUS expression in ALS disease relevant tissues, and this differs between the two mutations. *Tissue was collected from male and female mice aged 14 months old and total protein was extracted and FUS expression quantified using quantitative western blots. FUS expression of male and female mice was assessed using an antibody raised against the N terminus of the FUS protein which is the same between mouse and human FUS and is unaffected by the presence of the C terminal mutation. FUS expression from both sexes was analysed in* ***A-B)*** *spinal cord and* ***C-D)*** *tibialis anterior tissue. Data are shown as mean average ± SEM. Significance was calculated using a one-way ANOVA with Tukey's multiple comparisons post-hoc test. Ns = not significant, *=p<0.05, **=p<0.01.*

5.4.6 Increased cytoplasmic FUS protein is observed in mice expressing the *hFUS*^{Q519lfs} mutation

It is known that mutations in the FUS nuclear localisation sequence cause increased cytoplasmic FUS protein in patients, likely due to issues with binding nuclear import receptors.

Sections of lumbar spinal cord were collected from mice aged 14-months and probed with an antibody against FUS to assess FUS localisation in ventral motor neurons.

FUS is more severely localised to the cytoplasm in mice expressing the *hFUS*^{Q519lfs} mutation (Figure 5.11C) compared to controls and mice expressing the *hFUS*^{P525L} mutation (Figure 5.11A, B). This difference in FUS localisation was quantified manually in ImageJ and found to be significant (Figure 5.11D). Primary and secondary only controls show staining is specific (Figure 8.13).

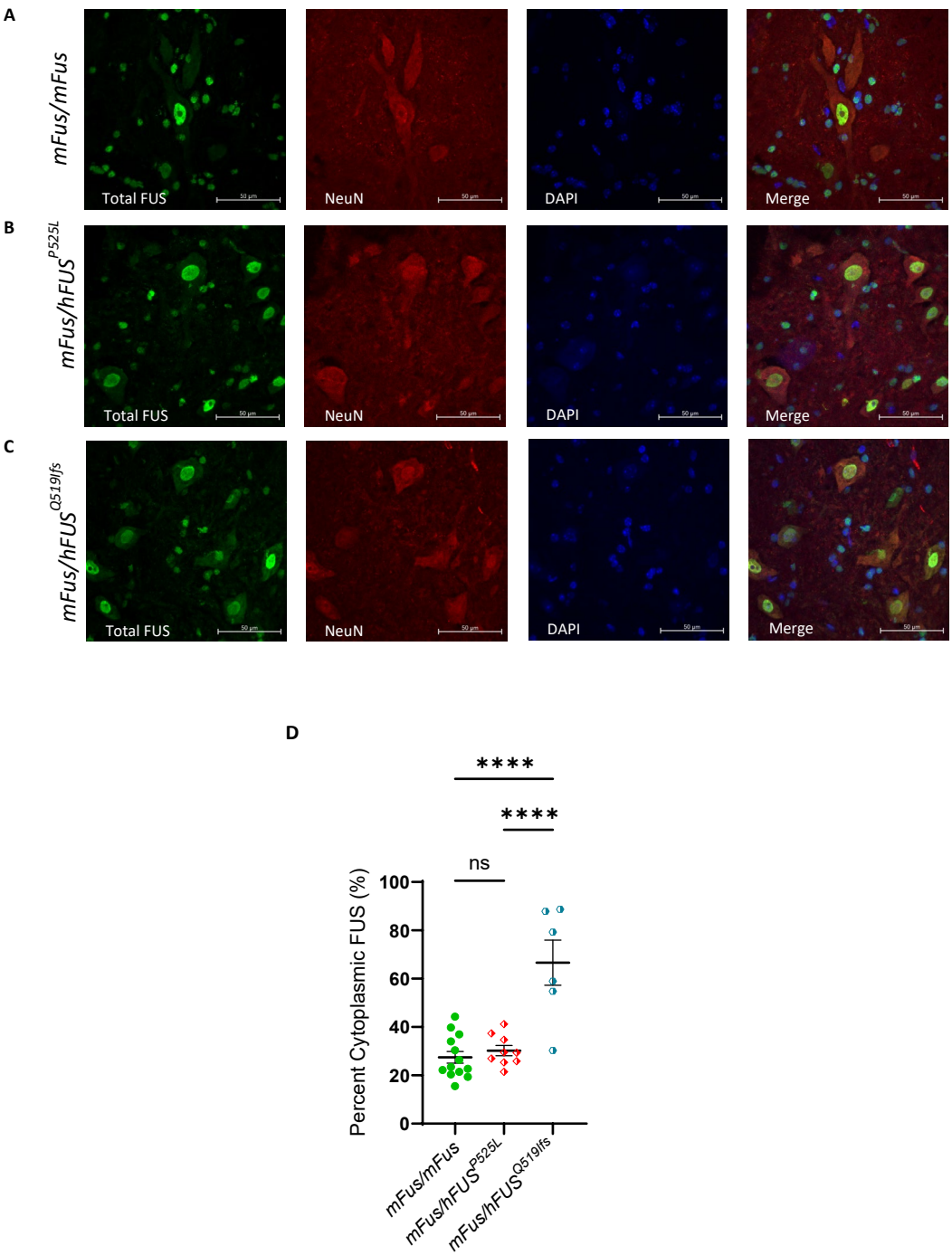


Figure 5.11: Cytoplasmic FUS is increased in mice expressing the hFUS^{Q519Ifs} mutation. *Spinal cord sections from 14-month-old mice which had been transcardially perfused with 4% PFA were stained using an antibody raised against the N terminus of the FUS protein (green) which is consistent between mouse and human FUS and unaffected by the C terminal mutations, and co-stained with a neuronal marker, NeuN (red). Cells were co-stained with DAPI to visualise nuclei (blue). Images shown are representative of sections stained from **A)** mFus/mFus controls, **B)** mice expressing the hFUS^{P525L} mutation and **C)** the hFUS^{Q519Ifs} mutation. **D)** FUS localisation in motor neurons positive for NeuN was manually assessed in ImageJ. By hand, the whole cell and nucleus were drawn around and the integrated density of FUS staining measured and shown as the percent of FUS staining which was nuclear, with the remaining FUS staining being cytoplasmic. Data are shown as mean average ± SEM with significance analysed using a one-way ANOVA with Tukey's multiple comparisons post-hoc test. ****=p<0.0001.*

5.4.7 There is little difference in transcript expression between mice expressing the two *FUS* mutations

Bulk RNA sequencing was carried out on 4-month-old SC and TA tissue of male mice.

A small number of transcripts were differentially expressed between mice expressing the two *FUS* mutations. In the SC, expression of 17 transcripts were changed; in the TA, there were 18 transcripts changed (Figure 5.12A, Supplementary Table 8.2, adjp<0.1). Three major *Gdpd3* transcripts were dysregulated in both tissues, with increased expression seen in *mFus/hFUS*^{Q519Ifs} mice compared to *mFus/hFUS*^{P525L} mice.

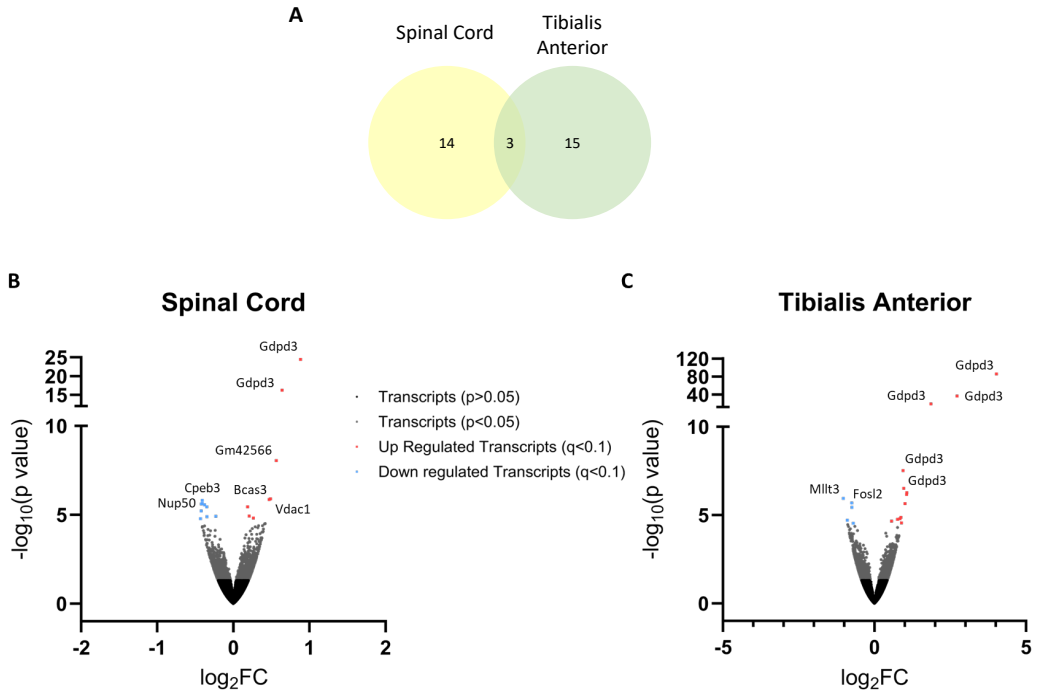


Figure 5.12: RNA sequencing data from spinal cord and tibialis anterior tissue collected from four-month-old male mice from the P525L x Q519Ifs cohort shows minimal transcript changes between the two FUS mutations. A) *The number of differentially expressed transcripts between the two FUS mutations in the SC and TA, and how many differentially expressed transcripts overlapped in both tissues.* ***B)*** *Volcano plot showing differentially expressed transcripts in the spinal cord of mFus/hFUS*^{Q519Ifs} *mice compared to mFus/hFUS*^{P525L} *mice.* ***C)*** *Volcano plot showing differentially expressed transcripts in the tibialis anterior of mFus/hFUS*^{Q519Ifs} *mice compared to mFus/hFUS*^{P525L} *mice.*

The proximity of the *Gdpd3* gene to the *FUS* gene locus on chromosome seven led us to speculate this differential expression may be an artefact of the humanisation process rather than a true phenotype. Upon further study this proved likely. SNP sequencing was employed to determine the genetic background of the regions surrounding the humanised *FUS* gene on chromosome seven in the two *FUS* mutant lines. In *mFus/hFUS*^{P525L} mice, the region surrounding the *Gdpd3* gene was of C57BL/6J or C3H origin, whereas in *mFus/hFUS*^{Q519Ifs} mice it was of 129S1/SvImJ origin. This means the differences in *Gdpd3* transcript expression are likely a result of differential regulation by the different genetic backgrounds. As the two mutant *FUS* lines were generated and maintained separately, meiotic recombination events have likely occurred independently within the *mFus/hFUS*^{P525L} mice which have shortened the 129S1/SvImJ region surrounding the *hFUS* gene on chromosome seven (Figure 5.13). The 129S1/SvImJ regions were originally present as the *hFUS* sequence was genetically targeted in 129S1/SvImJ embryonic stem cells.

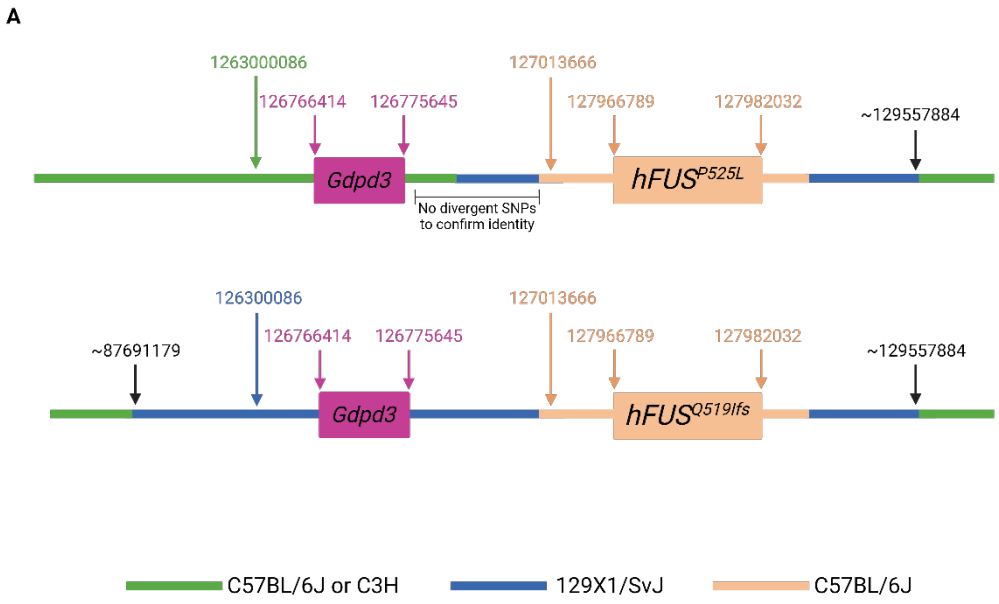


Figure 5.13: Genetic background surrounding the hFUS sequence in mFus/hFUS^{P525L} and mFus/hFUS^{Q519Ifs} mice. A) *Schematic highlighting the shortening of the 129S1/SvImJ region surrounding the hFUS sequence in mFus/hFUS^{P525L} mice compared to mFus/hFUS^{Q519Ifs} mice as determined by divergent SNP sequencing. Created with BioRender.com.*

Transcript expression was also compared between mice expressing either *FUS* mutation and controls. This comparison is also studying the effect of humanising the *FUS* gene as control mice express only mouse *Fus*, which must be considered when analysing expression changes. The stringency was relaxed to see the wider picture of transcript expression changes in the two *FUS* mutant models. In both tissues, mice expressing the *hFUS^{Q519Ifs}* mutation had more differentially expressed transcripts than mice expressing the *hFUS^{P525L}* mutation ($p<0.05$).

GO terms were studied for the list of transcripts which were differentially expressed in both *FUS* mutant mice, to see if overlapping disease mechanisms could be pulled out. The fold change of overlapping transcripts had a strong positive correlation

between *FUS* mutants which could suggest those transcripts are consistently affected in the presence of *FUS* mutations, representing shared disease mechanisms in FUS-ALS.

In the SC, the *cytoplasm* was the top hit of the overlapping transcripts, indicating the effect mutant FUS is likely having in this cellular component. Other terms included *protein binding, mRNA* and *DNA binding* which were unsurprising given the known roles of the FUS protein (Figure 5.14B).

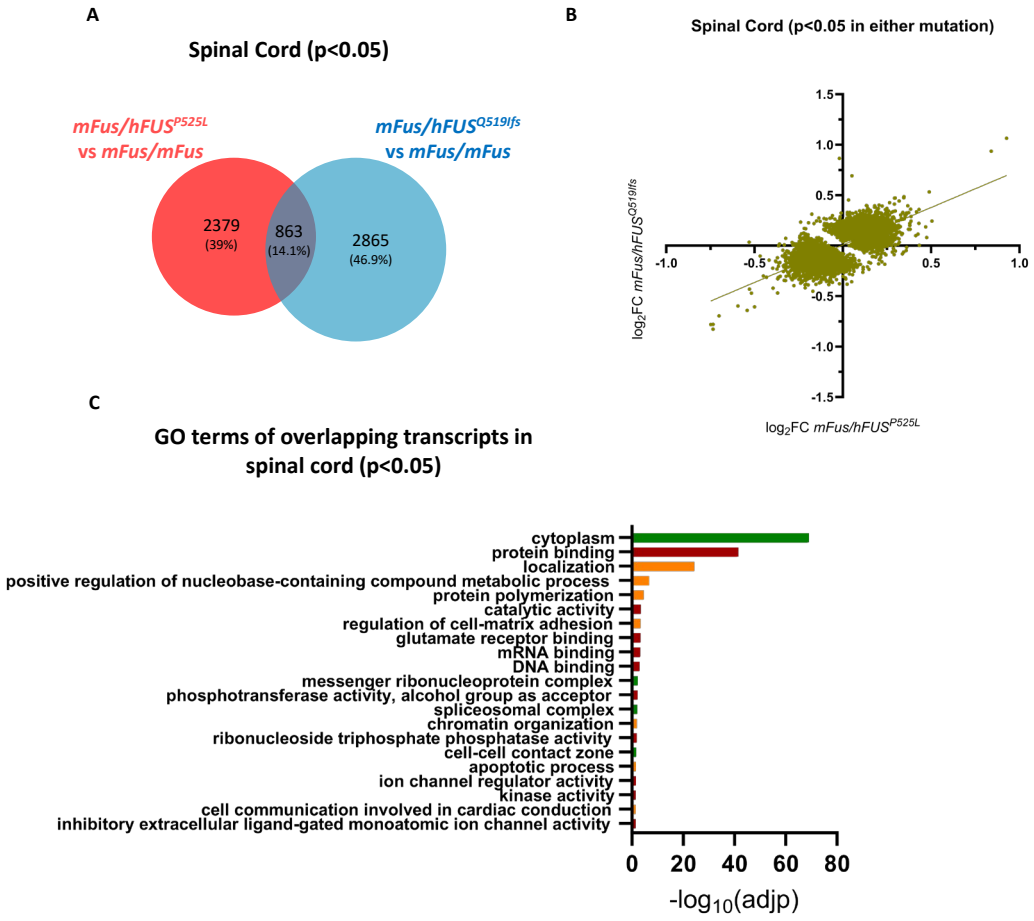


Figure 5.14: RNA sequencing data from spinal cord tissue collected from 4-month-old male mice from the P525L x Q519Ifs cohort highlighting differentially expressed transcripts between mutant FUS mice and wildtype controls. A) *The number of differentially expressed transcripts between the two FUS mutations versus controls in the SC* ***B)*** *Graph comparing the fold change of transcripts which were significantly differentially expressed in both FUS mutant mice versus controls (p<0.05)* ***C)*** *GO term analysis of overlapping transcripts from B.*

In the TA, the top hit was also the *cytoplasm*, followed by *protein binding* and *organonitrogen compound metabolic processes*. Organonitrogen compounds in the body include amino acids, urea, and creatine. Interestingly, *striated muscle cell development* was a hit for both mutations indicating a potential role of FUS in muscle development (Figure 5.15B).

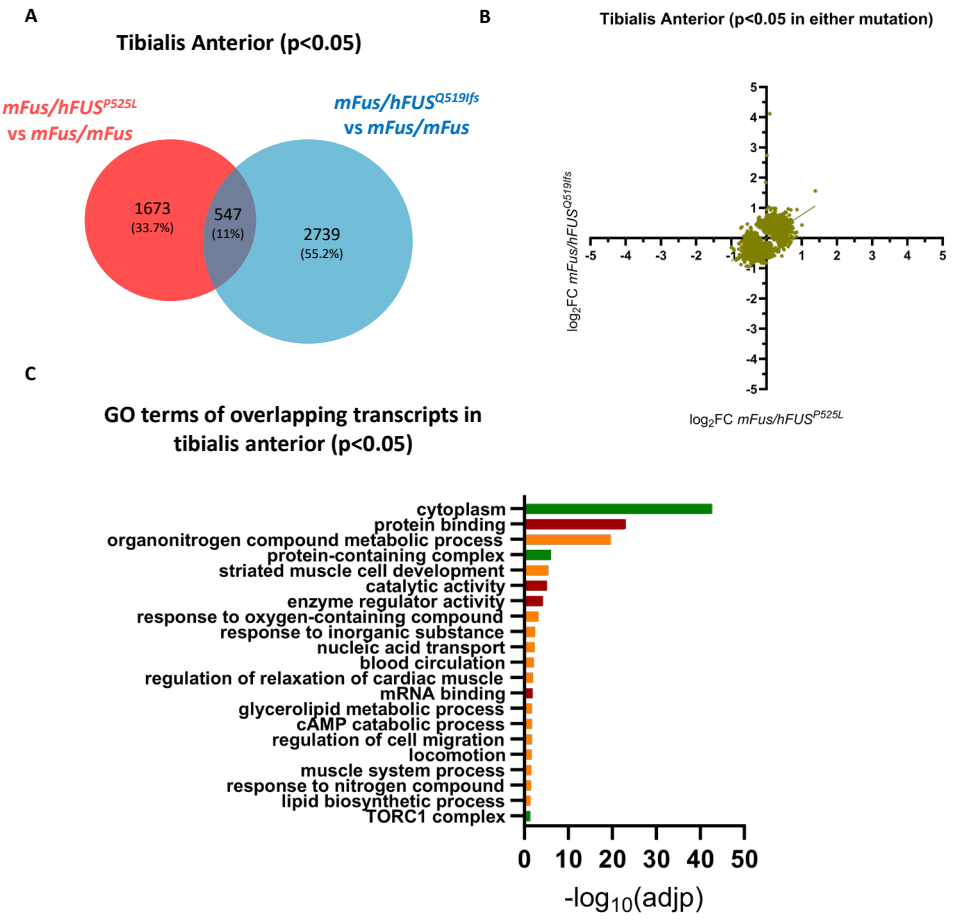


Figure 5.15: RNA sequencing data from tibialis anterior tissue collected from 4-month-old male mice from the P525L x Q519Ifs cohort highlighting differentially expressed transcripts between mutant FUS mice and wildtype controls. A) *The number of differentially expressed transcripts between the two FUS mutations versus controls in the TA* ***B)*** *Graph comparing the fold change of transcripts which were significantly differentially expressed in both FUS mutant mice versus controls (p<0.05)* ***C)*** *GO term analysis of overlapping transcripts from B.*

5.5 Discussion

The differing severity of *FUS* mutations has been debated based on clinical data such as disease onset, and is thought to correlate with how severely the NLS is disrupted (Grassano et al., 2022). Further data *in vitro* and *in vivo* has found that different *FUS* mutations lead to distinct cellular phenotypes, likely due to the extent of cytoplasmic FUS is localised (An et al., 2020; Korobeynikov et al., 2022; Salam et al., 2021; Verbeeck et al., 2012).

In this chapter, two different FUS-ALS patient mutations were compared: FUS^{P525L} and $FUS^{Q519Ifs}$. The $FUS^{Q519Ifs}$ mutation more severely disrupts the C terminus of the FUS protein compared to the FUS^{P525L} mutation. The $FUS^{Q519Ifs}$ mutation produced a severe phenotype in the ALS patient from which it was sequenced, possibly more severe than the phenotype caused by expression of the FUS^{P525L} mutation; however, it is not possible to say conclusively due to the low patient numbers. Mouse genetics provides a tool to probe further the phenotype severity of distinct *FUS* mutations.

In this chapter, animals expressing either $hFUS^{P525L}$ or $hFUS^{Q519Ifs}$ mutations were bred in such a way that the effect of the *FUS* mutations could be directly compared in litter mate controls.

5.5.1 Heterozygous expression of the $hFUS^{Q519Ifs}$ mutation produces a more severe phenotype than heterozygous expression of the $hFUS^{P525L}$ mutation

No difference in survival was observed in the $hFUS^{P525L}$ or $hFUS^{Q519Ifs}$ mice compared to controls up to 14 months of age. It would have been interesting to further age the cross cohort to see if a decrease in survival developed, however this

was not possible due to time constraints of this project and the closure of MRC Harwell.

Overall, phenotyping data presented in this chapter showed mice expressing the *hFUS*^{Q519lfs} mutation had a more severe outward phenotype than mice expressing the *hFUS*^{P525L} mutation and controls. For example, *mFus/hFUS*^{Q519lfs} mice were smaller, had altered anxiety phenotypes, trended towards a weaker grip strength, and displayed altered marble burying behaviour compared to *mFus/hFUS*^{P525L} mice. This was mirrored by what was seen at the *FUS* RNA and protein level; *FUS* expression was increased in mice expressing the *hFUS*^{Q519lfs} or the *hFUS*^{P525L} mutation compared to controls, but there were also trends towards increased *FUS* expression in *mFus/hFUS*^{Q519lfs} mice compared to *mFus/hFUS*^{P525L} mice, which was significant at the protein level in the TA of both sexes.

This difference in phenotype severity is consistent with what has been seen by others when using mouse models of FUS-ALS. In 2012, Verbeeck and colleagues produced three transgenic lines expressing human wildtype or mutant FUS under the control of the SBT promoter. The *FUS*$^{\Delta 14}$ mutant produced a larger accumulation of FUS in the cytoplasm compared to the F*US*^{R521C} mutation, likely due to a more disrupted NLS (Verbeeck et al., 2012). Whilst this project was ongoing, Korobeynikov and colleagues published on their targeted *Fus* knock-in models which included a comparison between the *Fus*^{P517L}, equivalent to human *FUS*^{P525L}, and *Fus*$^{\Delta 14}$ mutations (Korobeynikov et al., 2022). To note, the *Fus*$^{\Delta 14}$ sequence was partially humanised, whereas the *Fus*^{P517L} mutation was knocked-in to the mouse *Fus* sequence. Using the power of mouse genetics, they concluded that both *FUS* mutations had an element of

FUS loss of function (LOF) as expression of mutant FUS was unable to fully rescue *Fus*$^{-/-}$ mouse survival. This supports what was seen in this cohort whereby compound heterozygous mice did not survive suggesting there was insufficient functional FUS protein to carry out wildtype FUS roles. In addition to LOF, Korobeynikov and colleagues found both *FUS* mutations exhibited mutation and dose-specific gain of function toxicity. In this study there was increased FUS expression in the *mFus/hFUS*^{Q519Ifs} mice; it would be interesting further work to see if this was largely driven by mutant or wildtype *FUS* mRNA and protein. The increased severity of the phenotype in *mFus/hFUS*^{Q519Ifs} mice suggests hFUS^{Q519Ifs} was more toxic than hFUS^{P525L}.

Many of the phenotypes observed in the *mFus/hFUS*^{Q519Ifs} mice were seen at the earliest timepoint studied such as weight changes aged 6 weeks, a grip phenotype aged 6 months and smaller TA muscles aged 14 months. This means it cannot be said whether these phenotypes are degenerative or a consequence of developmental effects of the *FUS* mutation. It is accepted that FUS-ALS has a distinct clinical profile compared to other forms of ALS, including an earlier, sometimes juvenile, disease onset and fast progression (Naumann et al., 2019) and is the most common ALS subtype in patients younger than 35 years old (Hubers et al., 2015). In addition to the disease onset and duration, there have been reports of wider abnormalities in FUS-ALS patients such as intellectual disabilities (Goldstein et al., 2022; Zou et al., 2013) including in patients revealed to have the *FUS*^{P525L} and *FUS*^{Q519Ifs} mutations (Baumer et al., 2010; Goldstein et al., 2022). FUS is well described as a widely expressed protein and it is becoming apparent that the role of FUS extends far beyond neuronal cells and tissues (Ali et al., 2023).

Fully humanised *hFUS*^{P525L} mice in chapter 3 previously showed a degenerative phenotype, with minor hints of developmental changes. In this chapter, mice expressing the *hFUS*^{Q519Ifs} mutation show an overall more severe phenotype compared to mice expressing the *hFUS*^{P525L} mutation, with more severe developmental changes as evidenced by the sub-viability and highly penetrant malocclusion phenotype. Expression of the *hFUS*^{Q519Ifs} mutation was particularly severe on the C57BL/6J background, where the phenotype displayed was the most severe ever modelled by the MMoN group at Harwell. The malocclusion phenotype was followed up in collaboration with Dr Karen Lui's group at King's College London. Using CT scans, bone density and structure were measured, and it was found that expression of the *hFUS*^{Q519Ifs} mutation led to a severe craniofacial phenotype; skulls from these mice had visibly decreased bone density compared to controls and were asymmetrical, explaining the misaligned jaw and malocclusion phenotype.

Together this suggests that *FUS* mutations can manifest with variable developmental involvement, mimicking what is seen in FUS-ALS patients.

5.5.2 Enhanced disruption of the FUS NLS in mice expressing the *hFUS*^{Q519Ifs} mutation leads to more severe cytoplasmic FUS localisation than in *hFUS*^{P525L} mice

As discussed in the introduction to this chapter, the *FUS*^{Q519Ifs} mutation produces a frameshift mutation leading to severe truncation of the FUS protein's C terminus abolishing the NLS. Although the NLS is disrupted with the P525L mutation, this is to a lesser extent. Disruption of the NLS likely alters the ability of the mutated FUS protein to bind to nuclear import receptors such as TNPO1 (Dormann et al., 2012; Zhang & Chook, 2012). This is supported by the significant increase of cytoplasmic FUS

to around 65% of total FUS in *mFus/hFUS*^{Q519Ifs} mice compared to around 30% in controls and *mFus/hFUS*^{P525L} mice. The antibody used bound total FUS and so it cannot be said whether FUS localised to the cytoplasm was wildtype or mutant FUS.

With increased FUS in the cytoplasm in *mFus/hFUS*^{Q519Ifs} mice, both loss of wildtype function and toxic gain of function mechanisms may be contributing to the phenotypes observed and may begin to explain why mice heterozygous for *hFUS*^{Q519Ifs} had a more severe phenotype than *mFus/hFUS*^{P525L} mice.

It was thought that the increase in cytoplasmic FUS may lead to a more severe dysregulation of transcript expression in *mFus/hFUS*^{Q519Ifs} mice compared to *mFus/hFUS*^{P525L} mice as there is less FUS protein in the nucleus to carry out this role. This was not the case. RNA sequencing data found transcript expression between the two *FUS* mutations was very similar, with only 17 and 18 transcripts differentially expressed in the SC and TA, respectively. Of course, significant transcriptional changes may have been present in very specific cell types, which may have been missed in this bulk RNA sequencing experiment.

The most significantly differentially expressed hits were *Gdpd3* transcripts located on chromosome seven near the *FUS* gene, but these expression changes were likely a product of the *FUS* humanisation process and minor localised genetic drift, rather than due to the *FUS* mutation. This suggests the effect of the *FUS* mutations on transcript regulation was largely similar and differences in phenotype severity are likely due to an effect of the toxic mutant FUS protein unrelated to transcript regulation, possibly in the cytoplasm where the majority is located. This toxic cytoplasmic function is supported by work *in vitro* comparing two *FUS* mutations

where authors found that in neuronal cells expressing $FUS^{\Delta NLS}$, there was increased cytoplasmic FUS and a subsequent depletion of synapses and mitochondrial function, in contrast to cells expressing FUS^{514G} which displayed milder cytoplasmic FUS localisation and increased numbers of synapses (Salam et al., 2021). The cohort of mice studied in this chapter provide an ideal system to model the dose-specific toxic cytoplasmic function of mutant FUS induced by distinct *FUS* mutations in more detail.

6 Chapter 6: Discussion

6.1 What was unknown know before this project?

6.1.1 Could genomically humanised mice address the historic lack of translation in ALS research?

As discussed at length in chapter 1 and chapter 2 there are many reasons why it was thought targeted knock-in, humanised mice may be the way to address some of the outstanding issues in the field of ALS research. Arguably, the biggest issue being the historic lack of translation from work done using existing disease models into successful disease modifying treatments for patients.

Before this DPhil project, targeted knock-in, genomically humanised *FUS* mice which expressed human *FUS* under the controls of the mouse *Fus* promoter had not been characterised. The humanised *FUS* mice had been generated by the Mouse Models of Neurodegeneration Group at MRC Harwell and UCL, but the effect of humanising the gene in this way, and the subsequent phenotype was unknown and unpublished.

Generally, targeted knock-in mice have a less severe phenotype than overexpressing transgenics, but whether this was also true of fully genomically humanised *FUS* mice was unclear. Whether humanised knock-in models of FUS-ALS, and the humanisation strategy implemented to produce the mice would produce a more translatable model was yet to be determined.

6.2 What was done to address that knowledge gap?

6.2.1 Genomically humanised *FUS* mice were generated and characterised.

Mice expressing the human *FUS* gene and protein in a physiologically relevant pattern of expression were generated. The aim of these humanised mice was to better replicate patient phenotypes to enable a better understanding of human disease pathogenesis, and to design and test human targeted therapies.

The humanisation strategy used was experimental and novel. Few genomically humanised mouse models exist, and so the design was based on what was known about *FUS* gene regulation and disease pathomechanisms (Devoy et al., 2021). The human *FUS* construct contained all introns, exons, and the 3'UTR, but was expressed under the control of the endogenous mouse *Fus* promoter; the rationale being human *FUS* would be expressed at normal levels, in a normal pattern of expression.

Genomically humanised *FUS* wildtype and FUS-ALS mutant mice were extensively characterised. Longitudinal pipelines focusing on motor and cognitive phenotypes were employed, alongside cellular and molecular study of ALS disease relevant tissue such as spinal cord and fast-twitch skeletal muscles. In the case of humanised FUS^{P525L} mice, primary neuronal cell cultures were also generated to study early disease changes in an *in vitro* system.

Finally, two distinct *FUS* mutations were compared in a controlled setting on the same genetic background to try and understand what about *FUS* mutations affects disease severity.

6.3 What was found?

6.3.1 Human FUS could functionally replace mouse FUS.

Humanising the *FUS* gene had very little effect on the mouse; homozygous humanised *FUS* mice had no overt phenotype, FUS localisation was predominantly nuclear and there was no motor neuron loss. That is not to say humanised *FUS* mice were identical. There was a reduction in *FUS* mRNA and protein across most tissues studied and male *hFUS/hFUS* mice were marginally but significantly heavier than controls reinforcing that *hFUS/hFUS* mice are the most valid control when studying humanised *FUS* mice with ALS-causing mutations. Perhaps the most surprising was the remarkably few transcriptomic changes between *mFus/mFus* and *hFUS/hFUS* mice. This suggests that despite any differences between the mouse and human FUS protein, these are not sufficient to affect the ability of the protein to bind nucleic acid and alter gene transcription and translation.

If researchers were interested in the biochemical differences between human and mouse FUS, the humanised *FUS* mice represent an ideal system for studying this, however this was not an avenue pursued in this project.

6.3.2 *hFUS/hFUS^{P525L}* male mice exhibit FUS-ALS relevant phenotypes.

Male *hFUS/hFUS^{P525L}* mice exhibit a replicable motor phenotype, with both pre- and post-symptom timepoints able to be studied, alongside disease relevant cellular and molecular changes.

The phenotypes observed in the *hFUS/hFUS^{P525L}* mice were occurring independently of detectable motor neuron degeneration and neuroinflammation, which were not found in the *hFUS/hFUS^{P525L}* mice in this project. It may be that

histological phenotypes would develop if mice were aged for longer, as motor neuron loss has been detected as late as 24 months in some FUS-ALS knock-in models (Lopez-Erauskin et al., 2018), or may have been present in tissue not studied in depth in this project, such as the cortex.

The phenotypes displayed by the *hFUS/hFUS*^{P525L} mice were mild, likely representing an early stage of disease. Changes were also seen from a young age, with some likely occurring during development. *FUS* mutations may cause cellular defects in a tissue-specific manner during development which predisposes those tissues to disease pathogenesis when exposed to additional pathogenic events, or 'hits'. These hits may be encountered as mice age, such as stochastic mutations, or environmental stressors like physical stress and localised trauma.

6.3.3 Early changes in skeletal muscle may drive symptom progression in humanised *FUS* mutant mice.

hFUS/hFUS^{P525L} male mice developed a degenerative motor phenotype in the absence of detectable spinal motor neuron loss. As discussed in chapter 3, work is ongoing to repeat motor neurons counts and lumbrical muscles have been stained and imaged to assess neuromuscular junction innervation in aged mice, which can often precede spinal cord motor neuron loss. Interestingly, other FUS-ALS mouse models are known to display a motor phenotype before motor neuron loss (Devoy et al., 2017; Lopez-Erauskin et al., 2018; Zhang et al., 2020). This could suggest that physiological changes in motor neurons such as at the synapse, prior to motor neuron loss, could be contributing to phenotypes, and/or that deficits in other cells and tissues may be driving symptom progression, such as changes in skeletal muscle.

Skeletal muscle changes were first picked up during discovery bulk RNA sequencing in pre-symptomatic mice; tibialis anterior (TA) muscle samples had over five times as many transcriptomic changes as spinal cord tissue samples of the same age hinting at a prominent muscle phenotype worth pursuing. The increased transcriptomic disruption in the TA muscle compared to the spinal cord could suggest the TA muscle is somehow more adversely affected by the presence of the *hFUS*^{P525L} mutation but more work would be needed to confirm this. Expression of the *hFUS*^{P525L} mutation could be restricted to specific tissues or cell types within the TA or spinal cord to see how this modulated the outward phenotype. The more severe muscle transcriptomic disruption could reflect a dose-specific toxic gain of mutant FUS function as *FUS* expression was significantly or trending towards increased expression in the muscle to a greater degree than was observed in the spinal cord. The idea of dose-sensitive toxicity is perhaps supported by the fact predominantly slow-twitch fibre muscles such as the soleus, which are the most resistant to ALS pathogenesis, do not exhibit increased *FUS* expression in mutant *hFUS/hFUS*^{P525L} mice.

TA muscle transcript changes pointed towards alterations in muscle fibre type composition and dysfunctional energy biogenesis as an early disease phenotype; however, whether early transcriptomic changes resulted in a functional deficit is unknown as muscle morphology was not studied in young mice, and no motor phenotype was observed at 6 months. Functional phenotypes were found in the muscles of aged *hFUS/hFUS*^{P525L} male mice, which displayed a progressive, degenerative grip deficit and defective muscle transduction.

Changes in the muscle were likely driving some of the phenotypes observed in the *hFUS/hFUS*^{P525L} male mice and represent a site of pathological change which should be studied in more detail. This is even more prevalent given the recent finding that mutations in *TARDBP* can cause myopathy (Ervilha Pereira et al., 2023). Of note, some of the genes and GO terms found to be dysregulated in muscle biopsies of patients expressing the TDP-43 frameshift variant were consistent with transcripts and GO terms which were differentially expressed in both mice expressing the *hFUS*^{P525L} and *hFUS*^{Q519Ifs} mutation in chapter 5, such as straited muscle cell development.

6.3.4 Both loss and gain of function mechanisms of FUS toxicity are at play in the humanised *FUS* mutant mice.

There is evidence for both loss and gain of mutant FUS function driving pathomechanisms in the humanised *FUS* mutant mice. This is clinically relevant as it influences whether FUS-ALS treatments should aim to restore FUS function or dampen the effect of mutant FUS.

Work using existing models has argued that FUS-ALS is mainly a result of gain of toxic function; although *Fus* knock-out is perinatal lethal, there is no evidence of ALS-relevant phenotypes such as motor neuron loss which is seen when mutant *FUS* is overexpressed (Table 1.1). However, work using targeted knock-in mouse models have shown that overexpression models may have artificially exaggerated the role of gain of toxic function due to the presence of wildtype mouse FUS performing its normal function. Korobeynikov and colleagues employed the power of mouse genetics to confirm that both LOF and GOF were at play in targeted *FUS* mutant knock-in mice (Korobeynikov et al., 2022). Authors compared survival and developmental

phenotypes, such as malocclusion, between *Fus* knock-out and *Fus* knock-in mutant mice. Homozygous *Fus* knock-out or Fus^{P517L} (equivalent to human FUS^{P525L}) was perinatal lethal, whereas $Fus^{-/P517L}$ mice survived for 21 ± 12 days. This partial rescue of lethality shows that FUS^{P517L} retains some FUS function, albeit reduced. Authors argue that increased mutant FUS and other RNA binding proteins in insoluble fractions means FUS cannot perform its normal role leading to FUS LOF. Data from our humanised knock-in mice suggests there is some overlap of phenotypes in humanised *FUS* mutant and $Fus^{-/-}$ mice, again supporting a role for LOF in FUS pathomechanisms; $Fus^{-/-}$ mice on a mixed background are smaller and develop malocclusion and experience seizures, phenotypes seen in heterozygous $hFUS^{Q519lfs}$, and $hFUS^{P525L}$ mice to a lesser extent.

FUS mutant mice do not have identical phenotypes to $Fus^{-/-}$ mice however, showing *FUS* mutations must also initiate gain of toxic function, which is likely dose sensitive. Korobeynikov and colleagues found $Fus^{+/P517L}$ mice had reduced survival compared to $Fus^{+/\Delta 14}$ mice suggesting the two *FUS* mutations were having diverse effects, likely due to disruption of the NLS to different extents leading to different levels of cytoplasmic localisation. Data comparing the humanised $hFUS^{P525L}$ and $hFUS^{Q519lfs}$ mutations supports their findings; expression of the $hFUS^{Q519lfs}$ mutation leads to more severe increase of FUS in the cytoplasm, increased FUS protein levels and a more severe phenotype, particularly on the C57BL/6 background.

When considering LOF and GOF, it must be considered that different tissues will likely be vulnerable to different extents, given the tissue-specific roles of FUS. There will also be a mix of gain and loss of function within different cellular

compartments; there is evidence of both GOF and LOF of *FUS* mutations within the nucleus and the cytoplasm. More work is needed to unpick the relevance of this in tissues preferentially affected in ALS.

6.3.5 The hFUS^{Q519Ifs} protein is more toxic than the hFUS^{P525L} protein.

Expression of the *hFUS^{Q519Ifs}* mutation produced a more severe phenotype than expression of the *hFUS^{P525L}* mutation, but also of other mutations previously characterised at MRC Harwell such as the partially humanised *FUS$^{\Delta 14}$* mice. The *FUS$^{\Delta 14}$* mice express a point mutation in the splice acceptor site of exon 14 meaning exon 14 is skipped and exon 15 is read out of frame resulting in the PY NLS being lost.

When trying to generate cohorts of *hFUS^{Q519Ifs}* mice on different genetic backgrounds, it was apparent that heterozygous expression of the *hFUS^{Q519Ifs}* mutation was sufficient to produce developmental phenotypes (smaller mice, malocclusion, and highly penetrant seizures) that were only observed to the same degree when the *hFUS^{P525L}*or *FUS$^{\Delta 14}$* mutations were expressed in homozygosity, suggesting the *hFUS^{Q519Ifs}* mutation was more toxic.

More work would need to be done to fully understand what about the *hFUS^{Q519ifs}* mutation was driving the increased severity. Few transcripts were found to be differentially expressed between the *hFUS^{P525L}* and *hFUS^{Q519ifs}* mice; it would be interesting to employ single cell RNA sequencing to see if specific cell types were more vulnerable to effects of the *FUS* mutations, which could have been missed in bulk RNA sequencing. There was increased cytoplasmic FUS in *hFUS^{Q519ifs}* mice, so it may be that the cytoplasmic effect of the mutant protein was driving the phenotype, rather than the effect on transcript expression. Work could be done to study biochemical

differences between the mutant FUS proteins produced by the distinct mutations to see if there were changes to protein structure and folding which could impact the ability of FUS to perform its function. Subcellular location and binding partners of the mutant proteins could be assessed to see if this could shed light on potential downstream pathways affected by the different mutations.

Some of the developmental phenotypes displayed by the *hFUS*^{Q519lfs} mice, which mimicked *Fus* knock-out mice, could suggest a stronger loss of FUS function phenotype of the *hFUS*^{Q519lfs} mutation than was seen in *hFUS*^{P525L} mice. If true, this would have implications for therapy as knocking down FUS may exacerbate disease pathogenesis associated with the *hFUS*^{Q519lfs} mutation. This highlights the need to better understand the role of individual mutations and their potentially unique effects on tissues preferentially affected in ALS.

6.3.6 Humanised models are not the answer for everything: different models are needed to answer different questions.

Although the humanised *FUS* mice exhibit some disease relevant phenotypes, they do not recapitulate all aspects of ALS clinicopathology seen in patients and other *in vivo* models. Most lacking appears to be histological changes such as spinal motor neuron loss and the absence of FUS inclusion pathology. It must be considered that for the study of certain phenotypes, the humanised *FUS*^{P525L} mice are not the most appropriate.

Whether a model is best suited to answer a particular research question should always be considered but is commonly overlooked. I think a 'one-size-fits-all' model likely does not exist, and rather people need to work with a range of models, both *in*

vitro and *in vivo*, to discover and subsequently validate findings. This is particularly important when pre-clinical work is being generated to support clinical trial rationale in which there will be a mixed group of participants with multiple familial ALS mutations, along with sporadic patients.

One major strength of the humanised *FUS* models, beyond studying the various phenotypes unearthed during this DPhil project, is that human specific pathology can be explored. The ability to study human protein biochemistry, without interference from the mouse *Fus* gene and protein, is unique to these genetically humanised mice. Human specific biochemistry will become increasingly relevant as we learn more about protein conformation in pathological inclusions of different diseases. In the last year, near atomic resolution of fibrils from TDP-ALS and TDP-FTLD using cryo-electron microscopy revealed distinct TDP-43 amyloid fibril structures between the two diseases (Arseni et al., 2023). The likelihood is that fold type influences phenotype and toxicity; certain folds may be more toxic due to different binding properties or the ability to propagate more quickly. With the many structural and functional similarities between TDP-43 and FUS, it is likely the same will be true of FUS inclusions in ALS and other FUSopathies. Although the mouse and human FUS protein share around 97.67% identity at the amino acid level, small differences can have large effects on protein conformation and post-translational modifications, highlighting the importance of being able to study human FUS protein biochemistry.

6.4 What does this work mean?

6.4.1 What does work characterising the humanised *FUS* mice mean for the FUS-ALS field?

The overall aim of this project was to complete a comprehensive assessment of a wide range of phenotypes in the humanised *FUS* mice, following up on potential pathomechanisms as they were discovered. Once published, this will set the scene for other researchers to analyse disease relevant changes in the humanised *FUS* mutant mice in more depth.

It was thought humanising the *FUS* gene may produce a more severe model of FUS-ALS, with the human FUS strain and associated toxicity more intrinsically toxic than mouse FUS. Although this has not been the case, the model is still valuable to the community. The humanised *FUS* mice provide a way to study the mutated human gene and protein, expressed in a physiologically relevant pattern of expression, under the control of the endogenous mouse *Fus* promoter, which ultimately leads to ALS-relevant phenotypes.

In addition, the humanised *FUS* wildtype mice are an ideal genetic template in which to introduce and study additional ALS patient *FUS* mutations. By making the *hFUS* mice freely available, other research groups can generate humanised mutant mice in much the same way as the $hFUS^{P525L}$ and $hFUS^{Q519Ifs}$ mice were generated.

Another learning point from this project was the presence of sex-specific differences in the humanised *FUS* mutant and even *FUS* wildtype mice. In my experience, male mice had a stronger outward phenotype, and even at the RNA and protein level there were sex specific differences in *FUS* expression. Phenotypic sex

differences are well known (Wilson et al., 2022); however, when compiling Table 1.1, the sex of mice used to generate the data was seldom reported. I would urge the field to study mice of both sexes where possible, to avoid phenotypes being missed, and to generate data most relevant to FUS-ALS patients, of which there is not a documented sex bias although one could be masked by low patient numbers. If using both sexes is not logistically possible, it is important to report this in publications to improve replicability and validity of *in vivo* data.

6.4.2 What does work characterising the humanised *FUS* mice mean for FUS-ALS patients?

Historically, there has been a lack of successful disease modifying treatments for ALS patients, in large part because we still do not know what causes motor neurons to degenerate. Having said that, the latter does not necessarily have to be known to address the former, as is the case with spinal muscular atrophy (SMA). SMA, a condition like ALS in that motor neurons degenerate leading to muscle weakness, is usually caused by mutations in *SMN1.* How defective *SMN1* leads to disease pathomechanisms and ultimately motor neuron death is not well understood. Despite this, three therapies are now available to treat SMA.

Not only are the humanised *FUS* mice useful in helping scientists to understand FUS-ALS disease pathomechanisms, but they can also play a role in designing and validating human targeted therapies. The addition of the full human *FUS* sequence ensures the physiological and pathological characteristics of the human gene and protein are present in the mouse. This means human targeted therapies such as *FUS* siRNAs, ASOs and small molecule drugs can be assessed for safety and efficacy in the

humanised mice, without interference from mouse *Fus*. Experiments such as this are already ongoing; collaborators in the USA are using the humanised *FUS* mutant mice to validate patient *FUS*-targeted antisense oligonucleotides (ASO) to better understand efficacy of ASO knock-down and how this mitigates disease pathogenesis.

6.5 Limitations of the project

Although the humanised *FUS* mice provide a unique tool to study human FUS-ALS, they are not without limitations.

1) Humanised *FUS* mice display reduced *FUS* expression compared to *mFus/mFus* mice.

The mild reduction of *FUS* mRNA and protein in the humanised *FUS* mice was an unexpected limitation of this project. It was hoped that by placing the humanised construct under the control of the mouse *Fus* promoter, and including all introns, exons and 3'UTR, expression levels would be comparable to *mFus/mFus*. Instead, there was a mild but significant reduction in *FUS* expression in all tissues studied, possibly reflecting the loss of important regulatory elements, mouse transcription factors being unable to bind the human gene sequence as efficiently, or human FUS being less able to regulate its own expression. The humanised construct could have been designed differently, containing human exons but mouse *Fus* introns but whether this would have maintained expression is speculative.

This reduction in FUS expression meant that, although expression levels were comparable or increased in the *hFUS/hFUS*^{P525L} mice compared to *hFUS/hFUS*, there may have been an overall reduction in FUS protein in fully humanised mutant mice compared to *mFus/mFus* mice. The decrease in FUS levels could explain the lack of

pathological phenotypes that were seen in other FUS^{P525L} models, such as motor neuron loss, as dose sensitive FUS toxicity has been proposed (Korobeynikov et al., 2022).

FUS expression was regulated in a tissue specific manner, with the TA muscle seeing the largest reduction in FUS protein in *hFUS/hFUS* mice compared to *mFus/mFus* mice. Whilst reduced FUS protein, and therefore loss of FUS function, may be a factor in the phenotypes observed in *hFUS/hFUS^{P525L}* mice, using *hFUS/hFUS* mice as the most valid comparison controlled for unforeseen effects of humanisation; *hFUS/hFUS* mice also experience reduced FUS expression in the muscle. When comparing *hFUS/hFUS^{P525L}* mice to *hFUS/hFUS* mice there were many mutant-specific changes occurring such as a decrease in mitochondria, fibre type changes and muscle electrophysiology deficits.

2) Expression of the human FUS protein may be having more of an effect than is known from experiments carried out on *hFUS/hFUS* mice.

Extensive characterisation was carried out to try and ensure changes in ALS-disease relevant tissues were minimal, however certain things were not studied in the humanised FUS wildtype mice, such as binding partners of the human versus the mouse protein or whether human FUS can comparatively bind nucleic acid in the mouse system. Whilst efforts have been made to study this to a degree, such as RNA sequencing in which only a small number of transcripts were affected, humanisation may be having more of an impact than is known from the experiments carried out during this project. Digging deeper into the *hFUS/hFUS* mice may reveal more changes; however, from the work carried out, any differences appear minor and are not overtly

affecting the transcriptome. Nevertheless, it is these very differences, however small, that necessitate using *hFUS/hFUS* mice as controls for *hFUS* mutant mice.

3) "The humanised *FUS* mice are just another mouse model, and we are no closer to understanding FUS-ALS."

A criticism of this project may be that the humanised *FUS* mice are just another model of FUS-ALS to add to the list of existing models. During this project, a standard series of investigations were performed to characterise the phenotype of the *hFUS* wildtype and *hFUS* mutant mice, which although not in themselves novel, are essential to initially characterise the model for the field. The data produced from such experiments has highlighted some interesting phenotypes to be followed up on in more detail which aim to help better our understanding of FUS-ALS pathology in patients going forwards.

To generate genomically humanised targeted FUS-ALS mouse models was novel and the case for doing so was strong for the reasons discussed throughout this thesis. For example, to enable study of human targeted therapies and human protein strains and associated toxicity. There is the potential to use and study the humanised *FUS* mutant mice in ways that may not be possible with other existing models.

4) Primary neuronal cultures are a mixed population, and neurons represent an early, immature neuronal state.

Whilst the primary 'motor neuron collection' protocol was followed and every effort was made to collect tissue from the ventral side of the developing spinal cord, this did not produce a pure motor neuron population. Thought was given to how a

pure population of motor neurons could be produced. Flow cytometry was considered however the FUS protein was not tagged making this more challenging. A fellow DPhil student tried to isolate motor neurons using immuno-panning which was unsuccessful, largely because too few neurons were isolated, confluence was low and cells did not thrive in the absence of supporting cells.

As discussed in section 4.5, primary neuronal cultures are likely modelling an immature neuronal state. As has been suggested, phenotypes displayed by the cells in this chapter may represent early changes that occur in disease; it would have to be confirmed if the phenotypes displayed are relevant to disease progression in aging models.

Additionally, only one stress granule (SG) marker was used in primary cell culture experiments: G3BP1. Although G3BP1 is specific for SGs and not other cytoplasmic RNA granules (Dormann et al., 2010) there is increasing evidence that different stressors induce SGs with different protein compositions (Szewczyk et al., 2023). If future work was done using additional stressors, multiple SG markers would increase confidence that all SG types were detected.

5) Genetic background has a large effect on the penetrance and phenotype of *FUS* mutations.

The mouse genetic background strain has a large effect on the penetrance of developmental phenotypes such as malocclusion brought about by expression of *FUS* mutations, particularly $hFUS^{Q519lfs}$. The C3H background was used to generate $hFUS^{Q519lfs}$ cohorts as the malocclusion phenotype was relatively rare and prevented serious welfare issues. It may be inferred that the C3H background in some way

reduces the penetrance of the *hFUS*^{Q519Ifs} mutation more generally, but this was necessary to proceed with this project. This observation further supports the argument that work comparing mutations on different mouse backgrounds cannot always be directly compared, hence the need for projects such as this.

6.6 Future work

I think the following hypothesis-driven experiments would be valuable next steps to build on the knowledge gained during this project:

Hypothesis 1: The addition of environmental risk factors would decrease the age of symptom onset in the humanised *FUS*^{P525L} mice.

Work could be done to test human targeted disease modifying therapies in the humanised *FUS* mutant mice, but also to assess disease modifying *factors.* It is important to better understand what environmental triggers push or delay phenoconversion and affect disease progression. Factors to test could include diet, exercise, localised tissue trauma, different types of stress and viruses all of which have been proposed to influence the risk of developing ALS (Chapman et al., 2023; Dormann et al., 2012; Dormann et al., 2010; Ngo et al., 2014; Shelkovnikova et al., 2019; Szewczyk et al., 2023).

Hypothesis 2: hFUS^{P525L} will be localised to the insoluble fraction in aged *hFUS/hFUS*^{P525L} mice. There would be increased FUS protein in the insoluble fraction of *mFus/hFUS*^{Q519Ifs} mice compared to *mFus/hFUS*^{P525L} mice.

The presence of the *hFUS*^{P525L} mutation likely changes liquid-liquid phase separation dynamics of the hFUS^{P525L} protein (Korobeynikov et al., 2022). This may lead

to an increase in insoluble FUS in the cytoplasm of aged mice as cytoplasmic FUS increases during aging.

As there was increased hFUS^{Q519Ifs} in the cytoplasm compared to hFUS^{P525L} in chapter 5, I hypothesise there would be increased FUS protein in the insoluble fraction in *mFus/hFUS^{Q519Ifs}* mice leading to a stronger loss of FUS function phenotype.

It would be interesting to assess what proteins were sequestered along with mutant FUS in the insoluble fraction, which would likely include other RNA binding proteins (Korobeynikov et al., 2022). I would be curious to see if the sequestered proteins in the humanised mice differed from those reported in targeted knock-in mice expressing mutant mouse FUS protein, and between *FUS* mutations. This could inform if human protein strains behave differently to artificial mouse strains, and if they differ between different mutations, which may more accurately represent what is happening in human ALS patients.

Hypothesis 3a: Studying FUS inclusions from FUS-ALS caused by different *FUS* mutations will tell us more about disease progression.

As discussed in section 6.3.6, TDP-43 amyloid fibril structure conformation was shown to be different in pathological inclusions from different TDP-43 proteinopathies. I hypothesise the same would be true of FUS inclusions in that inclusions may have different conformational structures and properties in different FUSopathies. It would be interesting to assess the atomic structure of inclusions from FUS-ALS patients expressing different *FUS* mutations, or who develop FUS-ALS early or later in life, to see if the inclusions differed in structure which could in turn cause differences in FUS toxicity and disease aetiology.

Alternatively, the structural conformation of inclusions may be similar across FUS-ALS, with the mutation perhaps affecting other inclusion properties such as rate of formation by influencing the levels of cytoplasmic localisation. Severe truncation *FUS* mutations may be more toxic as the FUS protein produced lacks the C-terminus which could in some way influence the properties of inclusion fibrils, perhaps altering what proteins are bound and sequestered in the cytoplasm.

Hypothesis 3b: FUS inclusions from FUS-ALS patients would seed FUS inclusion pathology in humanised *FUS* mice.

It would be interesting to see if human patient inclusions could seed FUS pathology in the humanised wildtype mice, either *in vivo* or using primary cultures *in vitro*. If this was successful, it would be valuable work to see if different *FUS* mutations had different seeding properties, such as an ability to induce higher numbers of inclusions more quickly. Further work could assess if seeding ability correlated with any specific properties of the *FUS* mutations, such as degree of NLS disruption, which in patients leads to earlier, more aggressive disease progression.

This could help to answer questions surrounding disease pathology spreading and why certain mutations are more toxic. It would also produce a model with which to study FUS inclusions further including their structure, binding partners, and post-transcriptional modifications.

Hypothesis 3c: Different neuronal populations and tissues would be differentially affected by FUS inclusion seeding in humanised *FUS* mice.

Given the evidence that upper and lower motor neurons are vulnerable to degeneration in ALS, I would hypothesise that these neuronal populations would be particularly susceptible to seeding by FUS inclusions. It would be interesting to compare the vulnerability of both susceptible and more resistant neuronal populations, along with other non-neuronal tissue such as muscle, to see if seeding pathology was different in different cell types. This could help us to understand why certain cell types are more susceptible or resistant to disease, and to study how inclusion pathology spreading could be prevented or slowed to try and prevent disease progression in patient tissue.

Hypothesis 4: There will be early structural and functional changes in skeletal muscle in the *hFUS/hFUS^{P525L}* mice.

The changes in the muscle brought about by the *hFUS^{P525L}* mutation could be studied in more detail, across multiple muscle types to see which muscle fibres were preferentially affected by mutant FUS.

I would like to repeat the muscle electrophysiology experiments at multiple timepoints: 4, 6, 12, and 18 months. Given what was seen in the RNA sequencing data, I would hypothesise that changes would be detectable from 4 to 6 months, and that muscles in the mutant mice would be able to produce larger contractions initially due to an increase in type II fibres. I would want to pair this with fibre type staining and mitochondrial copy counts to see if fibre type changes reflect an early or even

developmental effect of mutant FUS that predisposes muscle tissue to dysfunction and subsequent atrophy.

In aged *hFUS/hFUS^{P525L}* mice, I would study mitochondrial changes in more detail, such as whether mitochondria were functional by analysing the electron transport chain complexes. This data would influence potential therapeutic targets, such as the treatments to target mitochondrial function perhaps in combination with reducing the effect of mutant FUS.

I would also want to carry out FUS staining in muscle tissue. Work has shown FUS is localised to the NMJ and causes NMJ structural abnormalities (So et al., 2018). If NMJ denervation is detected in the humanised *FUS^{P525L}* mice, I would study FUS localisation, aggregation, and inflammation in more detail to see what could cause this early disease symptom. More recently, work has highlighted FUS may play a role in synaptic function, as FUS co-localises with pre- and post-synaptic markers (Salam et al., 2021). It would be interesting to see the effect of mutant FUS on synaptic transmission, both in the motor cortex and at NMJs.

Hypothesis 5: Primary muscle cultures from *hFUS/hFUS^{P525L}* mice would show deficits, different to those seen in neuronal cultures.

In addition to looking at cellular stress response in more detail in primary neuronal cultures, I would like to produce primary muscle cultures from satellite cells. Given the muscle changes seen in the *hFUS/hFUS^{P525L}* mice, I hypothesise primary muscle cultures would provide a useful tool to study early disease changes. FUS localisation, expression, gene and protein dysregulation and fibre changes could all be studied.

It would be interesting to see whether muscle cells would be inherently different when collected from *hFUS/hFUS*^{P525L} mice vs *hFUS/hFUS* mice. A recent study on MedRxiv analysed the expression profile of ALS patient skeletal muscle tissue; it would be valuable to see if the expression changes authors reported were also detected in the *in vitro* muscle cultures, or *in vivo* in the adult *hFUS*^{P525L} mice, and could help explain some of the early changes occurring at the site of the muscle (Freydenzon et al., 2023).

The primary muscle cultures could also be stressed, perhaps overstimulated to induce damage, to see what pathways were activated and whether these were different in the *FUS* mutant mice.

6.7 Overall summary of thesis

In this thesis, genomically humanised *FUS* wildtype and *FUS* mutant mice expressing ALS causing patient mutations were characterised in depth. Genomically humanised *FUS* wildtype mice were overtly phenotypically normal, suggesting human FUS could functionally replace mouse FUS. Distinct phenotypes were found to be associated with expression of two FUS-ALS mutations, $hFUS^{P525L}$ and $hFUS^{Q519lfs}$, with both producing mutation-specific developmental and age-dependent phenotypes, particularly affecting skeletal muscle.

The humanised *FUS* mutant mice may more accurately represent pathogenesis occurring in human patients, as the mutant FUS protein is expressed in a physiologically relevant pattern of expression, which I hope enables *in vivo* work using the humanised mice to be more translatable to FUS-ALS patients. The humanised *FUS* mutant mice would be useful for assessing human targeted therapies, but also human protein specific biochemistry, as the mice express the human *FUS* gene and protein, without interference from the moue *Fus* gene and protein.

7 Chapter 7: Materials and Methods

7.1 Materials and equipment

7.1.1 Reagents and consumables

Table 7.1: Reagents and consumables

Reagent name	Manufacturer	Cat/part no.
Animal housing		
Rat and Mouse Breeding 3 (RM3) diet	Special Diet Services	
Aspen Chips bedding	Datesand	
Tissue collection		
Pentobarbitone		
Isoflurane		
RNAlater Stabilization Solution	ThermoFisher Scientific	AM7020
16% Formaldehyde (w/v), Methanol-free	ThermoFisher Scientific	28908
Isopentane	Fisher scientific	10030290 (manuf no. P/1030/08)
OCT Compound	VWR	361603E
Sodium azide	Sigma-Aldrich	S2002-100G
General reagents		
Bovine serum albumin, Lyophilized powder	Merck	A9418
Sucrose	Merck	S0389-500G
Chloroform	Fisher scientific	11398187
Ethanol	Fisher scientific	10437341
Methanol	Merck	106009
Triton X-100	Fisher scientific	11436631
Tween 20	Sigma-Aldrich	P9416
EDTA	ThermoFisher Scientific	17892
10% SDS	Fisher Scientific Ltd	10265153
Molecular Biology Grade Agarose	Severn Biotech Ltd	30-10-50
GelRed	Biotium	BT41003-5

GelGreen	Biotium	BT41005-5
Proteinase K Solution (20 mg/mL)	ThermoFisher Scientific	AM2546
DEPC Treated Water	ThermoFisher Scientific	AM9916
EXOsap	ThermoFisher Scientific	78200.200.UL
RNA extraction and RT-PCR		
Rneasy Mini Kit	Qiagen	74104
Rneasy Lipid Tissue Mini Kit	Qiagen	74804
Rneasy Fibrous Tissue Mini Kit	Qiagen	74704
RNAse ZAP	Sigma-Aldrich	R2020
QIAzol Lysis Reagent	Qiagen	79306
UltraPure Phenol:Chloroform:Isoamyl Alcohol (25:24:1, v/v)	ThermoFisher Scientific	15593031
Agilent RNA 6000 Nano Kit	Agilent	5067-1511
High-Capacity cDNA Reverse Transcription Kit	Applied Biosystems	4368814
Fast SYBR Green Master Mix	ThermoFisher Scientific	4385612
Protein extraction and western blotting		
RIPA buffer	ThermoFisher Scientific (Pierce)	89900
cOmplete, EDTA-free Protease Inhibitor	Sigma-Aldrich	11873580001
DC Protein Assay Reagents Package	BioRad	500-0116
Protein standard – 2 mg/vial BSA	Merck	P5619
Protein loading buffer. 4x	LI-COR	928-40004
NuPAGE Sample Reducing Agent (10X)	ThermoFisher Scientific	NP0004
NuPAGE 4-12% Bis-Tris Protein Gels, 1.0 mm, 15-wells	ThermoFisher Scientific	NP0323BOX
NuPAGE 4-12% Bis-Tris Protein Gels, 1.0 mm, 10-wells	ThermoFisher Scientific	NP0321BOX
NuPAGE MOPS SDS Running Buffer (20X)	ThermoFisher Scientific	NP0001
NuPAGE Antioxidant	ThermoFisher Scientific	NP0005
Chameleon Duo Pre-stained Protein Ladder	LI-COR	928-60000
iBlot™ Transfer Stack, nitrocellulose, mini	Invitrogen	IB301002
REVERT Total Protein Stain Kit	LI-COR	926-11010

Non-fat dried milk from bovine	Sigma-Aldrich	M7409
DNA		
MyTaq Extract-PCR Kit	Meridian Bioscience	BIO-21127
MyTaq Red 2x master mix	Meridian Bioscience	BIO-25043
Q5 High fidelity polymerase 2 x master mix	NEB	M0492L
Tris-HCl pH 8	Invitrogen	15568025
0.5M EDTA	Invitrogen	AM9260G
5M NaCl	Invitrogen	AM9760G
10% SDS	Fisher Scientific	10265153
Proteinase K	Invitrogen	AM2546
UltraPure Phenol:Chloroform:Isoamyl Alcohol (25:24:1, v/v)	ThermoFisher Scientific	15593031
D/C HIGH VACUUM GREASE	VWR (DOW CORNING)	291-0039 (manuf no. 636082B)
Sodium Acetate (3 M), pH 5.5	ThermoFisher Scientific	AM9740
TE Buffer Solution pH 8.0	Merck	8890-100ML
NFL quantification		
NF-light Advantage Assay Kit	Quanterix	103186
Disc Kit for Simoa HD-1/X (rev 2)	Quanterix	103347
Histology		
Mouse Ig Blocking Reagent (M.O.M.® (Mouse on Mouse) Blocking Reagent)	2B Scientific (Vector Labs)	MKB-2213
Normal Goat Serum	Abcam PLC	ab7481
Sudan Black B	Merck	199664
Chrome potassium sulphate	BDH Chemicals Ltd	6044080
Gallocyanine	Sigma-Aldrich	124508
Chrome alum	Merck Life Science	243361
Xylene	Pioneer Research Chemicals Ltd	25059
D.P.X	Sigma	06522
Clearium	Leica	3601100
Cresyl Violet acetate	Sigma-Aldrich	C5042

ProLong Gold Antifade Mountant	ThermoFisher Scientific	P36930
Prolong Glass Antifade Mountant with NucBlue	ThermoFisher Scientific	P36981
ProLong™ Gold Antifade Mountant with DAPI	ThermoFisher Scientific	P36935
Muscle ATPase staining		
Sodium barbital	Sigma-Aldrich	B0500
Calcium Chloride	Sigma-Aldrich	C1016
Cobalt(II) chloride	Sigma-Aldrich	232696
Sodium Acetate	Sigma-Aldrich	S2889
Ammonium sulfide, 20% solution	Sigma-Aldrich	A1952
Sodium hydroxide	Honeywell	71463
Hydrochloric acid	Honeywell	35328
Adenosine 5'-Triphosphate Disodium Salt	Merck	A3377
Mammalian cell culture		
HBSS (10X)	ThermoFisher Scientific	14185052
Poly-L-Ornithine Hydrobromide, MW 30,000	Merck	P3655
Laminin Mouse Protein Natural	ThermoFisher Scientific	23017015
Trypsin (2.5%) no phenol red	ThermoFisher Scientific	15090046
500ML LEIBOVITZ L 15 MED	Fisher scientific	15460554
Bovine Serum Albumin solution	Merck	A1595
DNAse I,LYO., 100 MG	Merck	11284932001
Neurobasal Medium	ThermoFisher Scientific	21103049
Horse serum heat inactivated	Merck	H1138
Glutamax	ThermoFisher Scientific	35050038
2-Mercaptoethanol (50 mM)	ThermoFisher Scientific	31350010
Penicillin-Streptomycin (5000 U/mL)	ThermoFisher Scientific	15070063
B-27 Supplement (50X) serum free	ThermoFisher Scientific	17504044
Rat CNTF	PeproTech	450-50
Human/Murine/Rat BDNF	PeproTech	450-02
Murine GDNF	PeproTech	450-44
Seahorse Xfe96 FluxPak mini	Agilent	102601-100
Seahorse XF Cell Mito Stress Test Kit	Agilent	103015-100

Seahorse XF DMEM Medium, pH 7.4	Agilent	103575-100
Seahorse XF 1.0 M Glucose Solution	Agilent	103577-100
TMRE-Mitochondrial Membrane Potential Assay Kit	Abcam	ab113852
Sodium arsenite solution	Merck	106277
CellTiter-Blue Cell Viability Assay	Promega	G8080
CellTox-Green Cytotoxicity Assay	Promega	G8741
Consumables		
Embedding Moulds	ThermoFisher Scientific	441228
Matrix D Lysing, 500 x 2mL tubes	MPBiomedicals	116913500
8-Well Non-Skirted PCR Plate Segment	4titude	503781
Strips of 8 Domed Caps	4titude	198733
MicroAmp Fast Optical 96-Well Reaction Plate	Applied Biosystems	4346906
PCR Seal	4titude	131135
Corning 96-Well Solid White Polystyrene Microplates	Fisher Scientific	10022561
SuperFrost Plus Adhesion slides	Fisher Scientific	10149870
High Precision Micrsocope Cover Glasses 13mm	Marienfeld	0117530
High Precision Micrsocope Cover Glasses 22x22mm	Marienfeld	0107052
High Precision Micrsocope Cover Glasses 24x50mm	Marienfeld	0107222
Costar Assay plate	Costar/Corning	3370
Nunc 24 Well Multidish Nunclon Delta SI	SLS	142475

7.1.2 Equipment

Table 7.2: Equipment

Equipment name	Manufacturer
Phenotyping	
PhotoBeam Open Field	Omnitech Electronics
EthovisionXT	Noldus
EchoMRI	Echo Medical Systems
Grip Strength Meter	Bioseb
Locotronic	Intellibio
Rotarod	Ugo Basile
Voluntary Running Wheels	TSE Systems
Isometric force transducers (muscle electrophysiology)	Dynamometer UFI Devices
PicoScope 3423 oscilloscope (muscle electrophysiology)	Pico Technology
Molecular biology	
Bertin Precellys 24 Lysis Homogeniser	Precellys
MicroCL 17R Microcentrifuge	ThermoFisher
Eppendorf ThermoMixer C	Eppendorf
accuSpin Micro 17R centrifuge	Fisher Scientific
NanoDrop 8000 Spectrophotometer	Thermo Fisher Scientific
2100 Bioanalyzer	Agilent
T100 Thermal Cycler	BioRad
Mini-Sub Cell GT Electrophoresis Cell	BioRad
ChemiDoc XRS+	BioRad
7500 Fast Real-Time PCR System	Applied Biosystems
Mini Gel Tank	Invitrogen
PowerPac Basic Power Supply	BioRad
PowerEase 90W	Invitrogen
iBlot Dry Blotting System	Invitrogen
Odyssey® CLx	LI-COR
NFL quantification	
HD-X ANALYZER™	Quanterix

Histology	
CryoStar NX70 Cryostat	Thermo Fisher Scientific
Nanozoomer slide scanner	Hamamatsu
Microscopy/imaging	
Axio Scan.Z1 Slide Scanner	Zeiss
AxioObserver LSM 700 inverted confocal	Zeiss
Plan-Apochromat 10x/0.3 M27 objective	Zeiss
Plan-Apochromat 20x/0.8 M27 objective	Zeiss
Plan-Apochromat 40x/1.4 Oil DIC M27 objective	Zeiss
Mammalian cell culture	
Invitrogen™ Countess II Automated Cell Counter	Thermo Fisher Scientific
Seahorse Xfe96 Analyzer	Agilent
FLUOstar Omega Microplate Reader	BMG Labtech

7.1.3 Software

Table 7.3: Software

Name	**Manufacturer**
Phenotyping	
Omnitech	Omnitech Electronics
EthovisionXT 8.5	Noldus
Fusion v6.5 SuperFlex Edition	Omnitech Electronics
EchoMRI	Echo Medical Systems
Locotronic Analysis	Intellibio
TSEphenomaster (Voluntary wheel running)	TSE Systems
PicoScope (muscle electrophysiology)	Pico Technology
Molecular biology	
7500 Software v2.3	Applied Biosystems
Image Lab v6.0.1	BioRad
Snapgene	Dotmatics
Empiria Studio	LI-COR
Image Studio Lite v5.2	LI-COR
Histology	

NDP.veiw 2	Hamamatsu
Microscopy/imaging	
ZEN Black	Carl Zeiss software
ZEN Blue	Carl Zeiss software
ImageJ	National Institutes of Health
Mammalian cell culture	
Seahorse_Wave	Agilent
MARS Data Analysis Software (plate reader)	BMG Labtech
Statistics	
GraphPad Prism 10	Dotmatics

7.2 Mice

7.2.1 Ethics statement

All animal husbandry and experiments were performed at the Mary Lyon Centre at MRC Harwell or at University College London Institute of Neurology (muscle electrophysiology). All animal work was done in accordance with the Animals (Scientific Procedures) Act 1986, Home Office guidelines and local ethics guidelines issued by the Medical Research Council. All reasonable measures were taken to minimise animal distress and suffering. Animal experiments were performed under Home Office Project License No. 20/0005.

7.2.2 Humane endpoints

Mice were monitored daily by ward staff and the following were used as humane endpoints:

- Weight loss exceeding 20% without recovery in 24 hours.
- Weight gain that results in a deterioration of condition such as reduced ability to move or rear for drinking and tautness of skin leading to lesions.
- Piloerect coat showing no improvement in up to 24 hours.
- Hunched appearance, not improving within a working day (8 hours maximum).
- Unexpected tremors impinging on the ability to feed not improving within a working day (8 hours maximum).
- Excessive activity or inactivity impinging on the welfare of the mouse.
- Seizures not returning to normal within 2-3 minutes, or repeated seizures.

7.2.3 Animal housing

Mice were fed ad libitum with free access to water (chlorinated to 9-13 ppm). Mice were kept under constant conditions with a regular 12h light (19:00-07:00) and dark (07:00-19:00) cycle, temperature of 21±2°C and humidity 55±10%. Mice were housed in same sex cages of up to five mice. Cages contained bedding, shredded paper, and a rodent tunnel for enrichment.

7.2.4 Generation of mouse lines

7.2.4.1 Generation of genomically humanised FUS mice

Quoted verbatim from the previously published report characterising the *hFUS/hFUS* mice (Devoy et al., 2021):

The official allele designation is $Fus^{tm3.1(FUS)Emcf}$ (MGI:6193752), referred to here as *hFUS*. A BAC targeting construct harbouring the mouse *Fus* locus (BAC RP24-297F14; strain C57BL/6J) was engineered to replace the mouse *Fus* gene from the ATG start site (g.106) to the end of the 3'UTR (g.14574) with the orthologous human *FUS* genomic sequence, and an FRT-flanked Neo cassette was inserted 1kb downstream from the humanised 3'UTR. This construct was electroporated into the 129X1/SvJ-129S1/SV mouse ES cell line R1, humanising *Fus* in the mouse genome via homologous recombination. Correctly targeted clones were initially identified through Loss-Of-Allele (LOA) copy via qPCR and ddPCR assays, while karyotype of positive clones was then screened employing ddPCR. Mice were generated by injection of modified ES cells into donor blastocysts, with the resultant chimeric male offspring crossed to C57BL/6J females to obtain GLT. Following confirmation of GLT, *hFUS* heterozygous mice were bred one further generation to the C57BL/6J strain, followed by crossing to the

Gt(ROSA)26Sortm2(CAG-flpo,-EYFP)Ics line (C57BL/6Ntac background) to excise the *FRT*-flanked Neo selection cassette. The Neo-negative line was then backcrossed for at least six further generations onto the C57BL6/J background before homozygotes were generated for long-read sequencing and experimental cohorts were bred. Genotyping was performed by LOA copy number qPCR using custom probe sets.

This line has been submitted to the European Mouse Mutant Archive (EMMA, EM:13073).

7.2.4.2 Generation of hFUS^{P525L} mice

hFUS^{P525L} mice, officially designated C57BL/6Ntac-Fus$^{em1(FUS*P525L)Emcf}$/H were generated using CRISPR mediated gene editing of a *hFUS/hFUS* embryo.

A 2 x 20 μl mixture of 1) Cas9 mRNA (100ng/μl), 2) small guide RNA (50ng/μl) [sequence: 5'-GGGAGCCAGGCTAATTAATA-3'] and 3) ssODN (50ng/μl, purchased from IDT as a PAGE-purified ultramer with four phosphorothioate bonds added at each end for stability) [sequence: 5'-ACTTAATTTTTTTTTTTTTTTTGCAGGGGTGAGCACAGACAGGATCGCAGGGAGAGGCTGTACTAATTAGCCTGGCTCCCCAGGTTCTGGAACAGCTTTTTGTCCTGTACCCAGTGTTACCCT-3'] were injected into the pronucleus of a one-cell-stage homozygous humanised *FUS* embryo. The injected zygotes were then implanted in pseudo pregnant female mice and the F0 progeny genotyped using Sanger sequencing. Correctly edited F0 animals were then crossed to C57BL/6J and C57BL/6N mice for one generation and the *hFUS^{P525L}* allele was confirmed at the F1 stage. Successfully generated *hFUS^{P525L}* mice were then backcrossed to C57BL/6J and C57BL/6N mice for at least 5-10 generations.

All work for this project was carried out on *hFUS*^{P525L} mice on the C57BL/6J background.

Two point mutations were introduced into the *hFUS* sequence, the first a C to T substitution meaning a leucine amino acid is coded for in the place of a proline at point 525 producing the *FUS*^{P525L} mutation. An additional silent mutation at amino acid position 526 was introduced to aid with genotyping.

7.2.4.3 Generation of hFUS^{Q519Ifs} mice

hFUS^{Q519Ifs} mice, officially designated C57BL/6Ntac-Fus$^{em2(FUS*Q519I)Emcf}$/H ((MGI:6193752), were generated using CRISPR mediated gene editing of a *hFUS/hFUS* embryo.

A 2 x 20 μl mixture of 1) cas9 mRNA (100ng/μl), 2) small guide RNA (50ng/μl) [sequence: 5'- TTGCAGGGGTGAGCACAGAC-3'] and 3) ssODN (50ng/μl, purchased from IDT as a PAGE-purified ultramer with phosphorothioate bond between first and last four nucleotides) [sequence: 5'-CAAAAAGCTGTTCCAGAACCTGGGGAGCCAGGCTAATTAATACGGCCTCTCCCTGCGATCCTGTGCTCACCCCTGCAAAAAAAAAAAAAAAAATTAAGTATCCATTATATTTGAGTTACC-3'] were injected into the pronucleus of a one-cell-stage homozygous humanised *FUS* embryo. Injected embryos were re-implanted in CD1 pseudo-pregnant females. Host females were allowed to litter and rear F0 progeny which were genotyped using Sanger sequencing.

Correctly edited F0 animals were then crossed to C57BL/6J and C57BL/6N mice for one generation and the *hFUS*^{Q519Ifs} allele was confirmed at the F1 stage. Successfully generated *hFUS*^{Q519Ifs} mice were backcrossed to C57BL/6J and C57BL/6N,

DBA and C3H mice. *hFUS*^{Q519Ifs} mice were subsequently maintained on the C3H background and were backcrossed with C3H mice for at least 5-10 generations.

The modification comprised a four-nucleotide deletion and a Q519I frameshift.

7.2.4.4 Generation of Fus$^{+/-}$ and Fus$^{-/-}$ mice

Fus knock-out mice, officially designated Fus$^{tm1.1(KOMP)Vlcg}$, were generated as part of the Knock-out Mouse Project (KOMP).

The *Fus* knock-out lines were generated by homologous recombination in VGB6 (C57BL6/Ntac) embryonic stem cells using targeting vectors made via BAC recombineering. The insertion of Velocigene cassette ZEN-Ub1 created a deletion of size 14268bp between positions 127566740-127581007 of Chromosome 7 (Build GRCm39) as detailed in (Valenzuela et al., 2003).

Cre-mediated excision of the parental Fus$^{tm1(KOMP)Vlcg}$ allele resulted in the removal of the neomycin selection cassette and critical exon(s) leaving behind the inserted lacZ reporter sequence.

Successfully generated *Fus*$^{+/-}$ mice were then backcrossed to C57BL/6J or DBA/2JCrl mice for at least 5-10 generations. Heterozygous *Fus*$^{+/-}$ mice on the congenic C57BL/6J or DBA/2JCrl background were then intercrossed to produce homozygous *Fus*$^{-/-}$ mice which were viable beyond weaning on a mixed C57BL/6J x DBA genetic background.

7.3 Mouse experimental procedures

7.3.1 Genotyping

Genotyping for all lines was performed in house using loss of allele copy count assays. Table 7.4 details the primer and probe sequences used.

Table 7.4: Genotyping primers

Assay	Primer	Sequence
Mouse *Fus* copy number qPCR assay	Forward primer	GGCGGTTGTGTGTGTATGTG
	Reverse primer	AACATGGACCCATTCTTCAGAAAG
	5'-FAM probe	CATCATTTTAGTTAAATTCTGTTTCC
Human *FUS* copy number qPCR assay	Forward primer	CCCAGCAGGAACTGGAATACAG
	Reverse primer	AACATGGACCCATTCTTCAGAAAG
	5'-FAM probe	TTCTGTCATGGGGAAATTCTGTTTCCC
Human FUS^{P525L} copy number qPCR assay	Forward primer	CAGGACAAAAAGCTGTTCCAGAAC
	Reverse primer	AGGATCGCAGGGAGAGGCT
	5'-FAM probe	AGCCAGGCTAATTAGTACAGC
Human $FUS^{Q519Ifs}$ copy number qPCR assay	Forward primer	GGAGCCAGGCTAATTAATACG
	Reverse primer	GGTAACTCAAATATAATGGATACTTAA TTTTT
	5'-FAM probe	CCTCTCCCTGCGATCCTGTGCTC

Mouse *Fus* KO copy number qPCR assay	Forward primer	GGCCATCCTGCTCTACAGA
	Reverse primer	GTGGTTCCCTTAACACATCTTTCAG
	5'-FAM probe	CTAGTTCCACGACAGCCTGGGC

7.3.2 Breeding and survival data

All mice bred at Harwell are documented on an internal system (Anonymus) which was used to export and analyse breeding and cohort data.

Survival analysis was also done using this exported data. Any mouse which had died from an unknown cause (e.g., found dead) or was culled due to any welfare issues (excluding fight wounds, unless it was due to issues with wound healing) was recorded as an event.

7.4 Phenotyping

Phenotyping tests were carried out at the same time each day and mice were acclimatised for 30 minutes prior to each test. The same experimenter carried out each test in a longitudinal pipeline and was blind to genotypes of the mice.

7.4.1.1 Weight checks

Mice were weighed inside a beaker, without the use of anaesthetic, every three to four weeks by MRC Harwell ward staff. Mice were also weighed before relevant *in vivo* tests.

7.4.1.2 Marble burying

Marble burying was used to assess the basic wellbeing of the mouse, to inform further tests. Mice were removed from the home cage and placed into open cage

bases containing 1.5L of Aspen Chips bedding and 9 marbles, with one mouse per cage base. Marbles were evenly spaced apart in 3 rows of 3, and placed on top of the bedding so they were fully visible. After 30 minutes, the number of marbles which were fully buried (2/3 of marble buried/not visible), partially buried (1/2 of marble buried/not visible), moved but not buried and not moved and not buried were recorded.

7.4.1.3 Open field

Open field was used to assess anxiety, activity, and exploratory drive according to manufacturer's instructions. Mice were removed from the home cage and placed into the self-contained arena. Lighting was set at 150-200 lux. Mice were recorded for 20 minutes via sensors in the open field equipment, and parameters such as distance travelled, and time spent in each zone were recorded.

7.4.1.4 Y maze

Y maze was used to assess anxiety, exploratory behaviour, and as a basic cognitive test. Y maze was used according to manufacturer's instructions. Y maze contains a start, familiar and novel arm. The start arm is randomised. For the habituation trial, the novel arm was blocked off. Mice were allowed to explore the start and familiar arm for 5 minutes. The mouse is then returned to the home cage for 2 minutes, before being placed back into the Y maze and recorded for 10 minutes with the novel arm open.

7.4.1.5 EchoMRI

EchoMRI measures body composition in conscious animals, providing measurements of whole-body fat mass, lean mass, and water content. Mice were

weighed, and then EchoMRI was performed using a mouse EchoMRI machine, then mice were returned to their home cage.

7.4.1.6 Grip strength

Grip strength was assessed using the force sensor equipment as per manufacturer's instructions. Mice were lowered onto the grid so only the forelimbs could grip and were pulled steadily downward. This was repeated 3 times. Mice were lowered onto the grid allowing fore and hindlimbs to grip and were pulled steadily downward. This was repeated 3 times.

7.4.1.7 Locotronic

Locotronic coordination was assessed as per manufacturer's instructions. The equipment contains a horizontal ladder within a corridor and mice are motivated to move from the illuminated start area to the darker finish area. Infrared sensors above and below the ladder detect errors in paw placement. Three runs were carried out per mouse with at least 30 minutes between runs, and the mean average total leg errors calculated. Runs which took longer than 30 seconds after exiting the start area were discounted (Stewart et al., 2019).

7.4.1.8 Accelerating rotarod test

Ability of mice to remain on a rotating rod was assessed as per manufacturer's instructions. Mice were trained for three consecutive days. Day 1: mice are placed on the rotarod at a constant speed of 4RPM for 300 seconds. If they fall off, they are placed back on. Day 2: mice are placed onto the rotarod, which is allowed to accelerate up to 40RPM. If the mice fall, they are replaced until 300 seconds and 40RPM is reached. Day 3: repeat as day 2. The following week, mice are trained for a

further day and then tested on two consecutive days. The acceleration and fall time are recorded, and the average taken.

7.4.1.9 Wheel-running test

Mice were singly housed in cages containing a voluntary running wheel attached to a computer for recording data for 2-3 weeks. Food and water were available ad libitum. After 2 weeks, the wheel was changed for one with rungs missing at irregular intervals, presenting a motor challenge. Only data recorded during the dark period (19:00-07:00) was analysed. Average maximum wheel running speed was calculated (in 5 minute bins) and analysed. Any mice which did not complete the 3 weeks were removed from analysis.

7.4.1.10 Muscle electrophysiology

Muscle strength, number of motor units and muscle fatigue were assessed in tibialis anterior (TA) and extensor digitorum longus (EDL) muscles of aged (21-month-old) *hFUS/hFUS*^{P525L} male mice using published muscle electrophysiology techniques by Dr Mhoriam Ahmed in the Greensmith lab at UCL (Ahmed et al., 2016; Ahmed et al., 2023). Briefly, the mice were anaesthetised using 1.5-2% isoflurane and the distal tendons of the TA and EDL muscles of both legs were exposed, freed, and attached to isometric force transducers. The sciatic nerve was also exposed and dissected, leaving only the deep peroneal branch intact which innervates the TA and EDL muscles. Silver wire electrodes were attached to the sciatic nerve to elicit isometric contractions.

Twitch force is first recorded for each muscle and is the amplitude of force produced by the muscle after one impulse is sent via the electrode, equivalent to one action potential.

For maximum tetanic force, the muscle is given a series of impulses via the electrodes and the maximum force generated by the muscle is recorded. This is repeated several times, careful not to fatigue the muscle.

Motor unit numbers were assessed by stimulating the muscle with impulses of increasing intensities and recording the twitch tension produced. The stepwise increase in twitch tension corresponds to individual motor units or axons being recruited which can be quantified.

To record muscle fatigue, the muscle is repeatedly stimulated and the difference in force between the first (strongest) and last (weakest) contraction is calculated.

7.4.1.11 Tail bleeds for NFL analysis

Tail bleeds were carried out by the phenotyping team at MRC Harwell. 10% total blood volume was collected from the lateral tail vein to quantify neurofilament light chain levels in blood plasma. EMLA cream was applied to the base of the tail then mice were placed in a plastic restrainer. Using a scalpel blade, a small incision was made in the lateral tail vein in the top third of the tail and blood was collected into a lithium heparin microcuvette. Total blood collected was then centrifuged at 4°C and the supernatant collected, frozen on dry ice and stored at -80°C until processing.

7.4.2 Tissue collection

Mice were culled via intraperitoneal injection of 0.2ml pentobarbitone. For the cohort of mice used in chapter 5 this injection was done after first anesthetising the mice with isoflurane as this protocol was brought in to reduce stress and suffering caused by injection of pentobarbitone.

The whole spinal cord (via hydraulic extrusion) brain (minus cerebellum and olfactory bulbs), tibialis anterior (TA), extensor digitorum longus (EDL) and soleus muscles were routinely dissected and processed, along with tail tissue for genotyping confirmation. If tissue was stored long term, it was either frozen immediately in liquid nitrogen and stored at -80°C, or stored in RNA later at -20°C. If fresh tissue was required, tissue was kept on ice until processing.

For motor neuron counts and FUS immunofluorescence studies in chapter 2 animals were culled via injection of pentobarbitone and the spinal cord was frozen in OCT over isopentane and dry ice. For FUS immunofluorescence studies in chapter 3 and 5, animals were transcardially perfused with 4% paraformaldehyde in PBS. Tissues were then dissected, post fixed overnight in 4% paraformaldehyde at 4°C and stored in PBS or 30% sucrose with 0.1% sodium azide before being frozen in OCT over isopentane and dry ice.

TA muscles were weighed after defrosting, prior to extraction of RNA or protein for downstream analysis.

7.5 Molecular biology

7.5.1 RNA extraction

Total RNA was extracted from several tissue types including spinal cord, brain, tibialis anterior muscle, extensor digitorum muscle and soleus muscle for *FUS* expression.

Tissue was submerged in 1ml Qiazol lysis reagent in Matrix D lysing tubes and homogenised for 2x30 seconds at 5500RPM using a Bertin Precellys 24 lysis homogeniser. For spinal cord and brain, the Rneasy Lipid Tissue Mini Kit was used, and all kit instructions followed. For muscle tissue the Rneasy Fibrous Tissue Mini Kit was used, and all kit instructions followed.

RNA was quality checked using a nanodrop spectrophotometer and Bioanalyzer before being stored at -80°C until further processing.

7.5.2 RT-PCR and quantitative RT-PCR

cDNA was prepared from total RNA and stored at -20°C until further processing.

RT-PCR was used to confirm the presence of the mouse *Fus* or human *FUS* sequence (Table 7.5). PCR reaction products were run on 1.5% agarose gels to assess for the presence/absence of mouse or human gene products.

For quantitative RT-PCR for *FUS* expression and *FUS* splicing analysis, qRT-PCR was performed using Fast SYBR Green Master Mix and 200nM or 250nM of each forward and reverse primer (Table 7.5). Thermal amplification conditions were 95°C for 20 secs, then 40 cycles of 95°C for 3 secs and 60°C for 30 secs. The specificity of

primer binding and amplification was confirmed by melt curve analysis. To control for non-specific amplification, no-template reactions were performed using all reagents except the sample. qRT-PCR reactions were carried out on 7500 Real-Time PCR machines. qRT-PCR data was analysed using the manufacturer's analysis software following the 2-ΔCt method.

Table 7.5: Primers used for RT-PCR experiments.

Target	Primer	Sequence	Experiment used in
Human *FUS*	Forward	CGGTCGTCTGGAACTTTGTT	Figure 2.3
	Reverse	CCATAACCGCCACCACTG	
Mouse *Fus*	Forward	CGGTCGTCTGGAACTTTGTT	Figure 2.3
	Reverse	CATAACCACCACCGCCAC	
Pan human-mouse *FUS*	Forward	CACAGGCTATGGAACTCAGTCA	Figure 2.3
	Reverse	GCCATAGCCAGGGTAGGAG	
Pan human-mouse *FUS*	hFUS_cons_2_F	CACAGGCTATGGAACTCAGTCA	Figure 2.3
	hFUS_cons_2_R	GCCATAGCCAGGGTAGGAG	
Human *FUS*	hFUS_P525L_1_F	ACCCAACAAGCAACCCAAAG	Figure 3.17
	hFUS_P525L_1_R	GGGGAGTTGACTGAGTTCCA	Figure 5.9
Pan human-mouse *FUS* (correctly spliced)	FUSex7-F	GGTGGCTTCAATAAATTTGGTGG	Figure 2.4
	FUSex10-R	AGTTTCCCTGTCTGTGTACAAA	Figure 8.3
Pan human-mouse *FUS* (intron 6 retained)	FUSin6-qF	TGTGTGCGTGTGTTTAATGC	Figure 2.4
	FUSin6-qR	GTCACCTTTCATACCTGTGGC	Figure 8.3
Pan human-mouse *FUS* (intron 7 retained)	FUSex7-F	GGTGGCTTCAATAAATTTGGTGG	Figure 2.4
	FUSin7-qR	ACACGCTAAGACATCTGCAA	Figure 8.3
Mouse *S16*	S16_F	TTCTGGGCAAGGAGCGATT	Figure 2.3
	S16_R	GATGGACTGTCGGATGGCA	Figure 2.4 Figure 3.17 Figure 5.9

			Figure 8.3
Mouse *Hprt1*	Hprt1_F	CATTATGCCGAGGATTTGG	Figure 2.3
	Hprt1_R	CACACAGAGGGCCACAATGT	Figure 2.4 Figure 3.17 Figure 5.9 Figure 8.3

7.5.3 RNA sequencing

Two separate RNA sequencing experiments were conducted:

1. *mFus/mFus, mFus/hFUS, hFUS/hFUS, hFUS/hFUS*^{P525L} and *Fus*$^{+/-}$ transcript expression
2. *mFus/mFus, mFus/hFUS*^{P525L} and *mFus/hFUS*^{Q519Ifs} transcript expression

For experiment 1, spinal cord and tibialis anterior muscle tissue was collected from 14-week-old *Fus*$^{+/-}$ male mice and 4-month-old male mice (all other genotypes). For experiment 2, spinal cord and tibialis anterior muscle tissue was collected from 4-month-old male mice. N of four-five was used for each genotype.

For experiment 1, tissue was stored in RNA later before being sent to Lexogen for total RNA extraction using SPLIT. For experiment 2, RNA extraction was carried out using procedures detailed in section 7.5.1 and RNA was sent to Lexogen for RNA sequencing.

For both experiments, CORALL libraries were prepared for Illumina sequencing. Total number of reads was up to 400 million per run, equating to around 25 million reads per sample. CORALL reads were then put through a workflow including sequencing QC, trimming, alignment to B6 reference using STAR and differential

expression using Deseq2. For analysis of results, FDR<0.1 was used unless otherwise stated.

7.5.4 SNP Sequencing Analysis

Transnetyx services performed MiniMUGA SNP analysis; an array-based platform with over 10,000 SNP markers that can be used to determine genetic background in 241 inbred strains of mice.

7.5.5 Protein extraction

Tissue was snap frozen in liquid nitrogen immediately after dissection and stored at -80°C until processed. Tissue was submerged in 500µl RIPA + protease inhibitors in Matrix D lysing tubes and homogenised for 2x30 seconds at 5500RPM using a Bertin Precellys 24 lysis homogeniser. Homogenate was centrifuged at 13,000xg for 10 minutes at 4°C. Supernatant (total protein) was aliquoted and stored at -80°C. Protein concentration was assessed using a DC or BSA assay.

7.5.6 Western blotting

Protein extracts were run on 4-12% Bis-Tris protein gels with 1X MOPS + 500µl antioxidant at 200v for 42 minutes. Protein was transferred to a nitrocellulose membrane. If total protein quantification was used to normalise data, total protein was stained prior to blocking following manufacturer's instructions. Membranes were blocked in 4% skimmed milk in PBST (0.1% Tween-20) for 90 minutes, the membrane was incubated with primary antibodies diluted in 4% milk/PBST either overnight at 4°C or for 90 minutes at room temperature. Membranes were washed 3x5 minutes in PBST then incubated with secondary antibodies diluted in 4% milk/PBST for 90 minutes at room temperature. Membranes were washed 2x5 minutes in PBST and 1x5 minutes in

PBS before being dried (10 minutes) and imaged on a Licor Odyssey Scanner. Blots were quantified using Empiria Studio.

Table 7.6: Antibodies used for western blotting.

Antibody	Concentration	Manufacturer	Cat/part no.
Primary Antibodies			
FUS 562	1:10,000	Novus	NB100-562
FUS 565	1:10,000	Novus	NB100-565
GAPDH Monoclonal Antibody (6C5)	1:2000	ThermoFisher Scientific	AM4300
Secondary antibodies			
IRDye 680RD Donkey anti-Mouse IgG (H+L)	1:15,000	LI-COR	926-68072
IRDye 800CW Goat anti-Rabbit IgG (H+L)	1:15,000	LI-COR	926-32211

7.5.7 DNA Extraction for mitochondrial copy count

Total DNA (genomic and mitochondrial) was isolated from tibialis anterior (TA) muscles. TA muscles were lysed overnight at 50°C with gentle shaking in 750µl tissue lysis buffer (Table 7.7) containing proteinase K (20ug/ml). The lysed samples were vortexed for 20 seconds. 1X volume of phenol:chloroform:isoamyl alcohol (25:24:1, pH 7.8-8.0) was added to the lysed sample which was then vortexed for 20 seconds. A pea sized blob of vacuum grease was added then tubes were centrifuged for 10 minutes at 13,000xg at room temperature. The upper aqueous phase was pipetted into a fresh micro-centrifuge tube. 2X volumes of chloroform was added to the aqueous phase, which was then vortexed for 20 seconds. A pea-sized blob of vacuum grease was added to the tube and then centrifuged for 10 minutes at 13,000xg at room temperature. The upper aqueous phase was collected into a fresh tube and 2.5X

volumes of 100% ice-cold ethanol added, along with 1:10 of sodium acetate (pH 5.2). The tube was vortexed for 20 seconds and kept at -20°C overnight. The next day, the precipitated DNA was centrifuged at 17,000xg for 15 minutes at 4°C. The supernatant was discarded. The DNA pellet was washed in ice-cold 70% ethanol and centrifuged at 17,000xg for 15 minutes at 4°C. The supernatant was discarded, and the pellet left to air-dry for 10 minutes at room temperature. 50µl of TE buffer was added to the DNA pellet which was left gently shaking at 4°C until the pellet dissolved. DNA concentration and quality was checked using a nanodrop.

Table 7.7: Tissue lysis buffer.

Reagent	Added
10 mM Tris-HCl pH 8	1 ml of 1M stock solution
25 mM EDTA	5 ml of 0.5M EDTA stock solution
100 mM NaCl	2 ml of 5M NaCl stock solution
0.5% (w/v) SDS	5 ml of 10% SDS stock solution
MilliQ water	87 ml
Total	100ml

7.5.8 Mitochondrial DNA copy count qRT-PCR assay

The ratio of mitochondrial DNA to genomic DNA was assayed as follows. Primers were designed to amplify a genomic gene (GAPDH) and a mitochondrial gene (mtND1) which is rarely deleted (He, 2002).

Total DNA was extracted from TA muscles using the protocol in section 7.5.7. Primer validation and melt curve analysis was carried out to ensure primers were specific and concentrations were appropriate. PCR products were then run on a 1% agarose gel to ensure that the size of the amplicon was as predicted.

qRT-PCR was performed using Fast SYBR Green master mix and 300nM of mtND1 and 50nM of GAPDH forward and reverse primer (Table 7.8). Thermal amplification conditions were 95°C for 20 secs, then 40 cycles of 95°C for 3 secs and 60°C for 30 secs. To control for non-specific amplification, no-template reactions were performed using all reagents except the sample. qRT-PCR reactions were carried out on 7500 Real-Time PCR machines. qRT-PCR data was analysed using the manufacturer's analysis software following the 2-ΔCt method.

Table 7.8: Primers used in mitochondrial copy count assay.

Target	Primer	Sequence
mtND1	mtND1_M_Fwd	CCCATTCGCGTTATTCTT
	mtND1_M_Rev	AAGTTGATCGTAACGGAAGC
GAPDH	GAPDH_M_Fwd	CAAGGAGTAAGAAACCCTGGACC
	GAPDH_M_Rev	CGAGTTGGGATAGGGCCTCT

7.5.9 Simoa assay for neurofilament light (NFL) quantification

Plasma was collected as per section 7.4.1.11.

NFL was measured using the NF-light Advantage Assay Kit for the Simoa immunoassay following all manufacturer's instructions. Each well was read in duplicate with a dilution of 1:40. The CV values (difference between duplicate readings) were very low indicating high repeatability of the test.

7.6 Histology, immunofluorescence, and immunohistochemistry

7.6.1 FUS immunofluorescence

Serial transverse sections (12μm) were cut from the OCT embedded spinal cords.

7.6.1.1 FUS staining in non-perfused spinal cord sections (chapter 2)

All steps were completed in a slide humidifier. Sections were post-fixed in 4% paraformaldehyde for 10 minutes. Slides were washed 3x10 minutes in PBS then blocked for 60 minutes in M.O.M blocking agent (45ul per 1.25ml). Slides were washed 3x10 minutes in PBS then incubated with an antibody against FUS (Santa Cruz, 1:400) in antibody buffer (3% NGS + 0.5% TX-100, 1:10) for 60 minutes at room temperature or overnight at 4°C. Slides were washed 3x10 minutes in PBS then incubated with anti-mouse IgG (1:1500) in antibody buffer for 60 minutes. Auto-fluorescent background was reduced by submerging slides in Sudan black B (0.1% in 80% ethanol/PBS) for 10 minutes. Slides were then washed 3x10 minutes in PBS and mounted.

7.6.1.2 FUS staining in perfused animals (chapter 3, 5)

All steps were completed in a slide humidifier. Slides were left at room temperature for 60 minutes. Sections were permeabilised in 0.3% (w/v) Triton X-100 in PBS (PBST) for 10-15 minutes then incubated with primary antibodies in 0.3% PBST + 1% BSA overnight at 4°C. Slides were washed 3x10 minutes in PBS then incubated with appropriate secondary antibodies in 0.3% PBST + 1% BSA for 120 minutes at room temperature. Auto-fluorescent background was reduced by submerging slides in Sudan black B (0.1% in 80% ethanol/PBS) for 10 minutes. Slides were then washed 3x10 minutes in PBS and mounted.

Table 7.9: IHC antibodies.

Antibody	Concentration	Manufacturer	Cat/part no.
Primary Antibodies			
FUS/TLS Antibody (H-6) mouse monoclonal	1:400	Santa Cruz Biotechnology	SC-373698
FUS 562	1:400	Novus	NB100-562
FUS 565	1:400	Novus	NB100-565
FUS^{P525L}	1:500	Generated by Marc-David Ruepp and Anny Devoy at King's College London	N/A
ChAT	1:250	Millipore (UK) Limited	AB144P
NeuN	1:200	Merck	MAB377
Secondary antibodies			
Alexa Fluor 488 goat anti mouse IgG (H+L)	1:1500	Invitrogen	A32723
Alexa Fluor 488 goat anti rabbit IgG (H+L)	1:1500	Invitrogen	A32731
Alexa Fluor 594 goat anti mouse IgG (H+L)	1:1500	Invitrogen	A11032
Alexa Fluor 594 goat anti rabbit IgG (H+L)	1:1500	Invitrogen	A11037
Alexa Fluor 488 donkey anti rabbit IgG (H+L)	1:500	Jackson	711-545-152
Alexa Fluor 594 donkey anti mouse IgG (H+L)	1:500	Jackson	715-585-150

7.6.2 Motor neuron counting

Spinal cord motor neurons in the unfixed ventral spinal cord were counted using published techniques (Austin et al., 2022).

Briefly, 20μm sections of mouse spinal cord from regions L3-L6 were cut, with every third section mounted on a slide (to ensure when counting the same motor neuron is not counted twice). Sections were stored at -80°C until processing. Sections were acclimatised at room temperature for one hour before staining for 30 minutes in gallocyanine solution (0.3g gallocyanine, 10g chrome alum, distilled water up to 100

ml) at room temperature. Sections were then rinsed and dehydrated in increasing concentrations of ethanol (70% EtOH, 90% EtOH, 100%EtOH, treat for 2 minutes with each solution). Sections were cleared in three changes of xylene and mounted in D.P.X.

Slides were imaged and ventral motor neurons counted. Only motor neurons of the sciatic motor pool were counted with the following criteria:

1. Large size and dark staining.
2. The cytoplasm stains more darkly than the nucleus, within the nucleus the dark nucleolus is visible.
3. Usually, three or more dendrites extend from the motor neuron.

7.6.3 Aggregation staining in spinal cord sections

Unfixed spinal cord sections on slides were left at room temperature for 60 minutes then dehydrated in Xylene (10 minutes, then 5 minutes then 1 minute) and 3 changes of 100% ethanol for 1 minute then 70% ethanol for 1 minute. Slides were stained in haematoxylin and eosin for 5 minutes then differentiated in 1% acid alcohol, dehydrated, cleared, and mounted.

7.6.4 Iba1 staining in spinal cord sections

All steps were completed in a slide humidifier. Perfused spinal cord sections on slides were left at room temperature for 60 minutes. Sections were permeabilised in 0.3% (w/v) Triton X-100 in PBS (PBST) for 10-15 minutes then incubated with primary antibodies in 0.3% PBST + 1% BSA overnight at 4°C. Slides were washed 3x10 minutes in PBS then incubated with appropriate secondary antibodies in 0.3% PBST + 1% BSA for 120 minutes at room temperature. Slides were then washed 3x10 minutes in PBS and mounted.

Iba1 staining was quantified using ImageJ. Spinal cord sections were imaged, and a standard sized region of interest (ROI) selected in the ventral horn of the spinal cord. The green channel (representing Iba1 staining) was segmented and the % area of the total ROI area covered by Iba1 staining was quantified.

Table 7.10: Antibodies used for Iba1 staining.

Antibody	Concentration	Manufacturer	Cat/part no.
Primary Antibodies			
Iba1	1:1000	Fujifilm	019-19741
Secondary antibodies			
Alexa Fluor 488 donkey anti rabbit IgG (H+L)	1:1000	Jackson	711-545-152

7.6.5 Muscle fibre typing

Unfixed TA muscles were sectioned at 12μm thickness in a series of 4 with 8 sections per slide. Slides were defrosted for 10 minutes at room temperature before staining.

For differential ATPase staining, muscle sections were preincubated in either (Table 7.12):

1. 20 mM sodium barbital, 36 mM $CaCl_2$, pH 10.3 for 15 min
2. 50 mM sodium acetate, 30 mM sodium barbital pH 4.2 for 5 min

Slides were rinsed in distilled water then incubated for 25 minutes in ATP incubating solution. Slides were then washed 3x3 minutes in 1% $CaCl_2$ before incubating for 10 minutes in 2% $CoCl_2$. Slides were washed 5 times in 5 mM sodium barbital. Now in a fume hood, a 1 % v/v solution of ammonium sulfide (0.1 ml stock NH_4SO_2 + 9.9 ml H_2O or 4.5ml in 200ml from 40-48% stock) was prepared. Slides were

stained with 1% $(NH_4)_2S$ for 30 seconds then washed with 5-6 times in tap water. Finally, slides were mounted using Aquamount.

For quantification, three transverse whole muscle sections at 400µm intervals were analysed from three to five animals of each genotype, with adjacent sections used for comparative pH 4.2 and pH 10.3 staining. A 500µm x 500µm area of muscle tissue was selected and fibre type was assessed manually based on fibre colour.

Table 7.11: Muscle fibre typing solution reagents.

Reagent solutions	Added
0.1 M Sodium Barbital Solution	5.15 mg barbital powder + 250ml deionised H_2O
0.18 M Calcium Chloride	2.65 g $CaCl_2 \cdot 2H_2O$ + 100ml deionised H_2O
1% w/v Calcium Chloride	10 g $CaCl_2 \cdot 2H_2O$ + 1000ml deionised H_2O
2% w/v Cobalt Chloride	8 g $CoCl_2 \cdot 6H_2O$ + 400ml deionised H_2O
Barbital Acetate Solution	1.47g Sodium barbital + 0.97g Sodium acetate + final vol of 50ml deionised H_2O
5mM sodium barbital	25 ml 0. 1 M Sodium Barbital + 500ml deionised water
1M Sodium Hydroxide	Used 1M stock
0.1M Sodium Hydroxide	1ml 1N NaOH + 9ml deionised water
1M Hydrochloric Acid	Used 1M stock
0.1M Hydrochloric Acid	10ml 1N HCl to 90ml deionised H_2O

Table 7.12: Muscle fibre typing solutions.

Incubating solutions	Added (ml)
10.85 pH ATP: TYPE 2 FIBRES DARK, TYPE 1 FIBRES LIGHT, TYPE 2C FIBRES INTERMEDIATE	
0.1 M Sodium Barbital	4
0.18 M Calcium Chloride	4
Deionised H_2O	12
4.48 pH ATP: TYPE 1 FIBRES DARKEST, TYPE 2C FIBRES INTERMEDIATE, TYPE 2A&B LIGHTEST	
Barbital Acetate Solution	5
0.1 N HCl	10

Deionised H_2O	4
ATP Incubating Solution (**pH 9.45-9.5**)	
ATP powder (disodium salt)	60mg
0.1 M Sodium Barbital	6
Deionised H_2O	21
0.18 M Calcium Chloride	3

7.6.6 Muscle fibre size and central nucleation analysis

TA muscles were embedded in OCT and flash frozen over isopentane pre-cooled in liquid nitrogen. 8µm muscle sections were cut, stained with haematoxylin and eosin, and imaged using a Nanozoomer slide scanner. For each animal, 3 lots of 500µm x 500µm areas of muscle tissue were selected for determination of muscle fibre size. Muscle fibre segmentation was performed manually in ImageJ (National Institutes of Health). The minimum 273erret diameter for each fibre was calculated in ImageJ. Central nucleation was manually assessed in 500 cells per muscle and expressed as a percentage.

7.6.7 Imaging

All fluorescence images were obtained using an inverted confocal microscope (Zeiss).

Muscle fibre type and H&E staining assays were imaged on a Nanozoomer slide scanner.

7.7 Mammalian cell culture and experimental procedures

7.7.1 Embryo dissection

Primary motor neurons were cultured from E12.5-E13.5-day-old embryos of *hFUS/hFUS* homozygous mice crossed with *hFUS/hFUS*^{P525L} mice. Pregnant females were culled using cervical dislocation and embryos dissected out and placed into HBSS on ice. Under a dissecting microscope, embryos were removed from the amniotic sac and placed ventral side down. This protocol was adapted from a collaborator at UCL (Fellows et al., 2020). The head and tail were removed and the skin overlaying the developing spinal cord peeled away. Once exposed, the spinal cord was removed from the embryo using curved forceps to cut away connecting tissue and hook underneath the cord. Next, the meninges and DRGs were peeled away from the cord, which was then flipped onto the ventral side and cut anterior to posterior leaving the ventral section, where motor neurons develop. The ventral spinal cord was cut into several pieces which were placed into a falcon with 1ml HBSS. Tails were collected for genotyping.

7.7.2 Primary cell culture disaggregation and seeding

Coverslips were coated in 1.5mg/ml poly-ornithin 1:100 in sterile milliQ H_2O at 37°C for 2 hours. The poly-ornithin was then aspirated and replaced with 1mg/ml laminin 1:333 in Neurobasal media and incubated overnight at 37°C. The laminin was aspirated, and coverslips rinsed once in Neurobasal prior to plating the cells.

10µl of 2.5% trypsin was added to 1ml HBSS containing the spinal cord sections, the tube was shaken and then placed into a 37°C water bath for 5 minutes, shaken, then returned to the water bath for a further 5 minutes. Tissue was dissociated in a

P1000 pipette and added to tube 1, which contained 800µl Leibovitz L15, 100µl 4% BSA in L15, 100µl 1mg/ml DNAse in L15, for 60 seconds and triturated. The supernatant was then added to tube 2 which contained 880µl Leibovitz L15, 100µl 4% BSA in L15, 20µl 1mg/ml DNAse in L15. 1ml of 4% BSA was then added to tube 2 below the supernatant, forming 2 layers. Tube 2 was centrifuged at 400xg for 5 minutes at room temperature. The supernatant was discarded and the cell pellet re-suspended in motor neuron media (MNM), the volume of which depended on the downstream application.

Cells were grown for 5 days at 37°C before downstream experiments.

Table 7.13: Motor neuron media components.

Motor neuron media (MNM)	**Final concentration**	**50ml media volume (µl)**
Neurobasal	N/A	46918.2
Heat inactivated horse serum	2%	1000
Glutamax (100X)	1X	500
β-mercaptoethanol (50mM)	24.8µM	24.8
Pen/Strep (100X)	1X	500
Add after filtering		
B27 supplement	1X	1000
CNTF	10ng/ml	5
BDNF	1ng/ml	2
GDNF	0.1ng/ml	50

7.7.3 Cell-type staining

Each well was washed 5 times in 0.5ml PBS then cells were fixed by adding 0.25ml 4% paraformaldehyde in PBS and incubating for 20 minutes at room temperature. Each well was washed 3x5 minutes in 0.5ml PBS with gentle agitation.

Cells were then permeabilised with 150µl of 0.2% Triton-X in PBS for 10 minutes at room temperature. Cells were then washed in 0.25ml in PBS. 0.5ml of blocking buffer (5% goat serum in PBS) was added to each well and cells were incubated for 60 minutes at room temperature. 250µl of primary antibody diluted in antibody buffer (1% goat serum in PBS) was added to each well and cells were incubated overnight at 4°C on a rocker.

The next day, cells were washed 3x10 minutes in 0.5ml PBS with agitation. 250µl of secondary antibody diluted in antibody buffer (1% goat serum in PBS) was applied to each well for 60 minutes at room temperature on a rocker.

After washing 3x10 minutes in PBS the coverslip was removed and mounted on a glass slide with mounting media.

Table 7.14: Cell-type staining antibodies.

Antibody	Concentration	Manufacturer	Cat/part no.
Primary antibodies			
GFAP	1:5000	abcam	AB7260
MAP2	1:1000	Merck	AB5622
Iba1	1:1000	Fujifilm	019-19741
Anti-Tau-1	1:1000	Merck	MAB3420
Islet1	2µg/µl	DSHB	40.2D6-A
Tubulin BETA III	1:1000	Merck	AB9354
ChAT	1:400	Merck	AB144P
NeuN	1:500	Merck	MAB377
Secondary antibodies			
Alexa Fluor 647 goat anti-mouse	1:1000	ThermoFisher	A21236
Alex Fluor 488 goat anti-chicken	1:1000	ThermoFisher	A11039
Alexa Fluor 488 goat anti-rabbit	1:1000	ThermoFisher	A11034

7.7.4 Staining for Stress Granule Markers

Cells were grown for 5 days in MNM. On day 5, 0.5mM sodium arsenite in MNM was applied for 60 minutes at 37°C to induce oxidative stress. Control cells had fresh MNM applied. After 60 minutes, cells were either fixed immediately in 4% paraformaldehyde or the sodium arsenite was removed, cells were washed once in MNM and then left in fresh MNM for 24 hours to allow cells to recover.

To stain the cells, they wells were washed 3x in PBS and fixed using 0.25ml of 4% paraformaldehyde for 20 minutes at room temperature. Wells were then washed 3x5 minutes in PBS with gentle agitation. PBS was aspirated and 150µL of 0.3% triton-X-PBS was added for 10 minutes at room temperature. Cells were washed once with PBS and then 0.5ml of blocking buffer (5% goat serum, 0.05% tritox-X-100) was added to each well and cells were incubated for 60 minutes at room temperature. Blocking buffer was removed and replaced with 250µL of primary antibodies in antibody buffer (1% goat serum) either for 60 minutes at room temperature or overnight at 4°C. After incubation with primary antibodies, cells were washed 3x10 minutes with PBS. 250µL of secondary antibodies in antibody buffer (1% goat serum) were added to the wells and incubated at room temperature for 60 minutes. Finally, cells were washed 3x10 minutes in PBS before mounting.

Table 7.15: Stress granule staining antibodies.

Antibody	Concentration	Manufacturer	Cat/part no.
Primary antibodies			
FUS 565	1:500	Novus	NB100-565
FUS^{P525L}	1:1000	Generated by Marc-David Ruepp and Anny Devoy at King's College London	N/A
Recombinant Anti-G3BP antibody	1:1000	abcam	ab181150
Secondary antibodies			
Alexa Fluor 647 goat anti-mouse	1:1000	ThermoFisher	A21236
Alexa Fluor 488 goat anti-rabbit	1:1000	ThermoFisher	A11034

7.7.5 Quantifying FUS localisation in primary cells

FUS localisation in primary cells was assessed semi-automatically using ImageJ.

Briefly, blue (DAPI) and red (G3BP1) channels were merged to generate whole cell images. Thresholding was carried out, any holes filled and watershed applied to separate cells and ROIs defined as each individual cell. Any cells which were not defined correctly were manually removed. The same was done for the blue (DAPI) channel alone to generate the nuclei ROIs. FUS staining was then quantified within the nuclei and whole cell ROIs to generate the percent of FUS staining which was nuclear.

7.7.6 Assessing mitochondrial function (Seahorse)

Cells were grown for 5 days at a density of 150,000 cells per well in MNM before performing the seahorse assay. The Agilent Seahorse XF Mito Stress Test Kit was used to assess mitochondrial function within the cell population according to manufacturer's instructions.

7.7.7 Assessing mitochondrial membrane potential (TMRE Assay)

Cells were plated at $1x10^5$ cells per well in a white-sided clear-bottomed 96 well plate and grown for 5 days in 200µl MNM.

A 20x solution of 400µM FCCP was made up in MNM then 10µl was added to the FCCP control wells and incubated for 10 minutes at 37°C. Meanwhile a 10x solution of 5µM TMRE in MNM base was made up. 20µl of the 5µM TMRE solution was added to all wells, including the FFCP controls, leading to a final concentration of 500nM. 20µl of MNM was added to non-TMRE control wells. Plates were incubated for 20 minutes at 37°C then media was gently aspirated and replaced with 100µl of PBS to wash cells. Plates were read on a fluorescence plate reader at excitation 549nm and emission 575nm.

7.7.8 Survival assay

Cells were plated at 50,000 cells per well and grown in white walled and bottomed 96 well plates.

After 5 days, MNM was removed and replaced with 50µl of either sodium arsenite or sucrose diluted in MNM. 50µl fresh MNM was added to control wells. Cells were then incubated for 60 minutes at 37°C. After the 60 minutes, MNM was removed from all wells and replaced with 50µl fresh MNM + 20µl CellTox-Green reagent. Plates were returned to the incubator and toxicity readings taken at 1, 4 and 24 hours post stress. After 23.5 hours, 4µl lysis buffer was added to positive control wells. Plates were read on a fluorescence plate reader at excitation 492nm and emission 520nm. After reading, media was removed and replaced with 100µl fresh MNM + 20µl

CellTiter-Blue reagent and incubated for 60 minutes at 37°C. Plates were read on a fluorescence plate reader at excitation 545±10nm and emission 595nm.

7.8 Statistical Analysis

Statistical analysis was conducted using GraphPad Prism. All data are displayed as mean average, with errors bars indicating standard error of the mean, unless otherwise specified. Data was analysed using an unpaired student T test (difference between two groups which are normally distributed and have equal variance), Mann Whitney test (difference between two groups which are not normally distributed and/or have unequal variance) or ANOVA/mixed effect analysis for multiple comparisons, followed by the appropriate post-hoc test. Tukey's post-hoc test was used to assess multiple pairwise comparisons. Sidak's post-hoc analysis was used to compare two variables.

8 Chapter 8: Supplementary Data

8.1 Chapter 2: Characterising *hFUS/hFUS* mice

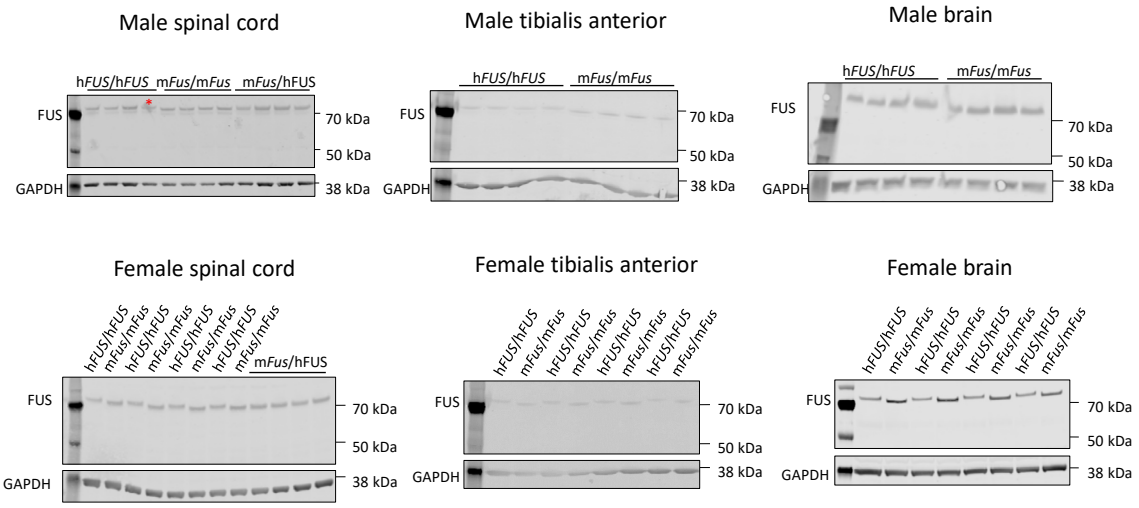


Figure 8.1: Images of immunoblots used for FUS expression quantification in 18-month-old mice in Figure 2.5. *Red asterisk indicates data point excluded due to anomaly on gel.*

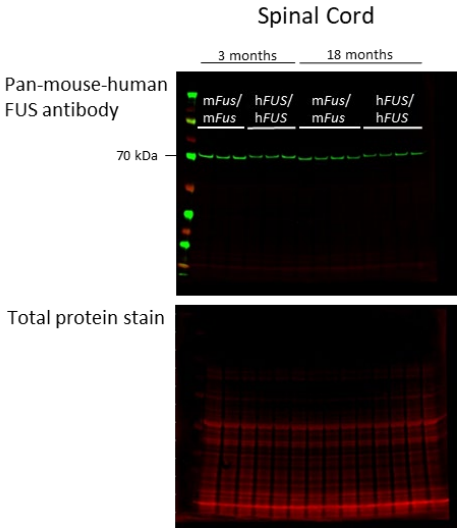


Figure 8.2: Images of immunoblots used for longitudinal FUS expression quantification in 3 and 18-month-old male mice in Figure 2.5.

Table 8.1: Transcripts differentially expressed in hFUS/hFUS mice compared to mFus/mFus mice.

Transcripts differentially expressed in *hFUS/hFUS* versus *mFus/mFus* mice (adjp<0.1)					
Transcript ID	Transcript name	Transcript type	Log_2FC	p value	adjp value
Spinal Cord					
FUS transcripts					
ENST00000474990	FUS-203	processed_transcript	4.97	1.78E-130	6.71E-126
ENST00000487509	FUS-206	retained_intron	4.24	1.84E-102	3.48E-98
ENST00000380244	FUS-202	protein_coding	4.54	1.38E-94	2.09E-90
ENST00000569760	FUS-212	retained_intron	4.36	1.18E-88	1.49E-84
ENST00000254108	FUS-201	protein_coding	4.23	5.28E-80	4.98E-76
ENST00000568685	FUS-210	protein_coding	4.02	3.80E-70	2.87E-66
ENST00000566605	FUS-209	nonsense_mediated_decay	2.50	5.41E-26	3.14E-22
ENST00000568901	FUS-211	retained_intron	2.37	2.24E-23	1.12E-19
ENST00000483853	FUS-204	retained_intron	1.96	3.83E-17	1.61E-13
ENST00000487045	FUS-205	retained_intron	1.71	3.32E-13	1.32E-09
ENST00000564766	FUS-208	retained_intron	1.06	7.36E-07	0.00185
Fus transcripts					
ENSMUST00000150411	Gm10167-201	processed_pseudogene (*Fus*)	–4.39	1.12E-132	8.48E-128
ENSMUST00000077609	Fus-201	protein_coding	–4.62	2.87E-119	7.22E-115
ENSMUST00000121616	Fus-204	protein_coding	–4.06	1.22E-80	1.32E-76
ENSMUST00000155941	Fus-211	retained_intron	–3.82	2.37E-79	1.99E-75
ENSMUST00000136289	Fus-207	retained_intron	–2.75	1.09E-30	6.88E-27
ENSMUST00000128851	Fus-206	retained_intron	–2.41	4.70E-24	2.53E-20
ENSMUST00000137464	Fus-208	processed_transcript	1.28	2.57E-20	1.21E-16
ENSMUST00000106251	Fus-203	protein_coding	–1.17	3.65E-18	1.62E-14
ENSMUST00000206627	Gm8309-201	processed_pseudogene (*Fus*)	–1.68	2.23E-12	8.41E-09
ENSMUST00000174196	Fus-213	retained_intron	–1.53	8.04E-11	2.76E-07

ENSMUST00000205351	Fus-216	retained_intron	–1.40	1.45E-09	4.37E-06
ENSMUST00000205261	Fus-215	retained_intron	–1.31	1.85E-08	5.38E-05
Non-*Fus* transcripts					
ENSMUST00000032944b	Gdpd3-201	protein_coding	2.97	2.20E-39	1.51E-35
ENSMUST00000205468	Gdpd3-202	retained_intron	1.63	3.03E-12	1.09E-08
ENSMUST00000206350	Gdpd3-204	retained_intron	1.50	1.02E-10	3.35E-07
ENSMUST00000117914	Rps15a-ps8-201	processed_pseudogene	1.48	6.51E-10	2.05E-06
ENSMUST00000119415	Rps15a-ps4-201	transcribed_processed_pseudogene	–0.95	4.48E-08	0.00013
ENSMUST00000161160	Hk1-220	retained_intron	–1.24	2.69E-07	0.00073
ENSMUST00000172457	Rps15a-207	protein_coding	–1.11	6.54E-07	0.00170
ENSMUST00000084586	Slx1b-201	retained_intron	0.96	1.03E-06	0.00250
ENSMUST00000207147	B230311B06Rik-201	lincRNA	–1.10	3.96E-06	0.00906
ENSMUST00000160101	Opa1-203	retained_intron	1.06	3.86E-06	0.00906
ENSMUST00000092723	Arid1b-201	protein_coding	0.60	6.45E-06	0.01432
ENSMUST00000042942	Sec23ip	protein_coding	0.52	6.98E-06	0.01504
ENSMUST00000167926	Acot7-206	protein_coding	–0.68	7.39E-06	0.01549
ENSMUST00000146138	Nup214-209	retained_intron	1.03	1.13E-05	0.02307
ENSMUST00000144507	Atp2b2-205	processed_transcript	–0.99	1.88E-05	0.03729
ENSMUST00000232272	Fyttd1-213	protein_coding	–0.81	2.30E-05	0.04450
ENSMUST00000206712	Rps13-206	retained_intron	–0.95	2.73E-05	0.05143
ENSMUST00000140932	Mgst1-207	protein_coding	–0.66	3.64E-05	0.06696
ENSMUST00000206351	Pak1-204	protein_coding	0.84	4.14E-05	0.07431
ENSMUST00000060315	Trim34a-201	protein_coding	–0.94	5.31E-05	0.09109
ENSMUST00000128482	Rps15a-203	protein_coding	0.87	5.23E-05	0.09109
ENSMUST00000106588	Rps15a-201	protein_coding	–0.72	5.85E-05	0.09816
ENSMUST00000106226	Tial1-202	protein_coding	–0.50	6.01E-05	0.09863

8.2 Chapter 3: Characterising *hFUS/hFUS^{P525L}* mice

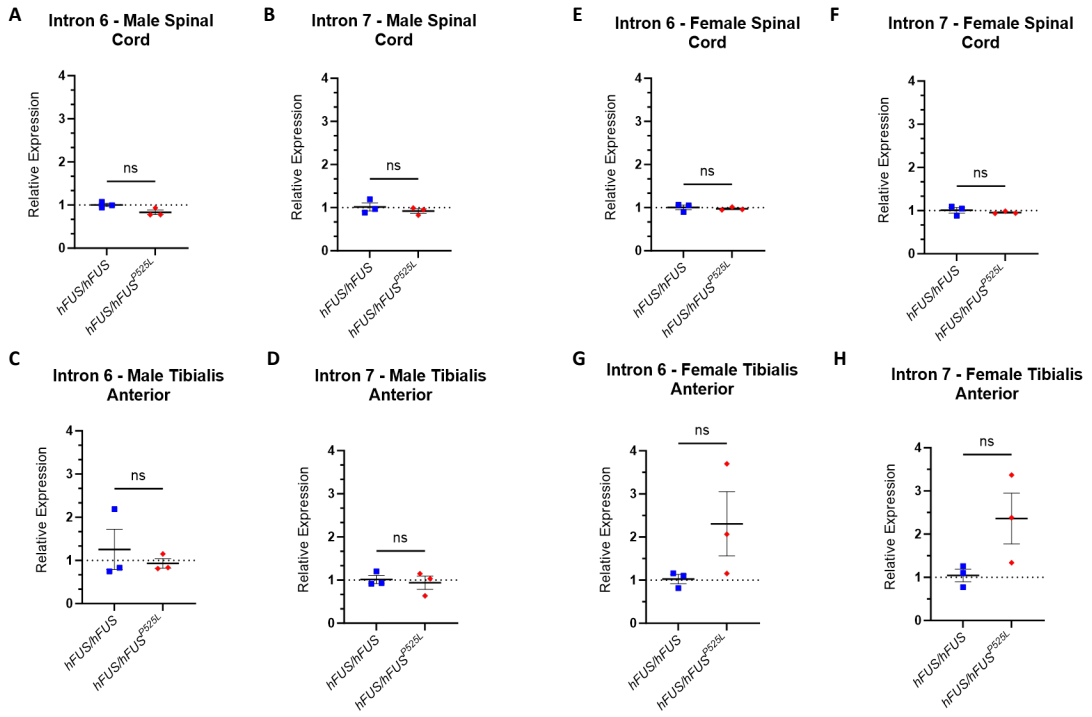


Figure 8.3: FUS intron 6 and 7 retention as a method of FUS autoregulation cannot explain FUS expression differences. *FUS transcripts with intron 6 and 7 retained were quantified as a percentage of correctly spliced FUS. Total RNA was extracted from 4-month-old male and female mice. Relative expression of FUS transcripts from male spinal cord with **A)** intron 6 retained and **B)** intron 7 retained. Relative expression of FUS transcripts from male tibialis anterior with **C)** intron 6 retained and **D)** intron 7 retained. Relative expression of FUS transcripts from female spinal cord with **E)** intron 6 retained and **F)** intron 7 retained. Relative expression of FUS transcripts from female tibialis anterior with **G)** intron 6 retained and **H)** intron 7 retained. Data are shown as mean average ± SEM with significance calculated using an Unpaired T Test. ns=not significant.*

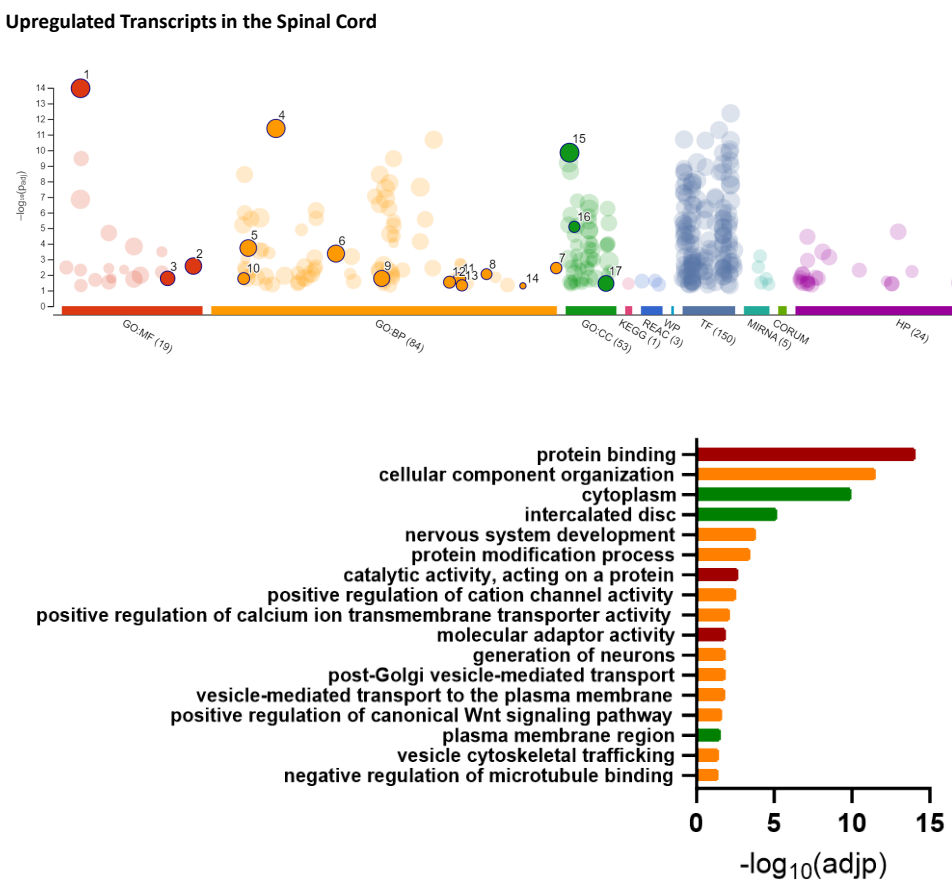


Figure 8.4: GO term analysis of transcripts which were upregulated in the spinal cord of hFUS/hFUS^{P525L} mice compared to hFUS/hFUS controls.

Downregulated Transcripts Spinal Cord

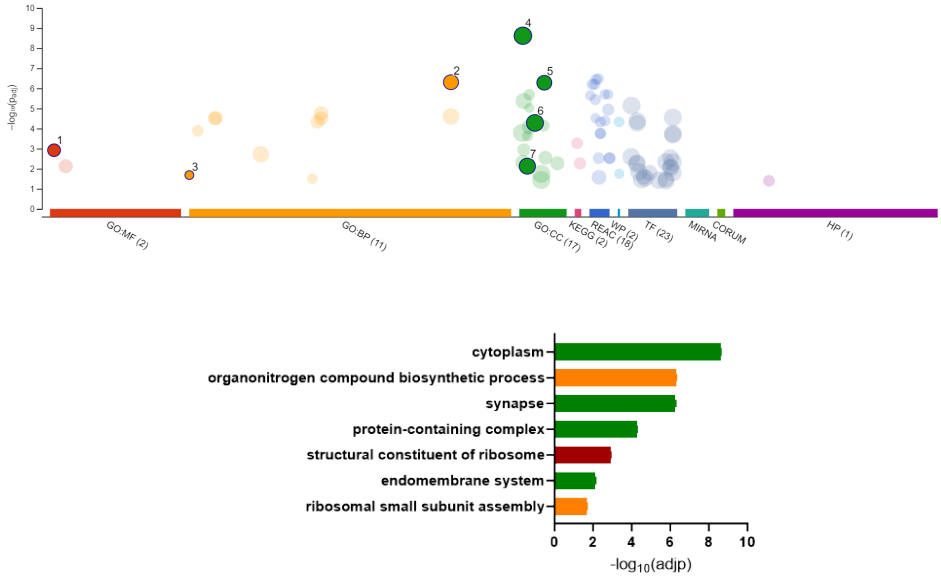


Figure 8.5: GO term analysis of transcripts which were downregulated in the spinal cord of hFUS/hFUS^{P525L} mice compared to hFUS/hFUS controls.

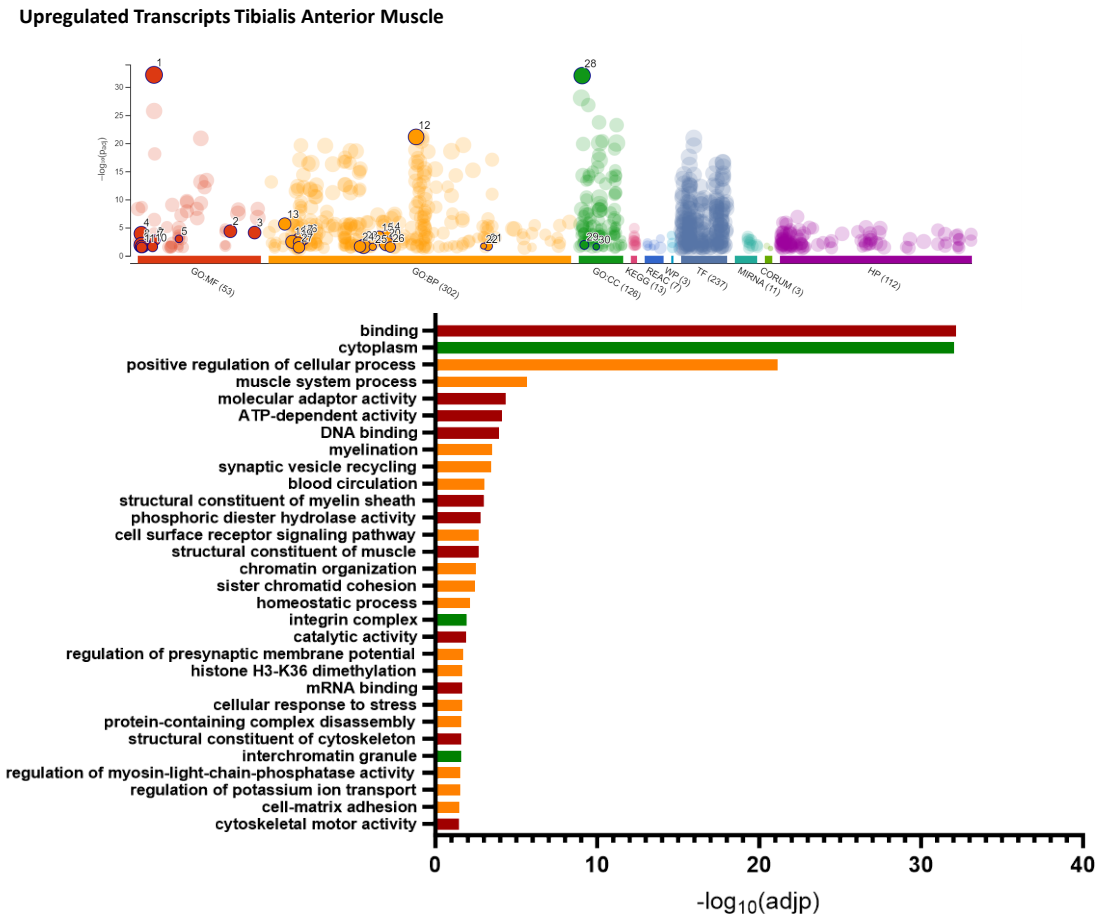


Figure 8.6: GO term analysis of transcripts which were upregulated in the tibialis anterior of hFUS/hFUS^{P525L} mice compared to hFUS/hFUS controls.



Figure 8.7: GO term analysis of transcripts which were downregulated in the tibialis anterior muscle of hFUS/hFUS^{P525L} mice compared to hFUS/hFUS controls.

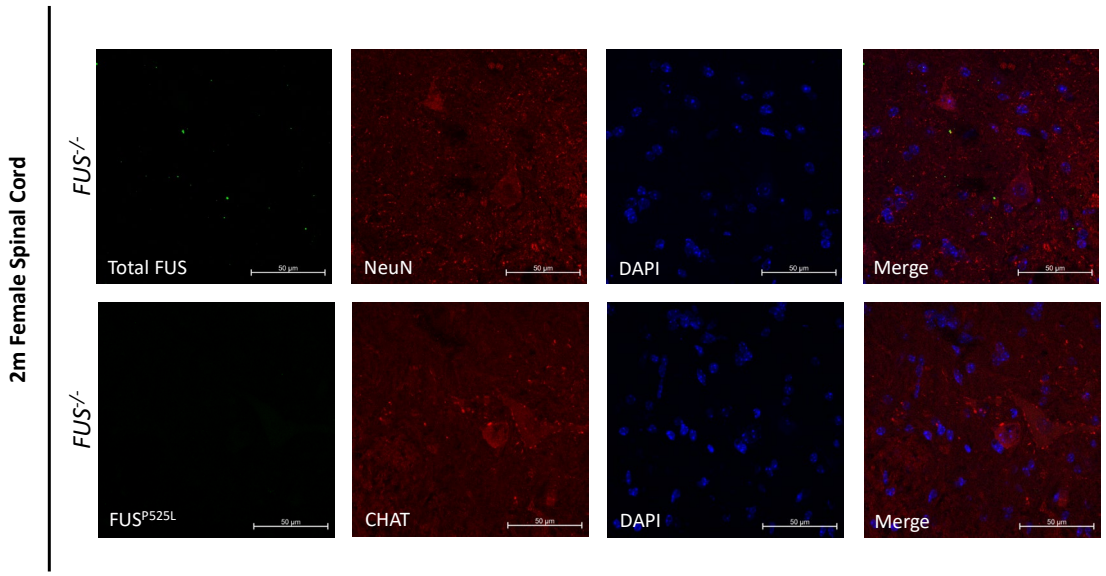


Figure 8.8: FUS staining in the spinal cord is specific. *FUS staining was carried out using an antibody raised against the C-terminus of the FUS protein and a FUS^{P525L} specific antibody, with ChAT or NeuN used as neuronal markers in Fus knock-out mice. Scale bars = 50µm.*

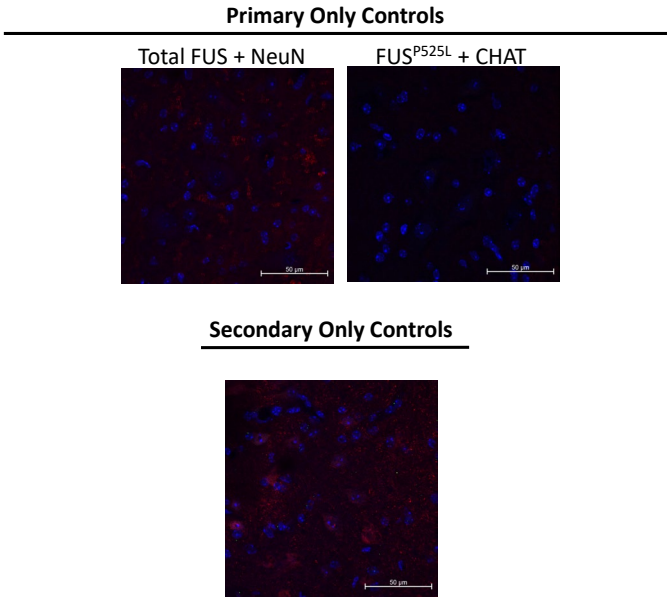


Figure 8.9: FUS, FUS^{P525L}, NeuN and ChAT staining is specific in spinal cord sections. A) *Sections were stained only with the primary antibodies raised against FUS, FUS^{P525L}, NeuN and ChAT.* ***B)*** *Sections were stained only with the relevant fluorescent-tagged secondary antibodies.*

8.3 Chapter 4: Primary cell cultures

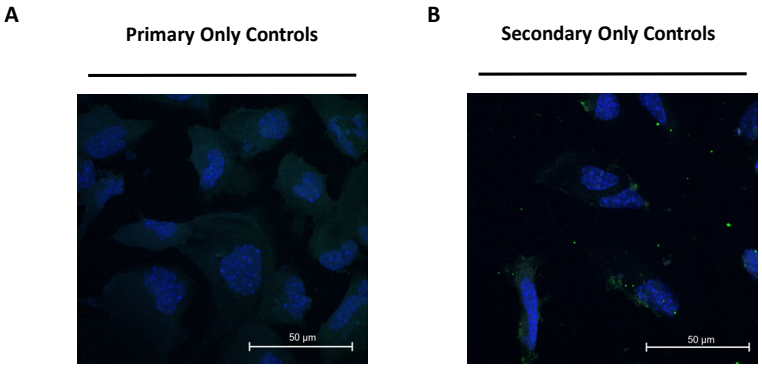


Figure 8.10: FUS and G3BP1 staining in cell cultures is specific. A) *Sections were stained only with the primary antibodies raised against FUS and G3BP1.* ***B)*** *Sections were stained only with the relevant fluorescent-tagged secondary antibodies.*

8.4 Chapter 5: Comparing *mFus/hFUS*^{P525L} and *mFus/hFUS*^{Q519Ifs} mice

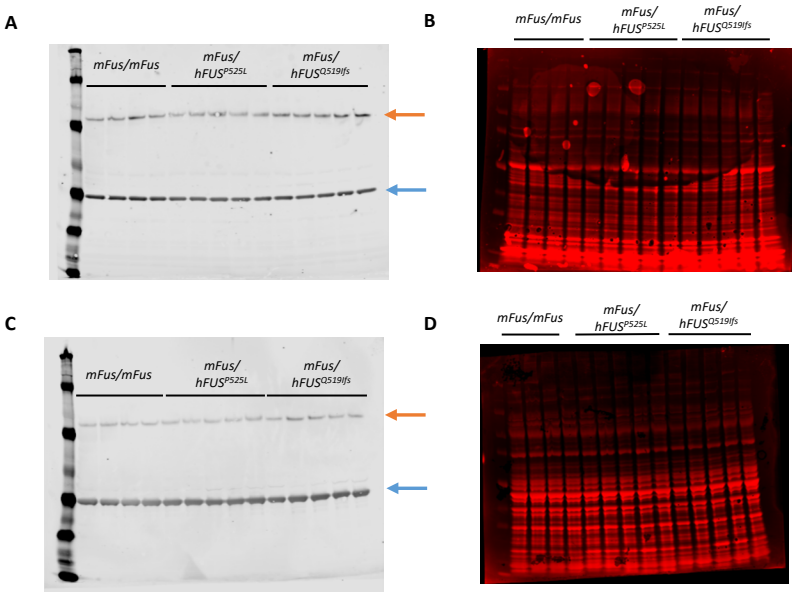


Figure 8.11: Western blot images used to quantify FUS expression in P525L x Q519Ifs male cohort mice. A) *Image of immunoblot used to quantify FUS expression in spinal cord tissue. Orange arrow indicates FUS protein band, blue arrow indicates GAPDH band which was used as an additional loading control.* ***B)*** *Total protein stain image used to normalise expression values in the spinal cord.* ***C)*** *Image of immunoblot used to quantify FUS expression in tibialis anterior tissue. Orange arrow indicates FUS protein band, blue arrow indicates GAPDH band which was used as an additional loading control.* ***D)*** *Total protein stain image used to normalise expression values in the tibialis anterior muscle.*

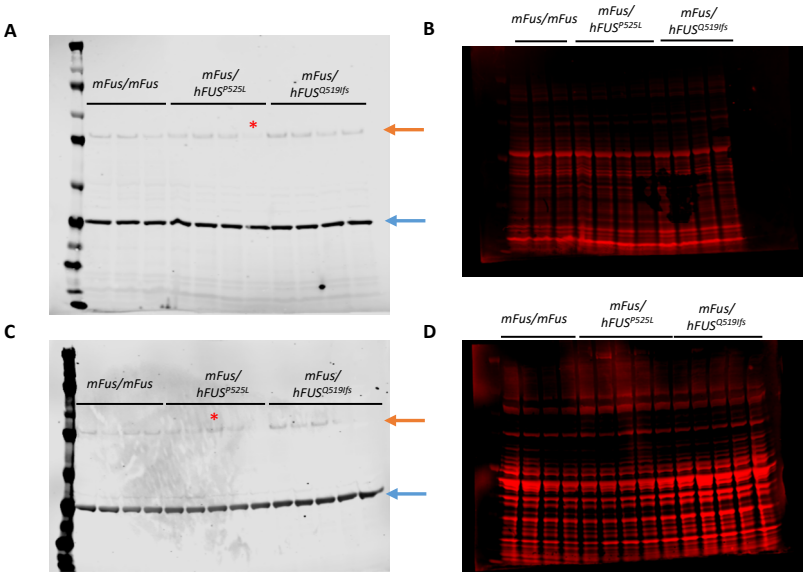


Figure 8.12: Western blot images used to quantify FUS expression in P525L x Q519Ifs female cohort mice. A) *Image of immunoblot used to quantify FUS expression in spinal cord tissue. Orange arrow indicates FUS protein band, blue arrow indicates GAPDH band which was used as an additional loading control. Red Asterix indicates an excluded data point due to issue when loading the gel.* ***B)*** *Total protein stain image used to normalise expression values in the spinal cord.* ***C)*** *Image of immunoblot used to quantify FUS expression in tibialis anterior tissue. Orange arrow indicates FUS protein band, blue arrow indicates GAPDH band which was used as an additional loading control. Red Asterix indicates an excluded data point due to issue when loading the gel.* ***D)*** *Total protein stain image used to normalise expression values in the tibialis anterior muscle.*

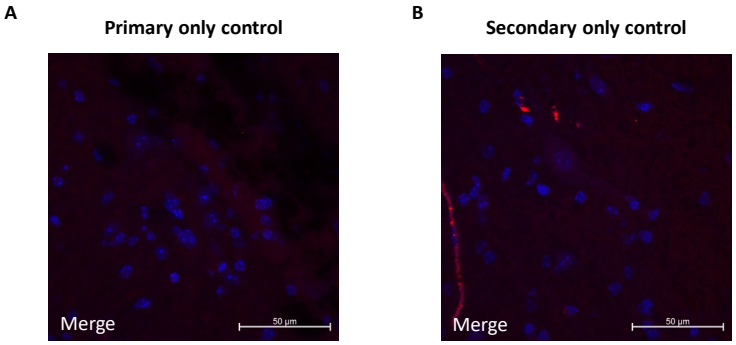


Figure 8.13: FUS and NeuN staining is specific in spinal cord sections of 14-month-old mice expressing either the hFUS^{P525L} or hFUS^{Q519Ifs} mutation or controls. A) *Sections were stained only with the primary antibodies raised against the N terminus of FUS and NeuN.* ***B)*** *Sections were stained only with the relevant fluorescent-tagged secondary antibodies.*

Table 8.2: Transcripts differentially expressed in mFus/hFUS^{Q519Ifs} mice compared to mFus/hFUS^{P525L} mice.

Transcripts differentially expressed in *mFus/hFUS^{Q519Ifs}* versus *mFus/hFUS^{P525L}* mice (adjp<0.1)					
Transcript ID	Transcript name	Transcript type	Log_2FC (in *mFus/hFUS^{Q519Ifs}* mice)	p value	adjp value
Spinal Cord					
ENSMUST00000032944	*Gdpd3*	protein coding	0.883818729292682000	0.000000000000000000	0.00000000000000000394
ENSMUST00000205468	*Gdpd3*	retained intron	0.640471549365685000	0.000000000000000060	0.00000000000031084505078
ENSMUST00000197120	*Gm42566*	coding	0.564782142896225000	0.000000009001704194	0.000307831278352053000
ENSMUST00000108061	*Bcas3*	protein coding	0.487923010430643000	0.000001284350720699	0.0267989148317886000000
ENSMUST00000020673	*Vdac1*	protein coding	0.472059129942299000	0.000001375655039739	0.0267989148317886000000
ENSMUST00000126781	*Nup50*	protein coding	-0.408540011725266000	0.000001567325486550	0.0267989148317886000000
ENSMUST00000230411	*Cpeb3*	protein coding	-0.406155824417233000	0.000002328532826080	0.031375079060910100000
ENSMUST00000195042	*Rab3gap2*	retained intron	-0.419721116123384000	0.000002451195306838	0.031375079060910100000
ENSMUST00000165033	*Egr1*	protein coding	-0.376940621420165000	0.000002752441359848	0.031375079060910100000
ENSMUST00000031565	*Fscn1*	protein coding	0.186900996618338000	0.000003521080847896	0.032936674172134500000
ENSMUST00000078374	*U2surp*	protein coding	-0.349228499213528000	0.000003531532160652	0.032936674172134500000
ENSMUST00000175665	*Gpc5*	protein coding	-0.421909656287720000	0.000006098633482669	0.052138742301708700000
ENSMUST00000206350	*Gdpd3*	retained intron	0.210060472219587000	0.000011922302888331	0.086855462381040700000

ENSMUST00000227181	*Itih3*	retained intron	-0.230624507384160000	0.000012005206578744	0.086855462381040700000
ENSMUST00000178504	*Atp9a*	protein coding	-0.346779366376225000	0.000012699280986788	0.086855462381040700000
ENSMUST00000146870	*Rngtt*	protein coding CDS not defined	0.265641434654388000	0.000015448846810451	0.099057040195691400000
ENSMUST00000201452	*Hsph1*	protein coding	-0.430050360413964000	0.000016518143007454	0.099683106428106100000
Tibialis Anterior					
ENSMUST00000032944	*Gdpd3*	protein coding	4.022895666004310000	0.000000000000000000	0.000000000000000000000000000000000000000
ENSMUST00000205468	*Gdpd3*	retained intron	2.727590661596110000	0.000000000000000000	0.000000000000000000000000000000004698448
ENSMUST00000206350	*Gdpd3*	retained intron	1.862819293455630000	0.000000000000000000	0.000000000000001668548040520720000000000
ENSMUST00000206858	*Gdpd3*	retained intron	0.943035739570078000	0.000000030746366329	0.000466852826342119000000000000000000000
ENSMUST00000205910	*Gdpd3*	retained intron	0.970734909020065000	0.000000305172560895	0.003706992131701270000000000000000000000
ENSMUST00000054459	*Tmem201*	protein coding	1.068922164327360000	0.000005396419379000	0.005462615456720770000000000000000000000
ENSMUST00000201372	*Ctbp1*	protein coding	1.063542771213250000	0.000006873731737 13	0.005964042439808260000000000000000000000
ENSMUST00000128930	*Mllt3*	protein coding CDS not defined	-1.025270953094250000	0.000011323048160938	0.008596458163780260000000000000000000000
ENSMUST00000031017	*Fosl2*	protein coding	-0.750548637170791000	0.000020826975560211	0.013686080535098200000000000000000000000

ENSMUST00000140500	*Larp1*	retained intron	1.009303680609490000	0.00000225337205859 8	0.013686080535098200000000000000000000000 0
ENSMUST00000236515	*Stub1*	protein coding	-0.739928904973034000	0.00000364219126212 9	0.020110193499698500000000000000000000000 0
ENSMUST00000175939	*Hnrnpk*	retained intron	0.873090922611467000	0.00001359698470834 5	0.068818871937172300000000000000000000000 0
ENSMUST00000207004	*Gdpd3*	retained intron	0.840198216979615000	0.00001631749135705 2	0.076235319620148400000000000000000000000 0
ENSMUST00000100962	*Gbp4*	protein coding	0.760640862981772000	0.00001766739553697 3	0.076646209666687100000000000000000000000 0
ENSMUST00000041388	*Serpine1*	protein coding	-0.893727854488446000	0.00001983676525298 6	0.080320384960355700000000000000000000000 0
ENSMUST00000081435	*H2-Q4*	protein coding	0.562165966506930000	0.00002220309580718 7	0.084282951684081900000000000000000000000 0
ENSMUST00000131217	*Rptor*	Nonsense mediated decay	0.895868041448151000	0.00002778730234787 8	0.099275858552981700000000000000000000000 0
ENSMUST00000167780	*Noct*	protein coding	-0.695548586895803000	0.00002959165681164 6	0.099848826006229100000000000000000000000 0

9 Chapter 9: References

Abramzon, Y. A., Fratta, P., Traynor, B. J., & Chia, R. (2020). The Overlapping Genetics of Amyotrophic Lateral Sclerosis and Frontotemporal Dementia. *Front Neurosci*, *14*, 42. https://doi.org/10.3389/fnins.2020.00042

Ahmed, M., Machado, P. M., Miller, A., Spicer, C., Herbelin, L., He, J., Noel, J., Wang, Y., Mcvey, A. L., Pasnoor, M., Gallagher, P., Statland, J., Lu, C.-H., Kalmar, B., Brady, S., Sethi, H., Samandouras, G., Parton, M., Holton, J. L., . . . Greensmith, L. (2016). Targeting protein homeostasis in sporadic inclusion body myositis. *Science Translational Medicine*, *8*(331), 331ra341-331ra341. https://doi.org/10.1126/scitranslmed.aad4583

Ahmed, M., Spicer, C., Harley, J., Taylor, J. P., Hanna, M., Patani, R., & Greensmith, L. (2023). Amplifying the Heat Shock Response Ameliorates ALS and FTD Pathology in Mouse and Human Models. *Mol Neurobiol*. https://doi.org/10.1007/s12035-023-03509-2

Ajmone-Cat, M. A., Onori, A., Toselli, C., Stronati, E., Morlando, M., Bozzoni, I., Monni, E., Kokaia, Z., Lupo, G., Minghetti, L., Biagioni, S., & Cacci, E. (2019). Increased FUS levels in astrocytes leads to astrocyte and microglia activation and neuronal death. *Scientific Reports*, *9*(1). https://doi.org/10.1038/s41598-019-41040-4

Al-Chalabi, A., Calvo, A., Chio, A., Colville, S., Ellis, C. M., Hardiman, O., Heverin, M., Howard, R. S., Huisman, M. H. B., Keren, N., Leigh, P. N., Mazzini, L., Mora, G., Orrell, R. W., Rooney, J., Scott, K. M., Scotton, W. J., Seelen, M., Shaw, C. E., . . . Pearce, N. (2014). Analysis of amyotrophic lateral sclerosis as a multistep process: a population-based modelling study. *Lancet Neurol*, *13*(11), 1108-1113. https://doi.org/10.1016/S1474-4422(14)70219-4

Aleksandrov, R., Dotchev, A., Poser, I., Krastev, D., Georgiev, G., Panova, G., Babukov, Y., Danovski, G., Dyankova, T., Hubatsch, L., Ivanova, A., Atemin, A., Nedelcheva-Veleva, M. N., Hasse, S., Sarov, M., Buchholz, F., Hyman, A. A., Grill, S. W., & Stoynov, S. S. (2018). Protein Dynamics in Complex DNA Lesions. *Molecular Cell*, *69*(6), 1046-1061.e1045. https://doi.org/10.1016/j.molcel.2018.02.016

Ali, Z., Godoy-Corchuelo, J. M., Martins-Bach, A. B., Garcia-Toledo, I., Fernández-Beltrán, L. C., Nair, R. R., Spring, S., Nieman, B. J., Jimenez-Coca, I., Bains, R. S., Forrest, H., Lerch, J. P., Miller, K., Fisher, E. M. C., Cunningham, T. J., & Corrochano, S. (2023). FUS-NLS mutation causes neurodevelopmental and systemic metabolic alterations. *Disease Models & Mechanisms*. https://doi.org/10.1242/dmm.050200

Alkaslasi, M. R., Piccus, Z. E., Hareendran, S., Silberberg, H., Chen, L., Zhang, Y., Petros, T. J., & Le Pichon, C. E. (2021). Single nucleus RNA-sequencing defines unexpected diversity of cholinergic neuron types in the adult mouse spinal cord. *Nat Commun*, *12*(1), 2471. https://doi.org/10.1038/s41467-021-22691-2

Alonso, A., Logroscino, G., Jick, S. S., & Hernan, M. A. (2009). Incidence and lifetime risk of motor neuron disease in the United Kingdom: a population-based study. *Eur J Neurol*, *16*(6), 745-751. https://doi.org/10.1111/j.1468-1331.2009.02586.x

An, H., Rabesahala De Meritens, C., Buchman, V. L., & Shelkovnikova, T. A. (2020). Frameshift peptides alter the properties of truncated FUS proteins in ALS-FUS. *Molecular Brain*, *13*(1). https://doi.org/10.1186/s13041-020-00618-0

An, H., Skelt, L., Notaro, A., Highley, J. R., Fox, A. H., La Bella, V., Buchman, V. L., & Shelkovnikova, T. A. (2019). ALS-linked FUS mutations confer loss and gain of function in the nucleus by promoting excessive formation of dysfunctional paraspeckles. *Acta Neuropathologica Communications*, *7*(1). https://doi.org/10.1186/s40478-019-0658-x

Andersen, P. M., & Al-Chalabi, A. (2011). Clinical genetics of amyotrophic lateral sclerosis: what do we really know? *Nature Reviews Neurology*, *7*(11), 603-615. https://doi.org/10.1038/nrneurol.2011.150

Anderson, P., & Kedersha, N. (2008). Stress granules: the Tao of RNA triage. *Trends Biochem Sci*, *33*(3), 141-150. https://doi.org/10.1016/j.tibs.2007.12.003

Andersson, M. K., Stahlberg, A., Arvidsson, Y., Olofsson, A., Semb, H., Stenman, G., Nilsson, O., & Aman, P. (2008). The multifunctional FUS, EWS and TAF15 proto-oncoproteins show cell type-specific expression patterns and involvement in cell spreading and stress response. *BMC Cell Biol*, *9*, 37. https://doi.org/10.1186/1471-2121-9-37

Arseni, D., Chen, R., Murzin, A. G., Peak-Chew, S. Y., Garringer, H. J., Newell, K. L., Kametani, F., Robinson, A. C., Vidal, R., Ghetti, B., Hasegawa, M., & Ryskeldi-Falcon, B. (2023). TDP-43 forms amyloid filaments with a distinct fold in type A FTLD-TDP. *Nature*, *620*(7975), 898-903. https://doi.org/10.1038/s41586-023-06405-w

Arseni, D., Hasegawa, M., Murzin, A. G., Kametani, F., Arai, M., Yoshida, M., & Ryskeldi-Falcon, B. (2022). Structure of pathological TDP-43 filaments from ALS with FTLD. *Nature*, *601*(7891), 139-143. https://doi.org/10.1038/s41586-021-04199-3

Arthur, K. C., Calvo, A., Price, T. R., Geiger, J. T., Chiò, A., & Traynor, B. J. (2016). Projected increase in amyotrophic lateral sclerosis from 2015 to 2040. *Nature Communications*, *7*(1), 12408. https://doi.org/10.1038/ncomms12408

Austin, A., Beresford, L., Price, G., Cunningham, T., Kalmar, B., & Yon, M. (2022). Sectioning and Counting of Motor Neurons in the L3 to L6 Region of the Adult Mouse Spinal Cord. *Current Protocols*, *2*(5). https://doi.org/10.1002/cpz1.428

Baade, I., Hutten, S., Sternburg, E. L., Pörschke, M., Hofweber, M., Dormann, D., & Kehlenbach, R. H. (2021). The RNA-binding protein FUS is chaperoned and imported into the nucleus by a network of import receptors. *Journal of Biological Chemistry*, *296*, 100659. https://doi.org/10.1016/j.jbc.2021.100659

Baechtold, H., Kuroda, M., Sok, J., Ron, D., Lopez, B. S., & Akhmedov, A. T. (1999). Human 75-kDa DNA-pairing Protein Is Identical to the Pro-oncoprotein TLS/FUS and Is Able to Promote D-loop Formation. *Journal of Biological Chemistry*, *274*(48), 34337-34342. https://doi.org/10.1074/jbc.274.48.34337

Balendra, R., Al Khleifat, A., Fang, T., & Al-Chalabi, A. (2019). A standard operating procedure for King's ALS clinical staging. *Amyotroph Lateral Scler Frontotemporal Degener*, *20*(3-4), 159-164. https://doi.org/10.1080/21678421.2018.1556696

Baron, D. M., Kaushansky, L. J., Ward, C. L., Sama, R. R. K., Chian, R.-J., Boggio, K. J., Quaresma, A. J. C., Nickerson, J. A., & Bosco, D. A. (2013). Amyotrophic lateral sclerosis-linked FUS/TLS alters stress granule assembly and dynamics. *Molecular Neurodegeneration*, *8*(1), 30. https://doi.org/10.1186/1750-1326-8-30

Baumer, D., Hilton, D., Paine, S. M. L., Turner, M. R., Lowe, J., Talbot, K., & Ansorge, O. (2010). Juvenile ALS with basophilic inclusions is a FUS proteinopathy with FUS mutations. *Neurology*, *75*(7), 611-618. https://doi.org/10.1212/wnl.0b013e3181ed9cde

Beeldman, E., Govaarts, R., De Visser, M., Klein Twennaar, M., Van Der Kooi, A. J., Van Den Berg, L. H., Veldink, J. H., Pijnenburg, Y. A. L., De Haan, R. J., Schmand, B. A., & Raaphorst, J. (2020). Progression of cognitive and behavioural impairment in early amyotrophic lateral sclerosis. *Journal of Neurology, Neurosurgery & Psychiatry*, *91*(7), 779-780. https://doi.org/10.1136/jnnp-2020-322992

Bensimon, G., Lacomblez, L., & Meininger, V. (1994). A Controlled Trial of Riluzole in Amyotrophic Lateral Sclerosis. *New England Journal of Medicine*, *330*(9), 585-591. https://doi.org/10.1056/nejm199403033300901

Berchtold, D., Battich, N., & Pelkmans, L. (2018). A Systems-Level Study Reveals Regulators of Membrane-less Organelles in Human Cells. *Mol Cell*, *72*(6), 1035-1049 e1035. https://doi.org/10.1016/j.molcel.2018.10.036

Berry, J. D., Blanchard, M., Bonar, K., Drane, E., Murton, M., Ploug, U., Ricchetti-Masterson, K., Savic, N., Worthington, E., & Heiman-Patterson, T. (2023). Epidemiology and economic burden of amyotrophic lateral sclerosis in the United States: a literature review.

Amyotrophic Lateral Sclerosis and Frontotemporal Degeneration, *24*(5-6), 436-448. https://doi.org/10.1080/21678421.2023.2165947

Birsa, N., Bentham, M. P., & Fratta, P. (2020). Cytoplasmic functions of TDP-43 and FUS and their role in ALS. *Seminars in Cell & Developmental Biology*, *99*, 193-201. https://doi.org/10.1016/j.semcdb.2019.05.023

Birsa, N., Ule, A. M., Garone, M. G., Tsang, B., Mattedi, F., Chong, P. A., Humphrey, J., Jarvis, S., Pisiren, M., Wilkins, O. G., Nosella, M. L., Devoy, A., Bodo, C., De La Fuente, R. F., Fisher, E. M. C., Rosa, A., Viero, G., Forman-Kay, J. D., Schiavo, G., & Fratta, P. (2021). FUS-ALS mutants alter FMRP phase separation equilibrium and impair protein translation. *Science Advances*, *7*(30), eabf8660. https://doi.org/10.1126/sciadv.abf8660

Burke, A., Kathleen, Janke, M., Abigail, Rhine, L., Christy, & Fawzi, L., Nicolas. (2015). Residue-by-Residue View of In Vitro FUS Granules that Bind the C-Terminal Domain of RNA Polymerase II. *Molecular Cell*, *60*(2), 231-241. https://doi.org/10.1016/j.molcel.2015.09.006

Caputo, M., La Bella, V., & Notaro, A. (2020). Differential subcellular expression of ^{P525L}FUS as a putative biomarker for ALS phenoconversion. *Neurology Genetics*, *6*(2), e410. https://doi.org/10.1212/nxg.0000000000000410

Chapman, L., Cooper-Knock, J., & Shaw, P. J. (2023). Physical activity as an exogenous risk factor for amyotrophic lateral sclerosis: a review of the evidence. *Brain*, *146*(5), 1745-1757. https://doi.org/10.1093/brain/awac470

Chen, S., Sayana, P., Zhang, X., & Le, W. (2013). Genetics of amyotrophic lateral sclerosis: an update. *Molecular Neurodegeneration*, *8*(1), 28. https://doi.org/10.1186/1750-1326-8-28

Chen, Y., Deng, J., Wang, P., Yang, M., Chen, X., Zhu, L., Liu, J., Lu, B., Shen, Y., Fushimi, K., Xu, Q., & Wu, J. Y. (2016). PINK1 and Parkin are genetic modifiers for FUS-induced neurodegeneration. *Hum Mol Genet*, *25*(23), 5059-5068. https://doi.org/10.1093/hmg/ddw310

Chiò, A., Logroscino, G., Hardiman, O., Swingler, R., Mitchell, D., Beghi, E., Traynor, B. G., & Consortium, O. B. O. T. E. (2009). Prognostic factors in ALS: A critical review. *Amyotrophic Lateral Sclerosis*, *10*(5-6), 310-323. https://doi.org/10.3109/17482960802566824

Coady, T. H., & Manley, J. L. (2015). ALS mutations in TLS/FUS disrupt target gene expression. *Genes & Development*, *29*(16), 1696-1706. https://doi.org/10.1101/gad.267286.115

Conte, A., Lattante, S., Zollino, M., Marangi, G., Luigetti, M., Del Grande, A., Servidei, S., Trombetta, F., & Sabatelli, M. (2012). P525L FUS mutation is consistently associated with a severe form of juvenile amyotrophic lateral sclerosis. *Neuromuscul Disord*, *22*(1), 73-75. https://doi.org/10.1016/j.nmd.2011.08.003

Crown, A., Mcalary, L., Fagerli, E., Brown, H., Yerbury, J. J., Galaleldeen, A., Cashman, N. R., Borchelt, D. R., & Ayers, J. I. (2020). Tryptophan residue 32 in human Cu-Zn superoxide dismutase modulates prion-like propagation and strain selection. *PLoS One*, *15*(1), e0227655. https://doi.org/10.1371/journal.pone.0227655

Crozat, A., Åman, P., Mandahl, N., & Ron, D. (1993). Fusion of CHOP to a novel RNA-binding protein in human myxoid liposarcoma. *Nature*, *363*(6430), 640-644. https://doi.org/10.1038/363640a0

Darnell, J. C., & Klann, E. (2013). The translation of translational control by FMRP: therapeutic targets for FXS. *Nature Neuroscience*, *16*(11), 1530-1536. https://doi.org/10.1038/nn.3379

De Giorgio, F., Maduro, C., Fisher, E. M. C., & Acevedo-Arozena, A. (2019). Transgenic and physiological mouse models give insights into different aspects of amyotrophic lateral

sclerosis. *Disease Models & Mechanisms*, *12*(1), dmm037424. https://doi.org/10.1242/dmm.037424

De Vos, K. J., & Hafezparast, M. (2017). Neurobiology of axonal transport defects in motor neuron diseases: Opportunities for translational research? *Neurobiol Dis*, *105*, 283-299. https://doi.org/10.1016/j.nbd.2017.02.004

Deng, H., Gao, K., & Jankovic, J. (2014). The role of FUS gene variants in neurodegenerative diseases. *Nature Reviews Neurology*, *10*(6), 337-348. https://doi.org/10.1038/nrneurol.2014.78

Deng, J., Wang, P., Chen, X., Cheng, H., Liu, J., Fushimi, K., Zhu, L., & Wu, J. Y. (2018). FUS interacts with ATP synthase beta subunit and induces mitochondrial unfolded protein response in cellular and animal models. *Proceedings of the National Academy of Sciences*, *115*(41), E9678-E9686. https://doi.org/10.1073/pnas.1806655115

Deng, J., Yang, M., Chen, Y., Chen, X., Liu, J., Sun, S., Cheng, H., Li, Y., Bigio, E. H., Mesulam, M., Xu, Q., Du, S., Fushimi, K., Zhu, L., & Wu, J. Y. (2015). FUS Interacts with HSP60 to Promote Mitochondrial Damage. *PLoS Genet*, *11*(9), e1005357. https://doi.org/10.1371/journal.pgen.1005357

Devoy, A., Kalmar, B., Stewart, M., Park, H., Burke, B., Noy, S. J., Redhead, Y., Humphrey, J., Lo, K., Jaeger, J., Mejia Maza, A., Sivakumar, P., Bertolin, C., Soraru, G., Plagnol, V., Greensmith, L., Acevedo Arozena, A., Isaacs, A. M., Davies, B., . . . Fisher, E. M. C. (2017). Humanized mutant FUS drives progressive motor neuron degeneration without aggregation in 'FUSDelta14' knockin mice. *Brain*, *140*(11), 2797-2805. https://doi.org/10.1093/brain/awx248

Devoy, A., Price, G., De Giorgio, F., Bunton-Stasyshyn, R., Thompson, D., Gasco, S., Allan, A., Codner, G. F., Nair, R. R., Tibbit, C., Mcleod, R., Ali, Z., Noda, J., Marrero-Gagliardi, A., Brito-Armas, J. M., Williams, C., Öztürk, M. M., Simon, M., O'Neill, E., . . . Cunningham, T. J. (2021). Generation and analysis of innovative genomically humanized knockin SOD1, TARDBP (TDP-43), and FUS mouse models. *iScience*, *24*(12), 103463. https://doi.org/10.1016/j.isci.2021.103463

Dichmann, D. S., & Harland, R. M. (2012). fus/TLS orchestrates splicing of developmental regulators during gastrulation. *Genes Dev*, *26*(12), 1351-1363. https://doi.org/10.1101/gad.187278.112

Dini Modigliani, S., Morlando, M., Errichelli, L., Sabatelli, M., & Bozzoni, I. (2014). An ALS-associated mutation in the FUS 3'-UTR disrupts a microRNA–FUS regulatory circuitry. *Nature Communications*, *5*(1). https://doi.org/10.1038/ncomms5335

Dodd, K. C., Power, R., Ealing, J., & Hamdalla, H. (2019). FUS-ALS presenting with myoclonic jerks in a 17-year-old man. *Amyotroph Lateral Scler Frontotemporal Degener*, *20*(3-4), 278-280. https://doi.org/10.1080/21678421.2019.1582665

Dormann, D., Madl, T., Valori, C. F., Bentmann, E., Tahirovic, S., Abou-Ajram, C., Kremmer, E., Ansorge, O., Mackenzie, I. R. A., Neumann, M., & Haass, C. (2012). Arginine methylation next to the PY-NLS modulates Transportin binding and nuclear import of FUS. *The EMBO Journal*, *31*(22), 4258-4275. https://doi.org/10.1038/emboj.2012.261

Dormann, D., Rodde, R., Edbauer, D., Bentmann, E., Fischer, I., Hruscha, A., Than, M. E., Mackenzie, I. R. A., Capell, A., Schmid, B., Neumann, M., & Haass, C. (2010). ALS-associated fused in sarcoma (FUS) mutations disrupt Transportin-mediated nuclear import. *The EMBO Journal*, *29*(16), 2841-2857. https://doi.org/10.1038/emboj.2010.143

Ervilha Pereira, P., Schuermans, N., Meylemans, A., LeBlanc, P., Versluys, L., Copley, K. E., Rubien, J. D., Altheimer, C., Peetermans, M., Debackere, E., Vanakker, O., Janssens, S., Baets, J., Verhoeven, K., Lammens, M., Symoens, S., De Paepe, B., Barmada, S. J., Shorter, J., . . . Dermaut, B. (2023). C-terminal frameshift variant of TDP-43 with pronounced aggregation-propensity causes rimmed vacuole myopathy but not

ALS/FTD. *Acta Neuropathol*, *145*(6), 793-814. https://doi.org/10.1007/s00401-023-02565-1

Fallini, C., Bassell, G. J., & Rossoll, W. (2012). The ALS disease protein TDP-43 is actively transported in motor neuron axons and regulates axon outgrowth. *Hum Mol Genet*, *21*(16), 3703-3718. https://doi.org/10.1093/hmg/dds205

Fellows, A. D., Rhymes, E. R., Gibbs, K. L., Greensmith, L., & Schiavo, G. (2020). IGF1R regulates retrograde axonal transport of signalling endosomes in motor neurons. *EMBO Rep*, *21*(3), e49129. https://doi.org/10.15252/embr.201949129

Folker, E. S., & Baylies, M. K. (2013). Nuclear positioning in muscle development and disease. *Front Physiol*, *4*, 363. https://doi.org/10.3389/fphys.2013.00363

Frey, D., Schneider, C., Xu, L., Borg, J., Spooren, W., & Caroni, P. (2000). Early and Selective Loss of Neuromuscular Synapse Subtypes with Low Sprouting Competence in Motoneuron Diseases. *The Journal of Neuroscience*, *20*(7), 2534-2542. https://doi.org/10.1523/jneurosci.20-07-02534.2000

Freydenzon, A., Wani, S., Bharti, V., Wallace, L. M., Henders, A. K., Mccombe, P. A., Henderson, R. D., Steyn, F. J., Wray, N. R., Ngo, S. T., & Mcrae, A. F. (2023). *RNA-seq analysis of skeletal muscle in motor neurone disease cases and controls*. Cold Spring Harbor Laboratory.

Fujii, R., Okabe, S., Urushido, T., Inoue, K., Yoshimura, A., Tachibana, T., Nishikawa, T., Hicks, G. G., & Takumi, T. (2005). The RNA Binding Protein TLS Is Translocated to Dendritic Spines by mGluR5 Activation and Regulates Spine Morphology. *Current Biology*, *15*(6), 587-593. https://doi.org/10.1016/j.cub.2005.01.058

Gao, C., Gu, J., Zhang, H., Jiang, K., Tang, L., Liu, R., Zhang, L., Zhang, P., Liu, C., Dai, B., & Song, J. (2022). Hyperosmotic-stress-induced liquid-liquid phase separation of ALS-related proteins in the nucleus. *Cell Rep*, *40*(3), 111086. https://doi.org/10.1016/j.celrep.2022.111086

Godoy-Corchuelo, J. M., Fernández-Beltrán, L. C., Ali, Z., Gil-Moreno, M. J., López-Carbonero, J. I., Guerrero-Sola, A., Larrad-Sainz, A., Matias-Guiu, J., Matias-Guiu, J. A., Cunningham, T. J., & Corrochano, S. (2022). Lipid Metabolic Alterations in the ALS–FTD Spectrum of Disorders. *Biomedicines*, *10*(5), 1105. https://doi.org/10.3390/biomedicines10051105

Goldstein, O., Inbar, T., Kedmi, M., Gana-Weisz, M., Abramovich, B., Orr-Urtreger, A., & Drory, V. E. (2022). FUS-P525L Juvenile Amyotrophic Lateral Sclerosis and Intellectual Disability. *Neurology Genetics*, *8*(4), e200009. https://doi.org/10.1212/nxg.0000000000200009

Gonzalez, A., Mannen, T., Çağatay, T., Fujiwara, A., Matsumura, H., Niesman, A. B., Brautigam, C. A., Chook, Y. M., & Yoshizawa, T. (2021). Mechanism of karyopherin-β2 binding and nuclear import of ALS variants FUS(P525L) and FUS(R495X). *Scientific Reports*, *11*(1). https://doi.org/10.1038/s41598-021-83196-y

Goodwin, L. O., Splinter, E., Davis, T. L., Urban, R., He, H., Braun, R. E., Chesler, E. J., Kumar, V., van Min, M., Ndukum, J., Philip, V. M., Reinholdt, L. G., Svenson, K., White, J. K., Sasner, M., Lutz, C., & Murray, S. A. (2019). Large-scale discovery of mouse transgenic integration sites reveals frequent structural variation and insertional mutagenesis. *Genome Res*, *29*(3), 494-505. https://doi.org/10.1101/gr.233866.117

Grassano, M., Brodini, G., De Marco, G., Casale, F., Fuda, G., Salamone, P., Brunetti, M., Sbaiz, L., Gallone, S., Cugnasco, P., Bombaci, A., Vasta, R., Manera, U., Canosa, A., Moglia, C., Calvo, A., Traynor, B. J., & Chio, A. (2022). Phenotype Analysis of Fused in Sarcoma Mutations in Amyotrophic Lateral Sclerosis. *Neurology Genetics*, *8*(5), e200011. https://doi.org/10.1212/nxg.0000000000200011

Groen, E. J. N., Fumoto, K., Blokhuis, A. M., Engelen-Lee, J., Zhou, Y., van den Heuvel, D. M. A., Koppers, M., van Diggelen, F., van Heest, J., Demmers, J. A. A., Kirby, J., Shaw, P. J., Aronica, E., Spliet, W. G. M., Veldink, J. H., van den Berg, L. H., & Pasterkamp, R. J.

(2013). ALS-associated mutations in FUS disrupt the axonal distribution and function of SMN. *Human Molecular Genetics*, *22*(18), 3690-3704. https://doi.org/10.1093/hmg/ddt222

Groppo, R., & Richter, J. D. (2009). Translational control from head to tail. *Current Opinion in Cell Biology*, *21*(3), 444-451. https://doi.org/10.1016/j.ceb.2009.01.011

Hardiman, O., Al-Chalabi, A., Chio, A., Corr, E. M., Logroscino, G., Robberecht, W., Shaw, P. J., Simmons, Z., & van den Berg, L. H. (2017). Amyotrophic lateral sclerosis. *Nat Rev Dis Primers*, *3*, 17071. https://doi.org/10.1038/nrdp.2017.71

He, L. (2002). Detection and quantification of mitochondrial DNA deletions in individual cells by real-time PCR. *Nucleic Acids Research*, *30*(14), 68e-68. https://doi.org/10.1093/nar/gnf067

Hewitt, C., Kirby, J., Highley, J. R., Hartley, J. A., Hibberd, R., Hollinger, H. C., Williams, T. L., Ince, P. G., Mcdermott, C. J., & Shaw, P. J. (2010). Novel FUS/TLS Mutations and Pathology in Familial and Sporadic Amyotrophic Lateral Sclerosis. *Archives of Neurology*, *67*(4). https://doi.org/10.1001/archneurol.2010.52

Hicks, G. G., Singh, N., Nashabi, A., Mai, S., Bozek, G., Klewes, L., Arapovic, D., White, E. K., Koury, M. J., Oltz, E. M., Van Kaer, L., & Ruley, H. E. (2000). Fus deficiency in mice results in defective B-lymphocyte development and activation, high levels of chromosomal instability and perinatal death. *Nature Genetics*, *24*(2), 175-179. https://doi.org/10.1038/72842

Hirayanagi, K., Sato, M., Furuta, N., Makioka, K., & Ikeda, Y. (2016). Juvenile-onset Sporadic Amyotrophic Lateral Sclerosis with a Frameshift FUS Gene Mutation Presenting Unique Neuroradiological Findings and Cognitive Impairment. *Internal Medicine*, *55*(6), 689-693. https://doi.org/10.2169/internalmedicine.55.5569

Hofweber, M., Hutten, S., Bourgeois, B., Spreitzer, E., Niedner-Boblenz, A., Schifferer, M., Ruepp, M. D., Simons, M., Niessing, D., Madl, T., & Dormann, D. (2018). Phase Separation of FUS Is Suppressed by Its Nuclear Import Receptor and Arginine Methylation. *Cell*, *173*(3), 706-719 e713. https://doi.org/10.1016/j.cell.2018.03.004

Hsiung, G. Y., DeJesus-Hernandez, M., Feldman, H. H., Sengdy, P., Bouchard-Kerr, P., Dwosh, E., Butler, R., Leung, B., Fok, A., Rutherford, N. J., Baker, M., Rademakers, R., & Mackenzie, I. R. (2012). Clinical and pathological features of familial frontotemporal dementia caused by C9ORF72 mutation on chromosome 9p. *Brain*, *135*(Pt 3), 709-722. https://doi.org/10.1093/brain/awr354

Huang, C., Xia, P. Y., & Zhou, H. (2010). Sustained Expression of TDP-43 and FUS in Motor Neurons in Rodent's Lifetime. *International Journal of Biological Sciences*, 396-406. https://doi.org/10.7150/ijbs.6.396

Huang, E. J., Zhang, J., Geser, F., Trojanowski, J. Q., Strober, J. B., Dickson, D. W., Brown Jr, R. H., Shapiro, B. E., & Lomen-Hoerth, C. (2010). Extensive FUS-Immunoreactive Pathology in Juvenile Amyotrophic Lateral Sclerosis with Basophilic Inclusions. *Brain Pathology*, *20*(6), 1069-1076. https://doi.org/10.1111/j.1750-3639.2010.00413.x

Hubers, A., Just, W., Rosenbohm, A., Muller, K., Marroquin, N., Goebel, I., Hogel, J., Thiele, H., Altmuller, J., Nurnberg, P., Weishaupt, J. H., Kubisch, C., Ludolph, A. C., & Volk, A. E. (2015). De novo FUS mutations are the most frequent genetic cause in early-onset German ALS patients. *Neurobiol Aging*, *36*(11), 3117 e3111-3117 e3116. https://doi.org/10.1016/j.neurobiolaging.2015.08.005

Humphrey, J., Birsa, N., Milioto, C., McLaughlin, M., Ule, A. M., Robaldo, D., Eberle, A. B., Krauchi, R., Bentham, M., Brown, A. L., Jarvis, S., Bodo, C., Garone, M. G., Devoy, A., Soraru, G., Rosa, A., Bozzoni, I., Fisher, E. M. C., Muhlemann, O., . . . Fratta, P. (2020). FUS ALS-causative mutations impair FUS autoregulation and splicing factor networks through intron retention. *Nucleic Acids Res*, *48*(12), 6889-6905. https://doi.org/10.1093/nar/gkaa410

Ishigaki, S., Masuda, A., Fujioka, Y., Iguchi, Y., Katsuno, M., Shibata, A., Urano, F., Sobue, G., & Ohno, K. (2012). Position-dependent FUS-RNA interactions regulate alternative splicing events and transcriptions. *Sci Rep*, *2*, 529. https://doi.org/10.1038/srep00529

Jayaprakash, K., Glasmacher, S. A., Pang, B., Beswick, E., Mehta, A. R., Dakin, R., Newton, J., Chandran, S., & Pal, S. (2020). Riluzole prescribing, uptake and treatment discontinuation in people with amyotrophic lateral sclerosis in Scotland. *Journal of Neurology*, *267*(8), 2459-2461. https://doi.org/10.1007/s00415-020-09919-9

Kamelgarn, M., Chen, J., Kuang, L., Jin, H., Kasarskis, E. J., & Zhu, H. (2018). ALS mutations of FUS suppress protein translation and disrupt the regulation of nonsense-mediated decay. *Proceedings of the National Academy of Sciences*, *115*(51), E11904-E11913. https://doi.org/10.1073/pnas.1810413115

Kapeli, K., Martinez, F. J., & Yeo, G. W. (2017). Genetic mutations in RNA-binding proteins and their roles in ALS. *Hum Genet*, *136*(9), 1193-1214. https://doi.org/10.1007/s00439-017-1830-7

Keszycki, R., Rodriguez, G., Dunn, J. T., Locci, A., Orellana, H., Haupfear, I., Dominguez, S., Fisher, D. W., & Dong, H. (2023). Characterization of apathy-like behaviors in the 5xFAD mouse model of Alzheimer's disease. *Neurobiol Aging*, *126*, 113-122. https://doi.org/10.1016/j.neurobiolaging.2023.02.012

Kia, A., McAvoy, K., Krishnamurthy, K., Trotti, D., & Pasinelli, P. (2018). Astrocytes expressing ALS-linked mutant FUS induce motor neuron death through release of tumor necrosis factor-alpha. *Glia*, *66*(5), 1016-1033. https://doi.org/10.1002/glia.23298

Kiernan, M. C., Vucic, S., Cheah, B. C., Turner, M. R., Eisen, A., Hardiman, O., Burrell, J. R., & Zoing, M. C. (2011). Amyotrophic lateral sclerosis. *Lancet*, *377*(9769), 942-955. https://doi.org/10.1016/S0140-6736(10)61156-7

King, A., Troakes, C., Smith, B., Nolan, M., Curran, O., Vance, C., Shaw, C. E., & Al-Sarraj, S. (2015). ALS-FUS pathology revisited: singleton FUS mutations and an unusual case with both a FUS and TARDBP mutation. *Acta Neuropathologica Communications*, *3*(1). https://doi.org/10.1186/s40478-015-0235-x

Kino, Y., Washizu, C., Kurosawa, M., Yamada, M., Miyazaki, H., Akagi, T., Hashikawa, T., Doi, H., Takumi, T., Hicks, G. G., Hattori, N., Shimogori, T., & Nukina, N. (2015). FUS/TLS deficiency causes behavioral and pathological abnormalities distinct from amyotrophic lateral sclerosis. *Acta Neuropathologica Communications*, *3*(1). https://doi.org/10.1186/s40478-015-0202-6

Korobeynikov, V. A., Lyashchenko, A. K., Blanco-Redondo, B., Jafar-Nejad, P., & Shneider, N. A. (2022). Antisense oligonucleotide silencing of FUS expression as a therapeutic approach in amyotrophic lateral sclerosis. *Nature Medicine*, *28*(1), 104-116. https://doi.org/10.1038/s41591-021-01615-z

Kraeuter, A.-K., Guest, P. C., & Sarnyai, Z. (2019). The Y-Maze for Assessment of Spatial Working and Reference Memory in Mice. In *Methods in Molecular Biology* (pp. 105-111). Springer New York. https://doi.org/10.1007/978-1-4939-8994-2_10

Kumar, S. T., Nazarov, S., Porta, S., Maharjan, N., Cendrowska, U., Kabani, M., Finamore, F., Xu, Y., Lee, V. M., & Lashuel, H. A. (2023). Seeding the aggregation of TDP-43 requires post-fibrillization proteolytic cleavage. *Nat Neurosci*, *26*(6), 983-996. https://doi.org/10.1038/s41593-023-01341-4

Kuroda, M. (2000). Male sterility and enhanced radiation sensitivity in TLS-/- mice. *The EMBO Journal*, *19*(3), 453-462. https://doi.org/10.1093/emboj/19.3.453

Kwiatkowski, T. J., Bosco, D. A., LeClerc, A. L., Tamrazian, E., Vanderburg, C. R., Russ, C., Davis, A., Gilchrist, J., Kasarskis, E. J., Munsat, T., Valdmanis, P., Rouleau, G. A., Hosler, B. A., Cortelli, P., de Jong, P. J., Yoshinaga, Y., Haines, J. L., Pericak-Vance, M. A., Yan, J., . . . Brown, R. H. (2009). Mutations in the FUS/TLS Gene on Chromosome 16 Cause

Familial Amyotrophic Lateral Sclerosis. *Science*, *323*(5918), 1205-1208. https://doi.org/doi:10.1126/science.1166066

Lagier-Tourenne, C., Polymenidou, M., & Cleveland, D. W. (2010). TDP-43 and FUS/TLS: emerging roles in RNA processing and neurodegeneration. *Human Molecular Genetics*, *19*(R1), R46-R64. https://doi.org/10.1093/hmg/ddq137

Lagier-Tourenne, C., Polymenidou, M., Hutt, K. R., Vu, A. Q., Baughn, M., Huelga, S. C., Clutario, K. M., Ling, S. C., Liang, T. Y., Mazur, C., Wancewicz, E., Kim, A. S., Watt, A., Freier, S., Hicks, G. G., Donohue, J. P., Shiue, L., Bennett, C. F., Ravits, J., . . . Yeo, G. W. (2012). Divergent roles of ALS-linked proteins FUS/TLS and TDP-43 intersect in processing long pre-mRNAs. *Nat Neurosci*, *15*(11), 1488-1497. https://doi.org/10.1038/nn.3230

Lai, S.-L., Abramzon, Y., Schymick, J. C., Stephan, D. A., Dunckley, T., Dillman, A., Cookson, M., Calvo, A., Battistini, S., Giannini, F., Caponnetto, C., Mancardi, G. L., Spataro, R., Monsurro, M. R., Tedeschi, G., Marinou, K., Sabatelli, M., Conte, A., Mandrioli, J., . . . Traynor, B. J. (2011). FUS mutations in sporadic amyotrophic lateral sclerosis. *Neurobiology of Aging*, *32*(3), 550.e551-550.e554. https://doi.org/10.1016/j.neurobiolaging.2009.12.020

Ling, S. C., Dastidar, S. G., Tokunaga, S., Ho, W. Y., Lim, K., Ilieva, H., Parone, P. A., Tyan, S. H., Tse, T. M., Chang, J. C., Platoshyn, O., Bui, N. B., Bui, A., Vetto, A., Sun, S., McAlonis-Downes, M., Han, J. S., Swing, D., Kapeli, K., . . . Cleveland, D. W. (2019). Overriding FUS autoregulation in mice triggers gain-of-toxic dysfunctions in RNA metabolism and autophagy-lysosome axis. *Elife*, *8*. https://doi.org/10.7554/eLife.40811

Ling, S. C., Polymenidou, M., & Cleveland, D. W. (2013). Converging mechanisms in ALS and FTD: disrupted RNA and protein homeostasis. *Neuron*, *79*(3), 416-438. https://doi.org/10.1016/j.neuron.2013.07.033

Liu, Y., Beyer, A., & Aebersold, R. (2016). On the Dependency of Cellular Protein Levels on mRNA Abundance. *Cell*, *165*(3), 535-550. https://doi.org/10.1016/j.cell.2016.03.014

Logroscino, G., Traynor, B. J., Hardiman, O., Chio, A., Mitchell, D., Swingler, R. J., Millul, A., Benn, E., Beghi, E., & Eurals. (2010). Incidence of amyotrophic lateral sclerosis in Europe. *J Neurol Neurosurg Psychiatry*, *81*(4), 385-390. https://doi.org/10.1136/jnnp.2009.183525

Lopez-Erauskin, J., Tadokoro, T., Baughn, M. W., Myers, B., McAlonis-Downes, M., Chillon-Marinas, C., Asiaban, J. N., Artates, J., Bui, A. T., Vetto, A. P., Lee, S. K., Le, A. V., Sun, Y., Jambeau, M., Boubaker, J., Swing, D., Qiu, J., Hicks, G. G., Ouyang, Z., . . . Da Cruz, S. (2018). ALS/FTD-Linked Mutation in FUS Suppresses Intra-axonal Protein Synthesis and Drives Disease Without Nuclear Loss-of-Function of FUS. *Neuron*, *100*(4), 816-830 e817. https://doi.org/10.1016/j.neuron.2018.09.044

Loughlin, F. E., Lukavsky, P. J., Kazeeva, T., Reber, S., Hock, E.-M., Colombo, M., Von Schroetter, C., Pauli, P., Cléry, A., Mühlemann, O., Polymenidou, M., Ruepp, M.-D., & Allain, F. H.-T. (2019). The Solution Structure of FUS Bound to RNA Reveals a Bipartite Mode of RNA Recognition with Both Sequence and Shape Specificity. *Molecular Cell*, *73*(3), 490-504.e496. https://doi.org/10.1016/j.molcel.2018.11.012

Lule, D., Ludolph, A. C., & Ludolph, A. G. (2008). Neurodevelopmental and neurodegenerative diseases - is there a pathophysiological link? Attention-deficit/hyperactivity disorder and amyotrophic lateral sclerosis as examples. *Med Hypotheses*, *70*(6), 1133-1138. https://doi.org/10.1016/j.mehy.2007.11.002

Mackenzie, I. R., Rademakers, R., & Neumann, M. (2010). TDP-43 and FUS in amyotrophic lateral sclerosis and frontotemporal dementia. *Lancet Neurol*, *9*(10), 995-1007. https://doi.org/10.1016/S1474-4422(10)70195-2

Mackenzie, I. R. A., & Neumann, M. (2012). FET proteins in frontotemporal dementia and amyotrophic lateral sclerosis. *Brain Research*, *1462*, 40-43. https://doi.org/10.1016/j.brainres.2011.12.010

Mackenzie, I. R. A., Neumann, M., Bigio, E. H., Cairns, N. J., Alafuzoff, I., Kril, J., Kovacs, G. G., Ghetti, B., Halliday, G., Holm, I. E., Ince, P. G., Kamphorst, W., Revesz, T., Rozemuller, A. J. M., Kumar-Singh, S., Akiyama, H., Baborie, A., Spina, S., Dickson, D. W., . . . Mann, D. M. A. (2010). Nomenclature and nosology for neuropathologic subtypes of frontotemporal lobar degeneration: an update. *Acta Neuropathologica*, *119*(1), 1-4. https://doi.org/10.1007/s00401-009-0612-2

Maharana, S., Wang, J., Papadopoulos, D. K., Richter, D., Pozniakovsky, A., Poser, I., Bickle, M., Rizk, S., Guillen-Boixet, J., Franzmann, T. M., Jahnel, M., Marrone, L., Chang, Y. T., Sterneckert, J., Tomancak, P., Hyman, A. A., & Alberti, S. (2018). RNA buffers the phase separation behavior of prion-like RNA binding proteins. *Science*, *360*(6391), 918-921. https://doi.org/10.1126/science.aar7366

Mamontova, E. M., Clement, M. J., Sukhanova, M. V., Joshi, V., Bouhss, A., Rengifo-Gonzalez, J. C., Desforges, B., Hamon, L., Lavrik, O. I., & Pastre, D. (2023). FUS RRM regulates poly(ADP-ribose) levels after transcriptional arrest and PARP-1 activation on DNA damage. *Cell Rep*, *42*(10), 113199. https://doi.org/10.1016/j.celrep.2023.113199

Marin, B., Boumediene, F., Logroscino, G., Couratier, P., Babron, M. C., Leutenegger, A. L., Copetti, M., Preux, P. M., & Beghi, E. (2017). Variation in worldwide incidence of amyotrophic lateral sclerosis: a meta-analysis. *Int J Epidemiol*, *46*(1), 57-74. https://doi.org/10.1093/ije/dyw061

Marrone, L., Poser, I., Casci, I., Japtok, J., Reinhardt, P., Janosch, A., Andree, C., Lee, H. O., Moebius, C., Koerner, E., Reinhardt, L., Cicardi, M. E., Hackmann, K., Klink, B., Poletti, A., Alberti, S., Bickle, M., Hermann, A., Pandey, U. B., . . . Sterneckert, J. L. (2018). Isogenic FUS-eGFP iPSC Reporter Lines Enable Quantification of FUS Stress Granule Pathology that Is Rescued by Drugs Inducing Autophagy. *Stem Cell Reports*, *10*(2), 375-389. https://doi.org/10.1016/j.stemcr.2017.12.018

Masrori, P., & Van Damme, P. (2020). Amyotrophic lateral sclerosis: a clinical review. *European Journal of Neurology*, *27*(10), 1918-1929. https://doi.org/10.1111/ene.14393

Mastrocola, A. S., Kim, S. H., Trinh, A. T., Rodenkirch, L. A., & Tibbetts, R. S. (2013). The RNA-binding protein fused in sarcoma (FUS) functions downstream of poly(ADP-ribose) polymerase (PARP) in response to DNA damage. *J Biol Chem*, *288*(34), 24731-24741. https://doi.org/10.1074/jbc.M113.497974

Masuda, A., Takeda, J., Okuno, T., Okamoto, T., Ohkawara, B., Ito, M., Ishigaki, S., Sobue, G., & Ohno, K. (2015). Position-specific binding of FUS to nascent RNA regulates mRNA length. *Genes Dev*, *29*(10), 1045-1057. https://doi.org/10.1101/gad.255737.114

Mejzini, R., Flynn, L. L., Pitout, I. L., Fletcher, S., Wilton, S. D., & Akkari, P. A. (2019). ALS Genetics, Mechanisms, and Therapeutics: Where Are We Now? *Front Neurosci*, *13*, 1310. https://doi.org/10.3389/fnins.2019.01310

Millecamps, S., Boillée, S., Le Ber, I., Seilhean, D., Teyssou, E., Giraudeau, M., Moigneu, C., Vandenberghe, N., Danel-Brunaud, V., Corcia, P., Pradat, P.-F., Le Forestier, N., Lacomblez, L., Bruneteau, G., Camu, W., Brice, A., Cazeneuve, C., Leguern, E., Meininger, V., & Salachas, F. (2012). Phenotype difference between ALS patients with expanded repeats inC9ORF72and patients with mutations in other ALS-related genes. *Journal of Medical Genetics*, *49*(4), 258-263. https://doi.org/10.1136/jmedgenet-2011-100699

Miller, T. M., Cudkowicz, M. E., Genge, A., Shaw, P. J., Sobue, G., Bucelli, R. C., Chio, A., Van Damme, P., Ludolph, A. C., Glass, J. D., Andrews, J. A., Babu, S., Benatar, M., McDermott, C. J., Cochrane, T., Chary, S., Chew, S., Zhu, H., Wu, F., . . . Group, O. L. E. W. (2022). Trial of Antisense Oligonucleotide Tofersen for SOD1 ALS. *N Engl J Med*, *387*(12), 1099-1110. https://doi.org/10.1056/NEJMoa2204705

Mitchell, J. C., Mcgoldrick, P., Vance, C., Hortobagyi, T., Sreedharan, J., Rogelj, B., Tudor, E. L., Smith, B. N., Klasen, C., Miller, C. C. J., Cooper, J. D., Greensmith, L., & Shaw, C. E. (2013). Overexpression of human wild-type FUS causes progressive motor neuron degeneration in an age- and dose-dependent fashion. *Acta Neuropathologica*, *125*(2), 273-288. https://doi.org/10.1007/s00401-012-1043-z

Mitsumoto, H., Brooks, B. R., & Silani, V. (2014). Clinical trials in amyotrophic lateral sclerosis: why so many negative trials and how can trials be improved? *Lancet Neurol*, *13*(11), 1127-1138. https://doi.org/10.1016/S1474-4422(14)70129-2

Molliex, A., Temirov, J., Lee, J., Coughlin, M., Kanagaraj, A. P., Kim, H. J., Mittag, T., & Taylor, J. P. (2015). Phase separation by low complexity domains promotes stress granule assembly and drives pathological fibrillization. *Cell*, *163*(1), 123-133. https://doi.org/10.1016/j.cell.2015.09.015

Moore, A., Young, C. A., & Hughes, D. A. (2019). Health Utilities and Costs for Motor Neurone Disease. *Value in Health*, *22*(11), 1257-1265. https://doi.org/10.1016/j.jval.2019.05.011

Murthy, A. C., Tang, W. S., Jovic, N., Janke, A. M., Seo, D. H., Perdikari, T. M., Mittal, J., & Fawzi, N. L. (2021). Molecular interactions contributing to FUS SYGQ LC-RGG phase separation and co-partitioning with RNA polymerase II heptads. *Nature Structural & Molecular Biology*, *28*(11), 923-935. https://doi.org/10.1038/s41594-021-00677-4

Muyderman, H., & Chen, T. (2014). Mitochondrial dysfunction in amyotrophic lateral sclerosis - a valid pharmacological target? *Br J Pharmacol*, *171*(8), 2191-2205. https://doi.org/10.1111/bph.12476

Nagano, S., Takahashi, Y., Yamamoto, K., Masutani, H., Fujiwara, N., Urushitani, M., & Araki, T. (2015). A cysteine residue affects the conformational state and neuronal toxicity of mutant SOD1 in mice: relevance to the pathogenesis of ALS. *Hum Mol Genet*, *24*(12), 3427-3439. https://doi.org/10.1093/hmg/ddv093

Nakaya, T., Alexiou, P., Maragkakis, M., Chang, A., & Mourelatos, Z. (2013). FUS regulates genes coding for RNA-binding proteins in neurons by binding to their highly conserved introns. *RNA*, *19*(4), 498-509. https://doi.org/10.1261/rna.037804.112

Naumann, M., Peikert, K., Günther, R., Van Der Kooi, A. J., Aronica, E., Hübers, A., Danel, V., Corcia, P., Pan-Montojo, F., Cirak, S., Haliloglu, G., Ludolph, A. C., Goswami, A., Andersen, P. M., Prudlo, J., Wegner, F., Van Damme, P., Weishaupt, J. H., & Hermann, A. (2019). Phenotypes and malignancy risk of different FUS mutations in genetic amyotrophic lateral sclerosis. *Annals of Clinical and Translational Neurology*, *6*(12), 2384-2394. https://doi.org/10.1002/acn3.50930

Neumann, M., Rademakers, R., Roeber, S., Baker, M., Kretzschmar, H. A., & Mackenzie, I. R. A. (2009). A new subtype of frontotemporal lobar degeneration with FUS pathology. *Brain*, *132*(11), 2922-2931. https://doi.org/10.1093/brain/awp214

Ngo, S. T., Steyn, F. J., & McCombe, P. A. (2014). Body mass index and dietary intervention: implications for prognosis of amyotrophic lateral sclerosis. *J Neurol Sci*, *340*(1-2), 5-12. https://doi.org/10.1016/j.jns.2014.02.035

Niccoli, T., Partridge, L., & Isaacs, A. M. (2017). Ageing as a risk factor for ALS/FTD. *Hum Mol Genet*, *26*(R2), R105-R113. https://doi.org/10.1093/hmg/ddx247

Nolan, M., Talbot, K., & Ansorge, O. (2016). Pathogenesis of FUS-associated ALS and FTD: insights from rodent models. *Acta Neuropathol Commun*, *4*(1), 99. https://doi.org/10.1186/s40478-016-0358-8

Oddoux, S., Brocard, J., Schweitzer, A., Szentesi, P., Giannesini, B., Brocard, J., Fauré, J., Pernet-Gallay, K., Bendahan, D., Lunardi, J., Csernoch, L., & Marty, I. (2009). Triadin Deletion Induces Impaired Skeletal Muscle Function. *Journal of Biological Chemistry*, *284*(50), 34918-34929. https://doi.org/10.1074/jbc.m109.022442

Patel, A., Lee, H. O., Jawerth, L., Maharana, S., Jahnel, M., Hein, M. Y., Stoynov, S., Mahamid, J., Saha, S., Franzmann, T. M., Pozniakovski, A., Poser, I., Maghelli, N., Royer, L. A., Weigert, M., Myers, E. W., Grill, S., Drechsel, D., Hyman, A. A., & Alberti, S. (2015). A Liquid-to-Solid Phase Transition of the ALS Protein FUS Accelerated by Disease Mutation. *Cell*, *162*(5), 1066-1077. https://doi.org/10.1016/j.cell.2015.07.047

Patel, T., Hammelman, J., Aziz, S., Jang, S., Closser, M., Michaels, T. L., Blum, J. A., Gifford, D. K., & Wichterle, H. (2022). Transcriptional dynamics of murine motor neuron maturation in vivo and in vitro. *Nat Commun*, *13*(1), 5427. https://doi.org/10.1038/s41467-022-33022-4

Payne, B. A., & Chinnery, P. F. (2015). Mitochondrial dysfunction in aging: Much progress but many unresolved questions. *Biochim Biophys Acta*, *1847*(11), 1347-1353. https://doi.org/10.1016/j.bbabio.2015.05.022

Perri, E. R., Parakh, S., Vidal, M., Mehta, P., Ma, Y., Walker, A. K., & Atkin, J. D. (2020). The Cysteine (Cys) Residues Cys-6 and Cys-111 in Mutant Superoxide Dismutase 1 (SOD1) A4V Are Required for Induction of Endoplasmic Reticulum Stress in Amyotrophic Lateral Sclerosis. *Journal of Molecular Neuroscience*, *70*(9), 1357-1368. https://doi.org/10.1007/s12031-020-01551-6

Picchiarelli, G., Demestre, M., Zuko, A., Been, M., Higelin, J., Dieterlé, S., Goy, M.-A., Mallik, M., Sellier, C., Scekic-Zahirovic, J., Zhang, L., Rosenbohm, A., Sijlmans, C., Aly, A., Mersmann, S., Sanjuan-Ruiz, I., Hübers, A., Messaddeq, N., Wagner, M., . . . Storkebaum, E. (2019). FUS-mediated regulation of acetylcholine receptor transcription at neuromuscular junctions is compromised in amyotrophic lateral sclerosis. *Nature Neuroscience*, *22*(11), 1793-1805. https://doi.org/10.1038/s41593-019-0498-9

Picchiarelli, G., Demestre, M., Zuko, A., Been, M., Higelin, J., Dieterle, S., Goy, M. A., Mallik, M., Sellier, C., Scekic-Zahirovic, J., Zhang, L., Rosenbohm, A., Sijlmans, C., Aly, A., Mersmann, S., Sanjuan-Ruiz, I., Hubers, A., Messaddeq, N., Wagner, M., . . . Storkebaum, E. (2019). FUS-mediated regulation of acetylcholine receptor transcription at neuromuscular junctions is compromised in amyotrophic lateral sclerosis. *Nat Neurosci*, *22*(11), 1793-1805. https://doi.org/10.1038/s41593-019-0498-9

Picher-Martel, V., Brunet, F., Dupre, N., & Chrestian, N. (2020). The Occurrence of FUS Mutations in Pediatric Amyotrophic Lateral Sclerosis: A Case Report and Review of the Literature. *J Child Neurol*, *35*(8), 556-562. https://doi.org/10.1177/0883073820915099

Piol, D., Robberechts, T., & Da Cruz, S. (2023). Lost in local translation: TDP-43 and FUS in axonal/neuromuscular junction maintenance and dysregulation in amyotrophic lateral sclerosis. *Neuron*, *111*(9), 1355-1380. https://doi.org/10.1016/j.neuron.2023.02.028

Prasad, A., Bharathi, V., Sivalingam, V., Girdhar, A., & Patel, B. K. (2019). Molecular Mechanisms of TDP-43 Misfolding and Pathology in Amyotrophic Lateral Sclerosis. *Front Mol Neurosci*, *12*, 25. https://doi.org/10.3389/fnmol.2019.00025

Qiu, H., Lee, S., Shang, Y., Wang, W.-Y., Au, K. F., Kamiya, S., Barmada, S. J., Finkbeiner, S., Lui, H., Carlton, C. E., Tang, A. A., Oldham, M. C., Wang, H., Shorter, J., Filiano, A. J., Roberson, E. D., Tourtellotte, W. G., Chen, B., Tsai, L.-H., & Huang, E. J. (2014). ALS-associated mutation FUS-R521C causes DNA damage and RNA splicing defects. *Journal of Clinical Investigation*, *124*(3), 981-999. https://doi.org/10.1172/jci72723

Reber, S., Jutzi, D., Lindsay, H., Devoy, A., Mechtersheimer, J., Levone, B. R., Domanski, M., Bentmann, E., Dormann, D., Muhlemann, O., Barabino, S. M. L., & Ruepp, M. D. (2021). The phase separation-dependent FUS interactome reveals nuclear and cytoplasmic function of liquid-liquid phase separation. *Nucleic Acids Res*, *49*(13), 7713-7731. https://doi.org/10.1093/nar/gkab582

Reber, S., Stettler, J., Filosa, G., Colombo, M., Jutzi, D., Lenzken, S. C., Schweingruber, C., Bruggmann, R., Bachi, A., Barabino, S. M., Mühlemann, O., & Ruepp, M. D. (2016). Minor intron splicing is regulated by

<scp>FUS</scp>

and affected by

<scp>ALS</scp>

-associated

<scp>FUS</scp>

mutants. *The EMBO Journal*, *35*(14), 1504-1521. https://doi.org/10.15252/embj.201593791

Robinson, H. K., Deykin, A. V., Bronovitsky, E. V., Ovchinnikov, R. K., Ustyugov, A. A., Shelkovnikova, T. A., Kukharsky, M. S., Ermolkevich, T. G., Goldman, I. L., Sadchikova, E. R., Kovrazhkina, E. A., Bachurin, S. O., Buchman, V. L., & Ninkina, N. N. (2015). Early lethality and neuronal proteinopathy in mice expressing cytoplasm-targeted FUS that lacks the RNA recognition motif. *Amyotroph Lateral Scler Frontotemporal Degener*, *16*(5-6), 402-409. https://doi.org/10.3109/21678421.2015.1040994

Rogelj, B., Easton, L. E., Bogu, G. K., Stanton, L. W., Rot, G., Curk, T., Zupan, B., Sugimoto, Y., Modic, M., Haberman, N., Tollervey, J., Fujii, R., Takumi, T., Shaw, C. E., & Ule, J. (2012). Widespread binding of FUS along nascent RNA regulates alternative splicing in the brain. *Sci Rep*, *2*, 603. https://doi.org/10.1038/srep00603

Rosen, D. R., Siddique, T., Patterson, D., Figlewicz, D. A., Sapp, P., Hentati, A., Donaldson, D., Goto, J., O'Regan, J. P., Deng, H.-X., Rahmani, Z., Krizus, A., Mckenna-Yasek, D., Cayabyab, A., Gaston, S. M., Berger, R., Tanzi, R. E., Halperin, J. J., Herzfeldt, B., . . . Brown, R. H. (1993). Mutations in Cu/Zn superoxide dismutase gene are associated with familial amyotrophic lateral sclerosis. *Nature*, *362*(6415), 59-62. https://doi.org/10.1038/362059a0

Rosenstein, J. M., Krum, J. M., & Ruhrberg, C. (2010). VEGF in the nervous system. *Organogenesis*, *6*(2), 107-114. https://doi.org/10.4161/org.6.2.11687

Rusina, R., Vandenberghe, R., & Bruffaerts, R. (2021). Cognitive and Behavioral Manifestations in ALS: Beyond Motor System Involvement. *Diagnostics*, *11*(4), 624. https://doi.org/10.3390/diagnostics11040624

Sabatelli, M., Moncada, A., Conte, A., Lattante, S., Marangi, G., Luigetti, M., Lucchini, M., Mirabella, M., Romano, A., Del Grande, A., Bisogni, G., Doronzio, P. N., Rossini, P. M., & Zollino, M. (2013). Mutations in the 3' untranslated region of FUS causing FUS overexpression are associated with amyotrophic lateral sclerosis. *Hum Mol Genet*, *22*(23), 4748-4755. https://doi.org/10.1093/hmg/ddt328

Saberi, S., Stauffer, J. E., Schulte, D. J., & Ravits, J. (2015). Neuropathology of Amyotrophic Lateral Sclerosis and Its Variants. *Neurologic Clinics*, *33*(4), 855-876. https://doi.org/10.1016/j.ncl.2015.07.012

Sadaki, S., Fujita, R., Hayashi, T., Nakamura, A., Okamura, Y., Fuseya, S., Hamada, M., Warabi, E., Kuno, A., Ishii, A., Muratani, M., Okada, R., Shiba, D., Kudo, T., Takeda, S., & Takahashi, S. (2023). Large Maf transcription factor family is a major regulator of fast type IIb myofibre determination. *Cell Rep*, *42*(4), 112289. https://doi.org/10.1016/j.celrep.2023.112289

Sahadevan, S., Hembach, K. M., Tantardini, E., Pérez-Berlanga, M., Hruska-Plochan, M., Megat, S., Weber, J., Schwarz, P., Dupuis, L., Robinson, M. D., De Rossi, P., & Polymenidou, M. (2021). Synaptic FUS accumulation triggers early misregulation of synaptic RNAs in a

mouse model of ALS. *Nature Communications*, *12*(1). https://doi.org/10.1038/s41467-021-23188-8

Salam, S., Tacconelli, S., Smith, B. N., Mitchell, J. C., Glennon, E., Nikolaou, N., Houart, C., & Vance, C. (2021). Identification of a novel interaction of FUS and syntaphilin may explain synaptic and mitochondrial abnormalities caused by ALS mutations. *Sci Rep*, *11*(1), 13613. https://doi.org/10.1038/s41598-021-93189-6

Sama, R. R. K., Ward, C. L., Kaushansky, L. J., Lemay, N., Ishigaki, S., Urano, F., & Bosco, D. A. (2013). FUS/TLS assembles into stress granules and is a prosurvival factor during hyperosmolar stress. *Journal of Cellular Physiology*, *228*(11), 2222-2231. https://doi.org/10.1002/jcp.24395

Sasayama, H., Shimamura, M., Tokuda, T., Azuma, Y., Yoshida, T., Mizuno, T., Nakagawa, M., Fujikake, N., Nagai, Y., & Yamaguchi, M. (2012). Knockdown of the Drosophila fused in sarcoma (FUS) homologue causes deficient locomotive behavior and shortening of motoneuron terminal branches. *PLoS One*, *7*(6), e39483. https://doi.org/10.1371/journal.pone.0039483

Scekic-Zahirovic, J., Oussini, H. E., Mersmann, S., Drenner, K., Wagner, M., Sun, Y., Allmeroth, K., Dieterlé, S., Sinniger, J., Dirrig-Grosch, S., René, F., Dormann, D., Haass, C., Ludolph, A. C., Lagier-Tourenne, C., Storkebaum, E., & Dupuis, L. (2017). Motor neuron intrinsic and extrinsic mechanisms contribute to the pathogenesis of FUS-associated amyotrophic lateral sclerosis. *Acta Neuropathologica*, *133*(6), 887-906. https://doi.org/10.1007/s00401-017-1687-9

Scekic-Zahirovic, J., Sanjuan-Ruiz, I., Kan, V., Megat, S., De Rossi, P., Dieterlé, S., Cassel, R., Jamet, M., Kessler, P., Wiesner, D., Tzeplaeff, L., Demais, V., Sahadevan, S., Hembach, K. M., Muller, H.-P., Picchiarelli, G., Mishra, N., Antonucci, S., Dirrig-Grosch, S., . . . Dupuis, L. (2021). Cytoplasmic FUS triggers early behavioral alterations linked to cortical neuronal hyperactivity and inhibitory synaptic defects. *Nature Communications*, *12*(1). https://doi.org/10.1038/s41467-021-23187-9

Scekic-Zahirovic, J., Sendscheid, O., El Oussini, H., Jambeau, M., Sun, Y., Mersmann, S., Wagner, M., Dieterle, S., Sinniger, J., Dirrig-Grosch, S., Drenner, K., Birling, M. C., Qiu, J., Zhou, Y., Li, H., Fu, X. D., Rouaux, C., Shelkovnikova, T., Witting, A., . . . Dupuis, L. (2016). Toxic gain of function from mutant FUS protein is crucial to trigger cell autonomous motor neuron loss. *EMBO J*, *35*(10), 1077-1097. https://doi.org/10.15252/embj.201592559

Schoen, M., Reichel, J. M., Demestre, M., Putz, S., Deshpande, D., Proepper, C., Liebau, S., Schmeisser, M. J., Ludolph, A. C., Michaelis, J., & Boeckers, T. M. (2015). Super-Resolution Microscopy Reveals Presynaptic Localization of the ALS/FTD Related Protein FUS in Hippocampal Neurons. *Front Cell Neurosci*, *9*, 496. https://doi.org/10.3389/fncel.2015.00496

Schwartz, J. C., Ebmeier, C. C., Podell, E. R., Heimiller, J., Taatjes, D. J., & Cech, T. R. (2012). FUS binds the CTD of RNA polymerase II and regulates its phosphorylation at Ser2. *Genes Dev*, *26*(24), 2690-2695. https://doi.org/10.1101/gad.204602.112

Schwartz, J. C., Podell, E. R., Han, S. S. W., Berry, J. D., Eggan, K. C., & Cech, T. R. (2014). FUS is sequestered in nuclear aggregates in ALS patient fibroblasts. *Molecular Biology of the Cell*, *25*(17), 2571-2578. https://doi.org/10.1091/mbc.e14-05-1007

Sephton, C. F., Tang, A. A., Kulkarni, A., West, J., Brooks, M., Stubblefield, J. J., Liu, Y., Zhang, M. Q., Green, C. B., Huber, K. M., Huang, E. J., Herz, J., & Yu, G. (2014). Activity-dependent FUS dysregulation disrupts synaptic homeostasis. *Proceedings of the National Academy of Sciences*, *111*(44), E4769-E4778. https://doi.org/10.1073/pnas.1406162111

Sévigny, M., Bourdeau Julien, I., Venkatasubramani, J. P., Hui, J. B., Dutchak, P. A., & Sephton, C. F. (2020). FUS contributes to mTOR-dependent inhibition of translation. *Journal of Biological Chemistry*, *295*(52), 18459-18473. https://doi.org/10.1074/jbc.ra120.013801

Shang, Y., & Huang, E. J. (2016). Mechanisms of FUS mutations in familial amyotrophic lateral sclerosis. *Brain Res*, *1647*, 65-78. https://doi.org/10.1016/j.brainres.2016.03.036

Sharma, A., Lyashchenko, A. K., Lu, L., Nasrabady, S. E., Elmaleh, M., Mendelsohn, M., Nemes, A., Tapia, J. C., Mentis, G. Z., & Shneider, N. A. (2016). ALS-associated mutant FUS induces selective motor neuron degeneration through toxic gain of function. *Nature Communications*, *7*(1), 10465. https://doi.org/10.1038/ncomms10465

Shefner, J. M., Musaro, A., Ngo, S. T., Lunetta, C., Steyn, F. J., Robitaille, R., De Carvalho, M., Rutkove, S., Ludolph, A. C., & Dupuis, L. (2023). Skeletal muscle in amyotrophic lateral sclerosis. *Brain*. https://doi.org/10.1093/brain/awad202

Shelkovnikova, T. A., An, H., Skelt, L., Tregoning, J. S., Humphreys, I. R., & Buchman, V. L. (2019). Antiviral Immune Response as a Trigger of FUS Proteinopathy in Amyotrophic Lateral Sclerosis. *Cell Rep*, *29*(13), 4496-4508 e4494. https://doi.org/10.1016/j.celrep.2019.11.094

Shelkovnikova, T. A., Peters, O. M., Deykin, A. V., Connor-Robson, N., Robinson, H., Ustyugov, A. A., Bachurin, S. O., Ermolkevich, T. G., Goldman, I. L., Sadchikova, E. R., Kovrazhkina, E. A., Skvortsova, V. I., Ling, S.-C., Da Cruz, S., Parone, P. A., Buchman, V. L., & Ninkina, N. N. (2013). Fused in Sarcoma (FUS) Protein Lacking Nuclear Localization Signal (NLS) and Major RNA Binding Motifs Triggers Proteinopathy and Severe Motor Phenotype in Transgenic Mice. *Journal of Biological Chemistry*, *288*(35), 25266-25274. https://doi.org/10.1074/jbc.m113.492017

Shelkovnikova, T. A., Robinson, H. K., Troakes, C., Ninkina, N., & Buchman, V. L. (2014). Compromised paraspeckle formation as a pathogenic factor in FUSopathies. *Hum Mol Genet*, *23*(9), 2298-2312. https://doi.org/10.1093/hmg/ddt622

Shepheard, S. R., Parker, M. D., Cooper-Knock, J., Verber, N. S., Tuddenham, L., Heath, P., Beauchamp, N., Place, E., Sollars, E. S. A., Turner, M. R., Malaspina, A., Fratta, P., Hewamadduma, C., Jenkins, T. M., Mcdermott, C. J., Wang, D., Kirby, J., & Shaw, P. J. (2021). Value of systematic genetic screening of patients with amyotrophic lateral sclerosis. *Journal of Neurology, Neurosurgery & Psychiatry*, *92*(5), 510-518. https://doi.org/10.1136/jnnp-2020-325014

Shiihashi, G., Ito, D., Yagi, T., Nihei, Y., Ebine, T., & Suzuki, N. (2016). Mislocated FUS is sufficient for gain-of-toxic-function amyotrophic lateral sclerosis phenotypes in mice. *Brain*, *139*(Pt 9), 2380-2394. https://doi.org/10.1093/brain/aww161

Smith, E. F., Shaw, P. J., & De Vos, K. J. (2019). The role of mitochondria in amyotrophic lateral sclerosis. *Neuroscience Letters*, *710*. https://doi.org/10.1016/j.neulet.2017.06.052

So, E., Mitchell, J. C., Memmi, C., Chennell, G., Vizcay-Barrena, G., Allison, L., Shaw, C. E., & Vance, C. (2018). Mitochondrial abnormalities and disruption of the neuromuscular junction precede the clinical phenotype and motor neuron loss in hFUSWT transgenic mice. *Hum Mol Genet*, *27*(3), 463-474. https://doi.org/10.1093/hmg/ddx415

Soo, K. Y., Sultana, J., King, A., Atkinson, R., Warraich, S. T., Sundaramoorthy, V., Blair, I., Farg, M. A., & Atkin, J. D. (2015). ALS-associated mutant FUS inhibits macroautophagy which is restored by overexpression of Rab1. *Cell Death Discovery*, *1*(1), 15030. https://doi.org/10.1038/cddiscovery.2015.30

Stoica, R., Paillusson, S., Gomez-Suaga, P., Mitchell, J. C., Lau, D. H., Gray, E. H., Sancho, R. M., Vizcay-Barrena, G., De Vos, K. J., Shaw, C. E., Hanger, D. P., Noble, W., & Miller, C. C. (2016). <scp>ALS</scp>

/

<scp>FTD</scp>

-associated

<scp>FUS</scp>

activates

<scp>GSK</scp>

-3β to disrupt the

<scp>VAPB</scp>

–

<scp>PTPIP</sc. *EMBO reports*, *17*(9), 1326-1342. https://doi.org/10.15252/embr.201541726

Sun, Z., Diaz, Z., Fang, X., Hart, M. P., Chesi, A., Shorter, J., & Gitler, A. D. (2011). Molecular determinants and genetic modifiers of aggregation and toxicity for the ALS disease protein FUS/TLS. *PLoS Biol*, *9*(4), e1000614. https://doi.org/10.1371/journal.pbio.1000614

Szewczyk, B., Gunther, R., Japtok, J., Frech, M. J., Naumann, M., Lee, H. O., & Hermann, A. (2023). FUS ALS neurons activate major stress pathways and reduce translation as an early protective mechanism against neurodegeneration. *Cell Rep*, *42*(2), 112025. https://doi.org/10.1016/j.celrep.2023.112025

Tauffenberger, A., Vaccaro, A., Aulas, A., Vande Velde, C., & Parker, J. A. (2012). Glucose delays age-dependent proteotoxicity. *Aging Cell*, *11*(5), 856-866. https://doi.org/10.1111/j.1474-9726.2012.00855.x

Tetter, S., Arseni, D., Murzin, A. G., Buhidma, Y., Peak-Chew, S. Y., Garringer, H. J., Newell, K. L., Vidal, R., Apostolova, L. G., Lashley, T., Ghetti, B., & Ryskeldi-Falcon, B. (2023). TAF15 amyloid filaments in frontotemporal lobar degeneration. *Nature*. https://doi.org/10.1038/s41586-023-06801-2

Thompson, A. G., Gray, E., Verber, N., Bobeva, Y., Lombardi, V., Shepheard, S. R., Yildiz, O., Feneberg, E., Farrimond, L., Dharmadasa, T., Gray, P., Edmond, E. C., Scaber, J., Gagliardi, D., Kirby, J., Jenkins, T. M., Fratta, P., McDermott, C. J., Manohar, S. G., . . . Turner, M. R. (2022). Multicentre appraisal of amyotrophic lateral sclerosis biofluid biomarkers shows primacy of blood neurofilament light chain. *Brain Commun*, *4*(1), fcac029. https://doi.org/10.1093/braincomms/fcac029

Tibshirani, M., Tradewell, M. L., Mattina, K. R., Minotti, S., Yang, W., Zhou, H., Strong, M. J., Hayward, L. J., & Durham, H. D. (2015). Cytoplasmic sequestration of FUS/TLS associated with ALS alters histone marks through loss of nuclear protein arginine methyltransferase 1. *Hum Mol Genet*, *24*(3), 773-786. https://doi.org/10.1093/hmg/ddu494

Todd, T. W., & Petrucelli, L. (2022). Modelling amyotrophic lateral sclerosis in rodents. *Nat Rev Neurosci*, *23*(4), 231-251. https://doi.org/10.1038/s41583-022-00564-x

Tsai, Y.-L., Coady, T. H., Lu, L., Zheng, D., Alland, I., Tian, B., Shneider, N. A., & Manley, J. L. (2020). ALS/FTD-associated protein FUS induces mitochondrial dysfunction by preferentially sequestering respiratory chain complex mRNAs. *Genes & Development*, *34*(11-12), 785-805. https://doi.org/10.1101/gad.335836.119

Turner, B. J., & Talbot, K. (2008). Transgenics, toxicity and therapeutics in rodent models of mutant SOD1-mediated familial ALS. *Prog Neurobiol*, *85*(1), 94-134. https://doi.org/10.1016/j.pneurobio.2008.01.001

Udagawa, T., Fujioka, Y., Tanaka, M., Honda, D., Yokoi, S., Riku, Y., Ibi, D., Nagai, T., Yamada, K., Watanabe, H., Katsuno, M., Inada, T., Ohno, K., Sokabe, M., Okado, H., Ishigaki, S., & Sobue, G. (2015). FUS regulates AMPA receptor function and FTLD/ALS-associated

behaviour via GluA1 mRNA stabilization. *Nature Communications*, *6*(1), 7098. https://doi.org/10.1038/ncomms8098

Valenzuela, D. M., Murphy, A. J., Frendewey, D., Gale, N. W., Economides, A. N., Auerbach, W., Poueymirou, W. T., Adams, N. C., Rojas, J., Yasenchak, J., Chernomorsky, R., Boucher, M., Elsasser, A. L., Esau, L., Zheng, J., Griffiths, J. A., Wang, X., Su, H., Xue, Y., . . . Yancopoulos, G. D. (2003). High-throughput engineering of the mouse genome coupled with high-resolution expression analysis. *Nature Biotechnology*, *21*(6), 652-659. https://doi.org/10.1038/nbt822

Vance, C., Rogelj, B., HortobáGyi, T., De Vos, K. J., Nishimura, A. L., Sreedharan, J., Hu, X., Smith, B., Ruddy, D., Wright, P., Ganesalingam, J., Williams, K. L., Tripathi, V., Al-Saraj, S., Al-Chalabi, A., Leigh, P. N., Blair, I. P., Nicholson, G., De Belleroche, J., . . . Shaw, C. E. (2009). Mutations in FUS, an RNA Processing Protein, Cause Familial Amyotrophic Lateral Sclerosis Type 6. *Science*, *323*(5918), 1208-1211. https://doi.org/10.1126/science.1165942

Vance, C., Scotter, E. L., Nishimura, A. L., Troakes, C., Mitchell, J. C., Kathe, C., Urwin, H., Manser, C., Miller, C. C., Hortobagyi, T., Dragunow, M., Rogelj, B., & Shaw, C. E. (2013). ALS mutant FUS disrupts nuclear localization and sequesters wild-type FUS within cytoplasmic stress granules. *Hum Mol Genet*, *22*(13), 2676-2688. https://doi.org/10.1093/hmg/ddt117

Verbeeck, C., Deng, Q., Dejesus-Hernandez, M., Taylor, G., Ceballos-Diaz, C., Kocerha, J., Golde, T., Das, P., Rademakers, R., Dickson, D. W., & Kukar, T. (2012). Expression of Fused in sarcoma mutations in mice recapitulates the neuropathology of FUS proteinopathies and provides insight into disease pathogenesis. *Molecular Neurodegeneration*, *7*(1), 53. https://doi.org/10.1186/1750-1326-7-53

Waibel, S., Neumann, M., Rosenbohm, A., Birve, A., Volk, A. E., Weishaupt, J. H., Meyer, T., Müller, U., Andersen, P. M., & Ludolph, A. C. (2013). Truncating mutations in <scp>FUS</scp>/<scp>TLS</scp> give rise to a more aggressive <scp>ALS</scp>-phenotype than missense mutations: a clinico-genetic study in <scp>G</scp>ermany. *European Journal of Neurology*, *20*(3), 540-546. https://doi.org/10.1111/ene.12031

Wang, W.-Y., Pan, L., Su, S. C., Quinn, E. J., Sasaki, M., Jimenez, J. C., Mackenzie, I. R. A., Huang, E. J., & Tsai, L.-H. (2013). Interaction of FUS and HDAC1 regulates DNA damage response and repair in neurons. *Nature Neuroscience*, *16*(10), 1383-1391. https://doi.org/10.1038/nn.3514

Wang, X., Arai, S., Song, X., Reichart, D., Du, K., Pascual, G., Tempst, P., Rosenfeld, M. G., Glass, C. K., & Kurokawa, R. (2008). Induced ncRNAs allosterically modify RNA-binding proteins in cis to inhibit transcription. *Nature*, *454*(7200), 126-130. https://doi.org/10.1038/nature06992

Wilson, L. A. B., Zajitschek, S. R. K., Lagisz, M., Mason, J., Haselimashhadi, H., & Nakagawa, S. (2022). Sex differences in allometry for phenotypic traits in mice indicate that females are not scaled males. *Nature Communications*, *13*(1). https://doi.org/10.1038/s41467-022-35266-6

Yadav, A., Matson, K. J. E., Li, L., Hua, I., Petrescu, J., Kang, K., Alkaslasi, M. R., Lee, D. I., Hasan, S., Galuta, A., Dedek, A., Ameri, S., Parnell, J., Alshardan, M. M., Qumqumji, F. A., Alhamad, S. M., Wang, A. P., Poulen, G., Lonjon, N., . . . Levine, A. J. (2023). A cellular taxonomy of the adult human spinal cord. *Neuron*, *111*(3), 328-344 e327. https://doi.org/10.1016/j.neuron.2023.01.007

Yamashita, S., Mori, A., Sakaguchi, H., Suga, T., Ishihara, D., Ueda, A., Yamashita, T., Maeda, Y., Uchino, M., & Hirano, T. (2012). Sporadic juvenile amyotrophic lateral sclerosis caused by mutant FUS/TLS: possible association of mental retardation with this mutation. *J Neurol*, *259*(6), 1039-1044. https://doi.org/10.1007/s00415-011-6292-6

Yang, L., Embree, L. J., Tsai, S., & Hickstein, D. D. (1998). Oncoprotein TLS Interacts with Serine-Arginine Proteins Involved in RNA Splicing. *Journal of Biological Chemistry*, *273*(43), 27761-27764. https://doi.org/10.1074/jbc.273.43.27761

Yasuda, K., Clatterbuck-Soper, S. F., Jackrel, M. E., Shorter, J., & Mili, S. (2017). FUS inclusions disrupt RNA localization by sequestering kinesin-1 and inhibiting microtubule detyrosination. *Journal of Cell Biology*, *216*(4), 1015-1034. https://doi.org/10.1083/jcb.201608022

Yasuda, K., Zhang, H., Loiselle, D., Haystead, T., Macara, I. G., & Mili, S. (2013). The RNA-binding protein Fus directs translation of localized mRNAs in APC-RNP granules. *J Cell Biol*, *203*(5), 737-746. https://doi.org/10.1083/jcb.201306058

Yokoi, S., Udagawa, T., Fujioka, Y., Honda, D., Okado, H., Watanabe, H., Katsuno, M., Ishigaki, S., & Sobue, G. (2017). 3'UTR Length-Dependent Control of SynGAP Isoform alpha2 mRNA by FUS and ELAV-like Proteins Promotes Dendritic Spine Maturation and Cognitive Function. *Cell Rep*, *20*(13), 3071-3084. https://doi.org/10.1016/j.celrep.2017.08.100

Zhang, W., Falcon, B., Murzin, A. G., Fan, J., Crowther, R. A., Goedert, M., & Scheres, S. H. (2019). Heparin-induced tau filaments are polymorphic and differ from those in Alzheimer's and Pick's diseases. *Elife*, *8*. https://doi.org/10.7554/eLife.43584

Zhang, X., Wang, F., Hu, Y., Chen, R., Meng, D., Guo, L., Lv, H., Guan, J., & Jia, Y. (2020). In vivo stress granule misprocessing evidenced in a FUS knock-in ALS mouse model. *Brain*, *143*(5), 1350-1367. https://doi.org/10.1093/brain/awaa076

Zhang, Z. C., & Chook, Y. M. (2012). Structural and energetic basis of ALS-causing mutations in the atypical proline–tyrosine nuclear localization signal of the Fused in Sarcoma protein (FUS). *Proceedings of the National Academy of Sciences*, *109*(30), 12017-12021. https://doi.org/10.1073/pnas.1207247109

Zhou, B., Wang, H., Cai, Y., Wen, H., Wang, L., Zhu, M., Chen, Y., Yu, Y., Lu, X., Zhou, M., Fang, P., Li, X., & Hong, D. (2020). FUS

P525L mutation causing amyotrophic lateral sclerosis and movement disorders. *Brain and Behavior*, *10*(6). https://doi.org/10.1002/brb3.1625

Zhou, B., Zheng, Y., Li, X., Dong, H., Yu, J., Zou, Y., Zhu, M., Yu, Y., Fang, X., Zhou, M., Zhang, W., Yuan, Y., Wang, Z., Deng, J., & Hong, D. (2022). FUS Mutation Causes Disordered Lipid Metabolism in Skeletal Muscle Associated with ALS. *Molecular Neurobiology*, *59*(12), 7265-7277. https://doi.org/10.1007/s12035-022-03048-2

Zhou, Y., Liu, S., Liu, G., Ozturk, A., & Hicks, G. G. (2013). ALS-associated FUS mutations result in compromised FUS alternative splicing and autoregulation. *PLoS Genet*, *9*(10), e1003895. https://doi.org/10.1371/journal.pgen.1003895

Zou, H., Wang, J. Y., Ma, G. M., Xu, M. M., Luo, F., Zhang, L., & Wang, W. Y. (2022). The function of FUS in neurodevelopment revealed by the brain and spinal cord organoids. *Mol Cell Neurosci*, *123*, 103771. https://doi.org/10.1016/j.mcn.2022.103771

Zou, Z. Y., Cui, L. Y., Sun, Q., Li, X. G., Liu, M. S., Xu, Y., Zhou, Y., & Yang, X. Z. (2013). De novo FUS gene mutations are associated with juvenile-onset sporadic amyotrophic lateral sclerosis in China. *Neurobiol Aging*, *34*(4), 1312 e1311-1318. https://doi.org/10.1016/j.neurobiolaging.2012.09.005

Manual References

Arce, V., Garces, A., de Bovis, B., Filippi, P., Henderson, C., Pettmann, B., & deLapeyrière, O. (1999). Cardiotrophin-1 requires LIFRbeta to promote survival of mouse motoneurons purified by a novel technique. *Journal of neuroscience research*, *55*(1), 119–126. https://doi.org/10.1002/(SICI)1097-4547(19990101)55:1<119::AID-JNR13>3.0.CO;2-6

Brain Research UK (2023). *Motor neurone disease.* Available at: https://www.brainresearchuk.org.uk/neurological-conditions/motor-neurone-disease#:~:text=Six%20people%20are%20diagnosed%20every%20day%20in%20the%20UK. (Accessed 9/11/2023)

Douglas, A. G. L., Baralle, D. (2023, July 11-14). Population-level penetrance of ALS genes is markedly reduced. [Oral Conference Presentation]. ENCALS 2023, Barcelona, Spain. https://www.encals.eu/wp-content/uploads/2023/07/Oral_presentations_0607_desg.pdf

Garrick, D., Fiering, S., Martin, D. I., & Whitelaw, E. (1998). Repeat-induced gene silencing in mammals. *Nature genetics*, *18*(1), 56–59. https://doi.org/10.1038/ng0198-56

Gurney, M. E., Pu, H., Chiu, A. Y., Dal Canto, M. C., Polchow, C. Y., Alexander, D. D., Caliendo, J., Hentati, A., Kwon, Y. W., & Deng, H. X. (1994). Motor neuron degeneration in mice that express a human Cu,Zn superoxide dismutase mutation. Science (New York, N.Y.), 264(5166), 1772–1775. https://doi.org/10.1126/science.8209258

Lyall, R. A., Donaldson, N., Polkey, M. I., Leigh, P. N., & Moxham, J. (2001). Respiratory muscle strength and ventilatory failure in amyotrophic lateral sclerosis. *Brain : a journal of neurology*, *124*(Pt 10), 2000–2013. https://doi.org/10.1093/brain/124.10.2000

Martin, D. I., & Whitelaw, E. (1996). The vagaries of variegating transgenes. *BioEssays : news and reviews in molecular, cellular and developmental biology*, *18*(11), 919–923. https://doi.org/10.1002/bies.950181111

Shaw, C. E., Enayat, Z. E., Powell, J. F., Anderson, V. E., Radunovic, A., al-Sarraj, S., & Leigh, P. N. (1997). Familial amyotrophic lateral sclerosis. Molecular pathology of a patient with a SOD1 mutation. Neurology, 49(6), 1612–1616. https://doi.org/10.1212/wnl.49.6.1612

Suzuki, N., Kato, S., Kato, M., Warita, H., Mizuno, H., Kato, M., Shimakura, N., Akiyama, H., Kobayashi, Z., Konno, H., & Aoki, M. (2012). FUS/TLS-immunoreactive neuronal and glial cell inclusions increase with disease duration in familial amyotrophic lateral sclerosis with an R521C FUS/TLS mutation. Journal of neuropathology and experimental neurology, 71(9), 779–788. https://doi.org/10.1097/NEN.0b013e318264f164

The Jackon Laboratory (2016). *How to spot and manage malocclusion in research mice.* Available at: https://www.jax.org/news-and-insights/jax-blog/2016/july/how-to-spot-malocclusion-in-research-mice. (Accessed 12/10/2023)

Yan, Q., & Johnson, E. M., Jr (1988). An immunohistochemical study of the nerve growth factor receptor in developing rats. *The Journal of neuroscience: the official journal of the Society for Neuroscience*, *8*(9), 3481–3498. https://doi.org/10.1523/JNEUROSCI.08-09-03481.1988

Zinszner, H., Sok, J., Immanuel, D., Yin, Y., & Ron, D. (1997). TLS (FUS) binds RNA in vivo and engages in nucleo-cytoplasmic shuttling. *Journal of cell science*, *110 (Pt 15)*, 1741–1750. https://doi.org/10.1242/jcs.110.15.1741